R-7911-5008

THE THREE-DIMENSIONAL RESPONSE OF A BRIDGE STRUCTURE SUBJECTED TO TRAVELING RAYLEIGH WAVES, SV-WAVES, AND P-WAVES

by

S.D. Werner
L.C. Lee

May 1980

Prepared Under
National Science Foundation Grant No. PFR77-23335

AGBABIAN ASSOCIATES
El Segundo, California

ABSTRACT

This report describes results of a continuation of a research program directed toward studying the three-dimensional response of structures subjected to arbitrarily incident traveling seismic waves. Toward this end, a methodology developed during the first phase of the program (named CAST-1) is used to analyze the three-dimensional dynamic response of a single-span bridge on an elastic half-space subjected to traveling Rayleigh waves, SV-waves, and P-waves with arbitrary excitation frequencies and angles of incidence. These analyses, when considered with those for SH-waves conducted during the first phase of the research program, show how the bridge response is influenced by each of the various types of seismic waves that propagate through an elastic half-space.

Results from the bridge analyses demonstrate that nonvertically incident seismic waves induce resonant responses that are different from those induced by vertically incident seismic waves. In addition, important non-resonant response characteristics are seen to be dependent on the wave type, the excitation frequency (or wavelength), and the angles of horizontal and vertical incidence of the seismic waves.

ACKNOWLEDGEMENTS

This research program has been supported by a National Science Foundation grant to Agbabian Associates (Grant No. PFR77-23335). This support is gratefully acknowledged.

Primary contributors to this work were S.D. Werner, principal investigator for the study, and L.C. Lee, who performed the calculations. M.D. Trifunac of the University of Southern California provided a critical review of this report and contributed helpful suggestions throughout the research program.

TABLE OF CONTENTS

CONTENTS (CONCLUDED)

LIST OF ILLUSTRATIONS

LIST OF ILLUSTRATIONS (CONTINUED)

LIST OF ILLUSTRATIONS (CONTINUED)

LIST OF ILLUSTRATIONS (CONTINUED)

LIST OF ILLUSTRATIONS (CONTINUED)

LIST OF ILLUSTRATIONS (CONTINUED)

LIST OF ILLUSTRATIONS (CONTINUED)

LIST OF ILLUSTRATIONS (CONCLUDED)

LIST OF TABLES

LIST OF TABLES (CONTINUED)

LIST OF TABLES (CONCLUDED)

THIS PAGE INTENTIONALLY BLANK

CHAPTER 1

INTRODUCTION, SUMMARY, AND RECOMMENDATIONS

1.1 PURPOSE AND SCOPE

In most analyses of the response of structures to earthquake ground motions, the seismic excitation is assumed to be identical all along the base of the structure. However, this assumption does not account for the spatial variations of the seismic waves, which cause the structure foundations to be subjected to excitations that differ in both amplitude and phase. Such excitations can have an important effect on the structure response.

To study the effects of spatially varying excitations, a grant was awarded to Agbabian Associates by the National Science Foundation in October 1976. The first year of this research program saw the development of a new methodology for computing the three-dimensional dynamic response of one or more arbitrarily configured, elastic, aboveground structures on an elastic half-space subjected to traveling seismic waves with arbitrary wavelength and direction of incidence. This methodology (named CAST-1) was used to analyze the response of a single-span bridge structure subjected to excitations from arbitrarily incident SH-waves. Results from these analyses showed that phase differences in the input ground motions led to bridge responses that were very different from those induced by excitations from vertically incident waves (in which such phase differences are neglected). In addition, the results showed that the nature of the bridge response to the spatially varying excitations was strongly dependent on the direction of incidence of the SH-waves as well as the excitation frequency. This demonstrated the importance of considering a range of directions of propagation when evaluating the effects of traveling waves on the three-dimensional response of a bridge structure (Werner et al., 1977).

The present report describes work carried out during the second part of this research program, which was initiated in July 1978. This work has analyzed the same bridge/soil system that was considered during the first year of the program, except now the bridge has been subjected to excitations from arbitrarily incident P-, SV-, and Rayleigh waves. These results, when considered with those from the previous SH-wave analyses, demonstrate how the three-dimensional response of the bridge is influenced by each of the various types of seismic waves that propagate through an elastic half-space.

To present these results, the report is divided into five chapters and one appendix. The remainder of this first chapter contains a summary of the results of the analyses and recommendations for future work along these lines. Chapter 2 provides background information on the CAST-1 methodology, the bridge/soil system being analyzed, and the general types of bridge response that are induced by the traveling seismic waves. Chapters 3 through 5 present the results of the bridge response analyses from Rayleigh wave, SV-wave, and P-wave excitations, respectively. Appendix A describes how analyses of traveling SH-wave effects for a structure on an elastic half-space, as described in our first report, can be used to represent Love wave effects in a layered soil medium.

1.2 SUMMARY OF RESULTS

1.2.1 SOIL/STRUCTURE SYSTEM AND RESPONSE CATEGORIES

The bridge structure considered in these analyses is shown in Figure 1-1. It has a single span and is supported by rigid rectangular foundations that, in turn, are bonded to the surface of an elastic half-space representation of the soil medium. In this report, this soil/structure system is subjected to arbitrarily incident Rayleigh, P-, and SV-waves of variable wavelength (or excitation frequency). The direction of incidence of these waves is defined by a horizontal angle, θ_H, and a vertical angle, θ_V (Fig. 1-1). Three different horizontal angles--corresponding to θ_H = 90 deg, 0 deg, and 45 deg--are considered in this study. For each value of θ_H, several different values of θ_V are considered when analyzing the response of this bridge/soil system to traveling SV-waves and P-waves.

Two different categories of response are observed from examination of the results of the calculations. The first is termed resonant response and corresponds to large response amplitudes of the bridge/elastic-half-space system that are analogous to those exhibited during normal modes of vibration by a finite-supported (i.e., fixed-base or free-free) bridge.* Whether or not a given resonant response actually occurs is dependent on the direction of incidence of the seismic waves; however, for those various directions for which a resonant response does occur, its deformed shapes and frequency (termed resonant frequency) are always similar and are nearly independent of the wave type. The second response category is termed phased-input-induced response and corresponds to significant nonresonant response characteristics that result from the phasing of the free-field excitations applied along the two foundations. These response characteristics are strongly dependent on the wave type, direction, and apparent wavelength of the incident seismic waves.

The following subsections contain a summary of the resonant response and phased-input-induced response characteristics of the bridge that result from the range of wave types, directions of incidence, and frequencies considered in this study. In this, reference is frequently made to the translations and rotations of the bridge with respect to its x-, y-, and z-axes. These axes and the directions they represent are shown in Figure 1-1.

1.2.2 RESONANT RESPONSE

From examination of the results from all the wave types and directions of incidence considered in this study, three basic types of resonant response occur most often. These types, shown in Figure 1-2, are as follows:

- Rocking in the y-Direction (Fig. 1-2a). This rocking response is induced by the various types of seismic waves propagating normal to the bridge span (θ_H = 90 deg). It features displacements along the y-axis that are symmetric about the midspan of

*The bridge/elastic half-space system considered in this study is actually continuous and semi-infinite and therefore does not possess discrete normal modes.

the bridge and are largest at that point. This resonant response does not occur when $\theta_H = 45$ deg, because this oblique angle of incidence introduces phase differences between the two foundations; these phase differences destroy the symmetry of the foundation driving forces and moments in the y-z plane.

- Vertical Displacement of Road Deck (Fig. 1-2b). This resonant response occurs for each of the various types of seismic waves, regardless of their direction of incidence. It features only small foundation motions and large vertical displacements of the road deck that are symmetric about its midspan and largest at that point.

- Sidesway in x-Direction (Fig. 1-2c). This sidesway response is induced by the various seismic waves that result in ground motions in a plane parallel to the bridge span ($\theta_H = 0$ deg) and oblique to the bridge span ($\theta_H = 45$ deg). It features large x-displacements of the road deck relative to the two foundations and occurs at a resonant frequency that is very close to the frequency for the resonant response involving vertical displacements of the road deck.

Table 1-1 summarizes the occurrence of each resonant response as a function of the wave type and the direction of incidence of the seismic wave. This table shows that the three resonant responses occur for all three wave types and, for each type, their occurrence is dependent on the direction of incidence of the seismic waves (as denoted by the angles θ_H and θ_V).* In particular, it is seen that for a given body wave type, nonvertically incident waves induce resonant responses that are different from those induced by vertically incident waves.

*This is because the direction of the incident waves controls both the orientation and the phasing of the excitations applied to the two foundations.

1.2.3 PHASED-INPUT-INDUCED RESPONSE

Phased-input-induced responses are dependent on the direction of incidence of the seismic waves, on the ratio of the bridge dimension in the direction of propagation to the apparent wavelength of the incident wave, and on the wave type. In the paragraphs that follow, the phased-input-induced responses are grouped according to the angle of horizontal incidence θ_H and, within this grouping, the effects of the other variables noted above are summarized.

1.2.3.1 Waves Propagating Normal to Bridge Span (θ_H = 90 deg)

When the nonvertically incident P-, SV-, and Rayleigh waves are propagating normal to the span length, they are directed along the 70-ft length of the rigid foundations (Fig. 1-1). Therefore, when the apparent wavelength of these waves becomes short relative to this foundation length, the bridge response falls well below that of the free field. This significant trend is attributed to self-canceling effects whereby the net loading applied to a rigid foundation decreases as the wavelength of the incident wave decreases (see Werner et al., 1977). These effects are not induced by vertically incident body waves. Also, in a more realistic setting that involves flexible foundations, these effects are expected to be less pronounced than suggested by this analysis.

1.2.3.2 Waves Propagating Parallel to Bridge Span (θ_H = 0 deg)

When the P-, SV-, and Rayleigh waves are propagating parallel to the bridge span, they apply what can be regarded as point loads at the two ends of the bridge (since the dimension of the foundations in a direction parallel to the bridge is small relative to the bridge span, see Fig. 1-1). The characteristics of the bridge response to such loads are dependent on the wave type and on the relative phasing of the loads applied to the two foundations (which, in turn, is dependent on the ratio of the bridge span length to the apparent wavelength of the incident wave). Unlike the results for θ_H = 90 deg, the phased-input-induced response amplitudes for θ_H = 0 deg are of the same order of magnitude throughout the frequency range.

To demonstrate phased-input-induced responses for each nonvertically incident wave type, the bridge response has been computed for the cases involving applied excitations that are (a) of equal amplitude and equal phase at the two foundations and (b) of equal amplitude and opposite phase at the two foundations. The contrasting bridge response for these two cases illustrates the influence of the phasing of the applied excitations. Also, as the excitation frequency increases for a given case, the deformed shapes of the bridge become more complex and irregular because of the increased influence of wave diffraction, wave scattering, and higher modes of vibration at these higher excitation frequencies.

The influence of the wave type on the bridge response is also clearly demonstrated by the above cases. For example, the response of the bridge to Rayleigh wave motion is affected by the elliptic retrograde nature of the ground surface motion; it therefore differs markedly from the bridge response to, say, P-waves, for which the horizontal and vertical components of free-field motion are in phase. Also, the bridge response to SV-waves is seen to change markedly with varying θ_V because of (a) variations in both amplitude and phase of the free-field ground surface motion and (b) apparent wavelength effects.

1.2.3.3 Waves Propagating Oblique to the Bridge Span (θ_H = 45 deg)

There are three main trends regarding phased-input-induced effects of obliquely incident P-, SV-, and Rayleigh waves on the bridge response. These are as follows:

- The response of the bridge is now fully three dimensional, as contrasted with its essentially two-dimensional response to waves propagating at θ_H = 90 deg and 0 deg.
- Nonvertically incident waves propagating in the plane defined by θ_H = 45 deg can generate large torsional deformations in the various elements of the bridge. Torsion in the end walls

is a consequence of the differences between the substantial rotations about the z-axis that occur at the foundations and the tops of the end walls. Torsional deformations in the road deck are induced as a result of the differences that occur between the rocking displacements (in the y-direction) of the two end walls. Large torsional effects are not induced by the vertically incident body waves.

- When subjected to nonvertically incident waves, the bridge experiences high-frequency displacements along the x-, y-, and z-axes that become small relative to those of the free field. This occurs when the apparent wavelength of the obliquely incident wave, projected along the length of the rigid foundation, is small relative to the foundation length and leads to the self-canceling effects previously noted in Section 1.2.3.1. As indicated in that section, such self-canceling effects are not induced by vertically incident body waves.

1.3 RECOMMENDATIONS

The work described in this report and in our prior report (Werner et al., 1977) has used a new methodology to illustrate basic structural response phenomena induced by traveling seismic waves. Although these results provide important insights into such phenomena, more work is required in the related areas of input motions, field measurements of structural response, analytical studies, and development of analytical methodologies. These areas are discussed below.

1.3.1 DEFINITION OF INPUT MOTIONS

Perhaps the most significant deficiency in the current technology for evaluating traveling wave effects involves the lack of ground motion data necessary to guide the specification of spatially varying input motions for seismic response analyses. Accordingly, research efforts should be directed

toward the following two areas: (a) defining the spatial variations of ground motions, both horizontally and vertically; and (b) defining the amplitude, frequency content, and direction of incidence of the seismic waves that comprise the ground motions. These efforts should stress the planning and deployment of horizontal and vertical arrays of strong motion instruments, and the development of theoretical and analytical techniques for interpreting measurements from such instruments.

1.3.2 FIELD MEASUREMENTS OF STRUCTURAL RESPONSE

Various types of structures are particularly susceptible to traveling wave effects (e.g., bridges) and, therefore, should be so instrumented as to promote further insights into their behavior during earthquakes. Selection of the type and location of instruments to measure the response of these structures to traveling seismic waves should be guided by analytical studies and by prior observations of structural response characteristics. It is noted that dense arrays of instruments may be required to provide sufficiently detailed measurements to fully interpret the nature of the structural response.

1.3.3 ANALYTICAL STUDIES OF STRUCTURAL RESPONSE

Existing methodologies should be used to carry out further analytical studies and parametric analyses of the three-dimensional response of the various types of structures that are susceptible to effects of traveling seismic waves. Such analyses should have two main goals. First, they should be directed toward providing insights into potential seismic response modes of the structures and, in particular, toward the discovery and enumeration of structural response phenomena that may not be intuitively obvious. Second, the analyses should assess the influence of various physical parameters related to the structural configuration, soil medium, and input motions. Results from analyses planned with these goals in mind should be used to provide guidance for (a) developing simplified design procedures that incorporate traveling wave effects, (b) planning instrumentation for field measurements of the seismic response of the structures (as per Sec. 1.3.2), and (c) interpreting observed the observed behavior of structures during earthquakes.

1.3.4 FURTHER METHODOLOGY DEVELOPMENT

The CAST-1 methodology developed as part of this research program is only the first step in the development of the type of methodology that merges continuum solutions (for analyzing foundation/soil interaction effects) with finite element techniques (for representing the superstructure). Because it provides a potentially powerful technique for analyzing three-dimensional traveling wave effects, the methodology should be further developed and extended. In particular, research should be directed toward incorporating such features as embedded footings and pile foundations, deformable footings, viscoelastic layered soil media, topographic irregularities, structure non-linearities (e.g., expansion joints of bridges), and transient excitations (through the use of Fast Fourier Transform techniques).

TABLE 1-1. RESONANT RESPONSE OF BRIDGE FOR VARIOUS DIRECTIONS OF INCIDENCE OF SEISMIC WAVES

θ_H, deg	Wave Type	θ_V,[1] deg	Types of Resonant Response[2] (Fig. 1-2)		
			Rocking in y-Direction (f = 4.2 Hz)	Vertical Displacement of Road Deck (f = 2.8 Hz)	Sidesway in x-Direction (f = 3.0 Hz)
90	Rayleigh	0	Yes	Yes	No
	SV	90	Yes	No	No
		≠90	Yes	Yes	No
	P	90[3]	No	Yes	No
		≠90	Yes	Yes	No
0	Rayleigh	0	No	Yes	Yes
	SV	90	No	No	Yes
		≠90	No	Yes[4]	Yes
	P	90[3]	No	Yes	No
		≠90	No	Yes	Yes
45	Rayleigh	0	No	Yes	No
	SV	90	Yes	No	Yes
		≠90	No	Yes	Yes
	P	90[3]	No	Yes	No
		≠90	No	Yes	Yes

AA10337

Notes:

(1) θ_V = 90 deg represents vertically incident wave (Fig. 1-1).

(2) Resonant frequency values shown correspond to those from the SV-wave results. In some cases, they differ slightly in the Rayleigh wave and P-wave results.

(3) Response to vertically incident P-waves is independent of θ_H.

(4) When θ_H = 0 deg for SV-waves, resonant response involving vertical displacement of road deck is induced in all θ_V cases considered except when θ_V = 45 deg.

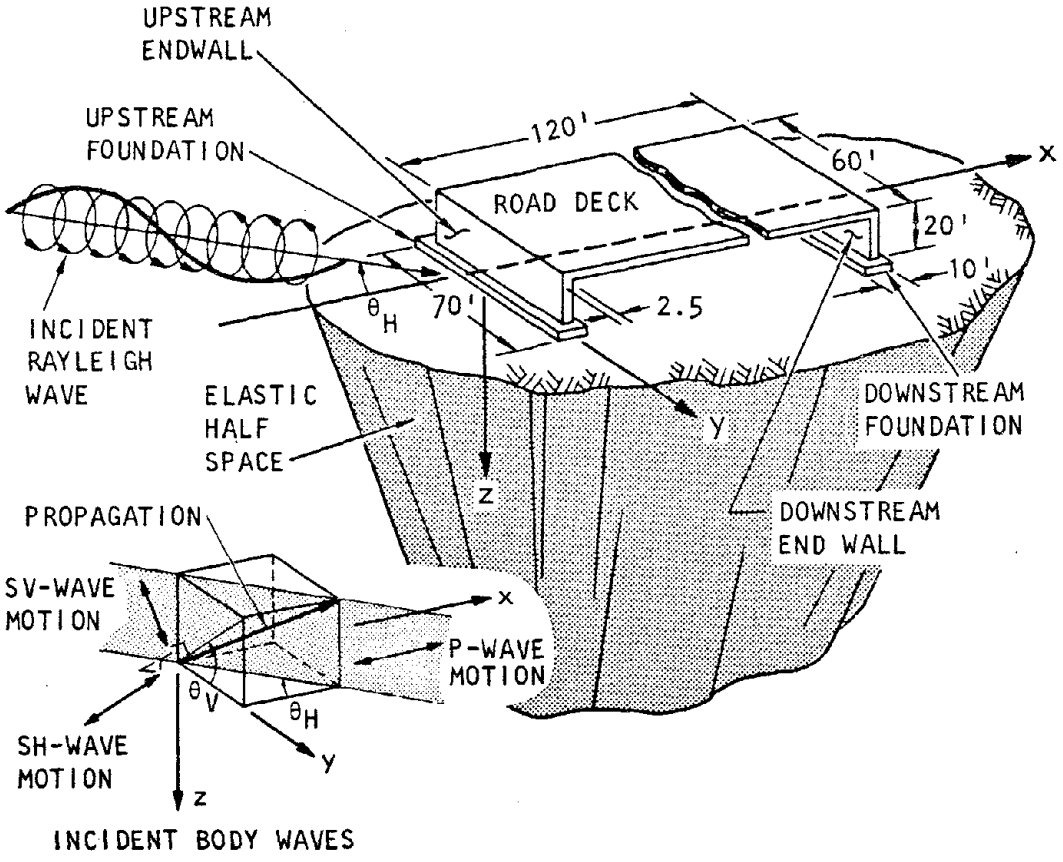

FIGURE 1-1. BRIDGE CONFIGURATION

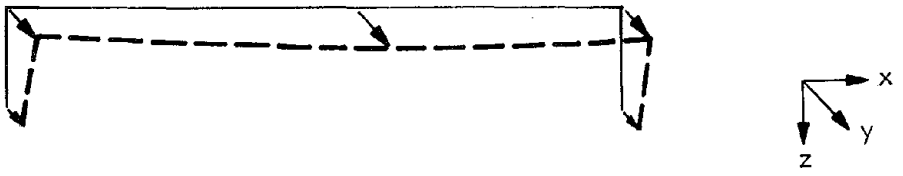

(a) Rocking in y-direction (4.2 Hz)

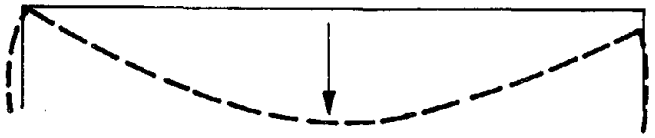

(b) Vertical displacement of road deck (2.8 Hz)

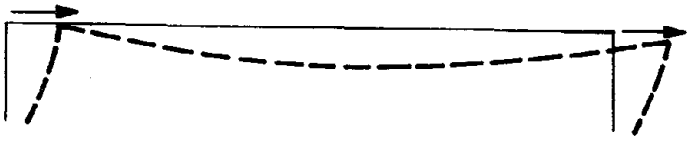

(c) Sidesway in x-direction (3.0 Hz)

FIGURE 1-2. DEFORMED SHAPES AT TIMES OF PEAK RESONANT RESPONSE

CHAPTER 2

BACKGROUND INFORMATION

This chapter presents background information pertinent to the analyses conducted during the second year of this research program. This includes a description of the CAST-1 methodology and the bridge/soil system being analyzed, together with a brief discussion of the general categories of bridge response that will be encountered.

2.1 CAST-1 METHODOLOGY

2.1.1 GENERAL DESCRIPTION

The methodology developed during this research program to analyze traveling seismic wave effects is named CAST-1 and has the following features (see Fig. 2-1):

a. It computes the three-dimensional dynamic response of one or more arbitrarily configured, elastic, aboveground structures.

b. It assumes each structure to be supported on any number of rigid foundations of arbitrary shape that are bonded to the surface of an elastic half-space.

c. It represents input motions as any desired combination of harmonic body and/or surface waves with arbitrary excitation frequencies, amplitudes, phase angles, and directions of incidence.

CAST-1 is organized into an input phase, a response analysis phase, and an output phase (Fig. 2-2). The input phase defines all input data required to fully describe the superstructure, foundations, soil medium, and input motions. It involves a single subprogram--Subprogram GREEN-- that computes Green's functions for an elastic half-space; for the other elements of the system, this phase involves defining the required input data. In the

response analysis phase, the computations of the dynamic response of the soil/structure system are carried out. This phase involves three separate subprograms--SAP, FOUND, and COMBINE--that are summarized in Figure 2-2 and in the subsections that follow. The final phase--the output phase--provides all printed and plotted output necessary to evaluate the system response characteristics. It involves Subprogram PLOT, which provides plots of frequency-dependent amplitudes and phase angles for any degree of freedom, as well as three-dimensional deformed shapes of the structure at specific times.

Within the context of these phases, the subsections that follow briefly summarize how the superstructure and foundation/soil systems are represented and how the overall system response analysis is carried out. More detailed descriptions of these aspects of CAST-1 are provided by Werner et al. (1977).

2.1.2 REPRESENTATION OF SUPERSTRUCTURE

CAST-1 uses a three-dimensional finite element model to represent the superstructure (see Subprogram SAP in Fig. 2-2). The model can comprise any combination of the various structural element types originally developed by Bathé et al. (1974) and shown in Figure 2-3; these elements are used to define the stiffness matrix and mass matrix of the superstructure. Once these matrices are defined, fixed-base mode shapes and frequencies are computed, using either a subspace iteration technique (Bathé and Wilson, 1972) or a determinant search solution (Bathé and Wilson, 1973). Damping in the superstructure is represented by specifying a damping ratio for each fixed-base normal mode of the superstructure.

2.1.3 REPRESENTATION OF FOUNDATION/SOIL SYSTEM

Foundation/soil interaction effects under the action of the incident wave motions are represented using a continuum solution based on the work of Wong (1975) and incorporated in CAST-1 as Subprogram FOUND (Fig. 2-2). This

solution characterizes the foundation/soil system in terms of complex, frequency-dependent driving force vectors and impedance matrices. The driving forces correspond to the reaction forces that result when each foundation is fixed and subjected to the incident waves transmitted through the soil medium (Fig. 2-4a). The elements of the jth column of the impedance matrix are computed as foundation reaction forces caused by a unit harmonic displacement of the jth foundation degree of freedom when all other foundation degrees of freedom are fixed (Fig. 2-4b). These quantities are derived for one or more foundations of arbitrary shape by first using Green's functions for an elastic half-space to define stress/displacement relationships for various subregions of each foundation, and then by imposing rigid-body displacement boundary conditions and equilibrium requirements. Details of this derivation are provided by Werner et al. (1977).

2.1.4 SYSTEM RESPONSE ANALYSIS

Once the superstructure and foundation/soil systems are characterized as described in Subsections 2.1.2 and 2.1.3, they are coupled by enforcing compatibility and equilibrium requirements at their interface (Gutierrez and Chopra, 1978). The response of this coupled system is then computed, using an extension of a procedure first described by Clough and Penzien (1975). This procedure computes the response for each structure degree of freedom as the superposition of (a) a pseudostatic component that represents the effects of the relative displacements associated with each support degree of freedom, and (b) a dynamic component that incorporates the effects of uniform shaking of the supports on the fixed-base structural response.

2.2 BRIDGE/SOIL SYSTEM

The bridge/soil system analyzed by CAST-1 in this study is described in this section. As previously noted, the system response under the action of Rayleigh waves, SV-waves, and P-waves has been computed during this year's effort (see Chapts. 3 to 5). For each wave type, parametric analyses are

carried out to show how the bridge response is influenced by the excitation frequency and direction of incidence of the incident wave. Parametric analyses of the response of this bridge/soil system to arbitrarily incident SH-waves have been carried out during the first year of the research program and are reported by Werner et al. (1977).

2.2.1 BRIDGE/SOIL SYSTEM MODEL

The bridge configuration considered in this study has a single span and is shown in Figure 2-5a to be 120 ft long, 70 ft wide, and 20 ft high. The bridge is modeled using the series of undamped beam elements shown in Figure 2-5b. Section and material properties for these elements are given in Table 2-1, and corresponding fixed-base mode shapes and frequencies are provided in Figure 2-6 for the first few modes of the bridge. This latter figure shows that the out-of-plane modes have significantly higher frequencies than do the corresponding in-plane modes, a direct result of the greater stiffness of the bridge in the y-direction.

The bridge is supported on two rigid rectangular foundations that rest on the surface of an elastic half-space representation of the soil medium. Material properties for the elastic half-space are provided in Table 2-1b. The low shear wave velocity of the soil medium (500 fps used in these calculations) is representative of a soft soil for which traveling wave effects at a given excitation frequency will be more pronounced than for a stiffer medium with a higher shear wave velocity. The mass of the foundations corresponds to that for a 2-ft thickness of reinforced concrete (with a unit weight of 150 pcf); this mass is somewhat greater than that considered in the earlier calculations involving SH-waves (Werner et al., 1977).

2.2.2 INCIDENT WAVE MOTIONS

The free-field excitations considered in this study correspond to planar harmonic Rayleigh, SV-, and P-waves. The circular frequency ω and direction of incidence of these waves are varied in the parametric analyses, while the amplitudes of the wave motions are fixed.

2.2.2.1 Rayleigh Waves

For Rayleigh waves, the excitation is normalized so that its horizontal component of free-field motion at the ground surface has an amplitude of 1.0. The corresponding vertical component of Rayleigh wave motion is 90 deg out of phase with respect to the horizontal component and, for a Poisson's ratio of the soil medium of 1/3, will have an amplitude that is 1.565 times the horizontal component. The direction of incidence of the Rayleigh wave motion is defined only in terms of the horizontal angle of incidence, θ_H, shown in Figure 2-5. Details of the definition of the free-field ground surface motion induced by Rayleigh waves are contained in Section 3.2.

2.2.2.2 P-Waves and SV-Waves

For P-waves and SV-waves, the direction of incidence of the excitations are defined using two angles--θ_H and θ_V--which are the horizontal and vertical angles of incidence (Fig. 2-5a). The amplitudes and phasing of the ground surface excitations from these waves are then determined assuming that the incident wave motion has a unit amplitude. For SV-waves, the resulting amplitudes and phase angles of the horizontal and vertical components of free-field motion at the ground surface are then determined as a function of θ_V, for a Poisson's ratio of the soil medium of 1/3. For P-waves, the horizontal and vertical components of free-field motion at the ground surface are always in phase; only the amplitudes of these components of motion vary according to θ_V and to the Poisson's ratio of the soil medium. Details of the definition of the free-field ground surface motion induced by SV-waves and P-waves are provided in Sections 4.2 and 5.2, respectively.

2.2.2.3 Excitation Cases and Dimensionless Frequencies

For each wave type, several different directions of incidence, as represented by appropriate combinations of θ_H and θ_V, are considered. These directions are summarized in Table 2-2 and are discussed more fully in

Chapters 3 through 5. For each direction, the excitation frequencies (wavelengths) are varied, and the amplitudes and phase angles of response at each degree of freedom of the bridge are computed as a function of a dimensionless frequency parameter, R_L, defined as

$$R_L = \frac{\ell}{\lambda} = \frac{\ell\omega}{2\pi V} \tag{2-1}$$

where λ and V are the wavelength and velocity, respectively, of the wave along its propagation path; ω is the circular frequency of excitation, and ℓ is a representative structure dimension in a direction parallel to the propagation path as defined by θ_H. Definitions of ℓ and corresponding values of R_L for various values of θ_H are given in Table 2-3.

2.3 BRIDGE RESPONSE CHARACTERISTICS

In Chapters 3 to 5, the bridge response to each of the arbitrarily incident wave types is described in terms of two basic categories, termed resonant response and phased-input-induced response. These are described in the subsections that follow.

2.3.1 RESONANT RESPONSE

When studying the dynamic response of structures subjected to harmonic input motions, it is typical to observe large amplitudes of response in the framework of finite-supported (e.g., fixed-base or free-free) structures that have discrete normal modes. However, the bridge/elastic-half-space system under consideration in this study does not possess such modes since it is actually a continuous semi-infinite system. Despite this, there are instances where the surface of the half-space moves so as to induce bridge-support motions whose frequency, phasing, and relative displacements are comparable in a general qualitative sense to those expected during fixed or free-free

modes of vibration; in such instances, large amplitudes of vibration of the bridge are observed. This type of behavior is termed "resonant response" throughout this report, by analogy with the finite-supported case, and the frequencies at which it occurs are termed "resonant frequencies." These differ from the modal frequencies of the finite-supported bridge because of three-dimensional soil/structure interaction effects and the phasing of the various components of the input motion.* Whether or not a given resonant response actually occurs is dependent on the direction of incidence of the seismic waves; however, for those various directions for which a resonant response does occur, its deformed shapes and resonant frequency are always similar and are essentially independent of wave type.

2.3.2 PHASED-INPUT-INDUCED RESPONSE

The second category of response observed for the bridge/soil system--termed phased-input-induced response--corresponds to nonresonant response characteristics that are related directly to the spatial variations of the traveling seismic waves. Unlike the resonant responses, the phased-input-induced response characteristics can be strongly dependent on the wave type and direction of incidence, as well as the phasing of the applied excitations.

It is appropriate here to note a fundamental characteristic of the phased-input-induced response to nonvertically incident body waves. This response to such waves can often be related to the apparent wavelength, λ_a, as projected onto the ground surface (Fig. 2-7) and computed in terms of λ and θ_V as

$$\lambda_a = \frac{\lambda}{\cos \theta_V} \qquad (2\text{-}2)$$

*Throughout this report, resonant frequencies of the bridge/soil system are compared to the frequencies of the corresponding fixed-base normal modes of the bridge. Similar comparisons could have been made involving free-free modes of vibration; however, eigenvectors and eigenvalues corresponding to such modes were not calculated.

The dimensionless frequency parameter R_L (Eq. 2-1) is expressed in terms of λ_a as

$$R_L = \frac{\ell}{\lambda} = \frac{\ell}{\lambda_a \cos \theta_V} \tag{2-3}$$

Equation 2-3 illustrates that, for response phenomena that occur at certain fixed values of λ_a, the corresponding value of R_L increases with increasing θ_V. This spreading of the dimensionless frequency scale that results when θ_V is increased is commonly referred to as apparent wavelength effects.

TABLE 2-1. BRIDGE/SOIL SYSTEM PROPERTIES

Element	Section Properties				Material Properties		
	Cross Sectional Area, ft^2	Moment of Inertia, ft^4			Young's Modulus, psi	Unit Weight, pcf	Poisson's Ratio
		About Strong Axis	About Weak Axis	Torsion			
Road Deck	9.82×10	3.56×10^4	3.29×10^2	1.01×10^3	3.54×10^6	150	0.15
End Walls	1.48×10^2	4.28×10^4	7.69×10	3.08×10^2			

(a) Bridge

Unit Weight	Poisson's Ratio	Shear Wave Velocity, fps	Other Wave Velocities, fps (for Poisson's Ratio = 1/3)	
			P-Wave Velocity	Rayleigh-Wave Velocity
110	0.33	500	1000	466.3

(b) Soil Medium

TABLE 2-2. SUMMARY OF EXCITATION CASES FOR EACH WAVE TYPE[1]

Wave Type	Angles of Incidence, deg[2]	
	Horizontal Angle, θ_H	Vertical Angle, θ_V
Rayleigh	0, 45, 90	0
SV[3]	↓	20, 45, 55, 60, 65, 90
P	↓	10, 45, 90

Notes:

(1) More complete description of excitation cases for each wave type provided in Chapters 3 to 5.

(2) Angles of incidence defined in Figures 2-1 and 2-5a.

(3) As discussed in Chapter 4, SV-wave excitations strongly influenced by θ_V. Therefore, several different θ_V values considered in order to fully represent θ_V effects.

TABLE 2-3. DEPENDENCE OF DIMENSIONLESS FREQUENCY ON θ_H

Angle of Incidence, θ_H, deg	Orientation of Incident Wave Propagation Path	Definition of ℓ (Eq. 2-1)		Dimensionless Frequency, R_L(1) (Eq. 2-1)
		Description	Numerical Value (Fig. 2-1)	
0	Within vertical plane parallel to x-z plane of bridge	Distance between the two bridge foundations	120 ft	$R_{Lx} = \frac{120 \text{ ft} \times \omega}{2\pi V}$
90	Within vertical plane normal to x-z plane of bridge (or parallel to y-z plane)	Length of foundations along y-axis	70 ft	$R_{Ly} = \frac{70 \text{ ft} \times \omega}{2\pi V}$
45	Within vertical plane oriented at 45 deg to x-z plane	Same as for θ_H = 0 deg and 90 deg		R_{Lx} and R_{Ly}

Note:

(1) V = Velocity of incident wave along its propagation path (V_P, V_S, V_R for P-wave, SV-wave, and Rayleigh wave, respectively)

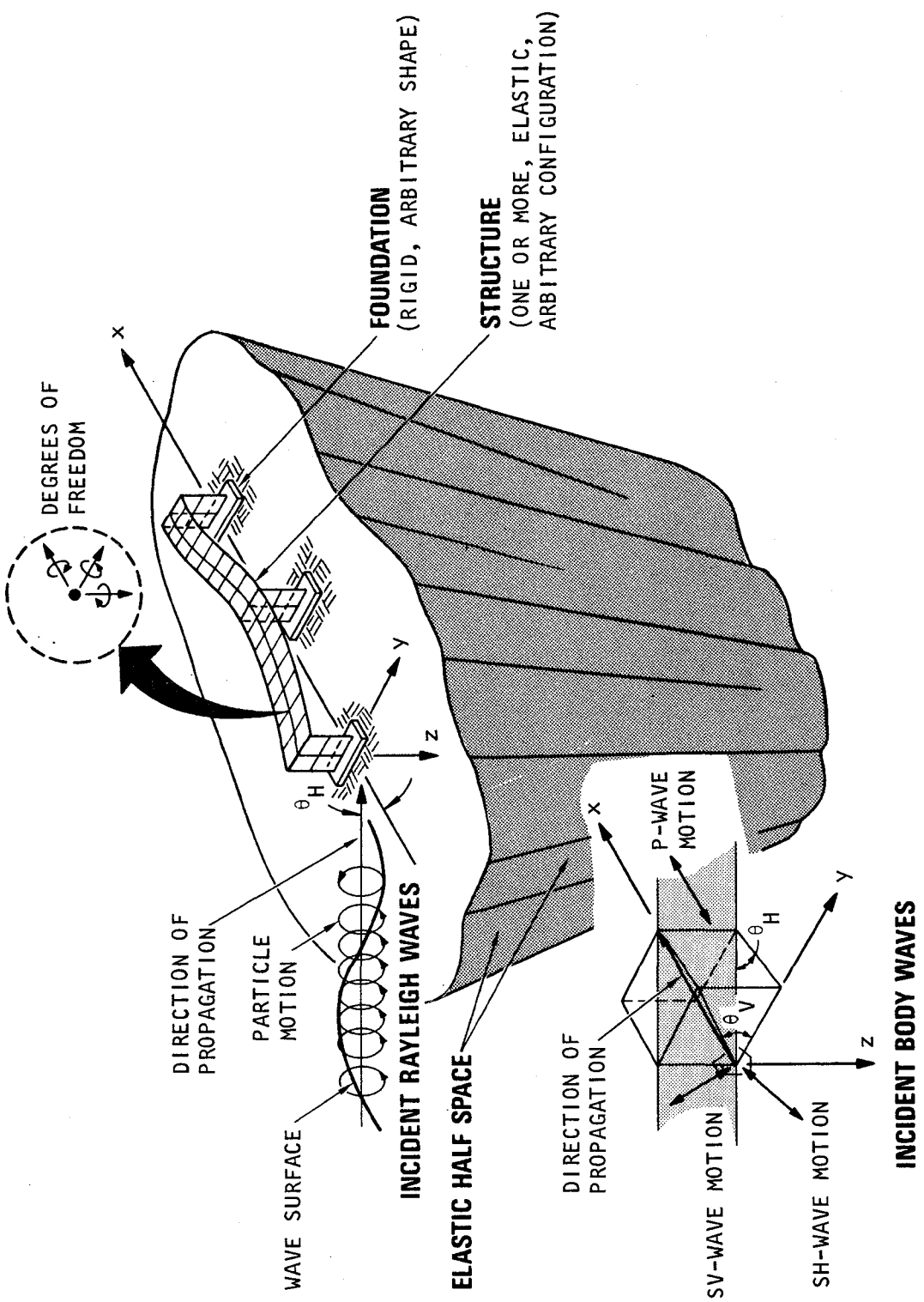

FIGURE 2-1. CAST-1 METHODOLOGY (Werner et al., 1977)

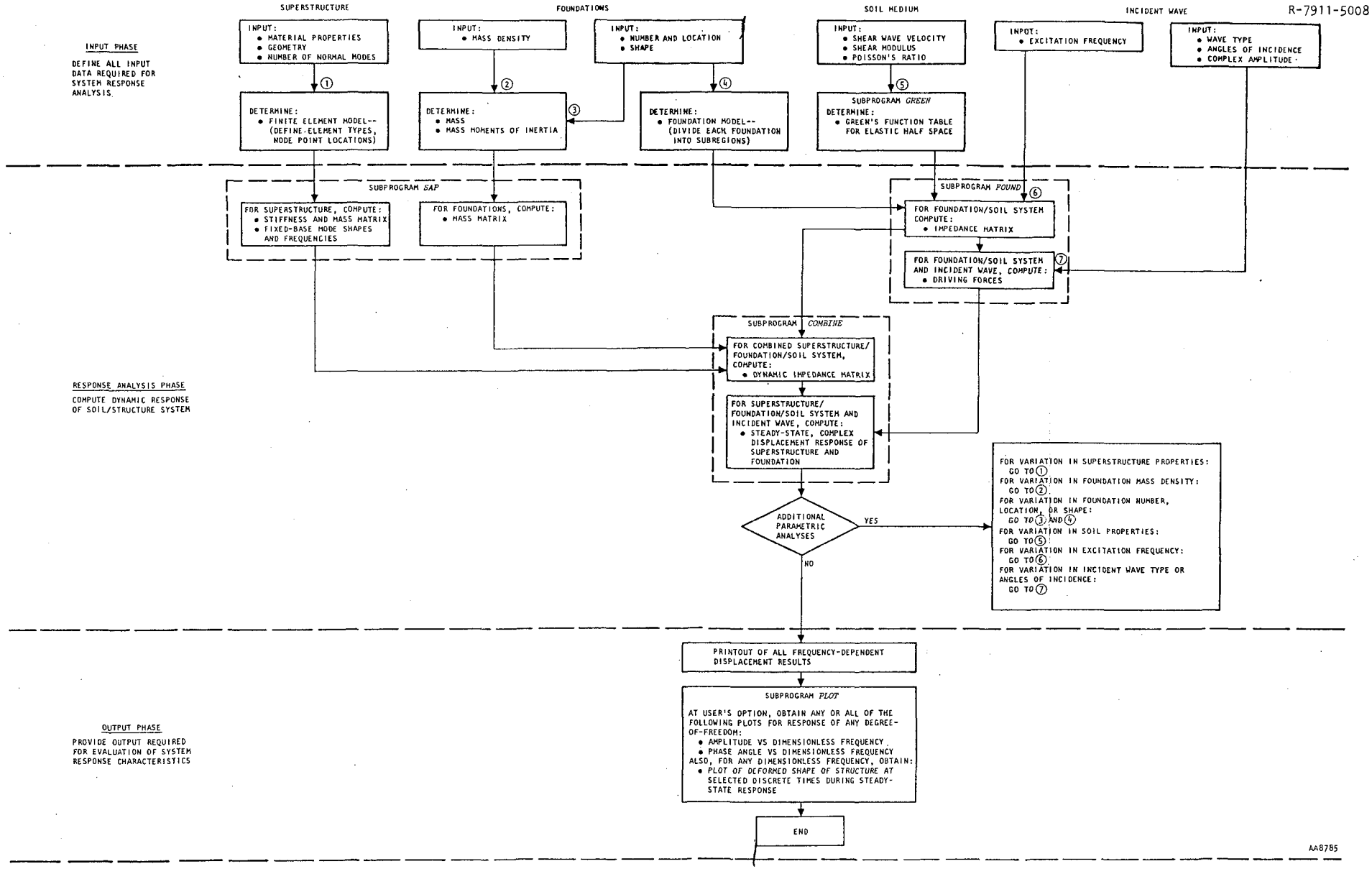

FIGURE 2-2. CAST-1 ANALYSIS PROCEDURE (Werner, et al., 1977)

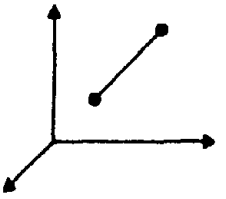

(a) Three-dimensional truss element

(b) Three-dimensional beam element

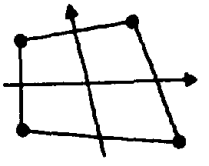

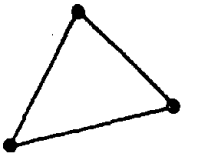

(c) Plane stress, plane strain and axisymmetric elements

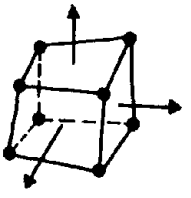

(d) Three-dimensional solid

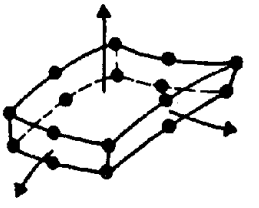

(e) Variable-number-nodes thick shell and three-dimensional element

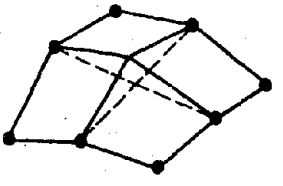

(f) Thin plate and shell element

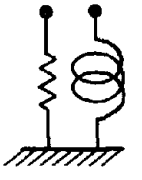

(g) Boundary element

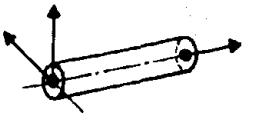

TANGENT

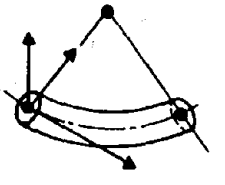

BEND

(h) Pipe element

FIGURE 2-3. SUPERSTRUCTURE ELEMENT TYPES IN SUBPROGRAM SAP (Bathé, et al., 1974)

Preceding page blank

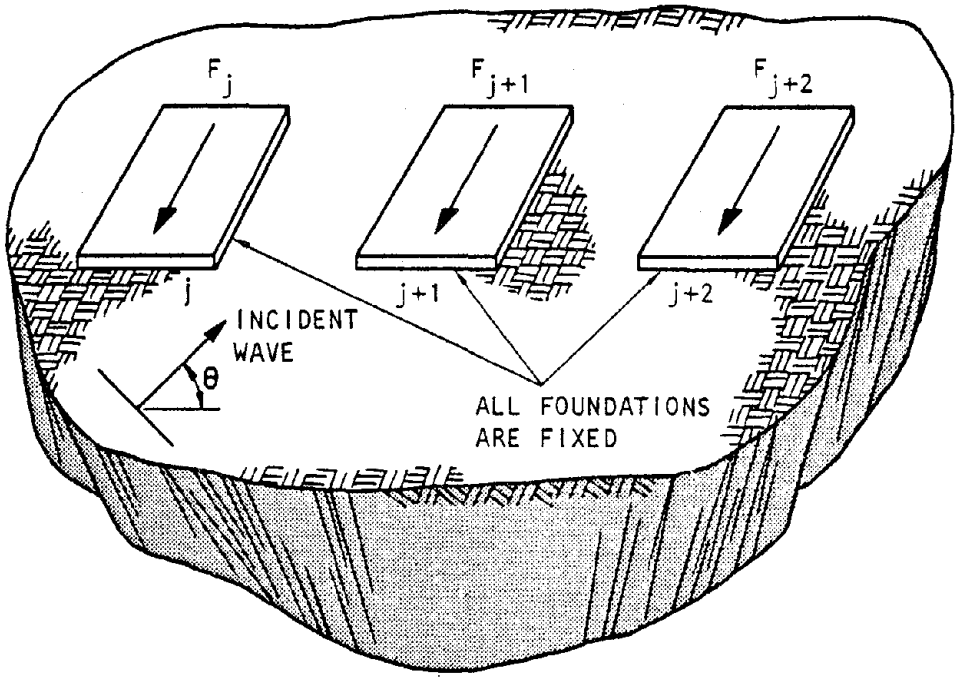

(a) Development of foundation driving forces (only longitudinal forces shown)

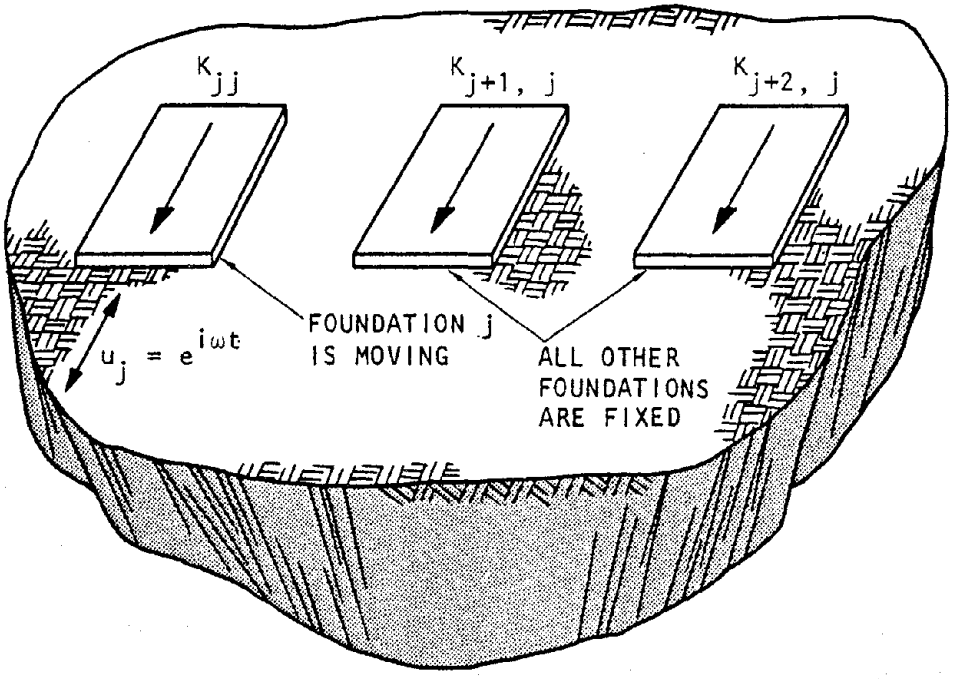

(b) Development of jth column of soil/foundation impedance matrix (only longitudinal forces shown)

FIGURE 2-4. DEVELOPMENT OF FOUNDATION/SOIL DRIVING FORCES AND IMPEDANCE MATRIX (Wong, 1975)

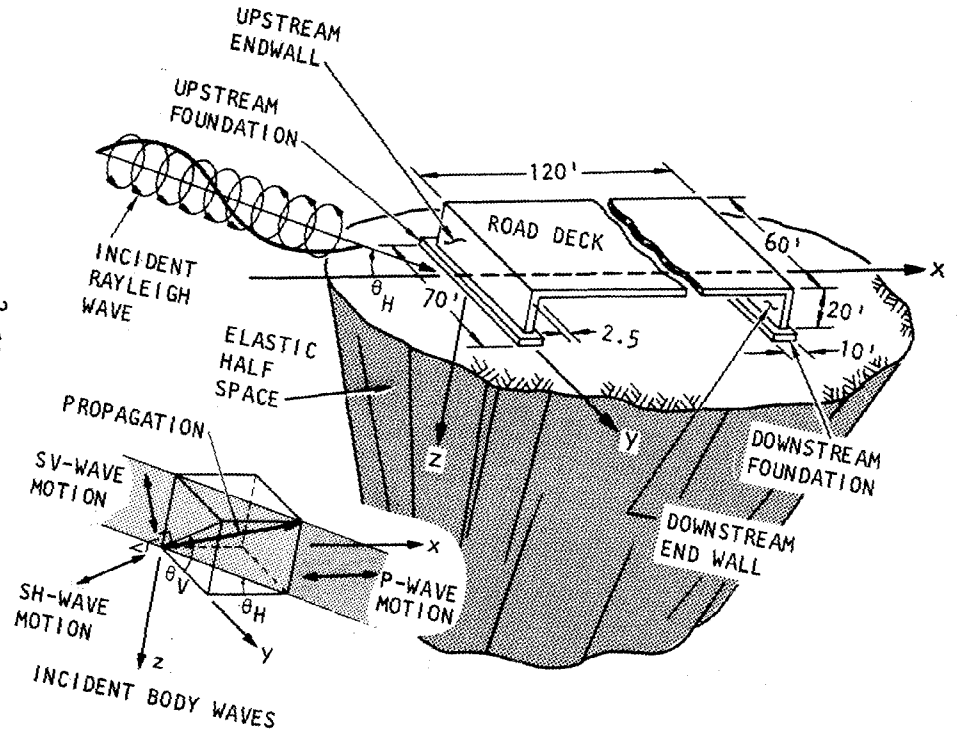

(a) Configuration

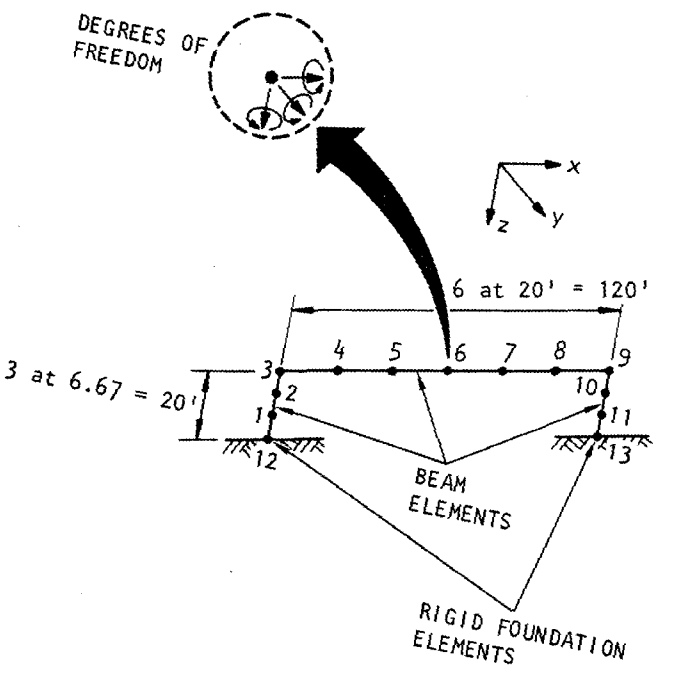

(b) Model

FIGURE 2-5. BRIDGE CONFIGURATION AND MODEL

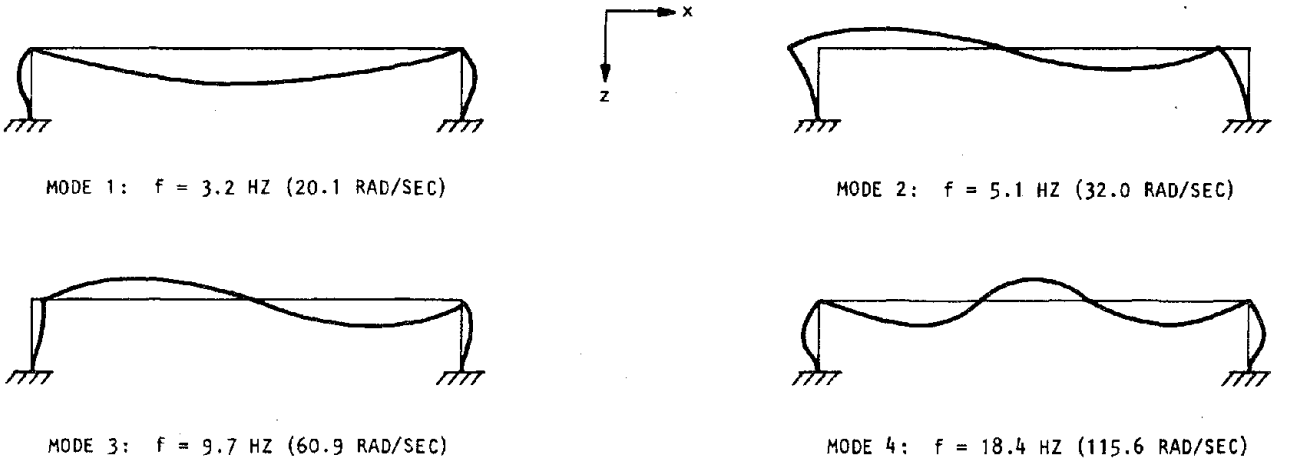

(a) In-plane modes (significant response in x-z plane)

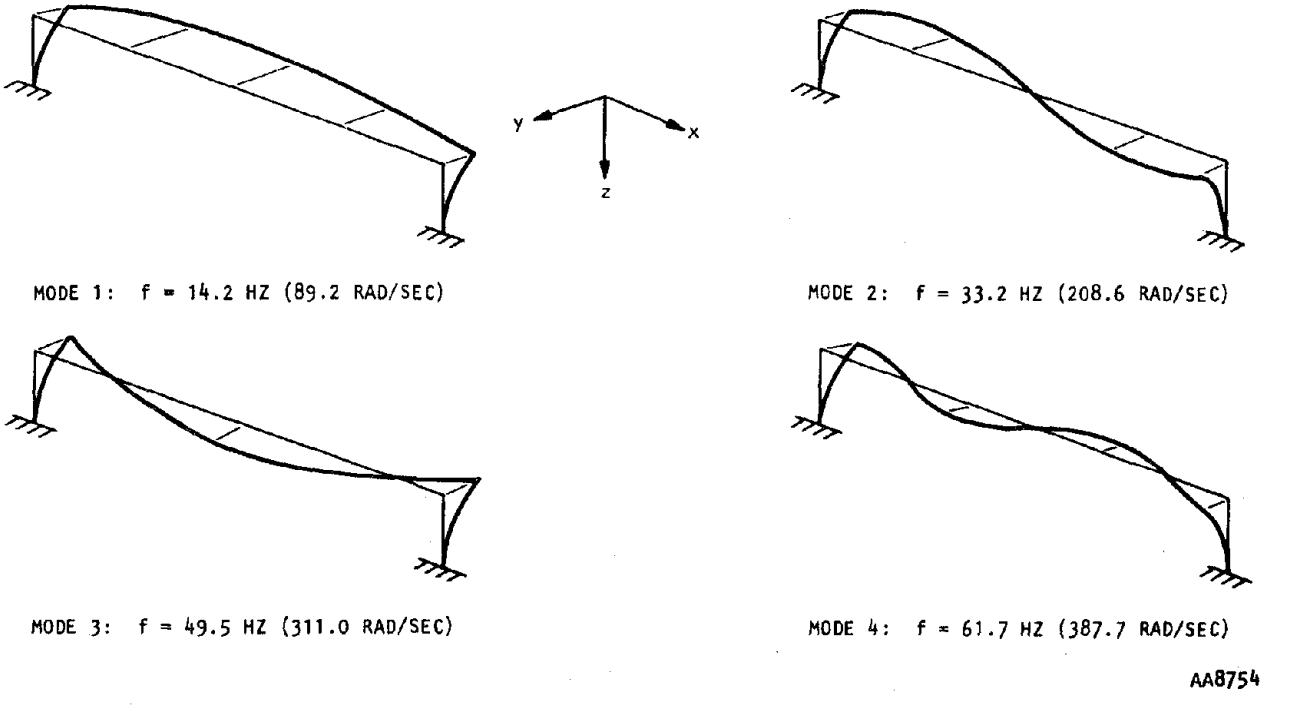

(b) Out-of-plane modes (significant response in y-direction)

FIGURE 2-6. FIXED-BASE MODE SHAPES AND FREQUENCIES OF BRIDGE

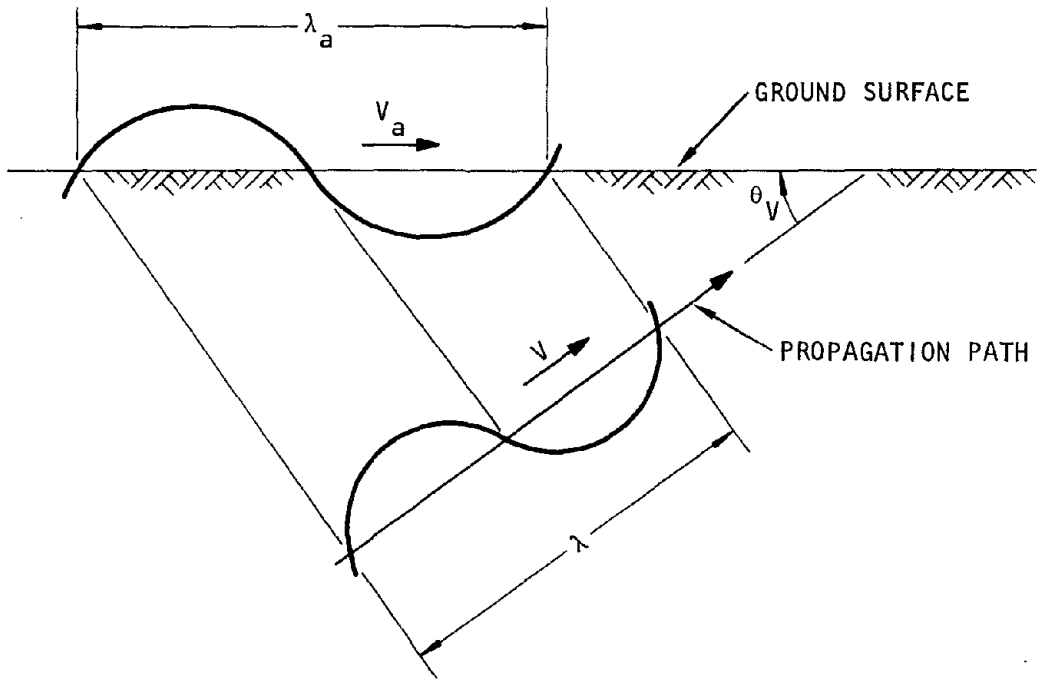

NOTE:

ALONG PROPAGATION PATH: WAVE LENGTH = λ

PROPAGATION VELOCITY = V

ALONG GROUND SURFACE: APPARENT WAVELENGTH = $\lambda_a = \frac{\lambda}{\cos \theta_V}$

APPARENT PROPAGATION VELOCITY = $V_a = \frac{V}{\cos \theta_V}$

FIGURE 2-7. APPARENT WAVELENGTH AND PROPAGATION VELOCITY

THIS PAGE INTENTIONALLY BLANK

CHAPTER 3

RAYLEIGH WAVE ANALYSIS

3.1 GENERAL DISCUSSION

The response of structures to propagating surface waves is a subject of growing interest among earthquake engineers. One reason for this is recent evidence of the important contributions of surface waves to the ground shaking recorded during major earthquakes. For example, accelerograms were synthesized by Trifunac (1971) at the site of the records from the May 18, 1940 Imperial Valley California earthquake, on the basis of energy propagating through low-velocity surface wave guides; these synthesized accelerograms were shown to have many of the characteristics of the actual recorded motions. Anderson (1974) showed that the largest accelerations in recordings from the June 27, 1966 Parkfield California earthquake are in time intervals consistent with surface wave arrivals. Hartzel et al. (1978) interpreted the strong ground motion recorded during the October 6, 1974 Acapulco Mexico earthquake as being composed mainly of high-frequency surface waves (1.0 to 4.0 Hz). Hanks (1975) used radial and transverse displacement records to show a strong influence of dispersed surface waves on motions measured at several accelerograph stations during the February 9, 1971 San Fernando, California earthquake.

Despite the potential importance of surface wave contributions to free-field earthquake motions, there have been very few studies of the response of structures to such waves. Our prior report (Werner et al., 1977) treated the response of this same bridge structure to arbitrarily incident SH-waves which, as shown in Appendix A, is equivalent to considering Love waves in a layered medium, provided the angle of vertical incidence of the SH-waves is properly chosen. For Rayleigh waves, however, the few studies that have been carried out have been based only on simple structural elements such as a single, rigid rectangular foundation (Luco and Wong, 1977) or a single spring/mass oscillator on a rigid foundation (Simpson, 1978; Wolf and Obernhuber, 1979). Nevertheless, the studies have provided insights into such Rayleigh wave effects

as (1) the rocking motions generated by Rayleigh waves that are normally incident to one of the sides of a rectangular foundation and (2) the fully three-dimensional response characteristics generated by obliquely incident Rayleigh waves. The potential importance of such response characteristics underscores the need to study Rayleigh wave effects further, using a more refined model of a three-dimensional, deformable structure of extended length. It is toward this end that the calculations described in this chapter are directed.

3.2 EXCITATION

The free field excitation induced along the ground surface by a horizontally propagating harmonic Rayleigh wave impinging on the structure with an angle θ_H (Fig. 3-1) is expressed as

$$u(x,y,0) = R_H \cos\theta_H \exp\left\{i\omega\left[t - \left(\frac{x\cos\theta_H + y\sin\theta_H}{V_R}\right)\right]\right\}$$

$$v(x,y,0) = R_H \sin\theta_H \exp\left\{i\omega\left[t - \left(\frac{x\cos\theta_H + y\sin\theta_H}{V_R}\right)\right]\right\} \qquad (3\text{-}1)$$

$$w(x,y,0) = iR_V \exp\left\{i\omega\left[t - \left(\frac{x\cos\theta_H + y\sin\theta_H}{V_R}\right)\right]\right\}$$

where

u,v,w = Free field displacements along the x, y, and z axes, respectively, at a location on the ground surface ($z = 0$) with coordinates x and y

ω = Circular frequency of excitation

R_H, R_V = Amplitudes of horizontal and vertical components of motion and the ground surface

V_R = Rayleigh wave velocity

In CAST-1, u, v, and w are determined in three separate steps. First, the Rayleigh wave velocity, V_R, is determined by applying a Newton-Raphson iterative technique to the following cubic equation (Knopoff, 1952).

$$\left(2 - \frac{V_R^2}{V_S^2}\right)^2 = 4\left(1 - \frac{V_R^2}{V_P^2}\right)^{1/2}\left(1 - \frac{V_R^2}{V_S^2}\right)^{1/2} \tag{3-2}$$

where V_P and V_S are the P-wave velocity and the shear wave velocity, respectively. Since Equation 3-2 involves ratios of the wave velocities, V_R is seen to be a function only of the Poisson's ratio of the soil medium. Next, the computed value of V_R is used to obtain R_H and R_V from the following expressions:

$$R_H = \left[\frac{2\left(\frac{V_R^2}{V_S^2} - 1\right)^{1/2}}{2 - \frac{V_R^2}{V_S^2}} - \left(\frac{V_R^2}{V_S^2} - 1\right)^{1/2}\right] A$$

$$R_V = \left[\frac{-2\left(\frac{V_R^2}{V_S^2} - 1\right)^{1/2}\left(\frac{V_R^2}{V_P^2} - 1\right)^{1/2}}{2 - \frac{V_R^2}{V_S^2}} - 1\right] A \tag{3-3}$$

where A is a function of the wave number (ω/V_R). For the present study, the Poisson's ratio is 1/3; therefore, Equations 3-2 and 3-3 yield $V_R = 0.9325\ V_S$ and $R_V = 1.565\ R_H$. Finally, these quantities are used in Equation 3-1 to define the free-field displacements that correspond to a particular excitation frequency ω and angle of incidence θ_H. It is noted that, for all values of ω and θ_H, the free-field excitations are normalized so that $R_H = 1.0$.

The nature of the resulting particle motions induced by the Rayleigh waves is illustrated in Figure 3-2. The motion of a particle along the ground surface follows an elliptic retrograde path in a vertical plane (Fig. 3-2a). This motion features a 90-deg phase difference between the peak horizontal and vertical components of motion (Eq. 3-1) and an aspect ratio of the elliptical path (i.e., the ratio of the peak vertical-to-horizontal displacement) that is a function of Poisson's ratio.* The corresponding spatial variation of the displacement of the overall ground surface is illustrated in Figure 3-2b.

3.3 RESULTS

As noted in Table 2-2 of Chapter 2, three different Rayleigh wave excitation cases are considered that correspond to angles of incidence of 90 deg, 0 deg, and 45 deg. Results from each of these cases are described in this section.

3.3.1 CASE 1: θ_H = 90 DEG

The first set of results ensues from the bridge response to Rayleigh waves that are propagating normal to the span of the bridge, or along its y-axis. The free field excitations for this case exhibit spatial variations as they propagate along the 70-ft length of each rigid foundation (Fig. 3-3a).

The most significant response characteristics for this case are depicted by the amplitude vs. dimensionless frequency plots given in Figures 3-3b to 3-3d and by the amplitudes and phase angles tabulated in Table 3-1. These results show that the most significant response components for this case are the displacements along the y- and z-axes, although displacements along the x-axis are also generated over a narrow frequency band. As noted in Table 2-3, the dimensionless frequency parameter used in the representation of these components is R_{Ly}--the ratio of the foundation length in the y-direction (70 ft) to the wavelength of the incident Rayleigh Wave.

---

*As previously noted, a Poisson's ratio of 1/3 leads to a peak vertical displacement that is 1.565 times the peak horizontal displacement. This is illustrated in Fig. 3-2a.

The results shown in Figure 3-3 and Table 3-1 show two principal types of response. The first corresponds to resonant responses (see Sec. 2-3) and is denoted by the prominent peak values of the y-displacements at $R_{Ly} = 0.58$ ($f = 3.9$ Hz) and the z-displacement at $R_{Ly} = 0.42$ ($f = 2.8$ Hz). The y-displacement peak corresponds to a resonance involving rocking of the bridge in the y-z plane, whereas the z-displacement peak (which occurs only at the midspan of the road deck) represents a resonance that involves bending of the road deck in the x-z plane (Fig. 3-4).* Comparisons with Figure 2-6 show that the resonant frequency at which the y-displacement peak occurs is much smaller than the frequency of the corresponding fixed-base mode (3.9 Hz vs. 14.2 Hz of Mode 1, Fig. 2-6b); this indicates that the underlying soil medium has an important effect on this particular resonant response. In contrast, the resonant frequency at which the z-displacement peak occurs is only slightly smaller than that of the corresponding fixed base mode (2.8 Hz vs. 3.2 Hz of Mode 1, Fig. 2-6a); therefore, the soil medium has only a small influence on this particular resonant response that is dominated by bending of the road deck in the x-z plane.

The second principal type of response observed for Case 1 occurs at higher values of R_{Ly}, which correspond to incident wavelengths that are short relative to the foundation length. For such conditions, Figure 3-3 shows that the bridge and foundation displacement amplitudes become small relative to the amplitudes of the Rayleigh wave excitation (given as the zero-frequency amplitude of motion). This phenomenon, which also has been observed in prior studies involving body wave excitation (e.g., Newmark et al., 1977), can be attributed to a self-canceling effect whereby the net loadings applied by short-wavelength excitations impinging on a rigid foundation are reduced; this, in turn, reduces the ability of the excitations to drive the foundation elements and to thereby induce significant structural responses (see discussion by Werner et al., 1977). However, in a more realistic setting with flexible rather than rigid foundations, this effect is expected to be less pronounced than suggested by this analysis.

---

*The resonance at 2.8 Hz also involves x-displacements of the two foundations that are of opposite phase (Table 3-1). These x-displacements, while prominent in Figure 3-4a, are much smaller than the z-displacements of the midspan of the road deck that occur at this frequency.

3.3.2 CASE 2: θ_H = 0 DEG

The second set of bridge response results is induced by Rayleigh waves that propagate parallel to the span of the bridge, or along its x-axis (Fig. 3-5a). For this case, the excitations applied at the two foundations differ in phase in a manner dependent on the ratio of the bridge span length (120 ft) to the wavelength of the incident Rayleigh wave. This ratio is used as the dimensionless frequency parameter for Case 2 and is denoted as R_{Lx} (see Table 2-3).

The significant bridge response components for this case are the displacements along the x- and z-axes, whose frequency-dependent amplitudes and phase angles are given in Figures 3-5b and 3-5c and in Table 3-2. These data show resonant response characteristics as well as important characteristics related directly to the phasing of the Rayleigh wave excitations.

3.3.2.1 Resonant Response Characteristics

Four sets of deformed shape plots that depict resonant responses of the bridge for this case are shown in Figure 3-6. The first of these plots (Fig. 3-6a) occurs at R_{Lx} = 0.72 (f = 2.8 Hz) and corresponds to the fundamental bending mode of the road deck in the x-z plane. This excitation frequency is identical to that observed for this same resonant response in Case 1 (θ_H = 90 deg). As in Case 1, this frequency is only slightly smaller than that of the corresponding fixed base mode (3.2 Hz for Mode 1 of Fig. 2-6a); since this resonant response primarily involves bending of the road deck, it is therefore not strongly influenced by the underlying soil medium. The same observations apply to the resonant responses shown in Figure 3-6c and 3-6d, which correspond to higher bending modes of the road deck and are analogous to the fixed-base Modes 3 and 4 of Figure 2-6a.* Only the resonant response

*It is noted that the resonant response shown in Figure 3-6d has a frequency (18.6 Hz) that is slightly higher than that of the corresponding fixed-base mode (Mode 4 of Fig. 2-6a, which has a frequency of 18.2 Hz) despite the presence of the soil medium. This may be caused by the relative phasing of the foundation rotations and translations induced by three-dimensional soil/structure interaction and the phased input motions. For example, the foundation rotations could be phased so as to restrain the end walls from deforming in a manner consistent with the deformations experienced by the road deck in the course of this resonant response. This, in turn, could effectively "stiffen" the bridge and increase its resonant frequency to a value greater than that occurring in its fixed-base condition.

shown in Figure 3-6b, which involves sidesway of the bridge coupled with bending of the road deck, is more strongly influenced by the soil medium. The excitation frequency for this response (f = 3.0 Hz, corresponding to R_{LX} = 0.78) is seen to fall below that of the corresponding fixed-base sidesway mode of the bridge (Mode 2 of Fig. 2-6a, which has a frequency of 5.1 Hz). Of course, this particular comparison may be influenced not only by the soil medium, but also by the fact that this resonant response involves coupled sidesway and road-deck bending, rather than pure sidesway motion.

3.3.2.2 Phased-Input-Induced Response Characteristics

In this subsection, two examples of the bridge response to phased Rayleigh wave excitations are presented. The first corresponds to the bridge response that occurs when the excitations applied at the two foundations are identical in amplitude and phase, while the second deals with the bridge response that occurs when these excitations are of identical amplitude and opposite phase. The markedly contrasting bridge response that results from each example illustrates the importance of the phasing of the Rayleigh wave excitations applied at the two foundations.

a. Equal-Amplitude/Equal-Phase Excitations

Excitations that are of equal amplitude and equal phase at the two foundations occur whenever the bridge span length is an integer multiple of the wavelength of the incident Rayleigh wave, i.e., when R_{LX} = 1.0, 2.0, 3.0, etc. Time-dependent deformed shapes provided for such excitations (Fig. 3-7) show that the bridge response at lower frequencies in this group (e.g., R_{LX} = 1.0) is comprised of two distinct patterns that occur at different times--one involving bending of the road deck that is nearly symmetric about its midspan and the other involving an essentially pure sidesway response. These marked changes in the bridge response during each cycle are a consequence of the 90-deg phase difference between the horizontal and vertical components of Rayleigh wave motion; i.e., the nearly symmetric bending of the road deck is caused by the identical *vertical* free-field excitations at the two foundations, while the sidesway response is caused by the identical *horizontal* excitations that occur about one-quarter of a cycle later.

As R_{Lx} increases within this group (corresponding to higher excitation frequencies), the above patterns of response become less distinct and the deformed shapes more complex (contrast, for example, the deformed shapes for R_{Lx} = 1.0 and 3.0 in Fig. 3-7). This is a direct consequence of the increased influence of wave diffraction and scattering and the higher modes of vibration that become important at these higher excitation frequencies.

b. Equal-Amplitude/Opposite-Phase Excitations

Excitations that are of equal amplitude and opposite phase at the two foundations occur whenever the ratio of the bridge span length to the ratio of the incident Rayleigh wave is such that R_{Lx} = 0.5, 1.5, 2.5, etc. For lower excitation frequencies within this group (R_{Lx} = 0.5), time-dependent deformed shapes show two distinct patterns of bridge response that differ markedly from those described above for the in-phase excitations (Fig. 3-8). One such pattern corresponds to symmetric bending of the road deck in the x-z plane and is a consequence of the *horizontal* excitations of equal amplitude and opposite phase that are applied at the two foundations. The second pattern, which is 90 deg out of phase with the first pattern for R_{Lx} = 0.5, involves nearly rigid body vertical motions of the bridge that are antisymmetric about its midspan; this is induced by *vertical* excitations of equal amplitude and opposite phase at the two foundations.

As R_{Lx} increases within this group, the above patterns of response become less distinct and the deformed shapes more complex--a trend also noted for the in-phase excitations. Again, this is a consequence of

---

*Note that the deformed shapes for R_{Lx} = 2.5 are not shown in Figure 3-8. This is because this particular value of R_{Lx} corresponds to a frequency (9.7 Hz) that is quite close to a resonant frequency indicated in Section 3.3.2.1 for this bridge/soil system (9.2 Hz, which corresponds to R_{Lx} = 2.37). Therefore, the response for R_{Lx} = 2.5 is much closer to the resonant response shown in Figure 3-6c than to the general pattern of response shown in Figure 3-8 for Rayleigh wave excitations of equal amplitude and opposite phase at the two foundations. Clearly, if this soil medium had a different Rayleigh wave velocity, or if the bridge had a different length, the response results for R_{Lx} = 2.5 would not have been as strongly influenced by this resonance phenomena and would have fit more closely within the response patterns shown in Figure 3-8.

the increased effects of wave diffraction and scattering and higher vibration modes, and can be seen for this out-of-phase excitation case by comparing the response characteristics for, say, $R_{Lx} = 0.5$ and 3.5 in Figure 3-8 and Table 3-2. Also, it is again noted that the marked differences between these response characteristics and those induced by the in-phase excitations clearly illustrate the importance of the phasing of the Rayleigh wave excitations applied at the two foundations.

3.3.3 CASE 3: $\theta_H = 45$ DEG

3.3.3.1 Excitations

The third and final case to be presented corresponds to Rayleigh waves that propagate at an angle of 45 deg with the x-y plane of the bridge (Fig. 3-9). When the wavelengths of such waves are projected along the x- and y-axes of the bridge, they are increased by a factor of $\frac{1}{\cos 45 \text{ deg}}$, or $\sqrt{2}$. This indicates that for a given excitation frequency, this oblique angle of incidence results in a change in the phasing of the excitations applied to the two foundations relative to that of Cases 1 and 2; this factor is of primary importance, as discussed subsequently. Also, the projections of the horizontal particle displacement amplitudes are reduced by the same factor. These effects on the projected particle motions are illustrated in Figure 3-9.

3.3.3.2 General Response Characteristics

The significant bridge response characteristics for this case are depicted in Figures 3-10a to 3-10d as amplitude vs. dimensionless frequency plots for displacements along the x-, y-, and z-axes and rotations about the z-axis; corresponding peak amplitudes and phase angles for these response components at selected frequencies are given in Table 3-3. In this, it is noted that both R_{Lx} and R_{Ly} are used as the dimensionless frequency parameters for this case.

Figures 3-10a to 3-10d show that, in contrast to the excitation cases for θ_H = 0 deg and 90 deg, the bridge response is now fully three dimensional. Characteristics of the three-dimensional response indicated by these figures and the associated phase angles (Table 3-3) are summarized as follows:

a. The bridge displacement amplitudes at moderate and higher frequencies fall well below those of the incident Rayleigh waves (Figs. 3-10a to 3-10c).

b. The frequency-dependent x-displacements and y-displacements differ markedly from those of Case 2 (θ_H = 0 deg) and Case 1 (θ_H = 90 deg), respectively. These differences are attributable to the oblique angle of incidence of the Rayleigh wave for Case 3, which alters the phasing of the excitations applied at the two foundations. The z-displacements are still dominated by a prominent resonant response peak at the same frequency as for Cases 1 and 2 (Figs. 3-10a to 3-10c).

c. At certain frequencies, the z-rotations of the foundations are markedly different from those of the road deck, indicating that prominent torsional deformations are induced in the end walls by the Case 3 excitations (Fig. 3-10d).

The following paragraphs provide more detailed descriptions of the resonant response characteristics of the bridge and the response characteristics induced by the phasing of these obliquely incident Rayleigh wave excitations.

3.3.3.3 Resonant Response Characteristics

As noted above, the oblique angle of incidence of the Rayleigh waves for Case 3 will change the phasing of the excitations applied to the two foundations, as compared to Cases 1 and 2 for which the Rayleigh waves

propagate along principal planes of the bridge. The extent to which these changes in phasing affect the occurrence of the resonant responses is summarized in Table 3-3. Of the various resonant responses noted for Cases 1 and 2, this table shows that only the response involving beam bending of the road deck in the x-z plane (which occurs at a frequency of 2.8 Hz) is also strongly present in Case 3. The resonant response associated with sidesway of the bridge in the x-direction is only faintly apparent in Case 3, with a peak x-displacement amplitude that is reduced markedly relative to that of Case 2 (Fig. 3-11). The resonant response that involved symmetric rocking in the y-direction at a frequency of $R_{Ly} = 0.58$ and was induced by the Case 1 ($\theta_H = 90$ deg) excitations does not occur at this frequency when $\theta_H = 45$ deg (Fig. 3-10b). This is because the resulting phase differences that occur between the excitations applied at the two foundations destroy the symmetry of the foundation driving forces and moments in the y-z plane.

3.3.3.4 Phased-Input-Induced Response Characteristics

Figure 3-10 and Table 3-3 indicate two main ways in which the phasing of the Rayleigh wave excitations with $\theta_H = 45$ deg affect the response of this bridge/soil system. The first, as indicated previously in Section 3.3.3.2, is the reduced amplitudes of bridge displacement along the x-, y-, and z-axes at moderate and higher excitation frequencies, as compared to the corresponding components of the free-field motion. This reduction was also observed in Case 1 but not in Case 2; it is undoubtedly related to the fact that a component of the excitation projected along the y-axis is now impinging along the length of the rigid foundations, leading to the self-canceling effects previously noted in Section 3.3.1 (Fig. 3-9).

The second phased-input-induced response characteristic corresponds to the manner in which the bridge displacements are affected by the phasing of the free-field excitations at the two foundations. To illustrate such effects, two sets of bridge response results--which correspond to two different phasings of the free-field excitations--are described below.

a. Equal-Amplitude/Equal-Phase Excitations

The first set of results corresponds to Rayleigh wave excitations that are of equal amplitude and equal phase at the two foundations; such excitations occur when $R_{Lx} = \sqrt{2}$, $2\sqrt{2}$, etc.* Time-dependent deformed shapes of the bridge response to such excitations are given in Figure 3-12, and the corresponding amplitudes and phase angles are provided in Table 3-3.

When $R_{Lx} = \sqrt{2}$, the following trends are observed from Figure 3-12 and Table 3-3:

- The y-components of displacement are largest in amplitude, are nearly symmetric about the midspan of the bridge, and have the largest amplitude at that point (Table 3-3).
- The y-components of foundation displacement are about 180 deg out of phase with the z-components and are about 90 deg out of phase with the x-components (Table 3-3). These phase differences are unlike those that exist among the various components of free-field motion; they are caused by foundation/soil interaction effects (wave diffraction and scattering at the foundations) and the effects of the overlying structure.
- The y- and z-components of displacement at the midspan of the road deck are essentially in phase with one another and are about 90 deg out of phase with the x-components of displacement along the road deck (Table 3-3). As a result, two distinct

*R_{Lx} is the ratio of the bridge span length to the wavelength of the incident wave *along its propagation path*. Projecting along the span of the bridge results in an increase in the *effective* wavelength that propagates along the x-axis by a factor of $\sqrt{2}$, or $\cos^{-1}$ 45 deg (Fig. 3-9). Therefore, when θ_H = 45 deg, dimensionless frequencies of $R_{Lx} = \sqrt{2}$, $2\sqrt{2}$, etc., correspond to excitations of equal amplitude and equal phase at the two foundations; similarly, dimensionless frequencies of $R_{Lx} = 0.5\sqrt{2}$, $2.5\sqrt{2}$, etc., correspond to excitations of equal amplitude and opposite phase at the two foundations.

deformed-shape configurations occur during a single response cycle. The first corresponds to maximum values of the y- and z-displacements at the midspan of the road deck, while the second, which occurs about one-quarter of a cycle later, involves sidesway of the bridge in the x-direction (Fig. 3-12a).

- The end walls are undergoing torsional deformations, as indicated by the differences that exist between the rotations about the z-axis of the foundations and the tops of the end walls. Peak values of the frequency-dependent rotations at the foundations occur when $R_{Lx} = \sqrt{2}$ (Fig. 3-10d, Table 3-3).

When $R_{Lx} = 2\sqrt{2}$, the bridge response characteristics differ from those noted above for $R_{Lx} = \sqrt{2}$. The differences are summarized as follows:

- The displacements along the y-axis are much smaller but are still symmetric about the midspan of the bridge (Table 3-3).

- The phase relationships between the various components of motion at the various locations along the bridge are much different than those existing at $R_{Lx} = \sqrt{2}$ (Table 3-3). As a result, the deformed shapes are now much different, with displacements of the foundations in the y- and z-directions being most prominent (Fig. 3-12b).

- The rotations about the z-axis at the foundations and the tops of the end walls are smaller than those corresponding to $R_{Lx} = \sqrt{2}$ (Fig. 3-10d, Table 3-3).

b. Equal-Amplitude/Opposite-Phase Excitations

The second set of deformed shape plots and tabulated amplitudes and phase angles correspond to Rayleigh wave excitations that are of equal amplitude and opposite phase at the two foundations; such excitations occur when $R_{Lx} = 0.5\sqrt{2}$, $1.5\sqrt{2}$, $2.5\sqrt{2}$, etc. Time-dependent deformed shape plots for $R_{Lx} = 1.5\sqrt{2}$ and $2.5\sqrt{2}$ are given in Figure 3-13 and, together with the amplitudes and phase angles from Table 3-3, show that the bridge response differs markedly from that induced by the equal-amplitude/equal-phase excitations.* The characteristics of this response are as follows:

- The y-components of displacement are antisymmetric about the midspan of the road deck and are largest at the tops of the two end walls. These components of displacement are much larger for $R_{Lx} = 0.5\sqrt{2}$ and $1.5\sqrt{2}$ than for $R_{Lx} = 2.5\sqrt{2}$ (Table 3-3).

- For each frequency, the end walls are rocking in opposite directions about the x-axis at a given instant of time (e.g., see Fig. 3-13a). This leads to torsional deformations of the road deck.

- The phase relationships that exist between the various components of motion along the bridge vary from one frequency in this group to the next, because of the differing effects of wave scattering and diffraction at the various frequencies (Table 3-3).

*The deformed shape for $R_{Lx} = \sqrt{2}/2$ (0.707) is very similar to that for the resonant response at $R_{Lx} = 0.72$ shown in Figure 3-11 and is therefore not included in Figure 3-13.

- When $R_{Lx} = 0.5\sqrt{2}$, the rotations about the z-axis are larger at the tops of the end walls than at the foundations; this indicates that the end walls are undergoing torsional deformations. In contrast, the rotations that occur at these locations when $R_{Lx} = 1.5\sqrt{2}$ and $2.5\sqrt{2}$ exhibit much smaller differences; therefore, even though these rotations are somewhat out of phase, the torsional deformations that occur in the end walls are much smaller than at low frequencies. It is noted that peak values of the frequency-dependent rotations within the road deck occur at $R_{Lx} = 0.5\sqrt{2}$ and $1.5\sqrt{2}$ (Fig. 3-10d, Table 3-3).

TABLE 3-1. BRIDGE RESPONSE TO INCIDENT RAYLEIGH WAVES WITH θ_H = 90 DEG[1] (CASE 1)

Description	Excitation Frequency[2]		Component of Response	Upstream Foundation		Downstream Foundation		Top of Upstream End Wall		Top of Downstream End Wall		Midspan of Road Deck	
	R_{Ly}	f, Hz		Amplitude	Phase Angle, rad	Amplitude	Phase Angle, rad	Amplitude	Phase Angle, rad	Amplitude	Phase Angle, rad	Amplitude	Phase Angle, rad
Resonance with Fundamental Beam Bending Mode of Road Deck in x-z Plane	0.42	2.80	Displacement along x-axis	1.256	-0.986π	1.250	0.014π	0.108	0.155π	0.108	1.155π	Small	--
			Displacement along y-axis	1.032	-0.038π	1.032	-0.038π	2.224	-0.024π	2.224	-0.024π	2.318	-0.024π
			Displacement along z-axis	1.586	0.231π	1.586	0.231π	1.616	0.229π	1.616	0.229π	20.786	0.133π
Resonance with Fundamental Rocking Mode of Bridge in y-direction	0.58	3.89	Displacement along y-axis	1.283	-0.207π	1.283	-0.207π	2.732	-0.134π	2.732	-0.134π	2.963	-0.134π
			Displacement along z-axis	0.605	0.569π	0.605	0.569π	0.603	0.569π	0.603	0.569π	1.207	-0.411π

AA10278

Note: (1) Incident Rayleigh wave motions normalized so that horizontal component of motion has unit amplitude and zero phase angle at upstream foundation, which is origin of coordinate system for this analysis. Vertical component of motion has amplitude that is 1.565 times amplitude of horizontal component (for soil with Poisson's ratio = 1/3) and is phased to be 90 deg ahead of horizontal component of Rayleigh wave motion.

(2) R_{Ly} = Ratio of foundation length (70 ft) to wavelength of incident Rayleigh wave.

f = Excitation frequency (Hz)

TABLE 3-2. BRIDGE RESPONSE TO INCIDENT RAYLEIGH WAVES WITH θ_H = 0 DEG(1) (CASE 2)

Description	Excitation Frequency(2)		Component of Response	Upstream Foundation		Downstream Foundation		Top of Upstream End Wall		Top of Downstream End Wall		Midspan of Road Deck	
	R_{Lx}	f, Hz		Amplitude	Phase Angle, rad	Amplitude	Phase Angle, rad	Amplitude	Phase Angle, rad	Amplitude	Phase Angle, rad	Amplitude	Phase Angle, rad
Resonance with Bridge Response Modes in x-z Plane	0.72	2.80	Displacement along x-axis	1.475	-0.428π	3.278	-1.700π	5.053	0.171π	4.796	0.155π	4.949	0.163π
			Displacement along z-axis	3.444	0.369π	1.385	-1.436π	3.495	0.369π	1.430	-1.442π	35.265	0.407π
	0.78	3.03	Displacement along x-axis	1.880	-0.360π	2.815	-2.317π	15.292	-0.313π	15.127	-0.316π	15.301	-0.315π
			Displacement along z-axis	1.047	0.342π	0.877	-0.798π	1.055	0.337π	0.866	-0.788π	15.584	-0.114π
	2.37(3)	9.20	Displacement along x-axis	0.729	-1.674π	0.921	-4.967π	0.569	-3.035π	0.636	-1.008π	0.637	-1.021π
			Displacement along z-axis	0.966	0.054π	0.822	-3.980π	1.025	-0.051π	0.786	-3.977π	0.239	-1.134π
	4.77	18.55	Displacement along x-axis	0.905	-1.617π	0.310	-9.957π	0.133	-6.434π	0.152	-0.705π	0.166	-0.579π
			Displacement along z-axis	0.559	-0.194π	1.442	-9.028π	0.650	-0.158π	1.412	-9.033π	4.803	-6.534π
Response to Excitations of Equal Amplitude and Phase at the Two Foundations	1.0	3.89	Displacement along x-axis	0.612	-1.775π	0.307	-2.099π	2.530	-0.923π	2.525	-0.929π	2.553	-0.926π
			Displacement along z-axis	1.556	0.477π	1.499	-1.469π	1.554	0.476π	1.495	-1.468π	3.038	-0.477π
	2.0	7.77	Displacement along x-axis	1.017	-1.969π	0.793	-4.047π	0.350	-2.938π	0.355	-0.952π	0.371	-0.945π
			Displacement along z-axis	1.915	0.404π	1.546	-3.651π	1.929	0.405π	1.559	-3.653π	0.945	-0.611π
	3.0	11.66	Displacement along x-axis	1.030	-1.985π	0.517	-5.913π	0.348	-2.915π	0.375	-0.926π	0.397	-0.921π
			Displacement along z-axis	1.103	0.129π	1.620	-5.710π	1.139	0.130π	1.641	-5.710π	0.763	-2.746π
Response to Excitations of Equal Amplitude and Opposite Phase at the Two Foundations	0.5	1.94	Displacement along x-axis	0.875	-0.005π	0.905	-0.981π	0.516	-0.514π	0.517	-0.526π	0.518	-0.520π
			Displacement along z-axis	1.636	0.502π	1.600	-0.514π	1.637	0.502π	1.601	-0.514π	2.051	1.001π
	1.5	5.83	Displacement along x axis	0.732	-1.937π	0.810	-2.961π	0.151	-2.485π	0.175	-0.626π	0.162	-0.561π
			Displacement along z axis	1.876	0.374π	1.859	-2.580π	1.892	0.374π	1.873	-2.580π	0.507	0.070π
	3.5 (3.48)	13.52	Displacement along x axis	1.468	-2.005π	0.599	-6.993π	0.072	-3.640π	0.173	-1.065π	0.097	-1.199π
			Displacement along z axis	1.022	0.264π	1.429	-6.681π	1.037	0.263π	1.455	-6.602π	0.618	-3.876π

AA9772

Note: (1) Incident Rayleigh wave motions normalized so that horizontal component of motion has unit amplitude and zero phase angle at upstream foundation, which is origin of coordinate system for this analysis. Vertical component of motion has amplitude that is 1.565 times amplitude of horizontal component (for soil with Poisson's ratio = 1/3) and is phased to be 90 deg ahead of horizontal component of Rayleigh wave motion.

(2) R_{Lx} = Ratio of bridge span length (120 ft) to wavelength of incident Rayleigh wave.
f = Excitation frequency (Hz).

(3) At R_{Lx} = 2.37, resonant response features beam bending of road deck in x-z plane that is approximately antisymmetric about its midspan. This resonance features vertical displacement amplitudes at intermediate node points of road deck (between end wall and midspan) that are large when compared to those at midspan; i.e., amplitudes at these node points range from 4.476 to 5.250 as compared to 0.239 at midspan. The amplitudes and phase angles of the displacements at these intermediate node points are not shown in this table, but are indicated in the deformed shape plot in Figure 3-6c.

TABLE 3-3. BRIDGE RESPONSE TO INCIDENT RAYLEIGH WAVES WITH θ_H = 45 DEG(1)

Description	Excitation Frequency(2) R_{Lx}	R_{Ly}	f, Hz	Component of Response	Upstream Foundation Amplitude	Upstream Foundation Phase Angle, rad	Downstream Foundation Amplitude	Downstream Foundation Phase Angle, rad	Top of Upstream End Wall Amplitude	Top of Upstream End Wall Phase Angle, rad	Top of Downstream End Wall Amplitude	Top of Downstream End Wall Phase Angle, rad	Midspan of Road Deck Amplitude	Midspan of Road Deck Phase Angle, rad
Resonance with Fundamental Beam Bending Mode of Road Deck in x-z Plane	0.720	0.420	2.80	Displacement along x-axis	0.900	-0.342π	0.828	-1.234π	1.151	-0.609π	1.240	-0.591π	1.202	-0.600π
				Displacement along y-axis	0.690	-0.023π	0.689	-1.048π	1.481	-0.011π	1.477	-1.034π	0.062	-1.531π
				Displacement along z-axis	2.007	0.498π	0.671	-0.549π	2.024	0.499π	0.660	-0.554π	11.583	-1.359π
				Rotation about z-axis ($\times 10^{-3}$)	1.350	0.535π	1.296	-0.548π	2.034	-1.025π	2.033	-1.020π	2.052	-1.023π
Resonance with Fundamental Sidesway Mode in x-z Plane	0.779	0.454	3.03	Displacement along x-axis	0.099	-1.346π	0.234	-1.251π	0.790	-0.986π	0.876	-0.976π	0.838	-0.981π
				Displacement along y-axis	0.708	-0.013π	0.686	-1.157π	1.568	-0.001π	1.528	-1.136π	0.346	-1.587π
				Displacement along z-axis	1.322	0.392π	1.270	-0.506π	1.331	0.391π	1.268	-0.504π	6.005	-1.864π
				Rotation about z-axis ($\times 10^{-3}$)	1.448	0.532π	1.389	-0.630π	2.083	-1.073π	2.084	-1.063π	2.102	-1.068π
Response to Applied Excitations of Equal Amplitude and Phase at the Two Foundations	1.414 ($\sqrt{2}$)	0.825	5.49	Displacement along x-axis	0.279	-1.858π	0.169	-1.992π	0.266	-0.941π	0.268	-0.957π	0.272	-0.949π
				Displacement along y-axis	1.217	-0.511π	1.179	-2.498π	2.168	-0.349π	2.150	-2.335π	2.551	-2.342π
				Displacement along z-axis	0.722	0.548π	0.726	-1.478π	0.723	0.548π	0.727	-1.478π	0.599	-2.447π
				Rotation about z-axis ($\times 10^{-3}$)	1.817	0.492π	1.927	-1.462π	0.416	-2.288π	0.467	-1.388π	0.068	-1.761π
	2.828 ($2\sqrt{2}$)	1.650	10.99	Displacement along x-axis	0.130	-2.964π	0.027	-3.148π	0.039	-1.953π	0.043	0.057π	0.044	0.052π
				Displacement along y-axis	0.335	-0.901π	0.334	-4.894π	0.060	-0.257π	0.071	-4.245π	0.151	-4.251π
				Displacement along z-axis	0.311	1.110π	0.259	-2.818π	0.318	1.110π	0.262	-2.818π	0.147	-3.854π
				Rotation about z-axis ($\times 10^{-3}$)	0.735	0.652π	0.760	-3.375π	0.096	-4.240π	0.092	-1.265π	0.007	-4.140π

Note: (1) Incident Rayleigh Wave motions normalized so that horizontal component of motion has unit amplitude and zero phase angle at upstream foundation, which is origin of coordinate system for this analysis. Vertical component of motion has amplitude that is 1.565 times amplitude of horizontal component (for soil with Poisson's ratio = 1/3) and is phased to be 90 deg ahead of horizontal component of Rayleigh Wave motion.

(2) R_{Lx} = Ratio of bridge span length (120 ft) to wavelength of incident Rayleigh wave.
R_{Ly} = Ratio of foundation length (70 ft) to wavelength of incident Rayleigh wave.
f = Excitation Frequency (Hz).

TABLE 3-3. (CONCLUDED)

Description	Excitation Frequency[2]			Component of Response	Upstream Foundation		Downstream Foundation		Top of Upstream End Wall		Top of Downstream End Wall		Midspan of Road Deck	
	R_{Lx}	R_{Ly}	f, Hz		Amplitude	Phase Angle, rad	Amplitude	Phase Angle, rad	Amplitude	Phase Angle, rad	Amplitude	Phase Angle, rad	Amplitude	Phase Angle, rad
Response to Applied Excitations of Equal Amplitude and Opposite Phase at the Two Foundations	0.707 $\left(\frac{\sqrt{2}}{2}\right)$	0.412	2.75	Displacement along x-axis	0.850	-0.216π	0.855	-1.101π	1.142	-0.581π	1.180	-0.564π	1.167	-0.572π
				Displacement along y-axis	0.689	-0.024π	0.690	-1.025π	1.467	-0.012π	1.467	-1.013π	0.006	-1.490π
				Displacement along z-axis	1.774	0.536π	0.957	-0.582π	1.785	0.538π	0.954	-0.586π	8.607	-1.213π
				Rotation about z-axis ($\times 10^{-3}$)	1.327	0.536π	1.275	-0.530π	2.018	-1.015π	2.017	-1.010π	2.035	-1.013π
	2.121 $(1.5\sqrt{2})$	1.237	8.24	Displacement along x-axis	0.071	-3.179π	0.146	-2.842π	0.055	-0.523π	0.059	-0.538π	0.059	-0.530π
				Displacement along y-axis	0.674	-0.504π	0.670	-3.505π	1.254	-0.233π	1.247	-3.232π	0.004	-3.601π
				Displacement along z-axis	0.198	0.386π	0.196	-2.609π	0.204	0.385π	0.202	-2.611π	0.023	-3.687π
				Rotation about z-axis ($\times 10^{-3}$)	1.603	0.552π	1.498	-2.448π	1.706	-3.235π	1.679	-1.231π	1.762	-3.233π
	3.536 $(2.5\sqrt{2})$	2.062	13.74	Displacement along x-axis	0.248	-3.015π	0.065	-4.056π	0.010	-2.495π	0.031	-0.090π	0.020	-0.178π
				Displacement along y-axis	0.091	-0.025π	0.088	-5.033π	0.168	0.432π	0.166	-4.567π	0.001	-5.123π
				Displacement along z-axis	0.245	1.336π	0.271	-3.692π	0.249	1.336π	0.276	-3.693π	0.096	-4.984π
				Rotation about z-axis ($\times 10^{-3}$)	0.439	1.274π	0.290	-3.687π	0.222	-4.572π	0.215	-0.564π	0.244	-4.567π

Note: (2) R_{Lx} = Ratio of bridge span length (120 ft) to wavelength of incident Rayleigh wave.
R_{Ly} = Ratio of foundation length (70 ft) to wavelength of incident Rayleigh wave.
f = Excitation frequency (Hz).

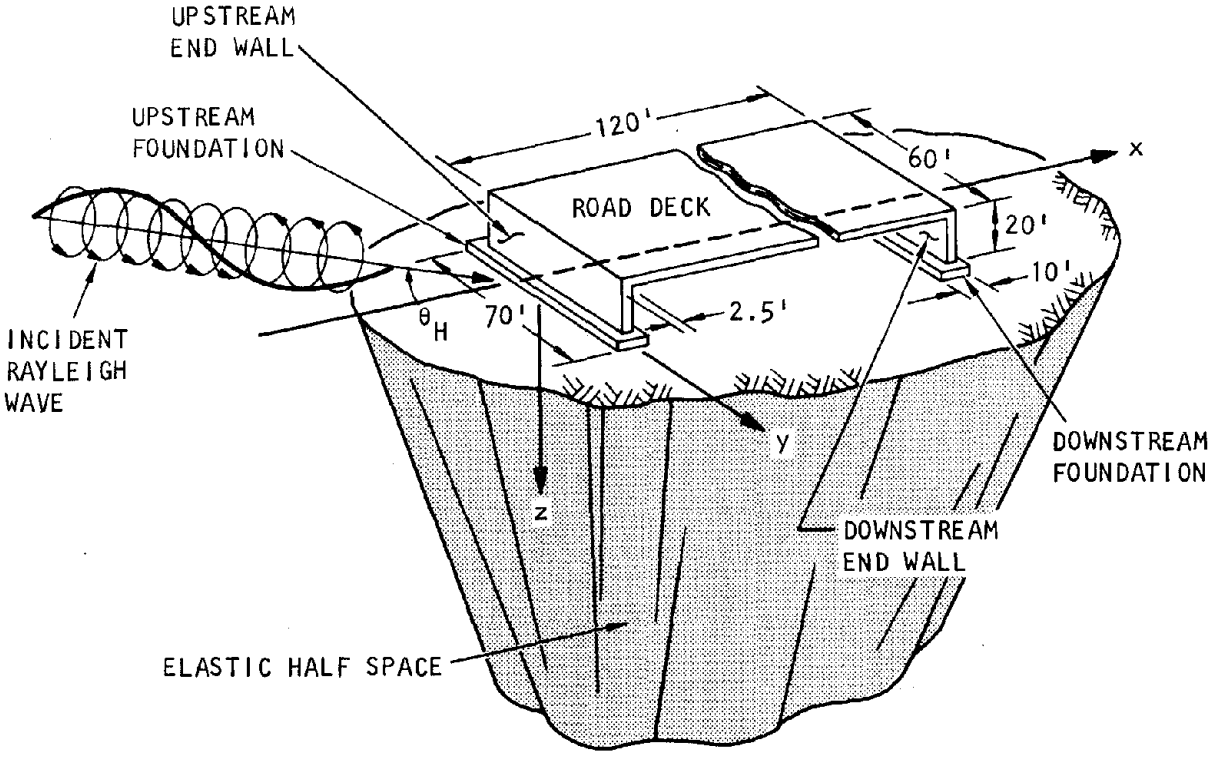

FIGURE 3-1. BRIDGE/SOIL SYSTEM SUBJECTED TO ARBITRARILY INCIDENT RAYLEIGH WAVES

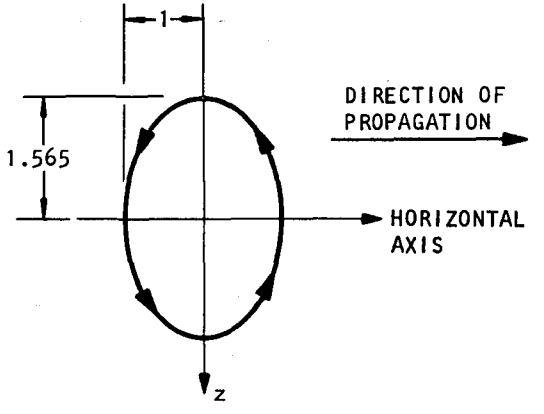

(a) Particle motion at a point

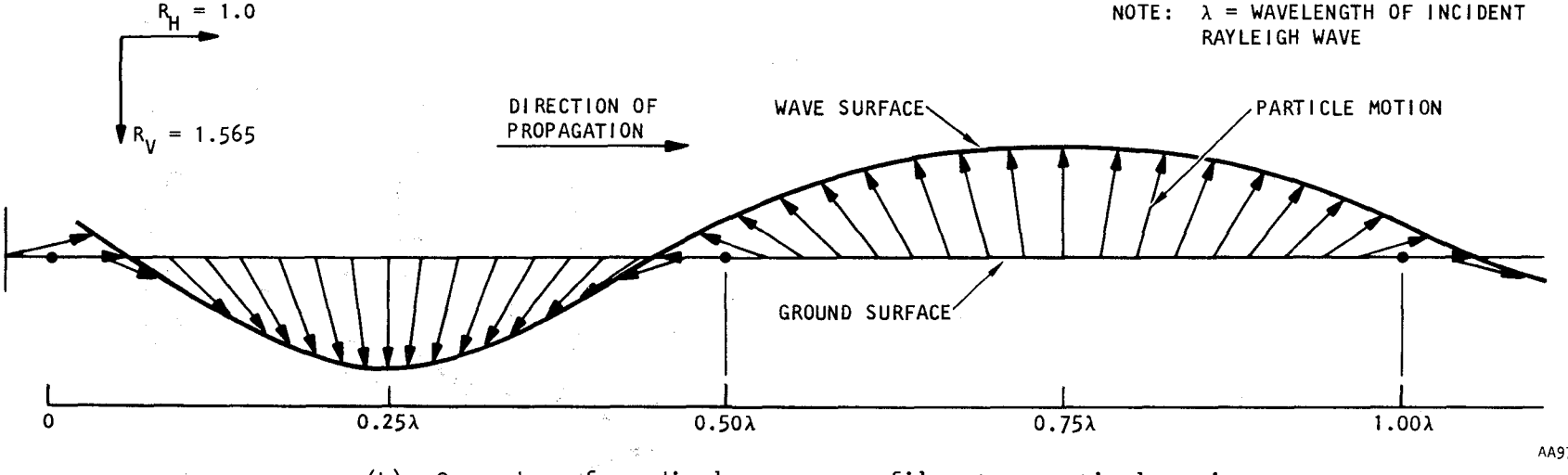

(b) Ground surface displacement profile at a particular time

FIGURE 3-2. RAYLEIGH WAVE MOTION AT SURFACE OF SOIL MEDIUM WITH POISSON'S RATIO = 1/3

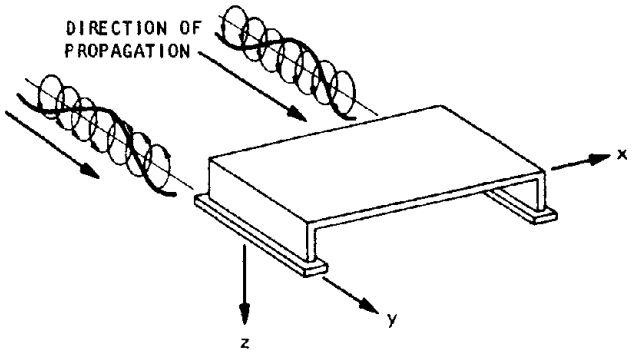

(a) Excitations from incident waves

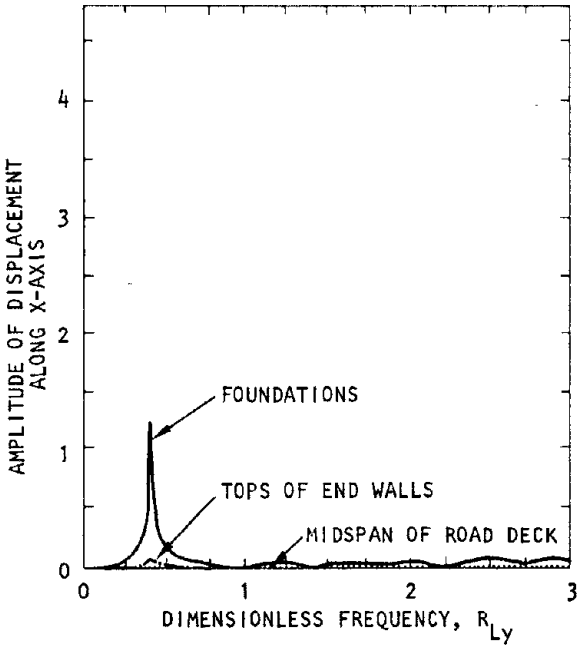

(b) Displacement along x-axis

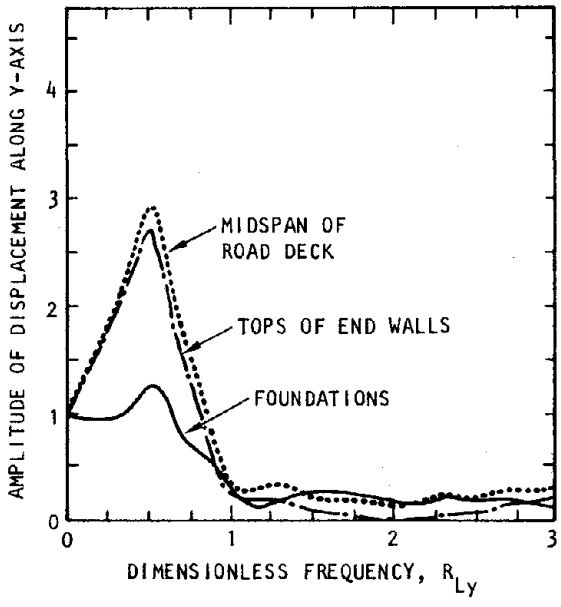

(c) Displacement along y-axis

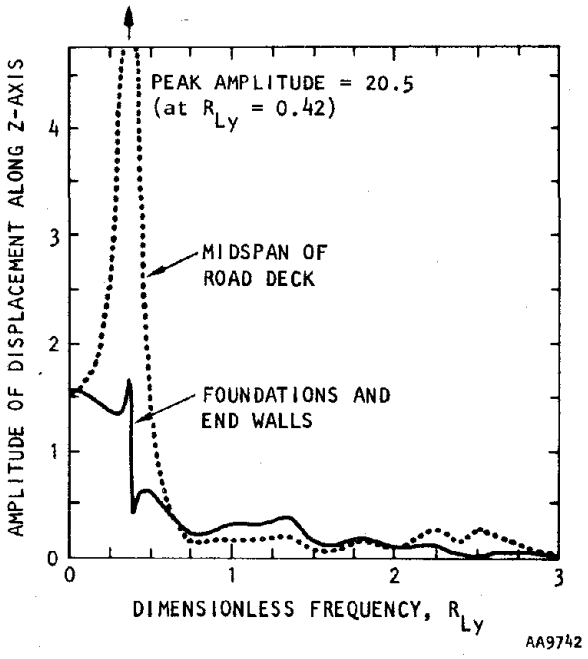

(d) Displacement along z-axis

FIGURE 3-3. FREQUENCY-DEPENDENT RESPONSE AMPLITUDES OF BRIDGE SUBJECTED TO INCIDENT RAYLEIGH WAVES WITH θ_H = 90 DEG

NOTE: DIFFERENT SCALE FOR FIGURES 3-4a AND 3-4b

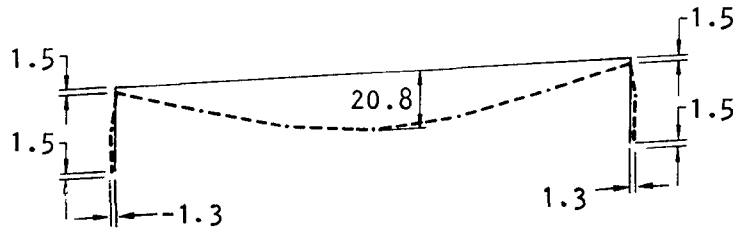

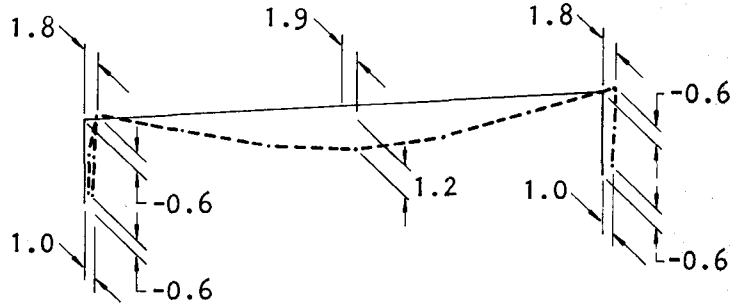

MAXIMUM Z-DISPLACEMENTS

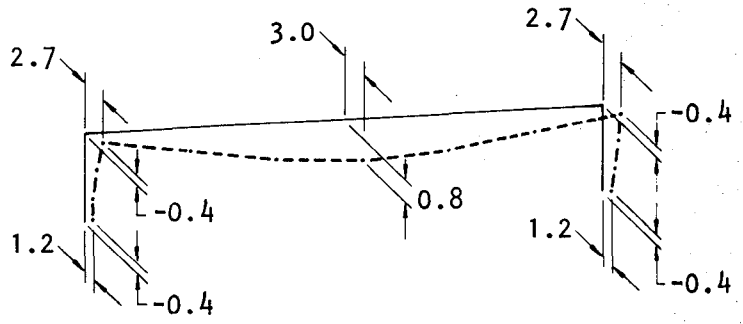

MAXIMUM Y-DISPLACEMENTS

(a) R_{Ly} = 0.42 (f = 2.8 Hz)

(b) R_{Ly} = 0.58 (f = 3.9 Hz)

FIGURE 3-4. CASE 1 (θ_H = 90 DEG): DEFORMED SHAPES OF BRIDGE AT TIMES OF PEAK RESONANT RESPONSE TO RAYLEIGH WAVE EXCITATIONS

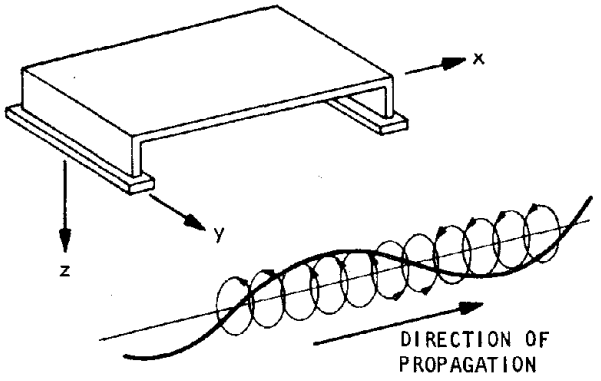

(a) Excitations from incident waves

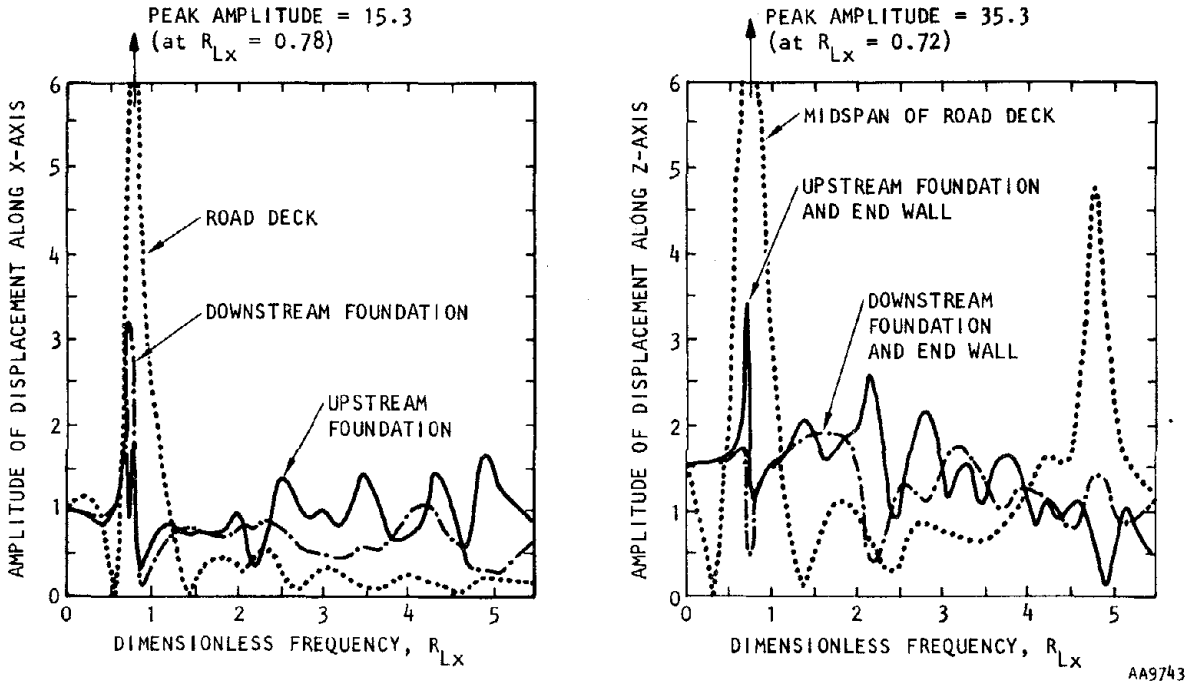

(b) Displacement along x-axis

(c) Displacement along z-axis

FIGURE 3-5. FREQUENCY-DEPENDENT RESPONSE AMPLITUDES OF BRIDGE SUBJECTED TO INCIDENT RAYLEIGH WAVES WITH θ_H = 0 DEG

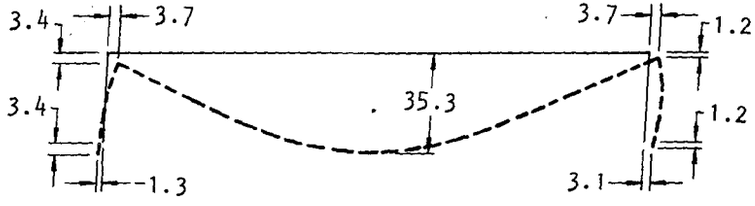

(a) R_{Lx} = 0.72 (f = 2.8 Hz)

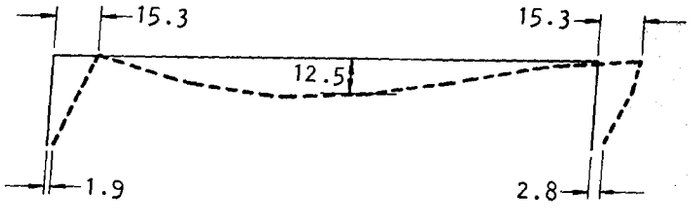

(b) R_{Lx} = 0.78 (f = 3.0 Hz)

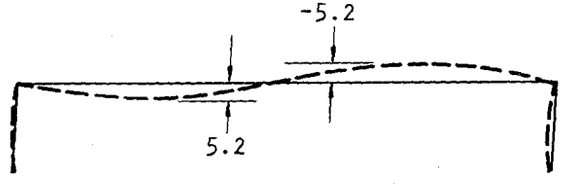

(c) R_{Lx} = 2.37 (f = 9.2 Hz)

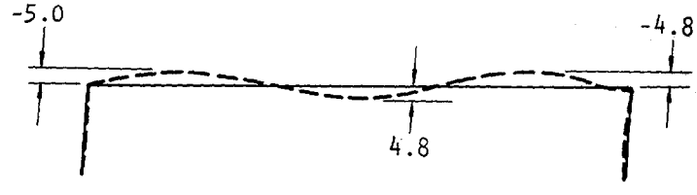

AA9739

(d) R_{Lx} = 4.77 (f = 18.6 Hz)

FIGURE 3-6. CASE 2 (θ_H = 0 DEG): DEFORMED SHAPES OF BRIDGE AT TIMES OF PEAK RESONANT RESPONSE TO RAYLEIGH WAVE EXCITATIONS

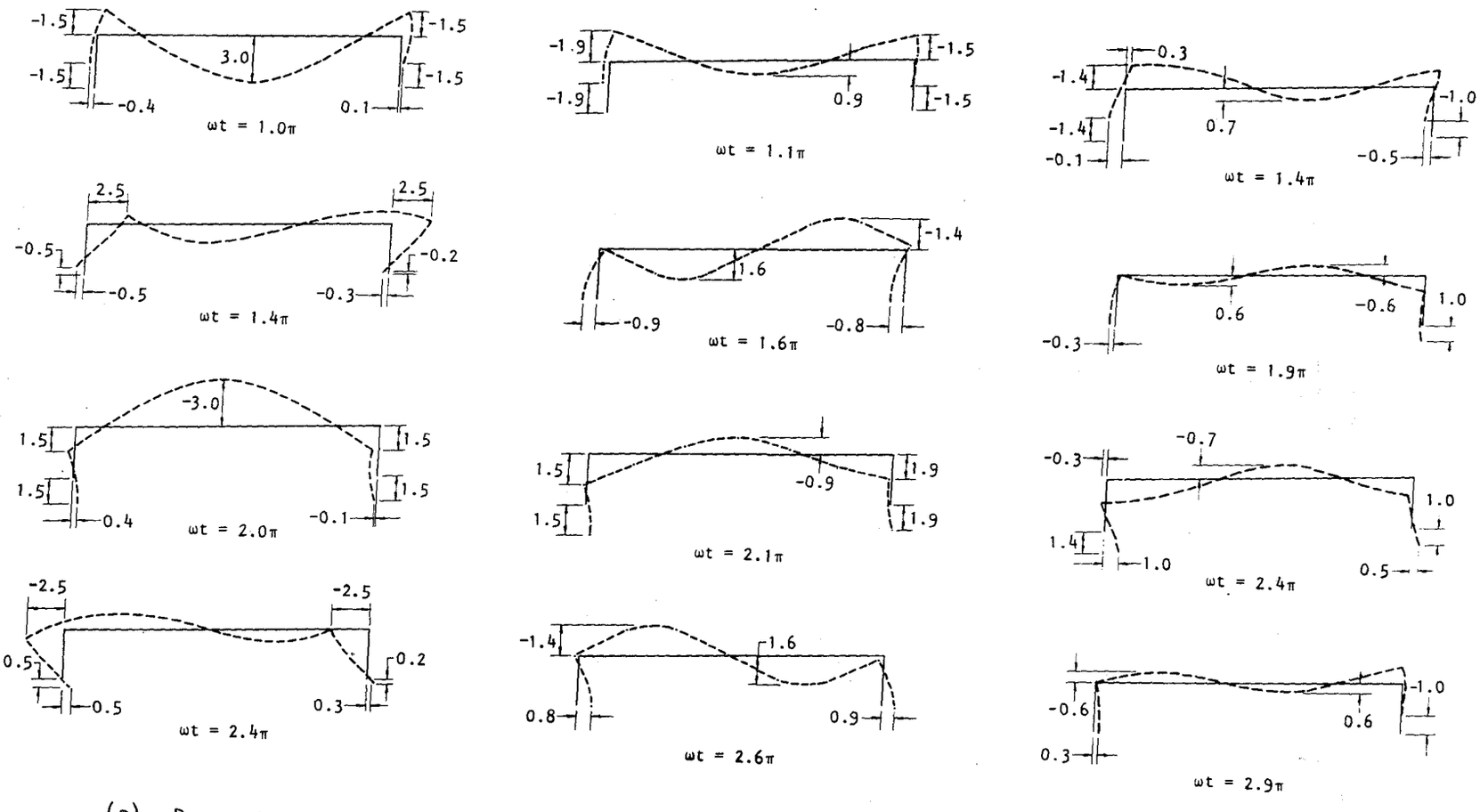

(a) R_{Lx} = 1.0

(b) R_{Lx} = 2.0

(c) R_{Lx} = 3.0

FIGURE 3-7. CASE 2 (θ_H = 0 DEG): BRIDGE RESPONSE TO APPLIED RAYLEIGH WAVE EXCITATIONS OF EQUAL AMPLITUDE AND EQUAL PHASE AT THE TWO FOUNDATIONS

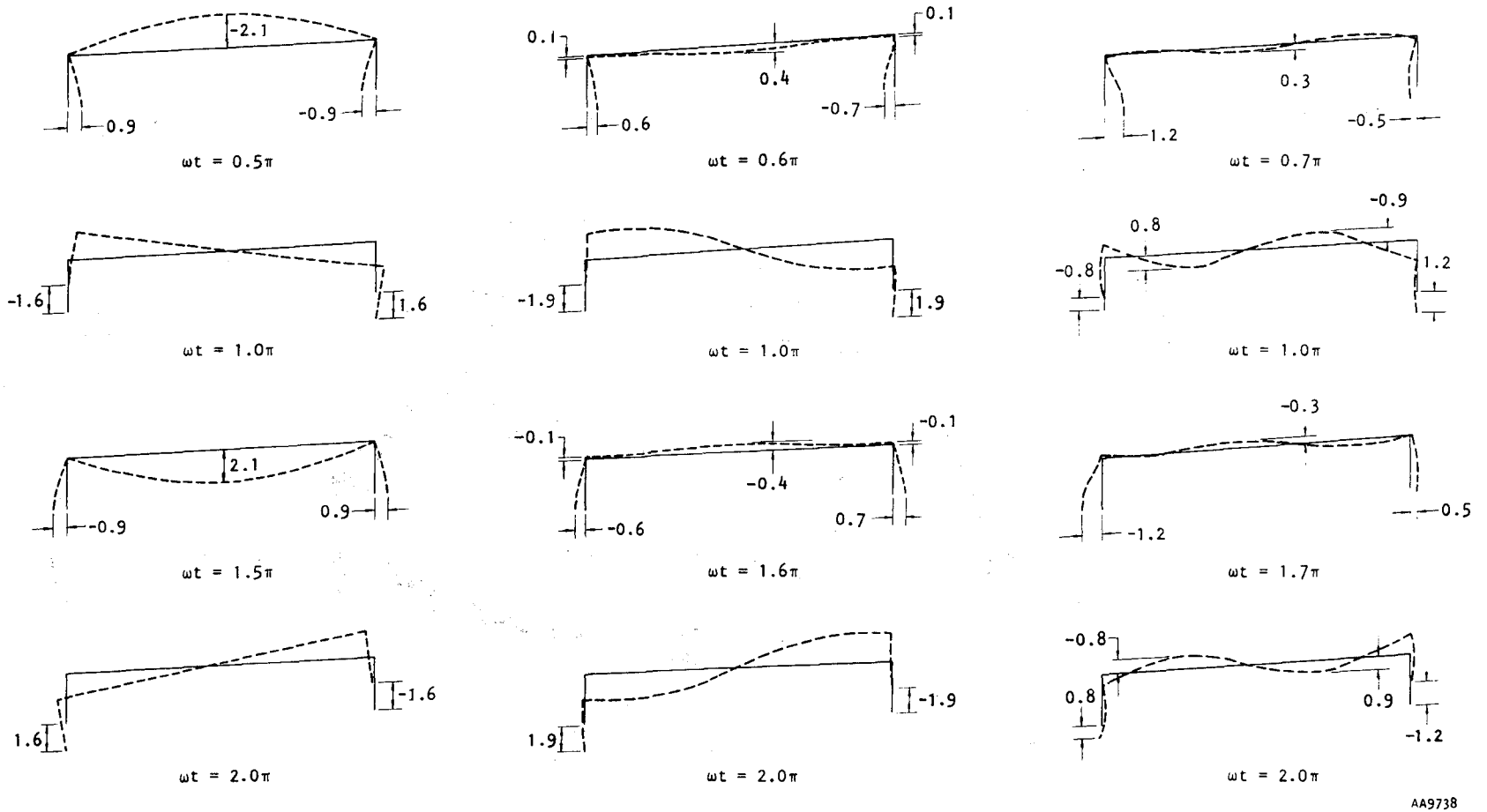

(a) $R_{Lx} = 0.5$ (b) $R_{Lx} = 1.5$ (c) $R_{Lx} \approx 3.5$ (3.48)

FIGURE 3-8. CASE 2 (θ_H = 0 DEG): BRIDGE RESPONSE TO APPLIED RAYLEIGH WAVE EXCITATIONS OF EQUAL AMPLITUDE AND OPPOSITE PHASE AT THE TWO FOUNDATIONS

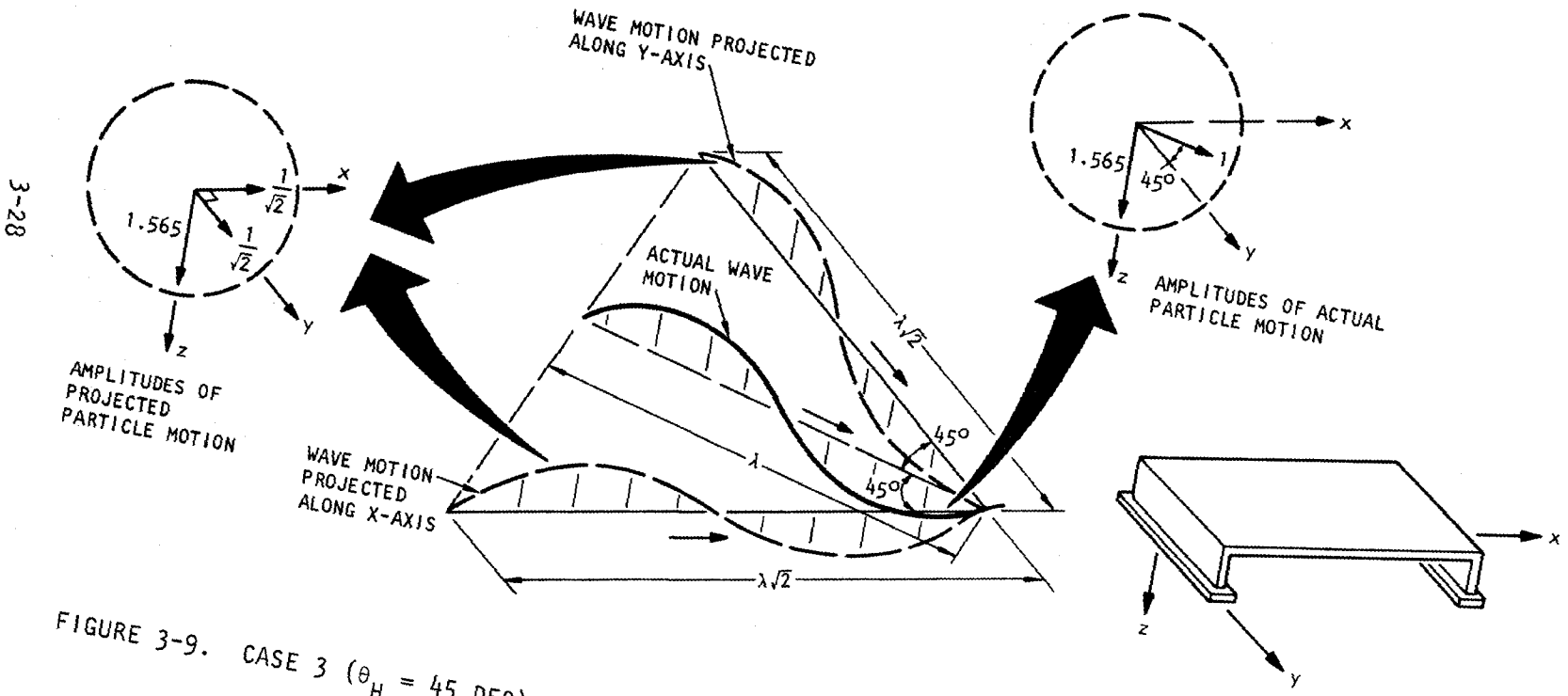

FIGURE 3-9. CASE 3 (θ_H = 45 DEG): RAYLEIGH WAVE MOTION PROJECTED ALONG X AND Y AXES OF BRIDGE

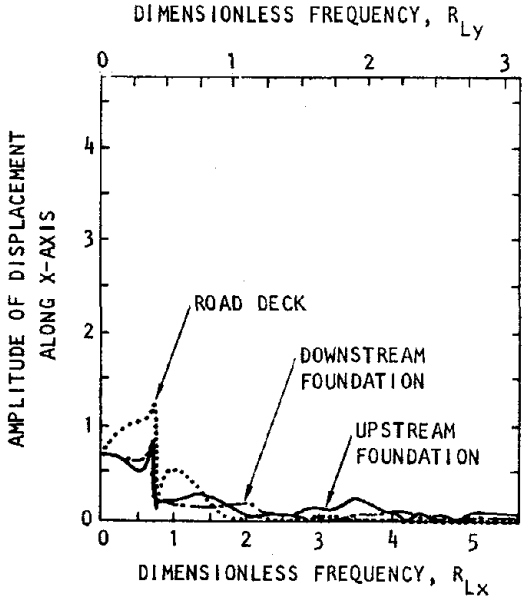

(a) Displacement along x-axis

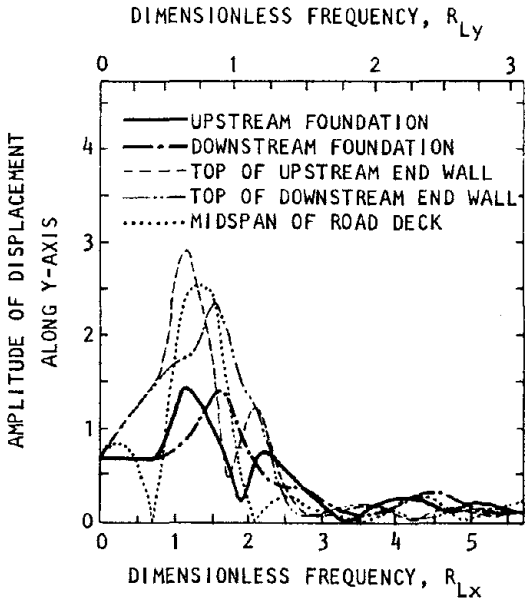

(b) Displacement along y-axis

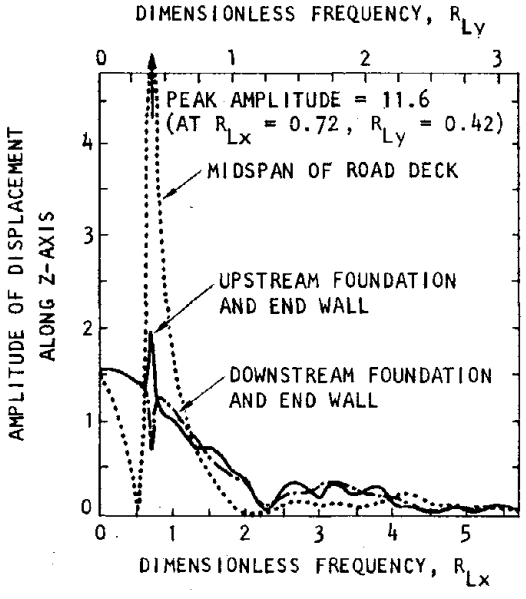

(c) Displacement along z-axis

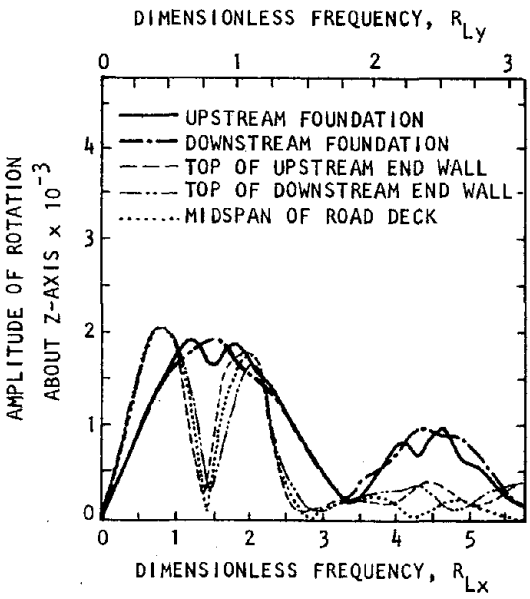

(d) Rotation about z-axis

FIGURE 3-10. FREQUENCY-DEPENDENT RESPONSE AMPLITUDES OF BRIDGE SUBJECTED TO INCIDENT RAYLEIGH WAVES WITH θ_H = 45 DEG

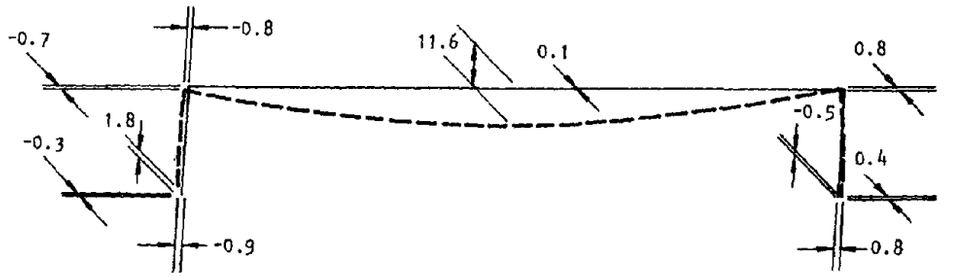

(a) R_{Lx} = 0.72 (f = 2.8 Hz)

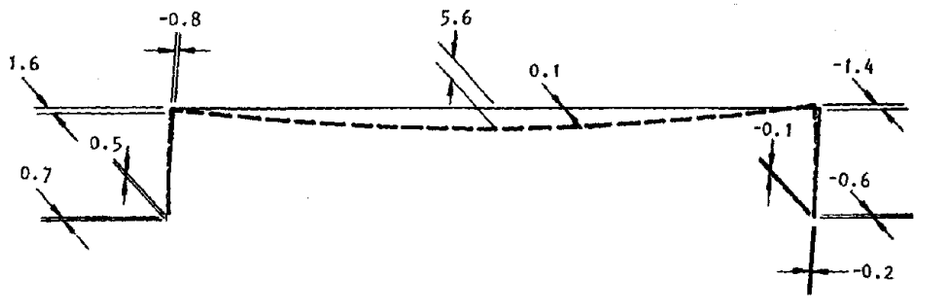

(b) R_{Lx} = 0.78 (f = 3.0 Hz)

AA10334

FIGURE 3-11. CASE 3 (θ_H = 45 DEG): DEFORMED SHAPES OF BRIDGE AT TIMES OF PEAK RESONANT RESPONSE TO RAYLEIGH WAVE EXCITATIONS

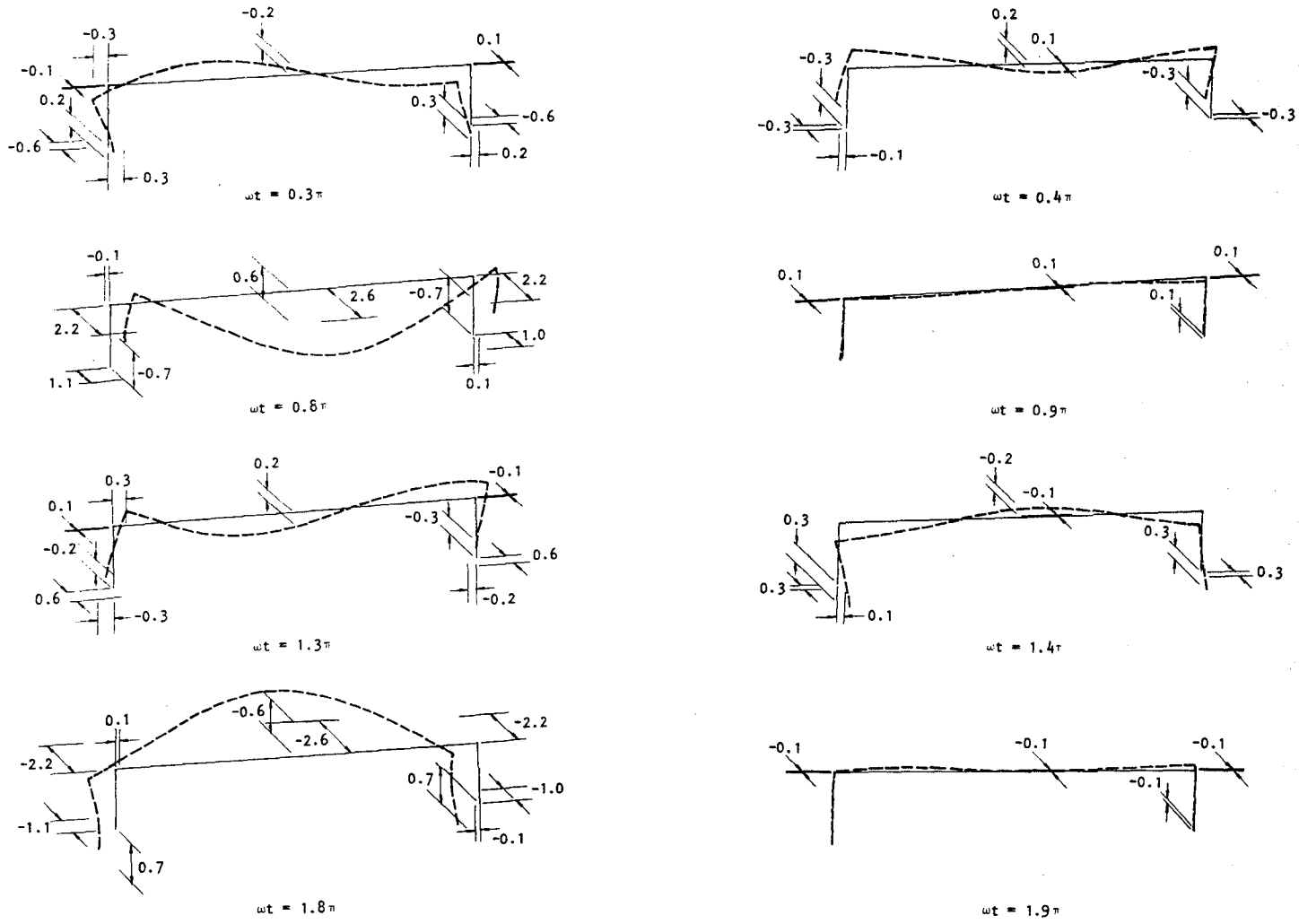

(a) $R_{Lx} = \sqrt{2}$

(b) $R_{Lx} = 2\sqrt{2}$

FIGURE 3-12. CASE 3 (θ_H = 45 DEG): BRIDGE RESPONSE TO APPLIED RAYLEIGH WAVE EXCITATIONS OF EQUAL AMPLITUDE AND EQUAL PHASE AT THE TWO FOUNDATIONS

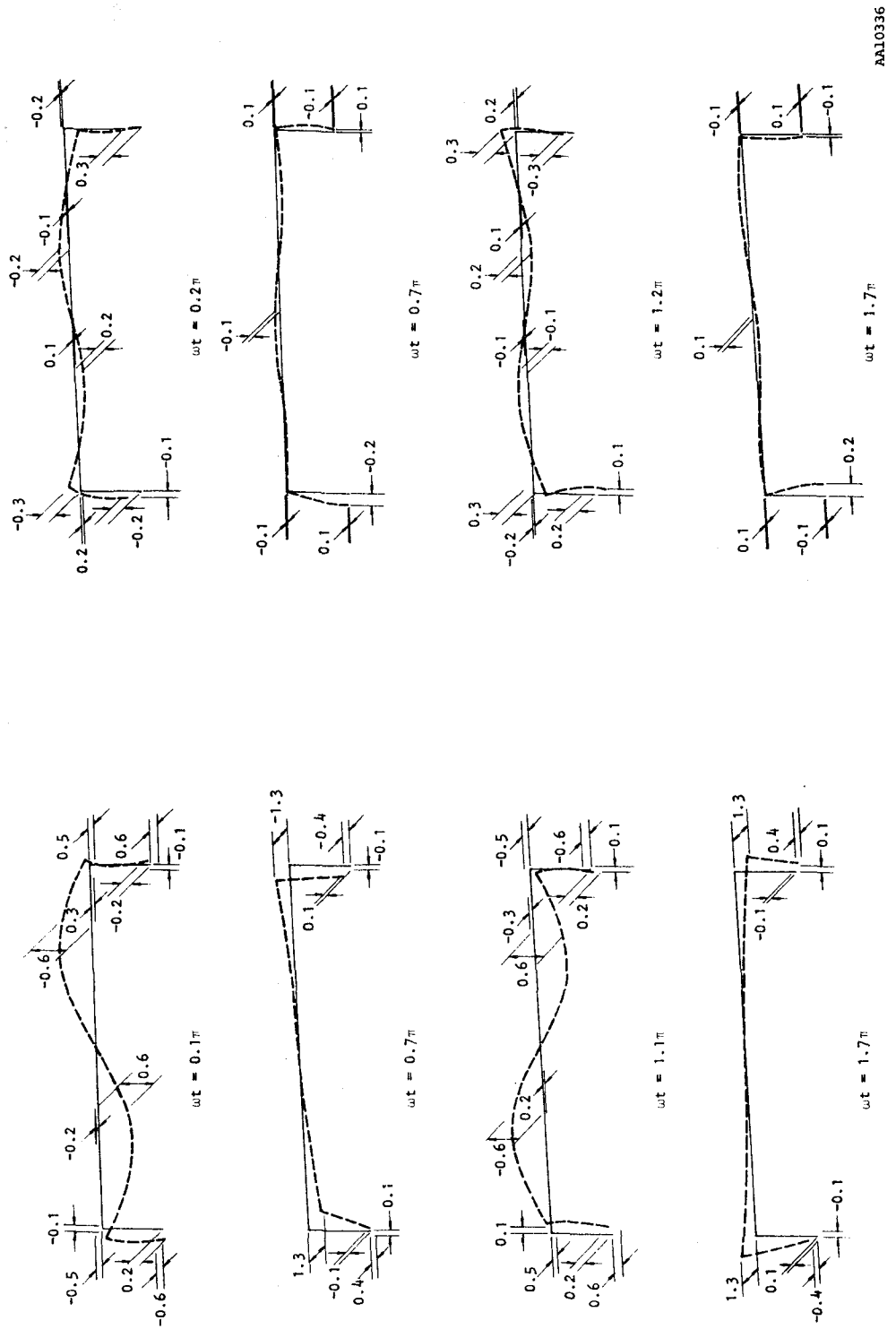

(a) $R_{Lx} = 1.5\sqrt{2}$ (b) $R_{Lx} = 2.5\sqrt{2}$

FIGURE 3-13. CASE 3 (θ_H = 45 DEG): BRIDGE RESPONSE TO APPLIED RAYLEIGH WAVE EXCITATIONS OF EQUAL AMPLITUDE AND OPPOSITE PHASE AT THE TWO FOUNDATIONS

CHAPTER 4

SV-WAVE ANALYSIS

4.1 GENERAL DISCUSSION

Of the various types of plane body waves that propagate within an elastic half-space, SV-waves are the most complex. This is because both the amplitudes and the phase angles of the horizontal and vertical components of wave motion along the ground surface are dependent on the vertical angle of incidence, θ_V (Fig. 4-1). As a result, the response of structures to such waves is correspondingly complex and interesting to investigate.

Despite this, there have been few studies of the response of structures to incident SV-waves, and these studies have been limited to consideration of very simple structural elements. For example, Wong and Luco (1978) analyzed the response of a rigid rectangular foundation to arbitrarily incident SV-waves. Their study showed that such waves lead to significant rocking of the foundation. Wolf and Obernhuber (1979) analyzed a single-mass structure on a rigid circular foundation and showed that the SV-wave-induced response of the foundation and structure was greatest in the vicinity of the critical angle of the SV-wave (which is the minimum value of θ_V at which the SV-wave excitations are real, as described in Sec. 4-2).

This chapter describes a study of SV-wave-induced effects that has features not contained in the prior studies mentioned above. One such feature is that, for the first time, the effects of traveling SV-waves on the response of a deformable bridge structure of extended length are investigated. A second feature is that the effects of the changes in the character of the SV-wave motion that result from variations in θ_V are studied to an extent not considered previously.

4.2 EXCITATION

The free-field motion generated along the ground surface by an SV-wave with angles of incidence θ_H and θ_V (Fig. 4-1) and a circular frequency ω is

$$\left\{u_{ff}\right\} = \left\{\begin{matrix} U_x \\ U_y \\ U_z \end{matrix}\right\} \exp\left[i\omega\left(t - \frac{x}{c}\cos\theta_H - \frac{y}{c}\sin\theta_H\right)\right] \qquad (4\text{-}1)$$

where U_x, U_y, and U_z are the amplitudes of ground-surface motion along the x, y, and z axes (Fig. 4-1), and c is the phase velocity, expressed in terms of the shear wave velocity V_s and $V_s/\cos\theta_V$. Now U_x, U_y, and U_z can in turn be expressed in terms of the amplitudes of the horizontal and vertical SV-wave motion in the plane of the wave (U_H and U_V respectively) as

$$\left\{\begin{matrix} U_x \\ U_y \\ U_z \end{matrix}\right\} = \begin{bmatrix} \cos\theta_H & 0 \\ \sin\theta_H & 0 \\ 0 & 1 \end{bmatrix} \left\{\begin{matrix} U_H \\ U_V \end{matrix}\right\} \qquad (4\text{-}2)$$

In Equation 4-2, U_H and U_V are computed considering that when an incident SV-wave reaches the ground surface, it is converted into a reflected SV-wave and a reflected P-wave (Fig. 4-1). Based on this consideration, expressions for U_H and U_V can be shown to be (Ewing, et al., 1957)

$$U_H = s\left[\frac{-2\sin\theta_V\,(\tan^2\theta_V - 1)(\tan^2\theta_V + 1)}{4\tan e\tan\theta_V + (\tan^2\theta_V - 1)^2}\right]$$

$$U_V = s\left[\frac{-4\tan e\sin\theta_V\,(1 + \tan^2\theta_V)}{4\tan e\tan\theta_V + (\tan^2\theta_V - 1)^2}\right] \qquad (4\text{-}3)$$

where s is the amplitude of the incident SV-wave and θ_V and e are, respectively, the angles that the incident and reflected SV-waves and the reflected P-wave make with the ground surface (Fig. 4-1). These angles are related through the expression

$$\cos e = \frac{V_P}{V_S} \cos \theta_V \tag{4-4}$$

where V_P and V_S are the P-wave and S-wave velocities of the elastic half-space. In terms of the Poisson's ratio of the elastic half-space ν, the angle e can be expressed as

$$\tan e = \sqrt{\left(\frac{1 - 2\nu}{2(1 - \nu)}\right)(1 + \tan^2 \theta_V) - 1} \tag{4-5}$$

Substituting Equation 4-5 into 4-3 shows that U_H and U_V are functions solely of the incident SV-wave amplitude s, the angle of incidence θ_V, and the Poisson's ratio ν.

Equation 4-4 indicates an important feature of the SV-wave problem, namely, that no real value of e exists until θ_V reaches the value $\theta_{V_{cr}}$, where

$$\theta_{V_{cr}} = \cos^{-1} \frac{V_S}{V_P} \tag{4-6}$$

Therefore, for an incident SV-wave there is no reflected P-wave when $\theta_V < \theta_{V_{cr}}$. Within this range, Equation 4-5 takes the form

$$\tan e = -i \sqrt{1 - \frac{(1 - 2\nu)}{2(1 - \nu)}(1 + \tan^2 \theta_V)} \tag{4-7}$$

Substituting Equation 4-7 into 4-3 leads to the following expressions for U_H and U_V, which are complex when $\theta_V < \theta_{V_{cr}}$

$$U_H = s\left\{\frac{-2 \sin\theta_V (\tan^4\theta_V - 1)}{(\tan^2\theta_V - 1)^4 + \dfrac{16\beta^2 \tan^2\theta_V}{\cos^2\theta_V}}\left[(\tan^2\theta_V - 1)^2 + i\left(\frac{4\beta \tan\theta_V}{\cos\theta_V}\right)\right]\right\}$$

$$U_V = s\left\{\frac{4\beta \tan\theta_V (\tan^2\theta_V + 1)}{(\tan^2\theta_V - 1)^4 + \dfrac{16\beta^2 \tan^2\theta_V}{\cos^2\theta_V}}\left[\frac{-4\beta \tan\theta_V}{\cos\theta_V} + i\left(\tan^2\theta_V - 1\right)^2\right]\right\} \quad (4\text{-}8)$$

where

$$\beta = \sqrt{\cos^2\theta_V - \frac{(1 - 2\nu)}{2(1 - \nu)}} \quad (4\text{-}9)$$

Amplitudes and phase angles corresponding to Equations 4-3 and 4-8 are plotted in Figure 4-2 for the case when $\nu = 1/3$ and $s = 1$. For this case, $\theta_{V_{cr}} = 60$ deg, and Figure 4-2 shows that when $\theta_V > \theta_{V_{cr}}$, U_H and U_V are in phase (although their relative amplitudes are functions of θ_V). When $\theta_V < \theta_{V_{cr}}$, however, two different types of free-field responses occur, as shown in Figure 4-2.

1. $\theta_V < 45$ deg. The free-field ground surface motions are elliptic retrograde, wherein the positive horizontal displacement vector, U_H, trails the positive vertical displacement vector, U_V, by 90 deg (where the positive vectors are defined in Fig. 4-1). The aspect ratio of this elliptic motion, or the ratio of the amplitudes of U_V and U_H, varies with θ_V within this range.

2. $45 \text{ deg} < \theta_V < 60 \text{ deg}$. The free-field ground surface motions are elliptic prograde, wherein the positive vertical displacement vector, U_H, is ahead of the positive vertical displacement vector, U_V, by 90 deg. As for $\theta_V < 45$ deg, the aspect ratio of this elliptic motion, or the ratio of the amplitudes of U_V to U_H, varies with θ_V within this range.

4.3 SCOPE OF CALCULATIONS

The frequency-dependent response of the bridge to arbitrarily incident SV-waves is computed for three different cases, which correspond to horizontal angles of incidence (θ_H) of 90 deg (Case 1), 0 deg (Case 2), and 45 deg (Case 3). For each case, results from the several different angles of vertical incidence (θ_V) listed in Table 4-1 are provided. This table shows that these values of θ_V encompass the range of different types of free-field ground surface motion that are induced by the SV-waves.

4.4 RESULTS FROM CASE 1: INCIDENT SV-WAVES WITH $\theta_H = 90$ DEG

The first case corresponds to SV-wave excitations that are propagating in a plane normal to the span of the bridge, or parallel to its y-z plane ($\theta_H = 90$ deg, as shown in Fig. 4-3). Results are presented first for vertically incident SV-waves in that plane, and then for nonvertically incident waves.

4.4.1 VERTICALLY INCIDENT SV-WAVES

When the SV-waves are vertically incident in the plane defined by $\theta_H = 90$ deg, the bridge foundations are subjected to uniformly distributed horizontal displacements that are directed along the y-axis of the bridge (i.e., normal to its span). The resulting principal bridge displacements are also directed along the y-axis (Fig. 4-4a, Table 4-2). The peak y-displacements of the bridge occur at a resonant dimensionless frequency, R_{Ly}, of 0.58 (which corresponds to 4.2 Hz); they denote rocking motions that are symmetric

about the midspan of the road deck and are largest at that point (Fig. 4-5a).* Rather small rotations about the z-axis occur and are a consequence of the bending of the road deck in the y-direction that is generated by this excitation (Fig. 4-4b). The displacements of the bridge along the x- and z-axes are negligible.

It is noted that this case results in identical excitation to that considered earlier by Werner et al. (1977) and corresponding to incident SH-waves for θ_V = 90 deg and θ_H = 0 deg. The bridge response is also identical, except for the effects of the increased foundation mass now considered (Sec. 2.2.1); this mass tends to slightly lower the frequencies at which the peak responses now take place.

4.4.2 NONVERTICALLY INCIDENT SV-WAVES

When the SV-waves are nonvertically incident in the plane defined by θ_H = 90 deg, the bridge foundations are subjected to nonuniformly distributed horizontal and vertical free-field excitations whose amplitudes and phase angles are dependent on θ_V and Poisson's ratio, as described in Section 4.2. The resulting bridge response (Figs. 4-6 to 4-11 and Tables 4-2 to 4-3) is markedly different from that induced by the vertically incident SV-waves and has the following characteristics:

- The bridge now undergoes not only y-displacements but significant z-displacements as well. The z-displacements are largest at the resonant frequency of R_{Ly} = 0.39 (which corresponds to 2.8 Hz)*; at that frequency, they are symmetric about the midspan of the road deck and are largest at that point (Fig. 4-11). The amplitudes of these midspan resonant-frequency z-displacements are generally quite large for each θ_V case investigated; the only exception to this trend, at θ_V = 60 deg, is caused by the vanishing free-field z-displacements at that angle of vertical incidence (Table 4-3, Figs. 4-2 and 4-9c).

- The y-displacements are similar to those induced by the vertically incident SV-waves in that they are usually largest

*This same resonant response and frequency was induced by the Rayleigh waves described in Chapter 3.

at the resonant frequency of $R_{Ly} = 0.58$; at that frequency, they denote rocking motions in the y-direction that are symmetric about the midspan of the road deck and are generally largest at that point (Figs. 4-5b, Table 4-2). Among the various θ_V results presented, the only exception to this trend occurs when $\theta_V = 55$ deg. At this angle, the elliptic prograde free-field motions induce rocking rotations (about the x-axis) that are phased so as to reduce the y-displacements of the road deck and cause them to be exceeded by the y-displacements of the foundation (Table 4-2 and Fig. 4-5c); along the road deck however, the *relative* displacements in the y-direction remain large. For all other θ_V angles investigated, the resonant-frequency rocking rotations are phased so that they enhance, rather than reduce, the y-displacements of the road deck (Table 4-2).

- The x-displacements of the bridge are usually negligible when compared to the y- and z-displacements. The only exception to this trend is at the previously noted resonant frequency for the z-displacements ($R_{Ly} = 0.39$ or 2.8 Hz). At this frequency, the significant bending of the road deck in the z-direction causes prominent x-displacements of the two foundations that are of equal amplitude and opposite phase (Table 4-3, Figs. 4-6a to 4-10a).

- The rotations of the bridge about the z-axis are generally small and are caused by the small degree of bending of the road deck that is occurring in the y-direction (Figs. 4-6d to 4-10d).

- As the dimensionless frequency R_{Ly} increases, the apparent wavelength of the SV-wave excitation decreases relative to the foundation length. This results in a self-canceling of the loads applied to the rigid foundations by the incident waves, which causes the higher-frequency bridge displacements to

become small relative to those of the free field* (Werner et al., 1977). However, as noted in Section 3.3.1, this effect would be somewhat less pronounced in a more realistic setting involving flexible foundations, rather than the rigid foundations considered in these analyses.

4.5 RESULTS FROM CASE 2: INCIDENT SV-WAVES WITH θ_H = 0 DEG

The second case corresponds to SV-wave excitations that are propagating in a plane parallel to the span of the bridge, or along its x-z plane (θ_H = 0 deg, as shown in Fig. 4-12).

4.5.1 VERTICALLY INCIDENT SV-WAVES

When the SV-waves are vertically incident in the plane defined by θ_H = 0 deg, the free-field displacements are directed along the x-axis (i.e., parallel to the span of the bridge) and are identical all along the ground surface. The resulting principal bridge displacements are also directed along the x-axis, although some z-displacements that are antisymmetric about the midspan of the road deck are generated (Tables 4-4 and 4-5, Fig. 4-13). The x-displacements of the road deck exhibit a significant peak at a resonant frequency of R_{Lx} = 0.72 (which corresponds to 3.0 Hz); at this frequency, they denote sidesway motions in the x-direction (Fig. 4-14a).† At higher frequencies, the x-displacements of the foundation are comparable in amplitude to those of the free field and are much larger than the road deck displacements (Fig. 4-13a). It is seen that, except for the slight effects of the increased foundation mass now considered (Sec. 2.2.1), these bridge response characteristics are identical to those previously shown by Werner et al. (1977) for the case involving SH-wave excitations with $\theta_H = \theta_V$ = 90 deg.

*The free-field displacements correspond to the zero-frequency displacement amplitudes in Figures 4-6 to 4-10.

†This same resonant response and frequency was induced by the Rayleigh waves in Chapter 3. Comparisons of this response at the corresponding fixed-base mode are described in that chapter.

4.5.2 NONVERTICALLY INCIDENT SV-WAVES

When the SV-waves are nonvertically incident in the plane defined by $\theta_H = 0$ deg, the two bridge foundations are subjected to horizontal and vertical components of free-field excitation whose amplitude and phase angle depend on θ_V and Poisson's ratio. The phasing of these components at the two foundations is dependent on the apparent wavelength of the SV-wave relative to the span length. The resulting bridge response (Tables 4-4 to 4-7 and Figs. 4-15 to 4-19) is strongly influenced by this phasing, as discussed in the paragraphs that follow.

4.5.2.1 Resonant Response Characteristics

a. Displacements along the z-Axis

The bridge response to nonvertically incident SV-waves features displacements along the z-axis whose most prominent feature is a significant peak at the midspan of the road deck when $R_{Lx} = 0.67$ ($f = 2.8$ Hz). This peak, which is not induced by the vertically incident SV-waves, represents bending of the road deck in the x-z plane; in this, the z-displacements are symmetric about the midspan of the road deck and are largest at that point (Fig. 4-20b). Virtually the same response at the same resonant frequency is induced by the nonvertically incident SV-waves with $\theta_H = 90$ deg (Case 1) and by the Rayleigh waves (Chapt. 3).

It is noted from Figures 4-16b and 4-20c that the above resonant response does not occur when $\theta_V = 45$ deg. This is because of the phasing of the vertical free-field excitations applied to the two foundations when $\theta_V = 45$ deg and $f = 2.8$ Hz. (Note from Fig. 4-2a that no horizontal free-field excitations are applied when $\theta_V = 45$ deg.) This phasing is demonstrated by computing the apparent wavelength, λ_a, to be

$$\lambda_a = \frac{V_S}{f \cos \theta_V} = \frac{500 \text{ fps}}{2.8 \text{ Hz } (0.707)} = 252 \text{ ft} \qquad (4\text{-}10)$$

which is about twice the span length of the bridge (120 ft). As shown in Figure 4-21, this leads to vertical free-field excitations that are of equal amplitude and opposite phase at the two foundations; such excitations cannot induce the symmetric vertical response represented by the resonant peak at 2.8 Hz.

Still another feature of the z-displacements is the secondary resonant peak at higher frequencies (R_{Lx} = 4.0 to 4.6). This peak, which was observed in the Rayleigh wave results (Chapt. 3), is depicted by the deformed shapes shown in Figure 4-22. It is analogous to Mode 4 of the in-plane fixed-base modes of the bridge (Fig. 2-6a) and occurs at about the same frequency as that mode.* This is because most of the strain energy induced in the bridge during this resonant response is concentrated in the road deck and is therefore not strongly affected by the soil medium.

b. Displacements along the x-Axis

The bridge response to nonvertically incident SV-waves features displacements along the x-axis whose most prominent feature is a significant peak at the road deck locations when R_{Lx} = 0.72 (f = 3.0 Hz). This peak represents a resonant response that involves sidesway of the bridge in the x-direction and was also induced by the vertically incident SV-waves with θ_H = 0 deg. However, it is now coupled with the previously noted resonance that involves large z-displacements at the midspan of the road deck (at R_{Lx} = 0.67 or f = 2.8 Hz); this z-displacement resonance was not induced by the vertically incident SV-waves. Because of this, the deformed shape of the road deck that now occurs when R_{Lx} = 0.72 is substantially altered from that induced at this frequency when the SV-waves are vertically incident (as seen by comparing Figs. 4-14b and 4-14c with Fig. 4-14a).

*This resonant frequency varies slightly with θ_V, possibly because of phasing relationships or, in some cases, poorly defined peaks (e.g., Fig. 4-16b). In fact, in some cases the resonant frequency slightly exceeds the frequency of the fixed-base mode; for example, when θ_V = 60 deg, the resonant frequency is 19.2 Hz, as compared to 18.4 Hz for Mode 4 of Figure 2-6a. This is probably because of effects of three-dimensional soil/structure interaction and the phased input motions (see discussion in footnote on p 3-6).

4.5.2.2 Phased-Input-Induced Response Characteristics

The above discussion of the vanishing resonant response at $R_{Lx} = 0.67$ when $\theta_V = 45$ deg illustrates one instance of how the size of the apparent wavelength of the SV-wave relative to the span length can influence the bridge response characteristics. The importance of this span-length to apparent-wavelength ratio is further illustrated by two additional sets of results that are described below for each value of θ_V. The first corresponds to the case where the free-field excitations are identical in amplitude and in phase at the two foundations. This occurs when the ratio of the bridge span length to the apparent wavelength of the incident SV-wave is 1.0, 2.0, 3.0, etc. The second set corresponds to free-field excitations that are of equal amplitude and opposite phase at the two foundations. Such excitations are induced when the ratio of the bridge span length to the apparent wavelength of the incident SV-wave is 0.5, 1.5, 2.5, etc. These two sets of results, considered together, serve to explain several of the pronounced peaks and valleys that exist in the amplitude vs. frequency plots of Figures 4-15 to 4-19. They also demonstrate that the phased-input-induced response characteristics are dependent on the angle of vertical incidence, θ_V, as well as on the apparent wavelength of the free-field excitations applied at the two foundations.

The results are presented in two ways for each θ_V. First, amplitudes and phase angles of the displacements at various locations along the bridge are given in Tables 4-6 and 4-7. Second, deformed shapes of the bridge at various times during a response cycle are provided to graphically illustrate how the bridge response is affected by the apparent wavelength of the SV-wave excitation (Figs. 4-23 to 4-32). The trends indicated by these results for each set of free-field excitations are described below.

a. Equal-Amplitude/Equal-Phase Excitations

(1) $\theta_V = 20$ deg. The two foundations are undergoing similar motions that deviate somewhat from the elliptic retrograde nature of the free-field excitations, because of soil/structure interaction effects (Table 4-6). The

resulting bridge response usually features small horizontal displacements of the road deck relative to the foundation (because the horizontal components of the free-field excitation are small).* The vertical displacements of the bridge are approximately symmetric about the midspan of the road deck, when the excitation frequencies are small. However, at higher frequencies, this symmetry becomes distorted because of increased effects of wave scattering and diffraction and higher modes of vibration (Table 4-6, Fig. 4-23).

(2) $\theta_V = 45$ deg. Because of the absence of horizontal components of free-field motion, the response of the two foundations at lower frequencies consists of primarily vertical displacements with only small, out-of-phase, horizontal displacement components; at high frequencies, however, the horizontal displacements of the two foundations become prominent. The road deck of the bridge experiences vertical displacements that are prominent over the entire frequency range and are approximately symmetric about the midspan of the bridge (Table 4-6). The deformed shape of the road deck becomes more complex as the frequency increases, because of the increased effects of wave scattering and diffraction and higher modes of vibration (Fig. 4-24).

(3) $\theta_V = 55$ deg. The two foundations are undergoing similar motions that deviate somewhat from the elliptic prograde nature of the free-field motions, because of soil/structure interaction effects (Table 4-6). Because both the horizontal and vertical components of the free-field excitation are prominent, the two components of the response at each foundation and bridge node point are likewise significant. The bridge response consists of two distinct patterns during a cycle. One pattern involves approximately in-phase horizontal displacements of the two foundations that are large relative to the road deck; the second pattern involves primarily vertical displacements of the road deck that are approximately symmetric about its midspan. The deformed shape of the bridge and the phasing of the foundation motions become more complex with increasing frequency, because of increased effects of wave scattering and diffraction and higher modes of vibration (Fig. 4-25).

*The only exception to this trend is at $R_{LX} = 1.06$ (1.0/cos 20 deg) where the structural response is influenced by the sidesway resonant response in the x-direction.

(4) $\theta_V = 60$ deg. Because the free-field excitations at the two foundations consist of very large horizontal components only, the foundations are undergoing primarily large, in-phase horizontal displacements; the vertical displacements of the two foundations are much smaller and are out of phase with one another (Table 4-6). The resulting bridge response features large horizontal displacements of the two foundations relative to the road deck and corresponding vertical displacements of the road deck that are approximately antisymmetric about its midspan. The deformed shape of the road deck becomes more complex as the frequency increases because of increased effects from wave scattering and diffraction and higher modes of vibration (Fig. 4-26).

(5) $\theta_V = 65$ deg. The free-field excitations at the two foundations consist of identical motions involving horizontal displacements that are larger than and in phase with the vertical displacements. The foundation displacements deviate somewhat from this pattern because of soil/structure interaction effects, although the horizontal displacements of the foundations are usually larger than the vertical (Table 4-6, Fig. 4-19). The resulting response of the bridge features prominent in-phase horizontal displacements of the two foundations that are large relative to the road deck, together with vertical displacements of the road deck that are neither antisymmetric nor symmetric about the midspan of the road deck. The deformed shape of the road deck and the phasing of the foundation motions become more complex as the excitation frequency is increased because of the increased effects of wave scattering and diffraction and higher modes of vibration (Fig. 4-27).

b. Equal-Amplitude/Opposite-Phase Excitations

(1) $\theta_V = 20$ deg. The two foundations are each undergoing horizontal and vertical displacements that deviate slightly from the elliptic retrograde nature of the field motions; these displacements are approximately 180 deg out of phase at the two foundations (Table 4-7). At low frequencies the resulting bridge response features two distinct patterns. One involves

approximately equal and opposite horizontal displacements of the two foundations accompanied by vertical displacements of the road deck that are symmetric about its midspan and largest at that point. The second pattern, which occurs about one-quarter of a cycle after the first pattern, involves vertical displacements that are antisymmetric about the midspan of the road deck. As the frequency increases, these patterns become less distinct and the deformed shapes more complex because of increased effects of wave scattering and diffraction and higher modes of vibration (Fig. 4-28).

(2) $\theta_V = 45$ deg. Despite the fact that the free-field excitations consist of only vertical displacements, the foundations are undergoing both horizontal and vertical displacements of significant amplitude (Table 4-7); the horizontal displacements are a consequence of the off-diagonal terms in the foundation/soil impedance matrix. The bridge response at low frequencies consists of sidesway displacements of the road deck relative to the foundation, as well as vertical displacements that are antisymmetric relative to the midspan of the road deck. At higher frequencies, no sidesway displacements are excited, and the deformed shapes corresponding to the antisymmetric vertical displacements become more complex because of increased effects of wave scattering and diffraction and higher modes of vibration (Fig. 4-29).

(3) $\theta_V = 55$ deg. The two foundations are undergoing horizontal and vertical displacements whose phase difference at each foundation deviates from the 90-deg value of the elliptic prograde free-field motions; also, the phase angles of the displacements of one foundation relative to the other differ from the 180-deg difference of the free-field motions, particularly at higher frequencies (Table 4-7). The resulting bridge response at low frequencies exhibits two distinct patterns. The first consists of vertical displacements that are antisymmetric about the midspan of the road deck. The second pattern, which occurs later in the response cycle, involves approximately equal and opposite horizontal displacements of the two foundations together with vertical displacements of the road deck that are symmetric

about the midspan of the road deck and largest at that point.* When the frequency increases, the deformed shape of the road deck becomes more complex because of the increased effects of wave scattering and diffraction and higher modes of vibration (Fig. 4-30).

(4) θ_V = 60 deg. Because the free-field motions consist of large horizontal components only (i.e., no vertical free-field displacements), the resulting motions of the two foundations involve large horizontal displacements of nearly opposite phase and relatively small vertical displacements. The bridge response to these large, nearly opposite phased horizontal motions of the foundations consists of vertical displacements of the road deck that are symmetric about its midspan and largest at that point*. As the frequency increases, the deformed shape of the road deck becomes more complex because of the increased effects of wave scattering and diffraction and higher modes of vibration (Fig. 4-31).

(5) θ_V = 65 deg. The free-field excitations at each of the two foundations consist of horizontal displacements that are larger than and in phase with the vertical displacements. Soil/structure interaction effects cause the foundation displacements to deviate somewhat from this pattern, particularly at higher frequencies, although the horizontal displacements of the foundation are still larger than the vertical (Table 4-7). The resulting bridge response features large horizontal displacements of the two foundations that are of opposite phase, together with vertical displacements of the road deck that are neither symmetric nor antisymmetric about its midspan. The

---

*When θ_V = 55 deg and 60 deg, the low-frequency bridge response involves approximately equal and opposite horizontal displacements of the foundations and corresponding vertical displacements of the road deck that are symmetric about its midspan and largest at that point. It is noted, however, that the vertical displacements of the road deck are of opposite phase to that induced directly by the horizontal displacements of the two foundations; e.g., inward displacements of foundations result in downward rather than upward vertical displacements of the road deck. This is attributed to the effects of foundation rotations about the y-axis that result from off-diagonal terms of the foundation/soil impedance matrix. Although not shown in Table 4-7, these rotations are phased to work against the effects of the horizontal foundation displacements; when transmitted through the end walls to the road deck, they result in the deformed shapes shown in Figures 4-30 and 4-31.

deformed shape of the road deck and the phasing of the foundation motions become more complex as the frequency increases, because of increased effects of wave scattering and diffraction and higher modes of vibration (Fig. 4-32).

4.6 RESULTS FROM CASE 3: INCIDENT SV-WAVES WITH θ_H = 45 DEG

The third and final case corresponds to SV-wave excitations that are propagating in a plane oblique to the x-z plane of the bridge (θ_H = 45 deg, as shown in Fig. 4-33a). The apparent wave motion from such a wave can be projected along the x- and y-axes of the bridge with the wavelength and particle motion relationships shown in Figure 4-33b.

4.6.1 VERTICALLY INCIDENT SV-WAVES

When the SV-waves are vertically incident in the plane defined by θ_H = 45 deg, the bridge foundations are subjected to uniformly distributed horizontal free-field displacements that can be resolved into identical components along the x- and y-axes. The resulting principal bridge displacements are also horizontal, although some small vertical displacements are generated that are antisymmetric about the midspan of the road deck (Fig. 4-34 and Tables 4-8 to 4-10). The features of these bridge response characteristics are described as follows:

- By comparing Figures 4-34a and 4-13a, it is seen that the bridge displacement components along the x-axis are similar to those generated by the Case 2 vertically incident SV-waves (θ_H = 0 deg, θ_V = 90 deg) in that: (a) a significant peak in the x-displacement of the road deck is exhibited at the same resonant frequency (R_{Lx} = 0.72, or f = 3.0 Hz); and (b) at higher frequencies, the x-displacements of the foundations substantially exceed those of the road deck.

- As seen from comparisons of Figures 4-34b and 4-4a, the bridge displacement components along the y-axis are similar to those

induced by the Case 1 vertically incident SV-waves ($\theta_H = \theta_V = 90$ deg); in each case, a prominent resonant response that is symmetric about the midspan of the road deck is induced at the same resonant frequency ($R_{Ly} = 0.58$, or $f = 4.2$ Hz). This resonant response corresponds to a rocking of the bridge in the y-direction.

- The rotations about the z-axis are small and are a consequence of the bending of the road deck in the y-direction (Fig. 4-34d). These rotational response characteristics are similar to those induced by the Case 1 vertically incident SV-waves.

Deformed shapes corresponding to the resonant responses noted above are provided in Figure 4-35.

4.6.2 NONVERTICALLY INCIDENT SV-WAVES

When the SV-waves are nonvertically incident in the plane defined by $\theta_H = 45$ deg, the bridge foundations are subjected to free-field displacement components directed along the x-, y-, and z-axes (Fig. 4-33b). The relative phasing and amplitudes of these displacements along the two foundations depends on their wavelength (or excitation frequency) and on the angle of vertical incidence, θ_V.

The bridge response to nonvertically incident SV-waves with $\theta_H = 45$ deg is shown in the form of amplitude vs. dimensionless frequency plots (Figs. 4-36 through 4-40) and as tabulated amplitudes and phase angles at selected frequencies (Tables 4-8 to 4-12). This response, unlike that for Cases 1 and 2, is now fully three dimensional over the entire frequency range. Also, the response is markedly different from that induced by the vertically incident SV-waves with $\theta_H = 45$ deg, as discussed in the paragraphs that follow.

4.6.2.1 Resonant Response Characteristics

For nonvertically incident SV-waves propagating in the plane defined by θ_H = 45 deg, resonant responses occur that involve sidesway of the bridge in the x-direction (at R_{Lx} = 0.72 or f = 3.0 Hz) and significant vertical displacements at the midspan of the road deck (at R_{Lx} = 0.67 or f = 2.8 Hz). These two resonant responses, which are depicted by the significant peaks that occur in the x-displacement and z-displacement vs. frequency curves, are coupled because of the close proximity of their resonant frequencies (see Tables 4-8 to 4-9 and Figs. 4-36a,c to 4-40a,c). These response characteristics differ from those induced by the vertically incident SV-waves with θ_H = 45 deg in that: (1) the resonance involving the vertical displacements is not excited by the vertically incident waves; and (2) the coupling that occurs between the sidesway and vertical displacement resonances at R_{Lx} = 0.72 results in a deformed shape of the road deck that differs markedly from that induced by the vertically incident SV-waves at that frequency (compare Figs. 4-41 and 4-35a). It is noted that this vertical displacement resonance was also induced by both the Case 1 and Case 2 nonvertically incident SV-waves (θ_H = 90 deg and 0 deg); the sidesway response was previously observed when the bridge was subjected to the Case 2 SV-wave excitations (θ_H = 0 deg).

Unlike the vertically incident wave results, the nonvertically incident SV-waves propagating at θ_H = 45 deg do not induce a resonant response involving rocking in the y-direction. This is because the finite apparent wavelength of the obliquely incident SV-wave excitations introduces phase differences between the y-components of free-field excitation applied at the two foundations. These phase differences, which are not induced by the vertically incident waves, destroy the symmetry of the applied loading in the y-direction; this, in turn, makes it difficult to excite the symmetric rocking resonant response that was generated by the vertically incident SV-wave excitations at R_{Ly} = 0.58 (f = 4.2 Hz) (see Figs. 4-36b to 4-40b and Table 4-10).

4.6.2.2 Phased-Input-Induced Response Characteristics

Three main types of phased-input-induced response characteristics are induced by the nonvertically incident SV-waves propagating at $\theta_H = 45$ deg. The first type corresponds to the reduction in amplitude of the displacements along the x-, y-, and z-axes that occur at higher frequencies; in all cases, the higher-frequency displacement amplitudes fall well below those of the free field (Figs. 4-36 to 4-40). These reductions occur because the nonvertically incident SV-waves with $\theta_H = 45$ deg have a finite apparent wavelength and are propagating oblique to the span of the bridge. The excitations are therefore affected by the significant dimension of the rigid foundation in the y-direction (Fig. 4-33b); as discussed previously, this results in self-canceling effects whereby the net foundation loading decreases as the projected apparent wavelength becomes small relative to the dimension of the rigid foundation. This decrease in net loading causes the observed reduction in bridge displacement at higher frequencies.

Another important feature of the phased-input-induced bridge response is the nature of the rotations about the z-axis of the foundations and road deck. These rotations, particularly at the foundations, are large when the vertical angle of incidence is near the critical angle (i.e., $\theta_V \approx 60$ deg).* Some features of these z-rotations are as follows (Figs. 4-36d to 4-40d):

- The z-rotations of the bridge are small for shallow angles of vertical incidence ($\theta_V = 20$ deg) and increase to very large values near the critical angle of incidence ($\theta_V \approx 60$ deg).
- At low excitation frequencies, the amplitudes of the z-rotations of the road deck are comparable to or larger than those of the foundations. At higher excitation frequencies and for $\theta_V \approx 60$ deg, the foundation rotations attain very

*The foundation rotations about the z-axis that occur when $\theta_H = 45$ deg and $\theta_V \approx 60$ deg are much larger than those induced by the Case 1^H excitations ($\theta_H = 90$ deg) or by the excitations induced by the Case 3 vertically incident SV-waves ($\theta_H = 45$ deg, $\theta_V = 90$ deg).

large amplitudes that are substantially greater than those of the road deck; they therefore indicate marked torsional deformations of the end walls.

- The large foundation rotations that occur when $\theta_V \approx 60$ deg may be attributed to free field displacement components in the x-direction that are nonuniformly distributed along the 70-ft length of the rigid foundation. This phenomenon is similar to that induced by nonvertically incident SH-waves that are propagating along the foundation length (Werner et al., 1977).

- The z-rotations induced in the road deck are due to differential y-displacements that are induced in the road deck because of bending in the y-direction. Because these y-displacements are larger at lower frequencies (Figs. 4-36b to 4-40b), the z-rotations of the road deck are also larger within that low-frequency range.

A third and final phased-input-induced response characteristic to be discussed corresponds to distinct zero-points or very small values that occur in the curves relating the y-displacements and z-displacements at the midspan of the road deck to the excitation frequency (Figs. 4-36b,c to 4-40b,c). These points occur when the free-field excitations applied at each foundation are phased so as to induce y-displacements and z-displacements that are approximately antisymmetric about the midspan of the road deck (Tables 4-11 and 4-12). The excitation frequencies at which this behavior occurs increase with increasing θ_V; this is a consequence of the spreading of the frequency scale because of apparent wavelength effects. Also, it is noted that when the bridge is undergoing antisymmetric y-displacements, (or, for that matter, any y-displacement response that is not symmetric about the midspan of the road deck), the resulting out-of-phase rocking displacements of the two end walls induce torsional deformations in the road deck.

TABLE 4-1. ANGLES OF VERTICAL INCIDENCE CONSIDERED FOR EACH CASE OF SV-WAVE MOTION

θ_V, deg	Significance	Amplitudes of Free-Field Ground Surface Motion (Eq. 4-3)	
		U_H	U_V
20	Elliptic retrograde motion	0.465	0.908
45	At interface between elliptic retrograde and elliptic prograde ranges of motion	0.0	1.414
55	Elliptic prograde motion	1.725	1.626
60	Critical angle of incidence. At interface between real and complex ranges of motion	3.441	0.0
65	U_H and U_V are in-phase and real	1.988	0.698
90	Motion from vertically incident SV-waves	2.0	0.0

TABLE 4-2. CASE 1 (θ_H = 90 DEG): RESONANT RESPONSE TO SV-WAVE EXCITATIONS AT R_{Ly} = 0.58 (f = 4.17 Hz)[1]

Vertical Angle of Incidence, θ_V, deg[2]	Component of Response	Upstream Foundation		Downstream Foundation		Top of Upstream End Wall		Top of Downstream End Wall		Midspan of Road Deck	
		Amplitude	Phase Angle, rad	Amplitude	Phase Angle, rad	Amplitude	Phase Angle, rad	Amplitude	Phase Angle, rad	Amplitude	Phase Angle, rad
90	Displacement along y-axis	3.585	0.817π	3.585	0.817π	4.570	0.787π	4.570	0.787π	5.018	0.787π
	Displacement along z-axis	Small	--	Small	--	Small	--	Small	--	Small	--
	Rotation about x-axis x 10^{-3}	4.077	0.675π	4.077	0.675π	4.154	0.677π	4.154	0.677π	4.154	0.677π
20	Displacement along y-axis	0.914	0.055π	0.914	0.055π	1.784	0.136π	1.784	0.136π	1.959	0.136π
	Displacement along z-axis	0.474	0.861π	0.474	0.860π	0.473	0.860π	0.473	0.860π	0.731	-0.123π
	Rotation about x-axis x 10^{-3}	3.742	0.218π	3.742	0.218π	3.773	0.218π	3.773	0.218π	3.773	0.218π
45	Displacement along y-axis	0.764	0.145π	0.764	0.145π	1.780	-1.693π	1.780	0.307π	1.954	-1.693π
	Displacement along z-axis	1.030	-0.994π	1.030	-0.994π	1.028	-0.994π	1.029	-0.994π	1.590	-1.978π
	Rotation about x-axis x 10^{-3}	4.768	-1.587π	4.768	0.413π	4.798	-1.588π	4.798	0.412π	4.798	-1.588π

Note: (1) R_{Ly} = Ratio of foundation length (70 ft) to wavelength of incident SV-wave

f = Excitation frequency (Hz)

(2) Amplitudes and phase angles of free-field motion are dependent on θ_V as shown in Figure 4-2.

AA10322

TABLE 4-2. (CONCLUDED)

Vertical Angle of Incidence, θ_V, deg (2)	Component of Response	Upstream Foundation		Downstream Foundation		Top of Upstream End Wall		Top of Downstream End Wall		Midspan of Road Deck	
		Amplitude	Phase Angle, rad	Amplitude	Phase Angle, rad	Amplitude	Phase Angle, rad	Amplitude	Phase Angle, rad	Amplitude	Phase Angle, rad
55	Displacement along y-axis	1.828	-0.721π	1.828	-0.721π	1.275	-0.840π	1.275	-0.840π	1.399	-0.840π
	Displacement along z-axis	1.373	0.870π	1.373	0.870π	1.371	0.870π	1.372	0.870π	2.120	-0.114π
	Rotation about x-axis x 10^{-3}	3.368	0.472π	3.368	0.472π	3.355	0.474π	3.355	0.474π	3.355	0.474π
60	Displacement along y-axis	5.134	0.822π	5.135	0.822π	6.481	0.792π	6.481	0.792π	7.116	0.792π
	Displacement along z-axis	0.104	0.147π	0.104	0.147π	0.104	0.147π	0.104	0.147π	0.160	-0.837π
	Rotation about x-axis x 10^{-3}	5.617	0.672π	5.617	0.672π	5.725	0.674π	5.725	0.674π	5.725	0.674π
65	Displacement along y-axis	3.005	0.798π	3.005	0.798π	4.036	0.744π	4.037	0.744π	4.432	0.744π
	Displacement along z-axis	0.592	0.984π	0.592	0.984π	0.591	0.984π	0.591	0.984π	0.914	Small
	Rotation about x-axis x 10^{-3}	4.690	0.594π	4.690	0.594π	4.754	0.596π	4.754	0.596π	4.754	0.596π

Note: (2) Amplitudes and phase angles of free-field motion are dependent on θ_V as shown in Figure 4-2.

TABLE 4-3. CASE 1 (θ_H = 90 DEG): RESONANT RESPONSE TO SV-WAVE EXCITATIONS AT R_{Ly} = 0.39 (f = 2.80 Hz)[1]

Vertical Angle of Incidence, θ_V, deg[2]	Component of Response	Upstream Foundation		Downstream Foundation		Top of Upstream End Wall		Top of Downstream End Wall		Midspan of Road Deck	
		Amplitude	Phase Angle, rad	Amplitude	Phase Angle, rad	Amplitude	Phase Angle, rad	Amplitude	Phase Angle, rad	Amplitude	Phase Angle, rad
90	Displacement along y-axis	2.557	0.977π	2.557	0.977π	2.821	0.972π	2.821	0.972π	2.940	0.972π
	All other displacements	Small	--	Small	--	Small	--	Small	--	Small	--
20	Displacement along x-axis	1.003	-0.660π	1.003	0.340π	0.083	0.465π	0.083	-0.535π	Small	--
	Displacement along y-axis	0.554	0.289π	0.554	0.289π	1.173	0.302π	1.173	0.302π	1.223	0.302π
	Displacement along z-axis	1.188	0.537π	1.188	0.537π	1.211	0.535π	1.211	0.535π	16.217	0.445π
45	Displacement along x-axis	1.817	-0.494π	1.817	-1.494π	0.151	-1.370π	0.151	-0.370π	Small	--
	Displacement along y-axis	0.143	0.396π	0.143	0.396π	0.870	-1.524π	0.870	0.476π	0.907	-1.524π
	Displacement along z-axis	2.152	-1.298π	2.152	-1.298π	2.194	-1.300π	2.194	-1.300π	29.369	-1.390π

AA10323

Note: (1) R_{Ly} = Ratio of foundation length (70 ft) to wavelength of incident SV-wave.

f = Excitation frequency (Hz)

(2) Amplitudes and phase angles of free-field motion are dependent on θ_V as shown in Figure 4-2.

TABLE 4-3. (CONCLUDED)

Vertical Angle of Incidence, θ_V, deg(2)	Component of Response	Upstream Foundation		Downstream Foundation		Top of Upstream End Wall		Top of Downstream End Wall		Midspan of Road Deck	
		Amplitude	Phase Angle, rad	Amplitude	Phase Angle, rad	Amplitude	Phase Angle, rad	Amplitude	Phase Angle, rad	Amplitude	Phase Angle, rad
55	Displacement along x-axis	2.268	-0.620π	2.268	0.380π	0.189	0.505π	0.188	-0.495π	Small	---
	Displacement along y-axis	1.853	-0.633π	1.853	-0.633π	1.339	-0.646π	1.339	-0.646π	1.396	-0.646π
	Displacement along z-axis	2.686	0.577π	2.686	0.577π	2.738	0.575π	2.738	0.575π	36.665	0.485π
60	Displacement along x-axis	0.130	-1.187π	0.130	-0.187π	0.011	-0.063π	0.011	0.938π	Small	--
	Displacement along y-axis	4.062	0.978π	4.062	0.978π	4.458	0.973π	4.458	0.973π	4.646	0.973π
	Displacement along z-axis	0.154	0.009π	0.154	0.009π	0.157	0.008π	0.157	0.008π	2.102	-0.083π
65	Displacement along x-axis	0.949	-0.514π	0.949	0.486π	0.079	0.611π	0.079	1.611π	Small	--
	Displacement along y-axis	2.390	0.972π	2.390	0.972π	2.656	0.940π	2.656	0.940π	2.768	0.940π
	Displacement along z-axis	1.124	0.683π	1.124	0.683π	1.146	0.681π	1.146	0.681π	15.346	0.591π

Note: (2) Amplitudes and phase angles of free-field motion are dependent on θ_V as shown in Figure 4-2.

TABLE 4-4. CASE 2 (θ_H = 0 DEG): RESONANT RESPONSE TO SV-WAVE EXCITATIONS AT R_{Lx} = 0.72 (f = 3.0 Hz)[1]

Vertical Angle of Incidence, θ_V, deg[2]	Component of Response	Upstream Foundation		Downstream Foundation		Top of Upstream End Wall		Top of Downstream End Wall		Midspan of Road Deck	
		Amplitude	Phase Angle, rad	Amplitude	Phase Angle, rad	Amplitude	Phase Angle, rad	Amplitude	Phase Angle, rad	Amplitude	Phase Angle, rad
90	Displacement along x-axis	5.886	0.563π	5.886	0.563π	34.913	0.559π	34.913	0.559π	35.120	0.559π
	Displacement along z-axis	0.343	1.792π	0.343	0.792π	0.357	1.782π	0.357	0.782π	Small	--
20	Displacement along x-axis	0.489	0.198π	0.925	-1.787π	4.215	-1.796π	4.115	0.202π	4.190	0.203π
	Displacement along z-axis	0.848	0.632π	0.734	-0.347π	0.855	0.629π	0.729	-0.341π	8.037	-1.688π
45	Displacement along x-axis	0.655	-0.538π	0.472	-0.554π	3.471	-0.432π	3.485	-0.432π	3.499	-0.432π
	Displacement along z-axis	1.570	-1.031π	1.548	-2.030π	1.574	-1.032π	1.551	-2.030π	0.712	-1.274π
55	Displacement along x-axis	0.518	-1.111π	0.947	-1.449π	2.959	-1.501π	3.173	-1.492π	3.084	-1.496π
	Displacement along z-axis	1.695	1.087π	1.962	-0.159π	1.695	1.092π	1.986	-0.161π	17.375	-0.366π
60	Displacement along x-axis	3.213	0.245π	5.417	0.178π	25.296	0.198π	25.636	0.199π	25.617	0.199π
	Displacement along z-axis	1.870	-0.803π	1.525	-0.859π	1.922	-0.801π	1.548	-0.855π	24.976	-0.686π
65	Displacement along x-axis	2.706	0.275π	3.889	0.193π	20.097	0.220π	20.249	0.222π	20.293	0.221π
	Displacement along z-axis	1.605	1.197π	0.209	-1.140π	1.633	1.200π	0.198	-1.121π	13.988	-0.541π

AA10324

Note: (1) R_{Lx} = Ratio of bridge span length (120 ft) to wavelength of incident SV-wave.

f = Excitation frequency (Hz)

(2) Amplitudes and phase angles of free-field motion are dependent on θ_V as shown in Figure 4-2.

TABLE 4-5. CASE 2 (θ_H = 0 DEG): RESONANT RESPONSE TO SV-WAVE EXCITATIONS AT R_{Lx} = 0.67 (f = 2.8 Hz)(1)

Vertical Angle of Incidence, θ_V, deg(2)	Component of Response	Upstream Foundation		Downstream Foundation		Top of Upstream End Wall		Top of Downstream End Wall		Midspan of Road Deck	
		Amplitude	Phase Angle, rad	Amplitude	Phase Angle, rad	Amplitude	Phase Angle, rad	Amplitude	Phase Angle, rad	Amplitude	Phase Angle, rad
90	Displacement along x-axis	3.873	0.891π	3.873	0.891π	13.979	0.890π	13.979	0.890π	14.052	0.890π
	Displacement along z-axis	0.065	2.024π	0.065	1.024π	0.071	2.012π	0.071	1.012π	Small	--
20	Displacement along x-axis	0.926	-0.119π	1.402	-1.232π	1.005	-1.402π	0.874	0.558π	0.943	0.580π
	Displacement along z-axis	1.945	0.755π	0.473	-0.909π	1.971	0.756π	0.490	-0.921π	17.674	-1.181π
45	Displacement along x-axis	0.160	-0.395π	0.342	-0.080π	1.648	-0.076π	1.632	-0.079π	1.649	-0.078π
	Displacement along z-axis	1.407	-1.014π	1.652	-1.970π	1.407	-1.014π	1.658	-1.970π	2.129	-1.927π
55	Displacement along x-axis	3.919	-0.884π	2.664	-1.757π	1.925	-1.146π	2.260	-1.098π	2.097	-1.120π
	Displacement along z-axis	1.257	0.199π	4.348	0.040π	1.320	0.195π	4.414	0.041π	45.652	0.119π
60	Displacement along x-axis	6.960	0.752π	4.138	0.125π	11.606	0.548π	12.054	0.559π	11.889	0.553π
	Displacement along z-axis	3.486	-0.322π	3.438	-0.322π	3.572	-0.320π	3.515	-0.319π	60.027	-0.204π
65	Displacement along x-axis	4.258	0.815π	3.126	0.252π	8.709	0.569π	8.839	0.579π	8.818	0.574π
	Displacement along z-axis	1.343	1.743π	1.855	-0.041π	1.385	1.749π	1.902	-0.041π	33.576	-0.052π

AA10325

Note: (1) R_{Lx} = Ratio of bridge span length (120 ft) to wavelength of incident SV-wave.

f = Excitation frequency (Hz)

(2) Amplitudes and phase angles of free-field motion are dependent on θ_V as shown in Figure 4-2.

TABLE 4-6. CASE 2 (θ_H = 0 DEG): RESPONSE OF BRIDGE TO FREE FIELD SV-WAVE EXCITATIONS OF EQUAL AMPLITUDE AND EQUAL PHASE AT THE TWO FOUNDATIONS

Vertical Angle of Incidence, θ_V, deg (1)	Excitation Frequency (2)		Component of Response	Upstream Foundation		Downstream Foundation		Top of Upstream End Wall		Top of Downstream End Wall		Midspan of Road Deck	
	R_{Lx}	f, Hz		Amplitude	Phase Angle, rad	Amplitude	Phase Angle, rad	Amplitude	Phase Angle, rad	Amplitude	Phase Angle, rad	Amplitude	Phase Angle, rad
20	$\frac{1.0}{\cos 20 \text{ deg}}$ (1.06)	4.43	Displacement along x-axis	0.363	0.501π	0.210	-3.747π	0.735	-2.613π	0.732	-0.622π	0.743	-0.618π
			Displacement along z-axis	0.943	0.794π	0.950	-1.174π	0.943	0.794π	0.950	-1.173π	1.209	-2.175π
	$\frac{2.0}{\cos 20 \text{ deg}}$ (2.13)	8.87	Displacement along x-axis	0.397	0.304π	0.228	-5.784π	0.173	-2.487π	0.172	-0.508π	0.182	-0.497π
			Displacement along z-axis	1.209	0.636π	0.807	-3.238π	1.226	0.637π	0.808	-3.239π	0.528	-4.296π
	$\frac{3.0}{\cos 20 \text{ deg}}$ (3.19)	13.30	Displacement along x-axis	0.482	0.174π	0.461	-7.531π	0.158	-4.616π	0.159	-0.683π	0.178	-2.650π
			Displacement along z-axis	0.653	0.570π	1.058	-5.431π	0.679	0.568π	1.081	-5.430π	0.720	-6.399π
45	$\frac{1.0}{\cos 45 \text{ deg}}$ (1.41)	5.89	Displacement along x-axis	0.126	-1.044π	0.232	-2.422π	0.176	-0.439π	0.176	-0.492π	0.180	-0.466π
			Displacement along z-axis	1.585	-1.031π	1.604	-3.045π	1.589	-1.031π	1.608	-3.045π	1.187	-2.020π
	$\frac{2.0}{\cos 45 \text{ deg}}$ (2.83)	11.79	Displacement along x-axis	0.269	-1.164π	0.481	-4.549π	0.061	-0.255π	0.092	-2.289π	0.084	-2.275π
			Displacement along z-axis	1.532	-1.363π	1.296	-5.336π	1.564	-1.363π	1.323	-5.337π	0.773	-4.347π
	$\frac{3.0}{\cos 45 \text{ deg}}$ (4.24)	17.68	Displacement along x-axis	1.129	-3.107π	0.771	-8.183π	0.060	-2.721π	0.136	-4.241π	0.095	-4.371π
			Displacement along z-axis	0.472	-1.372π	0.507	-7.443π	0.536	-1.401π	0.576	-7.464π	3.553	-6.670π
55	$\frac{1.0}{\cos 55 \text{ deg}}$ (1.74)	7.26	Displacement along x-axis	1.908	-0.657π	1.994	-2.628π	0.305	-3.642π	0.317	-3.611π	0.322	-3.627π
			Displacement along z-axis	2.130	0.770π	2.401	-1.207π	2.143	0.769π	2.415	-1.207π	1.346	-0.219π
	$\frac{2.0}{\cos 55 \text{ deg}}$ (3.49)	14.53	Displacement along x-axis	2.949	-0.807π	2.082	-4.711π	0.227	-5.774π	0.313	-5.843π	0.311	-5.814π
			Displacement along z-axis	2.004	0.421π	1.547	-3.658π	2.066	0.421π	1.621	-3.659π	1.909	-0.664π
	$\frac{3.0}{\cos 55 \text{ deg}}$ (5.23)	21.79	Displacement along x-axis	1.830	-0.927π	2.318	-7.073π	0.274	-8.185π	0.110	-5.972π	0.261	-8.125π
			Displacement along z-axis	1.491	0.552π	1.229	-5.445π	1.544	0.552π	1.259	-5.448π	1.610	-3.424π

AA10326

Note: (1) Amplitudes and phase angles of free-field motion are dependent on θ_V as shown in Figure 4-2.

(2) R_{Lx} = Ratio of bridge span length (120 ft) to wavelength of incident SV-wave.

f = Excitation frequency (Hz)

TABLE 4-6. (CONCLUDED)

Vertical Angle of Incidence, θ_V, deg (1)	Excitation Frequency (2)		Component of Response	Upstream Foundation		Downstream Foundation		Top of Upstream End Wall		Top of Downstream End Wall		Midspan of Road Deck	
	R_{Lx}	f, Hz		Amplitude	Phase Angle, rad	Amplitude	Phase Angle, rad	Amplitude	Phase Angle, rad	Amplitude	Phase Angle, rad	Amplitude	Phase Angle, rad
60	$\frac{1.0}{\cos 60\ deg}$ (2.00)	8.33	Displacement along x-axis	3.437	-1.115π	3.455	-1.114π	0.614	-1.802π	0.615	0.198π	0.643	0.198π
			Displacement along z-axis	1.652	-2.690π	1.865	-1.702π	1.700	-2.684π	1.913	-1.696π	0.059	-0.781π
	$\frac{2.0}{\cos 60\ deg}$ (4.00)	16.67	Displacement along x-axis	4.247	-1.209π	4.211	-3.205π	0.459	-4.212π	0.459	-0.211π	0.558	-0.211π
			Displacement along z-axis	0.422	-3.939π	0.337	-4.788π	0.424	-5.930π	0.342	-4.765π	0.251	-1.224π
	$\frac{3.0}{\cos 60\ deg}$ (6.00)	25.00	Displacement along x-axis	2.527	-1.419π	2.547	-5.261π	0.226	-6.236π	0.222	-0.624π	0.291	-2.428π
			Displacement along z-axis	0.121	-6.837π	0.297	-6.311π	0.122	-8.851π	0.326	-6.302π	0.209	-2.753π
65	$\frac{1.0}{\cos 65\ deg}$ (2.37)	9.86	Displacement along x-axis	1.811	-1.068π	1.876	-1.059π	0.565	-1.905π	0.550	0.100π	0.595	-1.903π
			Displacement along z-axis	1.856	0.777π	0.415	-4.647π	1.879	0.782π	0.390	-4.642π	0.518	-2.143π
	$\frac{2.0}{\cos 65\ deg}$ (4.73)	19.72	Displacement along x-axis	2.479	-1.336π	2.506	-3.262π	0.250	-4.305π	0.283	-0.378π	0.351	-4.344π
			Displacement along z-axis	0.174	0.798π	0.548	-7.342π	0.178	0.786π	0.550	-7.347π	0.734	-5.196π
	$\frac{3.0}{\cos 65\ deg}$ (7.10)	29.58	Displacement along x-axis	1.609	-1.350π	1.683	-5.374π	0.154	-6.318π	0.123	-1.159π	0.079	-6.607π
			Displacement along z-axis	0.262	-0.080π	0.786	-9.252π	0.230	0.023π	0.764	-9.241π	0.214	-7.308π

Note: (1) Amplitudes and phase angles of free-field motion are dependent on θ_V as shown in Figure 4-2.

(2) R_{Lx} = Ratio of bridge span length (120 ft) to wavelength of incident SV-wave.

f = Excitation frequency (Hz)

TABLE 4-7. CASE 2 (θ_H = 0 DEG): RESPONSE OF BRIDGE TO FREE FIELD SV-WAVE EXCITATIONS OF EQUAL AMPLITUDE AND OPPOSITE PHASE AT THE TWO FOUNDATIONS

Vertical Angle of Incidence, ε_V, deg (1)	Excitation Frequency (2)		Component of Response	Upstream Foundation		Downstream Foundation		Top of Upstream End Wall		Top of Downstream End Wall		Midspan of Road Deck	
	R_{Lx}	f, Hz		Amplitude	Phase Angle, rad	Amplitude	Phase Angle, rad	Amplitude	Phase Angle, rad	Amplitude	Phase Angle, rad	Amplitude	Phase Angle, rad
20	$\frac{0.5}{\cos 20\ deg}$ (0.53)	2.22	Displacement along x-axis	0.423	0.308π	0.449	-0.651π	0.363	-0.201π	0.363	-0.206π	0.364	-0.204π
			Displacement along z-axis	0.967	0.829π	0.941	-0.196π	0.968	0.829π	0.942	-0.196π	1.334	-0.679π
	$\frac{1.5}{\cos 20\ deg}$ (1.60)	6.65	Displacement along x-axis	0.342	0.367π	0.408	-4.613π	0.112	-2.277π	0.135	-0.359π	0.126	-0.322π
			Displacement along z-axis	1.090	0.666π	1.111	-2.285π	1.103	0.665π	1.122	-2.284π	0.193	-3.567π
	$\frac{2.5}{\cos 20\ deg}$ (2.66)	11.09	Displacement along x-axis	0.730	0.359π	0.240	-6.845π	0.084	-3.156π	0.113	-0.932π	0.100	-1.027π
			Displacement along z-axis	0.756	0.736π	0.940	-4.300π	0.756	0.735π	0.943	-4.300π	0.244	-5.620π
45	$\frac{0.5}{\cos 45\ deg}$ (0.71)	2.95	Displacement along x-axis	0.530	-0.386π	0.401	-0.360π	2.987	-0.267π	2.997	-0.267π	3.009	-0.267π
			Displacement along z-axis	1.570	-1.022π	1.537	-2.013π	1.574	-1.023π	1.539	-2.013π	0.438	-1.118π
	$\frac{1.5}{\cos 45\ deg}$ (2.12)	8.84	Displacement along x-axis	0.984	-0.941π	0.833	-3.029π	0.445	-0.573π	0.467	-0.565π	0.481	-0.569π
			Displacement along z-axis	0.625	-1.451π	0.599	-4.490π	0.660	-1.466π	0.637	-4.504π	0.024	-3.459π
	$\frac{2.5}{\cos 45\ deg}$ (3.54)	14.73	Displacement along x-axis	0.451	-1.529π	0.505	-5.726π	0.074	-0.906π	1.105	-2.637π	0.098	-2.743π
			Displacement along z-axis	1.099	-1.251π	1.223	-6.283π	1.121	-1.251π	1.252	-6.284π	0.283	-5.409π
55	$\frac{0.5}{\cos 55\ deg}$ (0.87)	3.63	Displacement along x-axis	1.368	-0.620π	1.449	-1.577π	0.505	-2.977π	0.490	-3.033π	0.500	-3.005π
			Displacement along z-axis	1.956	0.903π	1.727	-0.196π	1.959	0.905π	1.735	-0.197π	3.205	-0.542π
	$\frac{1.5}{\cos 55\ deg}$ (2.62)	10.90	Displacement along x-axis	1.765	-0.753π	2.704	-3.652π	0.230	-4.934π	0.156	-5.076π	0.204	-4.991π
			Displacement along z-axis	1.659	0.779π	1.680	-2.264π	1.659	0.779π	1.682	-2.266π	0.454	-0.705π
	$\frac{2.5}{\cos 55\ deg}$ (4.36)	18.16	Displacement along x-axis	1.378	-0.869π	2.017	-5.917π	0.151	-7.031π	0.071	-6.316π	0.076	-6.878π
			Displacement along z-axis	1.148	0.655π	0.964	-4.669π	1.162	0.659π	1.035	-4.664π	1.919	-1.451π

AA10327

Note: (1) Amplitudes and phase angles of free-field motion are dependent on θ_V as shown in Figure 4-2.

(2) R_{Lx} = Ratio of bridge span length (120 ft) to wavelength of incident SV-wave.

f = Excitation frequency (Hz)

TABLE 4-7. (CONCLUDED)

Vertical Angle of Incidence, θ_V, deg (1)	Excitation Frequency (2)		Component of Response	Upstream Foundation		Downstream Foundation		Top of Upstream End Wall		Top of Downstream End Wall		Midspan of Road Deck	
	R_{Lx}	f, Hz		Amplitude	Phase Angle, rad	Amplitude	Phase Angle, rad	Amplitude	Phase Angle, rad	Amplitude	Phase Angle, rad	Amplitude	Phase Angle, rad
60	$\frac{0.5}{\cos 60\ deg}$ (1.00)	4.17	Displacement along x-axis	2.909	-0.983π	2.911	0.017π	0.089	-0.986π	0.088	0.061π	0.007	0.571π
			Displacement along z-axis	0.445	-1.268π	0.376	-1.201π	0.452	-1.262π	0.385	-1.194π	4.012	-0.941π
	$\frac{1.5}{\cos 60\ deg}$ (3.00)	12.50	Displacement along x-axis	4.397	-1.112π	4.431	-2.114π	0.169	-3.133π	0.189	-0.097π	0.016	0.135π
			Displacement along z-axis	0.403	-3.817π	0.121	-3.350π	0.408	-3.815π	0.125	-3.353π	1.337	-1.081π
	$\frac{2.5}{\cos 60\ deg}$ (5.00)	20.83	Displacement along x-axis	3.481	-1.317π	3.584	-4.317π	0.389	-5.346π	0.375	-0.356π	0.013	-1.123π
			Displacement along z-axis	0.859	-6.153π	0.730	-6.059π	0.837	-8.143π	0.713	-6.037π	2.568	-2.255π
65	$\frac{0.5}{\cos 65\ deg}$ (1.18)	4.93	Displacement along x-axis	1.760	-0.981π	1.790	0.012π	0.068	-1.126π	0.044	0.224π	0.031	-1.342π
			Displacement along z-axis	1.002	0.919π	0.771	-2.030π	1.012	0.919π	0.770	-2.030π	1.443	-0.969π
	$\frac{1.5}{\cos 65\ deg}$ (3.55)	14.79	Displacement along x-axis	2.469	-1.191π	2.475	-2.137π	0.139	-3.111π	0.120	-0.304π	0.046	-2.780π
			Displacement along z-axis	0.675	0.803π	0.469	-6.422π	0.688	0.804π	0.483	-6.423π	0.855	-3.242π
	$\frac{2.5}{\cos 65\ deg}$ (5.92)	24.65	Displacement along x-axis	1.821	-1.417π	1.702	-4.385π	0.422	-5.453π	0.418	-0.439π	0.015	-5.885π
			Displacement along z-axis	0.232	0.181π	0.468	-8.383π	0.263	0.221π	0.476	-8.381π	0.687	-6.392π

Note: (1) Amplitudes and phase angles of free-field motion are dependent on θ_V as shown in Figure 4-2.

(2) R_{Lx} = Ratio of bridge span length (120 ft) to wavelength of incident SV-wave.

f = Excitation frequency (Hz)

TABLE 4-8. CASE 3 (θ_H = 45 DEG): RESONANT RESPONSE TO INCIDENT SV-WAVES — SIDESWAY OF BRIDGE IN X-Z PLANE (R_{Lx} = 0.72, R_{Ly} = 0.42, f = 3.0 Hz)(1)

Vertical Angle of Incidence, θ_V, deg(2)	Component of Response	Upstream Foundation		Downstream Foundation		Top of Upstream End Wall		Top of Downstream End Wall		Midspan of Road Deck	
		Amplitude	Phase Angle, rad	Amplitude	Phase Angle, rad	Amplitude	Phase Angle, rad	Amplitude	Phase Angle, rad	Amplitude	Phase Angle, rad
90	Displacement along x-axis	4.162	0.563π	4.162	0.563π	24.688	0.559π	24.688	0.559π	24.835	0.559π
	Displacement along y-axis	1.903	0.970π	1.903	0.970π	2.135	0.963π	2.135	0.963π	2.239	0.963π
	Displacement along z-axis	0.243	1.792π	0.243	0.792π	0.252	1.782π	0.252	0.782π	small	--
	Rotation about z-axis x 10^{-3}	0.023	0.400π	0.023	-0.600π	0.116	0.963π	0.116	-0.037π	small	--
20	Displacement along x-axis	0.285	-0.662π	0.499	-0.675π	2.397	-0.574π	2.428	-0.573π	2.427	-0.574π
	Displacement along y-axis	0.350	0.285π	0.354	-0.656π	0.769	0.302π	0.775	-0.642π	0.069	-0.187π
	Displacement along z-axis	0.891	0.765π	0.837	-0.098π	0.895	0.763π	0.838	-0.097π	1.891	-1.456π
	Rotation about z-axis x 10^{-3}	0.564	-1.131π	0.533	-0.169π	1.058	-0.671π	1.057	-0.669π	1.068	-0.670π
45	Displacement along x-axis	0.362	-0.465π	0.996	-0.374π	4.153	-0.284π	4.099	-0.286π	4.151	-0.285π
	Displacement along y-axis	0.073	0.188π	0.067	-2.160π	0.560	0.443π	0.592	-0.198π	0.324	0.108π
	Displacement along z-axis	1.319	1.057π	1.339	0.178π	1.317	1.058π	1.345	0.176π	5.304	-0.219π
	Rotation about z-axis x 10^{-3}	0.055	-0.323π	0.054	-0.499π	0.670	-0.364π	0.668	-0.380π	0.676	-0.372π
55	Displacement along x-axis	1.627	-1.284π	1.079	-1.287π	7.389	-1.358π	7.585	-1.355π	7.531	-1.357π
	Displacement along y-axis	1.320	-0.652π	1.336	-1.204π	0.910	-0.684π	0.929	-1.205π	0.655	-0.948π
	Displacement along z-axis	1.179	1.099π	1.404	0.063π	1.170	1.107π	1.419	0.058π	16.588	-0.254π
	Rotation about z-axis x 10^{-3}	1.343	-0.098π	1.322	-0.706π	0.919	0.566π	0.914	-1.450π	0.930	0.558π
60	Displacement along x-axis	4.191	0.326π	5.344	0.297π	28.130	0.305π	28.317	0.306π	28.391	0.305π
	Displacement along y-axis	2.849	0.948π	2.926	0.491π	3.072	0.930π	3.183	0.497π	2.544	0.709π
	Displacement along z-axis	1.076	-0.670π	0.751	-0.788π	1.113	-0.668π	0.756	-0.784π	13.692	-0.585π
	Rotation about z-axis x 10^{-3}	2.276	-0.471π	2.237	-1.018π	2.700	0.234π	2.686	0.207π	2.726	0.220π
65	Displacement along x-axis	2.779	0.370π	3.366	0.281π	18.622	0.315π	18.690	0.316π	18.767	0.315π
	Displacement along y-axis	1.681	0.942π	1.749	0.562π	1.864	0.897π	1.937	0.539π	1.684	0.714π
	Displacement along z-axis	0.997	-0.742π	0.304	0.626π	1.013	-0.737π	0.296	0.617π	9.006	-0.352π
	Rotation about z-axis x 10^{-3}	1.113	-0.468π	1.092	-0.934π	1.394	0.246π	1.383	0.209π	1.405	0.228π

AA10328

Note: (1) R_{Lx} = Ratio of bridge span length (120 ft) to wavelength of incident SV-wave
R_{Ly} = Ratio of foundation length (70 ft) to wavelength of incident SV-wave
f = Excitation frequency (Hz)

(2) Amplitudes and phase angles of free-field motion are dependent on θ_V as shown in Figure 4-2.

TABLE 4-9. CASE 3 (θ_H = 45 DEG): RESONANT RESPONSE TO INCIDENT SV-WAVES — BENDING OF ROAD DECK IN X-Z PLANE (R_{Lx} = 0.67, R_{Ly} = 0.39, f = 2.80 Hz)(1)

Vertical Angle of Incidence, θ_V, deg (2)	Component of Response	Upstream Foundation		Downstream Foundation		Top of Upstream End Wall		Top of Downstream End Wall		Midspan of Road Deck	
		Amplitude	Phase Angle, rad	Amplitude	Phase Angle, rad	Amplitude	Phase Angle, rad	Amplitude	Phase Angle, rad	Amplitude	Phase Angle, rad
90	Displacement along x-axis	2.739	0.891π	2.739	0.891π	9.886	0.890π	9.886	0.890π	9.937	0.890π
	Displacement along y-axis	1.808	0.977π	1.808	0.977π	1.995	0.972π	1.995	0.972π	2.079	0.972π
	Displacement along z-axis	0.046	2.024π	0.046	1.024π	0.050	2.012π	0.050	1.012π	small	--
	Rotation about z-axis x 10^{-3}	0.019	0.478π	0.019	-0.522π	0.094	0.972π	0.094	-0.028π	small	--
20	Displacement along x-axis	0.386	0.016π	0.380	-0.586π	1.293	-0.223π	1.315	-0.220π	1.311	-0.222π
	Displacement along y-axis	0.348	0.284π	0.353	-0.578π	0.740	0.299π	0.750	-0.568π	0.160	-0.146π
	Displacement along z-axis	1.001	0.834π	0.682	-0.078π	1.006	0.834π	0.680	-0.079π	2.845	-0.945π
	Rotation about z-axis x 10^{-3}	0.524	-1.129π	0.498	-0.104π	1.002	-0.634π	1.001	-0.635π	1.011	-0.634π
45	Displacement along x-axis	0.782	-0.767π	1.152	0.132π	1.793	0.071π	1.675	0.052π	1.742	0.062π
	Displacement along y-axis	0.061	0.209π	0.056	-2.103π	0.523	0.449π	0.547	-0.148π	0.330	0.141π
	Displacement along z-axis	0.795	0.800π	2.230	0.253π	0.794	0.791π	2.255	0.253π	15.320	0.268π
	Rotation about z-axis x 10^{-3}	0.050	-0.296π	0.048	-0.465π	0.595	-0.336π	0.593	-0.353π	0.599	-0.344π
55	Displacement along x-axis	3.809	-0.843π	1.866	-1.662π	3.238	-1.016π	3.555	-0.989π	3.411	-1.002π
	Displacement along y-axis	1.316	-0.646π	1.325	-1.164π	0.929	-0.670π	0.941	-1.164π	0.691	-0.919π
	Displacement along z-axis	1.695	0.354π	3.894	0.194π	1.752	0.349π	3.956	0.195π	42.236	0.225π
	Rotation about z-axis x 10^{-3}	1.245	-0.099π	1.230	-0.667π	0.896	0.592π	0.893	-1.422π	0.908	0.585π
60	Displacement along x-axis	5.119	0.792π	2.931	0.394π	11.862	0.650π	12.109	0.656π	12.047	0.653π
	Displacement along y-axis	2.802	0.959π	2.849	0.526π	2.993	0.945π	3.065	0.531π	2.508	0.735π
	Displacement along z-axis	1.922	-0.219π	1.884	-0.226π	1.972	-0.217π	1.924	-0.223π	32.624	-0.110π
	Rotation about z-axis x 10^{-3}	2.105	-0.473π	2.081	-0.983π	2.514	0.255π	2.506	0.230π	2.540	0.243π
65	Displacement along x-axis	3.056	0.886π	2.591	0.422π	7.744	0.657π	7.759	0.666π	7.791	0.661π
	Displacement along y-axis	1.646	0.956π	1.690	0.593π	1.796	0.915π	1.846	0.570π	1.625	0.740π
	Displacement along z-axis	0.566	0.051π	1.307	0.200π	0.597	0.053π	1.339	0.200π	21.780	0.132π
	Rotation about z-axis x 10^{-3}	1.027	-0.471π	1.016	-0.904π	1.288	0.266π	1.281	0.233π	1.299	0.250π

AA10330

Note: (1) R_{Lx} = Ratio of bridge span length (120 ft) to wavelength of incident SV-wave

R_{Ly} = Ratio of foundation length (70 ft) to wavelength of incident SV-wave

f = Excitation frequency (Hz)

(2) Amplitudes and phase angles of free-field motion are dependent on θ_V as shown in Figure 4-2.

TABLE 4-10. CASE 3 (θ_H = 45 DEG): COUPLED THREE-DIMENSIONAL RESPONSE TO INCIDENT SV-WAVES AT EXCITATION FREQUENCY OF 4.17 Hz (R_{Lx} = 1.00, R_{Ly} = 0.58) (1)

Vertical Angle of Incidence, θ_V, deg (2)	Component of Response	Upstream Foundation		Downstream Foundation		Top of Upstream End Wall		Top of Downstream End Wall		Midspan of Road Deck	
		Amplitude	Phase Angle, rad	Amplitude	Phase Angle, rad	Amplitude	Phase Angle, rad	Amplitude	Phase Angle, rad	Amplitude	Phase Angle, rad
90	Displacement along x-axis	1.023	1.037π	1.023	1.037π	1.740	0.052π	1.740	0.052π	1.760	0.052π
	Displacement along y-axis	2.535	0.817π	2.535	0.817π	3.232	0.787π	3.232	0.787π	3.548	0.787π
	Displacement along z-axis	0.090	1.050π	0.090	0.050π	0.091	1.050π	0.091	0.050π	small	--
	Rotation about z-axis x 10^{-3}	0.074	-0.250π	0.074	-1.250π	0.351	0.787π	0.351	-0.213π	small	--
20	Displacement along x-axis	0.135	-1.572π	0.116	-0.910π	0.156	-0.255π	0.155	-0.306π	0.156	-0.280π
	Displacement along y-axis	0.675	0.260π	0.355	-1.328π	1.401	0.291π	0.831	-1.196π	0.880	-1.535π
	Displacement along z-axis	0.705	0.802π	0.773	-0.481π	0.707	0.801π	0.774	-0.481π	0.794	-1.795π
	Rotation about z-axis x 10^{-3}	0.757	-1.140π	0.710	-0.527π	1.103	-0.900π	1.184	-0.854π	1.155	-0.876π
45	Displacement along x-axis	0.035	-0.749π	0.062	-1.497π	0.163	-0.936π	0.164	-0.922π	0.165	-0.929π
	Displacement along y-axis	0.112	0.314π	0.112	-2.685π	0.800	0.468π	0.800	-0.532π	Small	--
	Displacement along z-axis	1.367	0.979π	1.374	-0.022π	1.371	0.979π	1.378	-0.022π	0.052	-1.341π
	Rotation about z-axis x 10^{-3}	0.074	-0.440π	0.085	-0.705π	1.098	-0.532π	1.098	-0.532π	1.113	-0.532π
55	Displacement along x-axis	0.885	-2.595π	0.927	-1.405π	0.135	-2.061π	0.134	-1.920π	0.133	-1.991π
	Displacement along y-axis	1.185	-0.666π	1.394	-1.456π	0.590	-0.755π	0.866	-1.488π	0.348	-1.255π
	Displacement along z-axis	1.778	0.885π	1.586	0.018π	1.782	0.886π	1.591	0.017π	1.863	-0.485π
	Rotation about z-axis x 10^{-3}	1.899	-0.104π	1.856	-0.931π	0.933	0.408π	0.890	-1.599π	0.927	0.405π
60	Displacement along x-axis	1.884	-0.958π	1.807	0.296π	1.213	-0.312π	1.219	-0.285π	1.229	-0.299π
	Displacement along y-axis	2.389	0.872π	3.630	0.250π	2.552	0.815π	4.242	0.247π	2.438	0.435π
	Displacement along z-axis	0.271	-1.215π	0.199	-0.905π	0.274	-1.208π	0.205	-0.901π	2.372	-0.798π
	Rotation about z-axis x 10^{-3}	3.308	-0.474π	3.141	-1.222π	3.817	0.109π	3.574	0.078π	3.751	0.094π
65	Displacement along x-axis	1.125	-0.966π	0.990	0.403π	0.979	-0.292π	0.967	-0.274π	0.984	-0.283π
	Displacement along y-axis	1.376	0.824π	2.286	0.326π	1.686	0.721π	2.816	0.294π	1.970	0.444π
	Displacement along z-axis	0.883	-1.031π	0.624	0.393π	0.887	-1.030π	0.621	0.393π	1.482	-0.612π
	Rotation about z-axis x 10^{-3}	1.649	-0.472π	1.517	-1.111π	2.111	0.128π	1.914	0.078π	2.039	0.105π

AA10329

Note: (1) R_{Lx} = Ratio of bridge span length (120 ft) to wavelength of incident SV-wave

R_{Ly} = Ratio of foundation length (70 ft) to wavelength of incident SV-wave

f = Excitation frequency (Hz)

(2) Amplitudes and phase angles of free-field motion are dependent on θ_V as shown in Figure 4-2.

TABLE 4-11. CASE 3 (θ_H = 45 DEG): ANTISYMMETRIC Y-DISPLACEMENT RESPONSE INDUCED BY OBLIQUELY INCIDENT SV-WAVES

Vertical Angle of Incidence, θ_V, deg[1]	Excitation Frequency[2]			Upstream Foundation		Downstream Foundation		Top of Upstream End Wall		Top of Downstream End Wall		Midspan of Road Deck	
	R_{Lx}[3]	R_{Ly}	f, Hz	Amplitude	Phase Angle, rad	Amplitude	Phase Angle, rad	Amplitude	Phase Angle, rad	Amplitude	Phase Angle, rad	Amplitude	Phase Angle, rad
20	0.75	0.44	3.14	0.354	0.288π	0.354	-0.713π	0.791	0.306π	0.791	-0.694π	0.003	-1.173π
45	1.00	0.58	4.17	0.112	0.314π	0.112	-2.685π	0.800	0.468π	0.800	-0.532π	Small	--
55	1.23	0.72	5.14	1.335	-0.666π	1.325	-1.665π	0.667	-0.748π	0.652	-1.749π	0.012	-2.365π
60	1.41	0.82	5.89	3.573	0.831π	3.554	-0.170π	4.188	0.801π	4.158	-0.199π	0.022	-0.770π
65	1.67	0.98	6.97	1.488	0.687π	1.472	-0.313π	2.141	0.599π	2.120	-0.403π	0.009	-0.922π

AA10331

Note: (1) Amplitudes and phase angles of free-field motion are dependent on θ_V as shown in Figure 4-2.

(2) R_{Lx} = Ratio of bridge span length (120 ft) to wavelength of incident SV-wave

R_{Ly} = Ratio of foundation length (70 ft) to wavelength of incident SV-wave

f = Excitation frequency (Hz)

(3) R_{Lx} as shown above corresponds to $\frac{0.5}{\cos 45 \text{ deg} \cos \theta_V}$

TABLE 4-12. CASE 3 (θ_H = 45 DEG): ANTISYMMETRIC Z-DISPLACEMENT RESPONSE INDUCED BY OBLIQUELY INCIDENT SV-WAVES

Vertical Angle of Incidence, θ_V, deg[1]	Excitation Frequency[2]			Upstream Foundation		Downstream Foundation		Top of Upstream End Wall		Top of Downstream End Wall		Midspan of Road Deck	
	R_{Lx}	R_{Ly}	f, Hz	Amplitude	Phase Angle, rad	Amplitude	Phase Angle, rad	Amplitude	Phase Angle, rad	Amplitude	Phase Angle, rad	Amplitude	Phase Angle, rad
20	0.59	0.35	2.46	0.864	0.815π	0.863	0.032π	0.865	0.815π	0.864	0.032π	0.114	0.126π
45	1.00	0.58	4.17	1.367	0.979π	1.374	-0.022π	1.371	0.979π	1.378	-0.022π	0.052	-1.341π
55	1.51	0.88	6.27	1.537	0.758π	1.799	-0.461π	1.551	0.758π	1.816	-0.461π	0.060	-0.252π
60	2.83	1.65	11.79	0.153	-3.472π	0.226	-2.341π	0.156	-3.452π	0.234	-2.328π	0.029	-1.138π

AA10332

Notes: (1) Amplitudes and phase angles of free-field motion are dependent on θ_V as shown in Figure 4-2.

(2) R_{Lx} = Ratio of bridge span length (120 ft) to wavelength of incident SV-wave

R_{Ly} = Ratio of foundation length (70 ft) to wavelength of incident SV-wave

f = Excitation frequency (Hz)

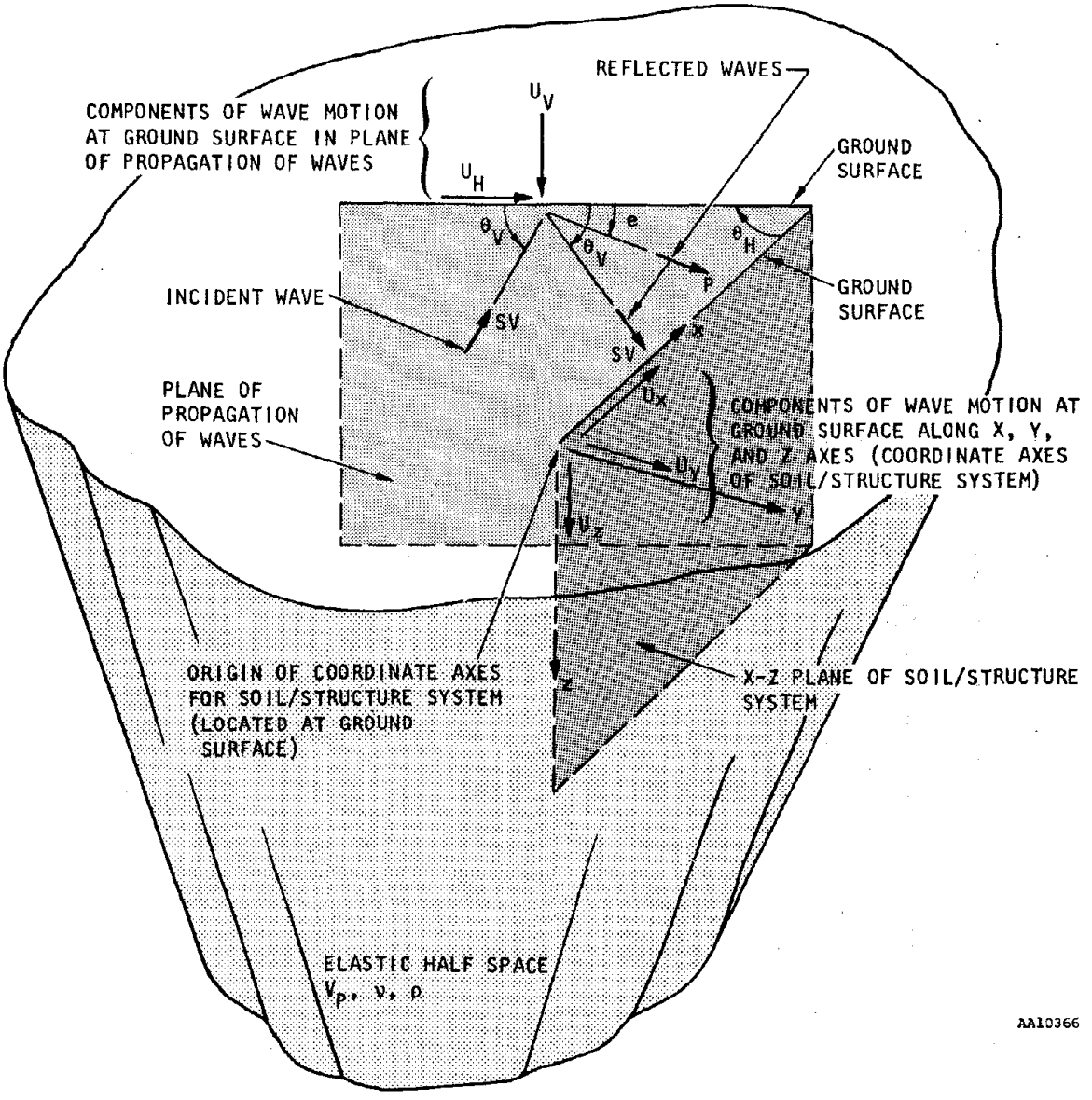

FIGURE 4-1. FREE-FIELD SV-WAVE GROUND MOTION

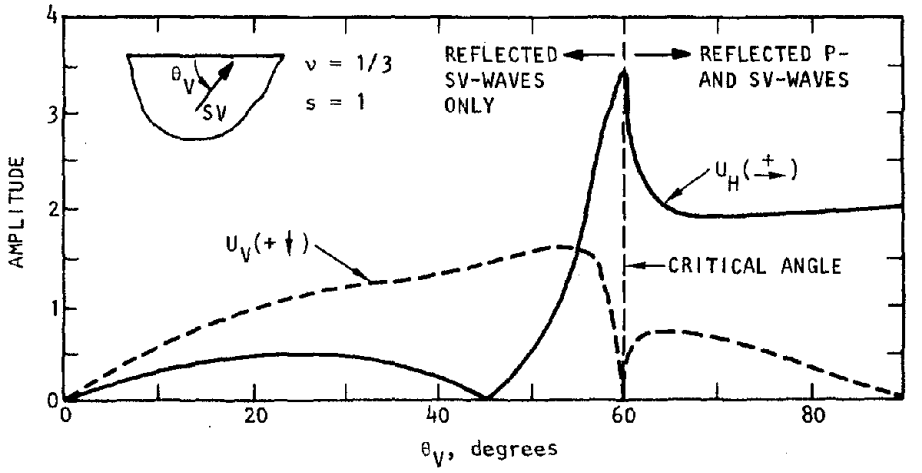

(a) Amplitude

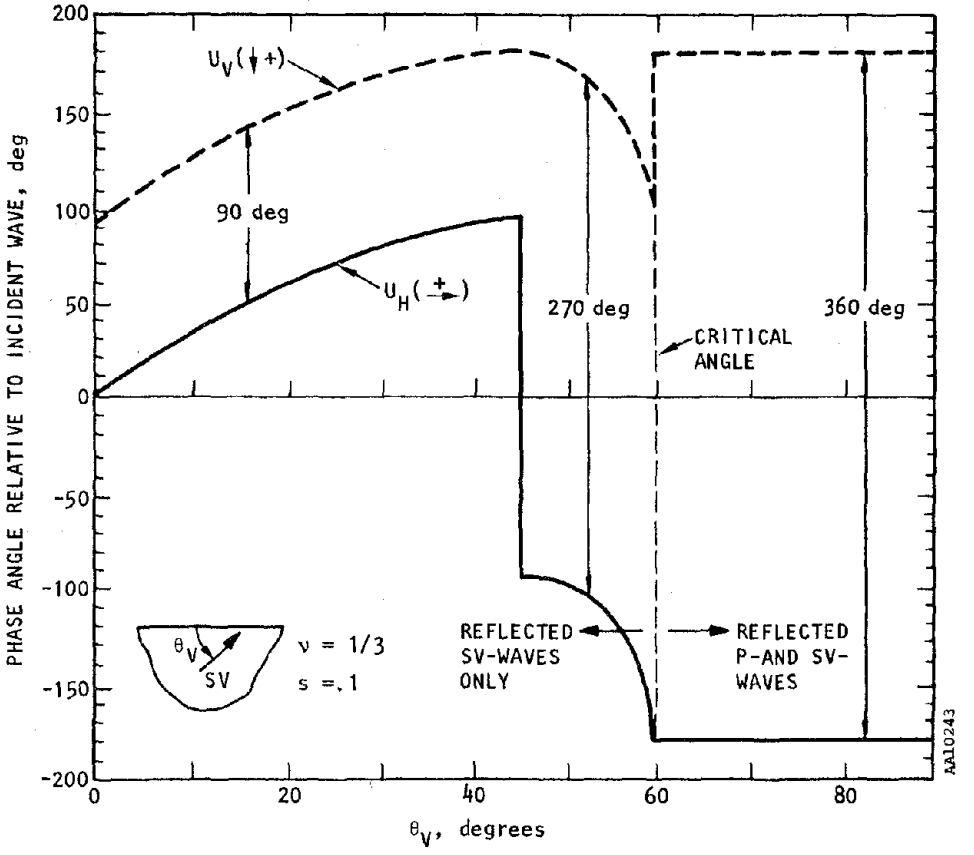

(b) Phase Angle

FIGURE 4-2. HORIZONTAL AND VERTICAL FREE-FIELD SV-WAVE GROUND SURFACE DISPLACEMENTS FOR POISSON'S RATIO = 1/3

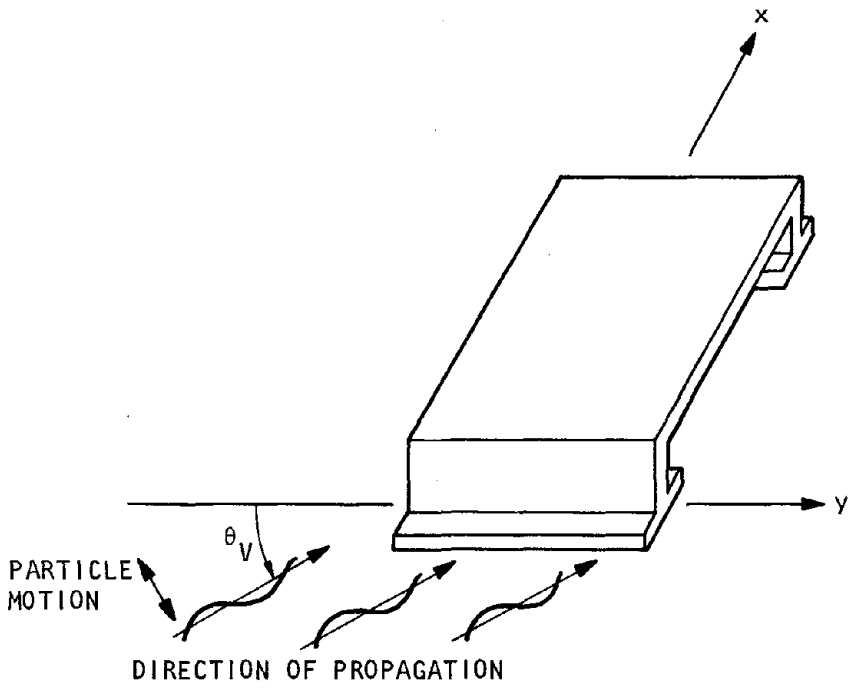

FIGURE 4-3. FREE-FIELD EXCITATIONS FROM INCIDENT SV WAVES FOR CASE 1 (θ_H = 90 deg)

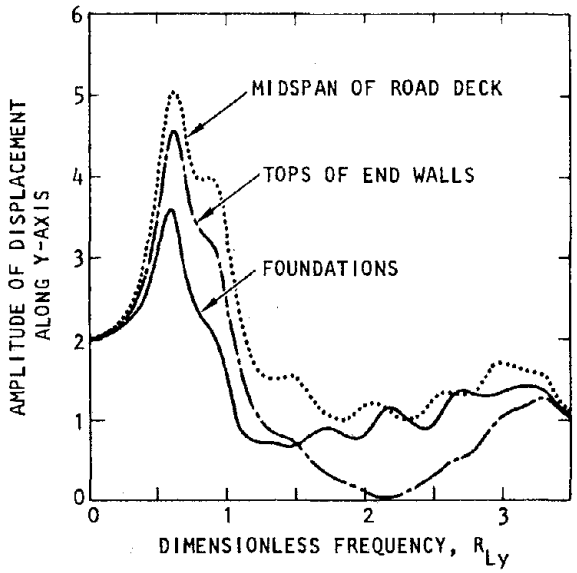

(a) Displacement along y-axis

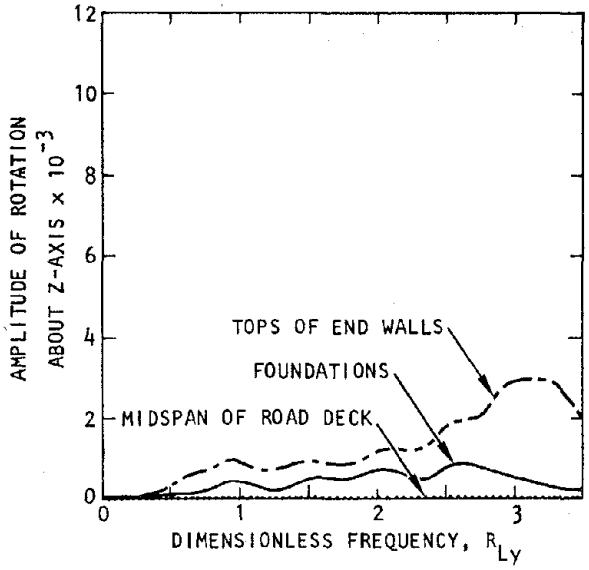

(b) Rotation about z-axis

FIGURE 4-4. FREQUENCY-DEPENDENT RESPONSE AMPLITUDES OF BRIDGE SUBJECTED TO INCIDENT SV-WAVES WITH $\theta_H = \theta_V = 90$ DEG

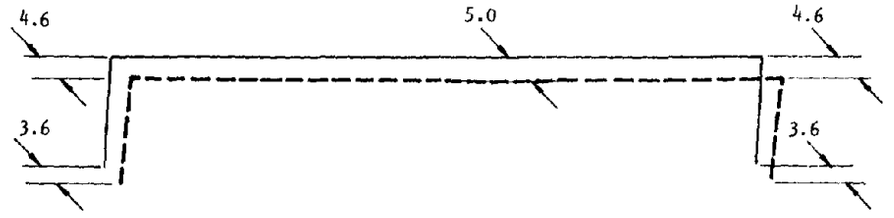

(a) θ_V = 90 deg

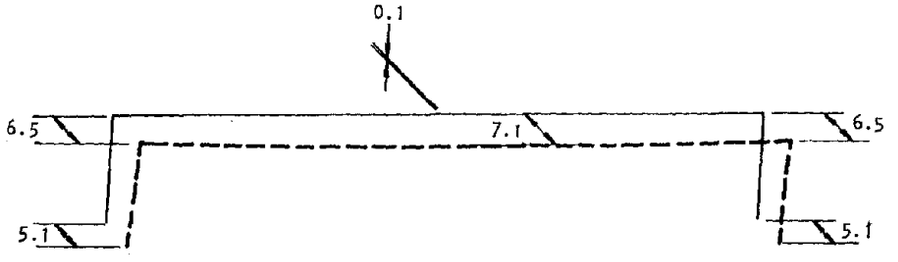

(b) θ_V = 60 deg

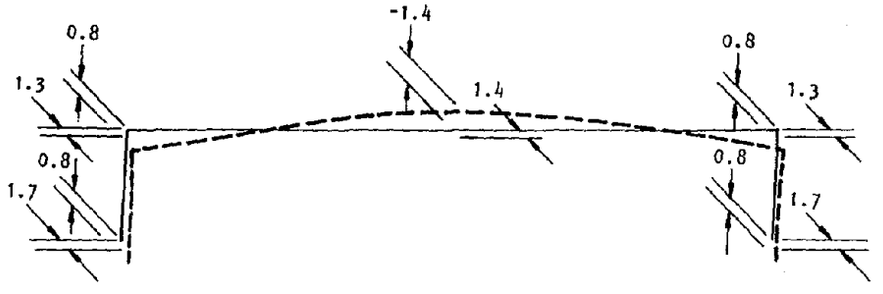

(c) θ_V = 55 deg

AA10260

FIGURE 4-5. CASE 1 (θ_H = 90 DEG): DEFORMED SHAPES OF BRIDGE AT TIMES OF PEAK RESONANT RESPONSE TO SV-WAVE EXCITATIONS (R_{Ly} = 0.58, f = 4.2 Hz)

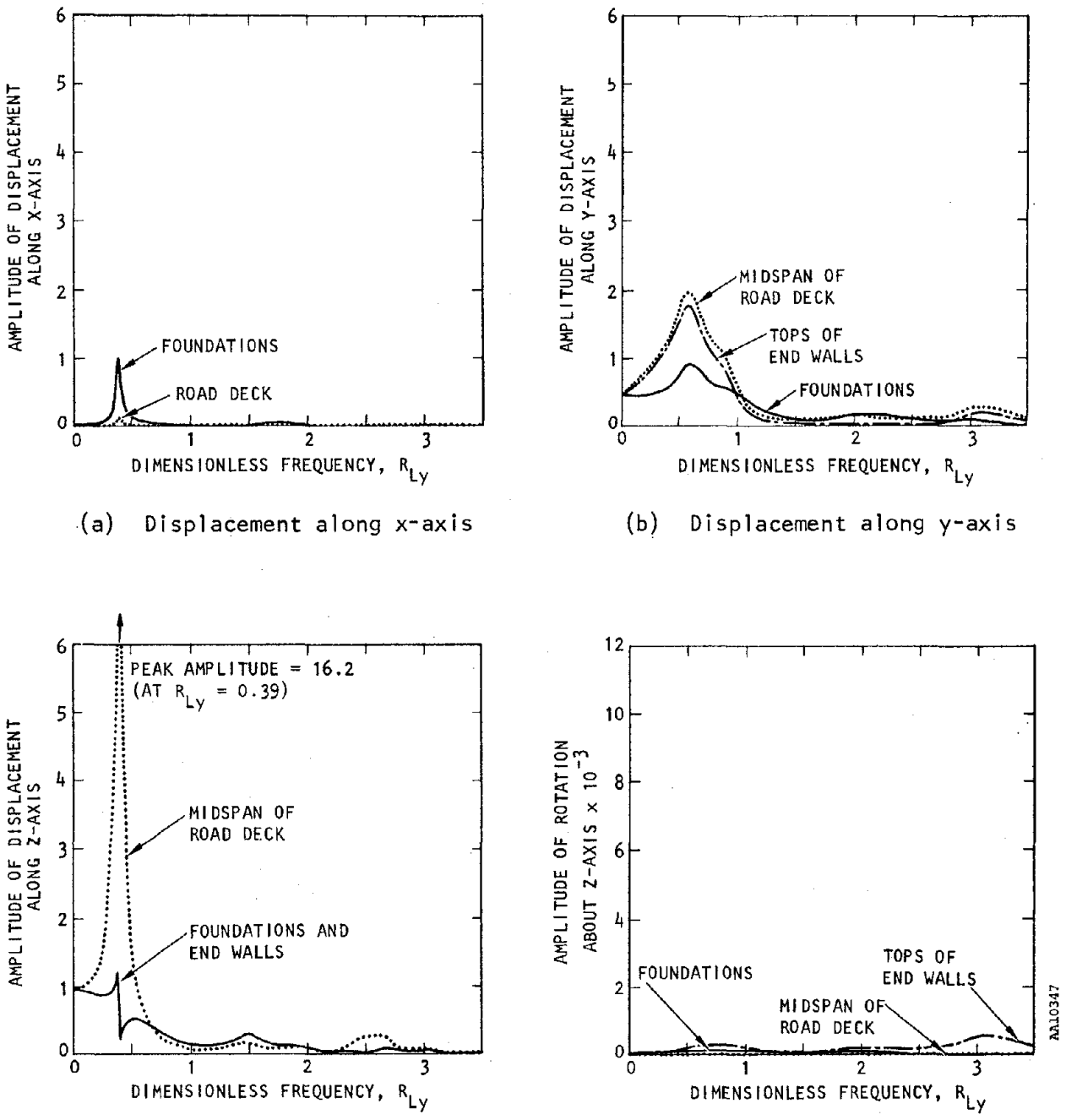

(a) Displacement along x-axis

(b) Displacement along y-axis

(c) Displacement along z-axis

(d) Rotation about z-axis

FIGURE 4-6. FREQUENCY-DEPENDENT RESPONSE AMPLITUDES OF BRIDGE SUBJECTED TO INCIDENT SV-WAVES WITH θ_H = 90 DEG, θ_V = 20 DEG

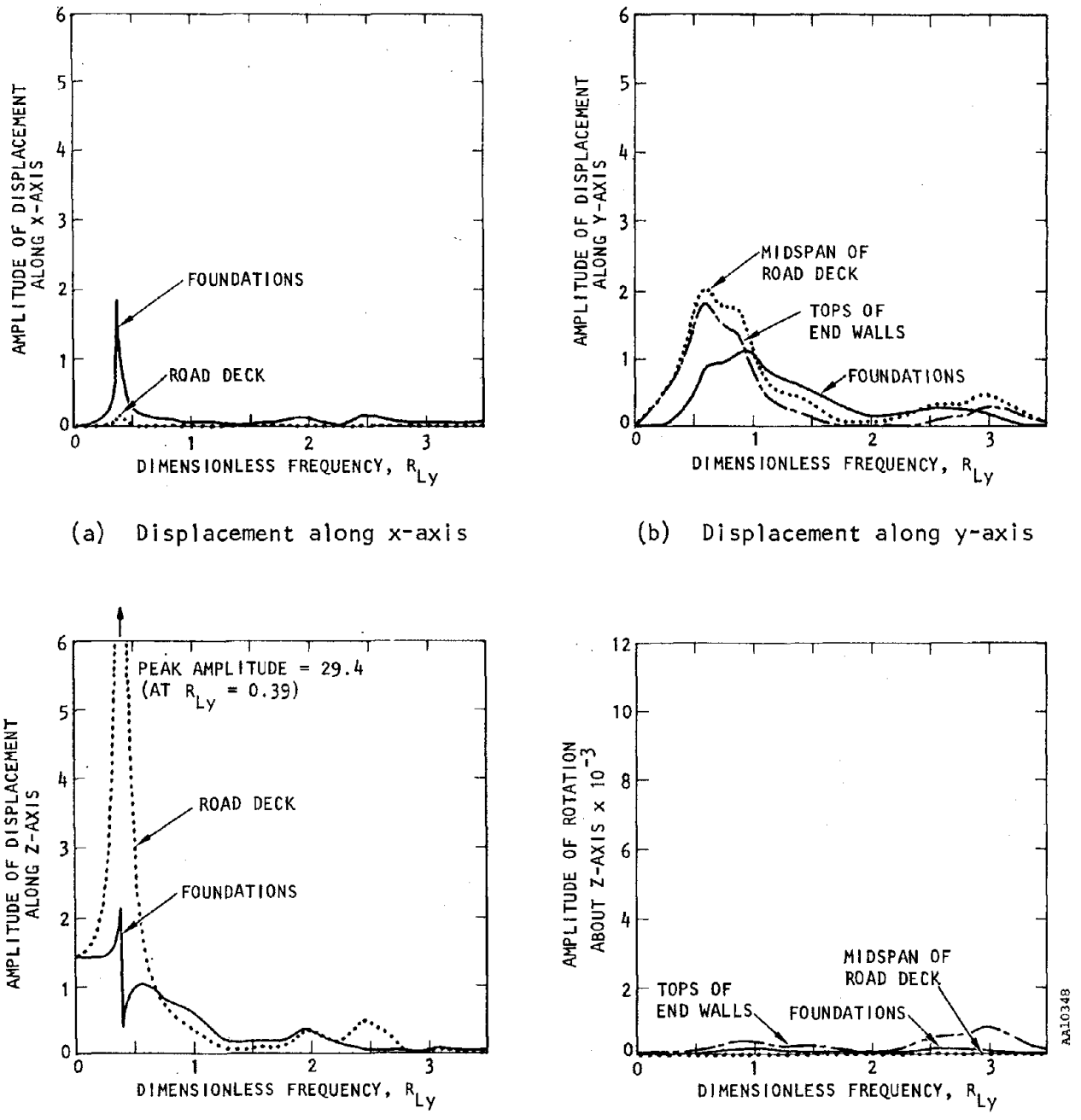

(a) Displacement along x-axis

(b) Displacement along y-axis

(c) Displacement along z-axis

(d) Rotation about z-axis

FIGURE 4-7. FREQUENCY-DEPENDENT RESPONSE AMPLITUDES OF BRIDGE SUBJECTED TO INCIDENT SV-WAVES WITH θ_H = 90 DEG, θ_V = 45 DEG

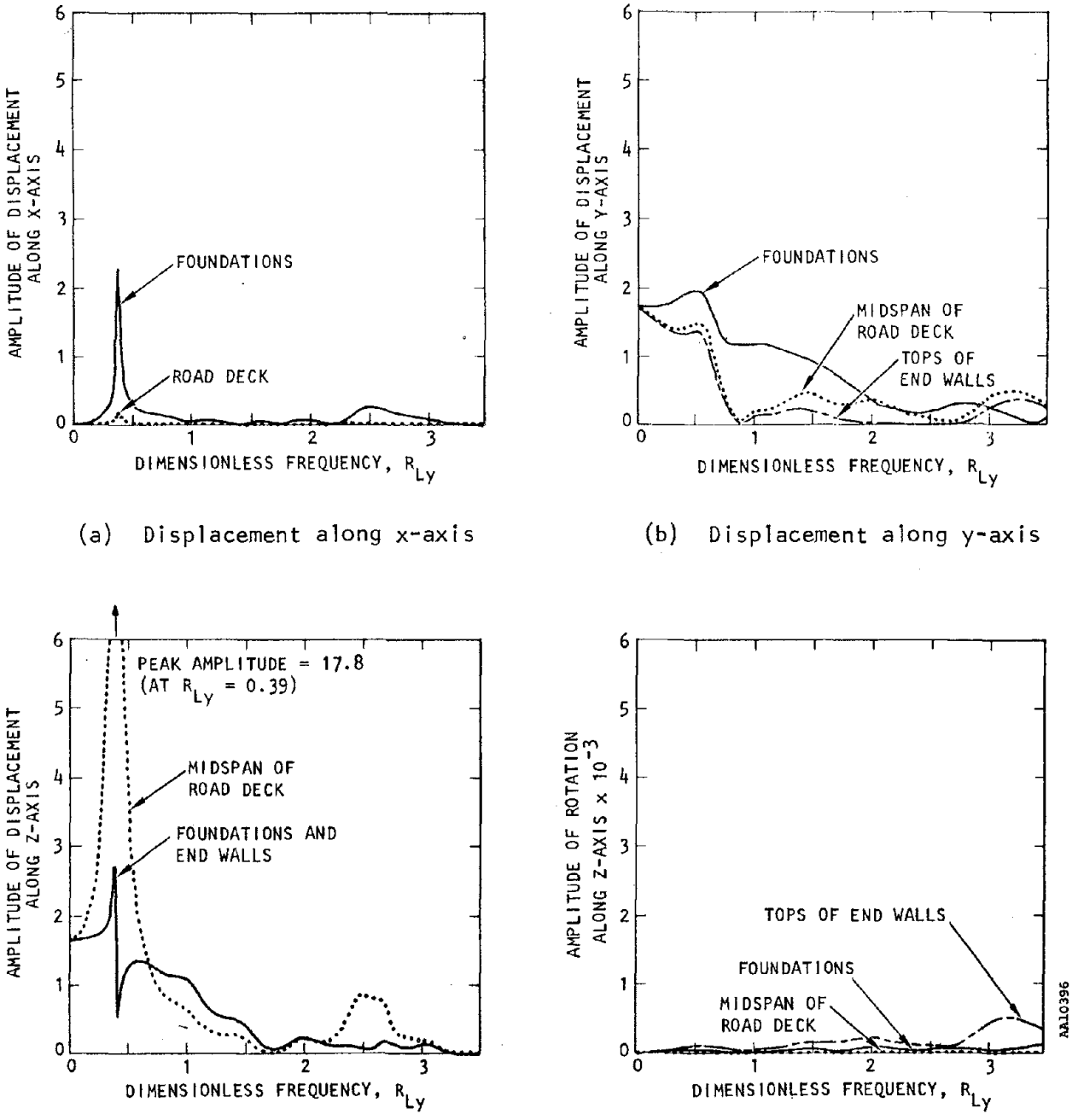

(a) Displacement along x-axis

(b) Displacement along y-axis

(c) Displacement along z-axis

(d) Rotation about z-axis

FIGURE 4-8. FREQUENCY-DEPENDENT RESPONSE AMPLITUDES OF BRIDGE SUBJECTED TO INCIDENT SV-WAVES WITH θ_H = 90 DEG, θ_V = 55 DEG

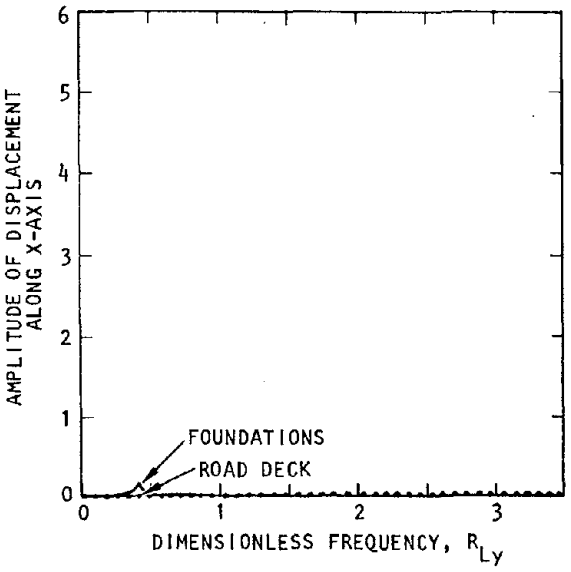

(a) Displacement along x-axis

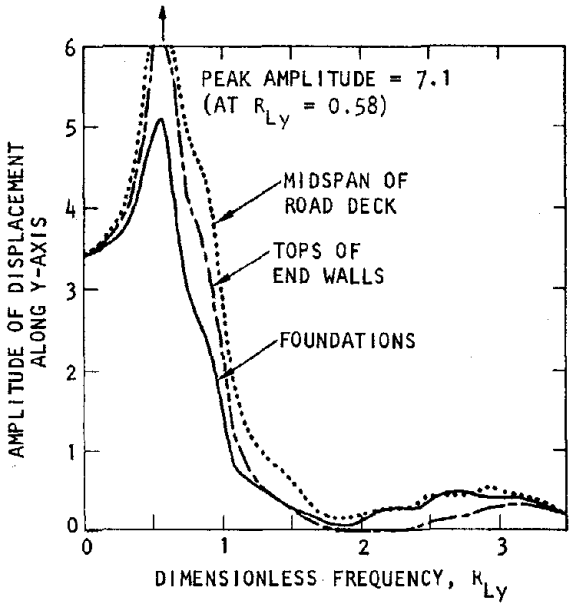

(b) Displacement along y-axis

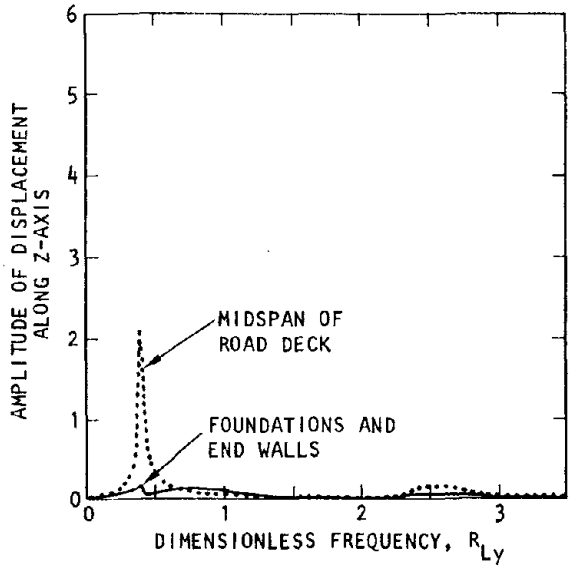

(c) Displacement along z-axis

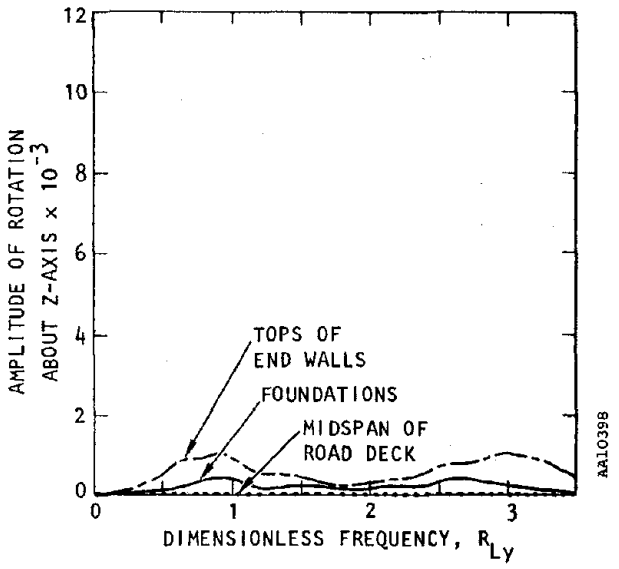

(d) Rotation about z-axis

FIGURE 4-9. FREQUENCY-DEPENDENT RESPONSE AMPLITUDES OF BRIDGE SUBJECTED TO INCIDENT SV-WAVES WITH θ_H = 90 DEG, θ_V = 60 DEG

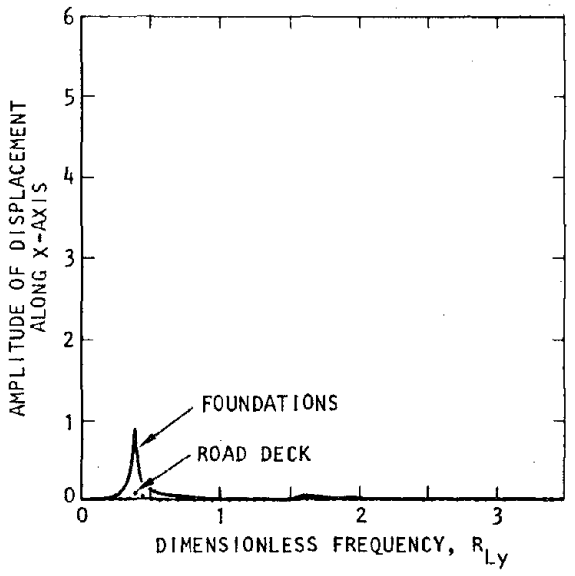

(a) Displacement along x-axis

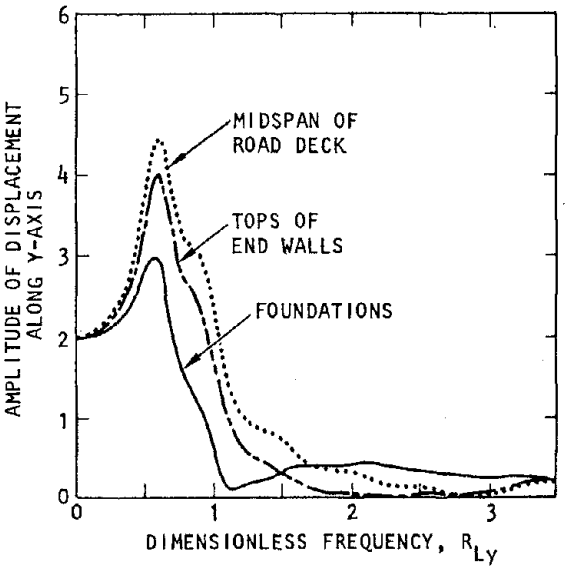

(b) Displacement along y-axis

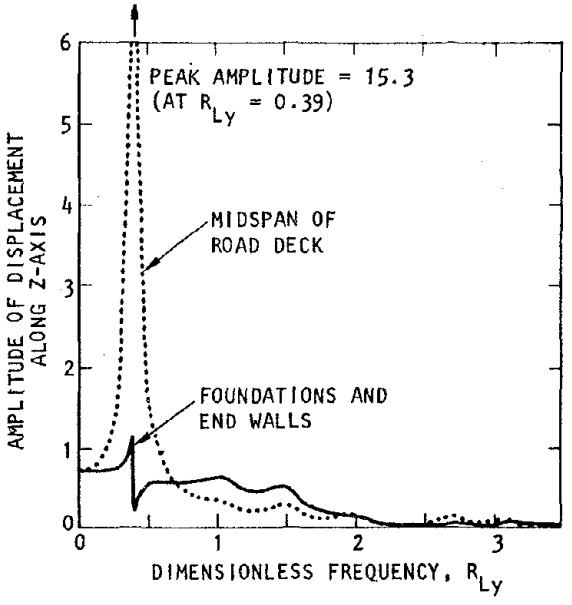

(c) Displacement along z-axis

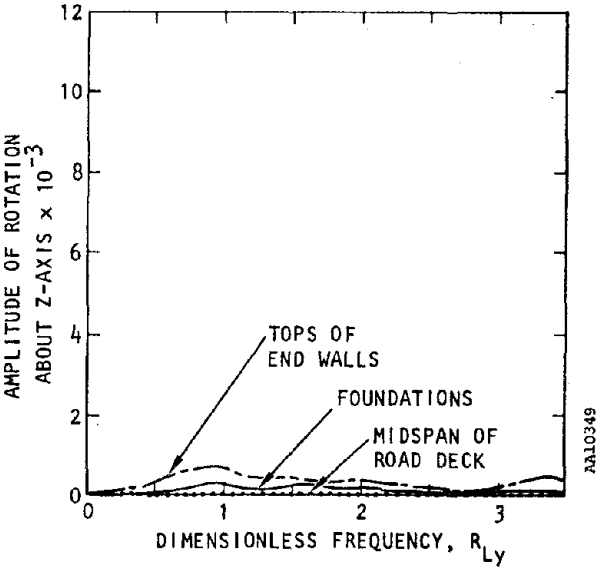

(d) Rotation about z-axis

FIGURE 4-10. FREQUENCY-DEPENDENT RESPONSE AMPLITUDES OF BRIDGE SUBJECTED TO INCIDENT SV-WAVES WITH θ_H = 90 DEG, θ_V = 65 DEG

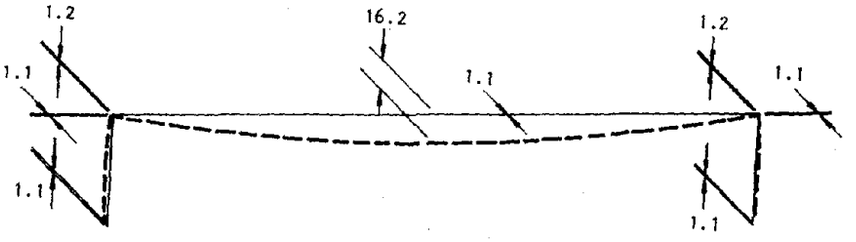

(a) θ_V = 20 deg

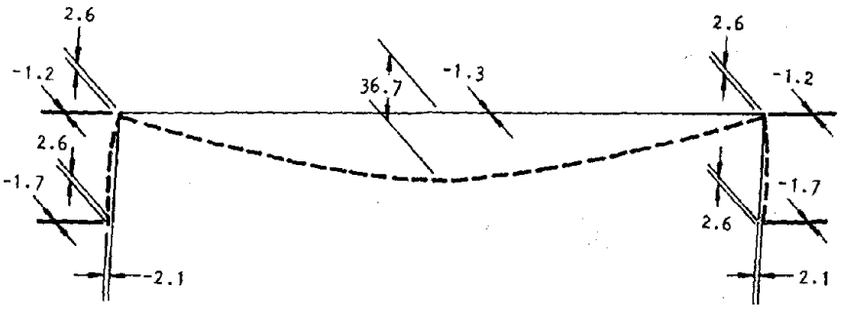

(b) θ_V = 55 deg

AA10261

FIGURE 4-11. CASE 1 (θ_H = 90 DEG): DEFORMED SHAPES OF BRIDGE AT TIMES OF PEAK RESONANT RESPONSE TO SV-WAVE EXCITATIONS (R_{Ly} = 0.39, f = 2.8 Hz)

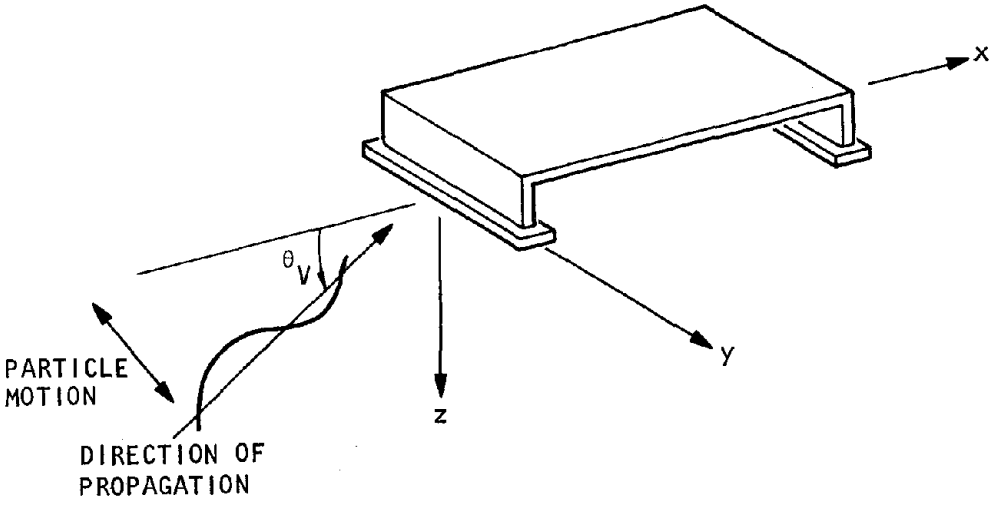

FIGURE 4-12. FREE-FIELD EXCITATIONS FROM INCIDENT SV-WAVES FOR CASE 2 (θ_H = 0 deg)

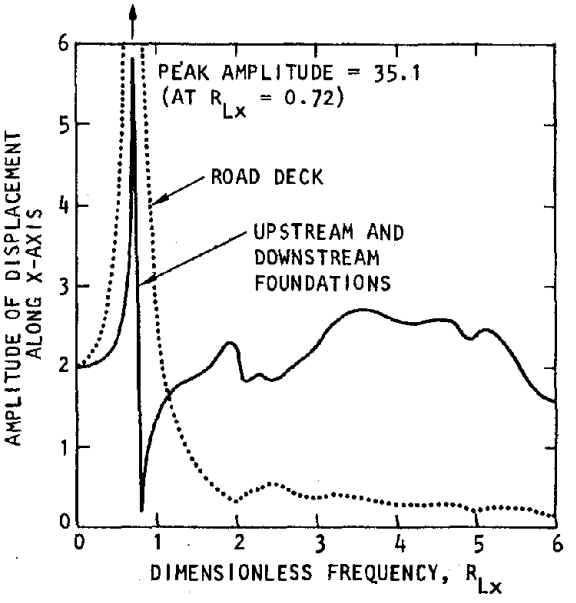

(a) Displacement along x-axis

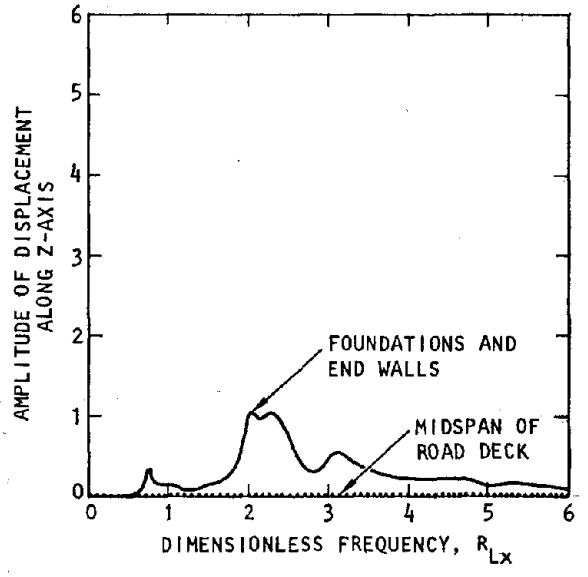

(b) Displacement along z-axis

FIGURE 4-13. FREQUENCY-DEPENDENT RESPONSE AMPLITUDES OF BRIDGE SUBJECTED TO INCIDENT SV-WAVES WITH θ_H = 0 DEG, θ_V = 90 DEG

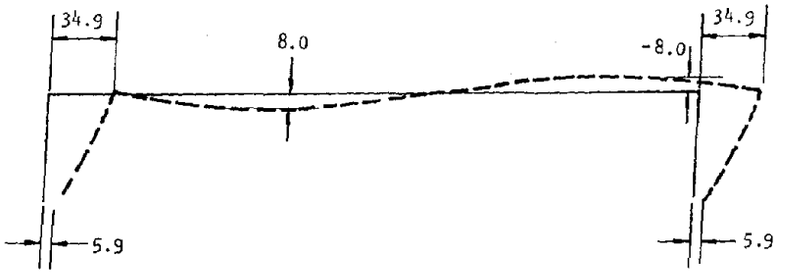

(a) θ_V = 90 deg

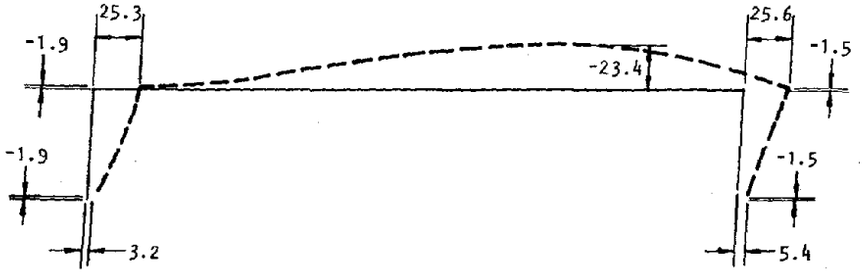

(b) θ_V = 60 deg

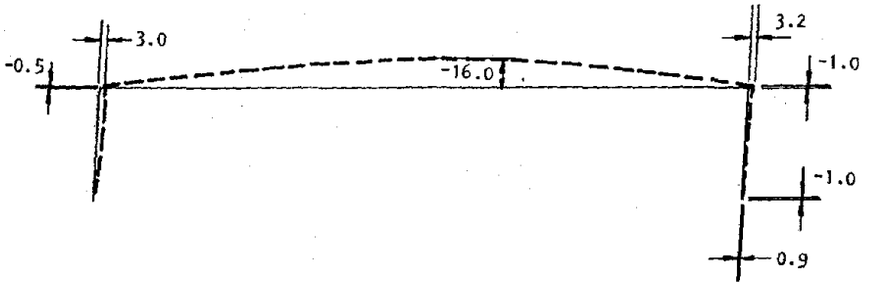

(c) θ_V = 55 deg

AA10262

FIGURE 4-14. CASE 2 (θ_H = 0 DEG): DEFORMED SHAPES AT TIMES OF PEAK RESONANT RESPONSE TO SV-WAVE EXCITATIONS (R_{Lx} = 0.72, f = 3.0 Hz)

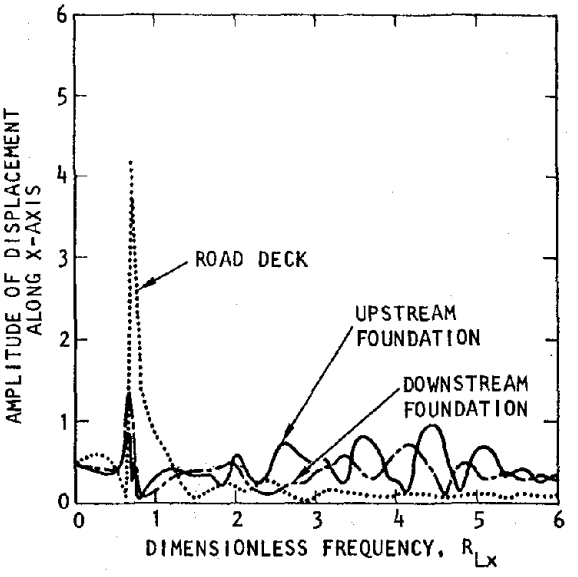

(a) Displacement along x-axis

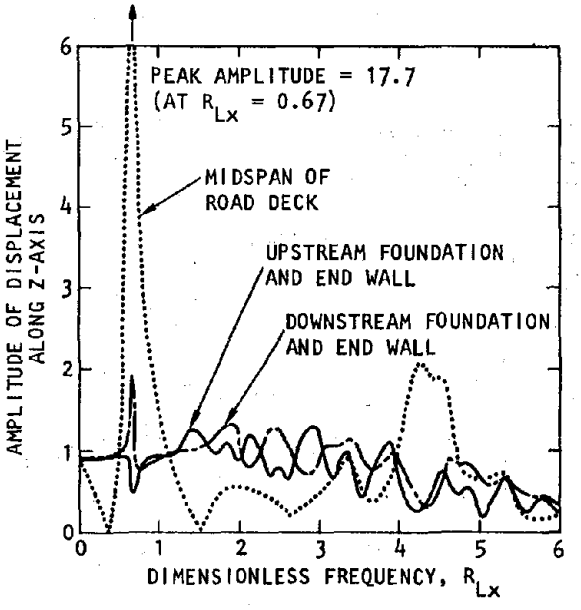

(b) Displacement along z-axis

FIGURE 4-15. FREQUENCY-DEPENDENT RESPONSE AMPLITUDES OF BRIDGE SUBJECTED TO INCIDENT SV-WAVES WITH θ_H = 0 DEG, θ_V = 20 DEG

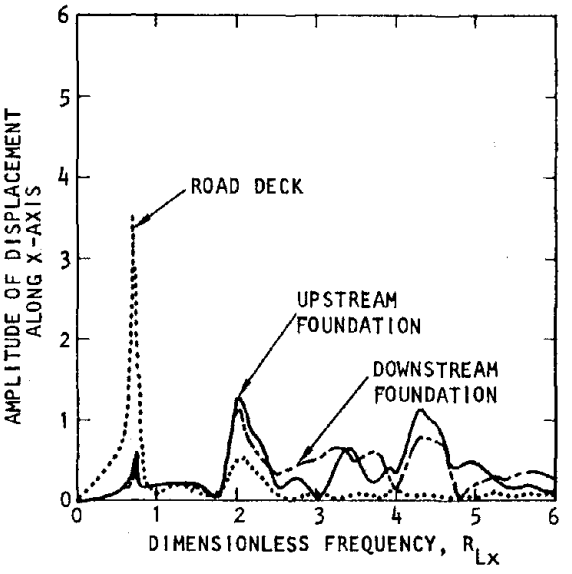

(a) Displacement along x-axis

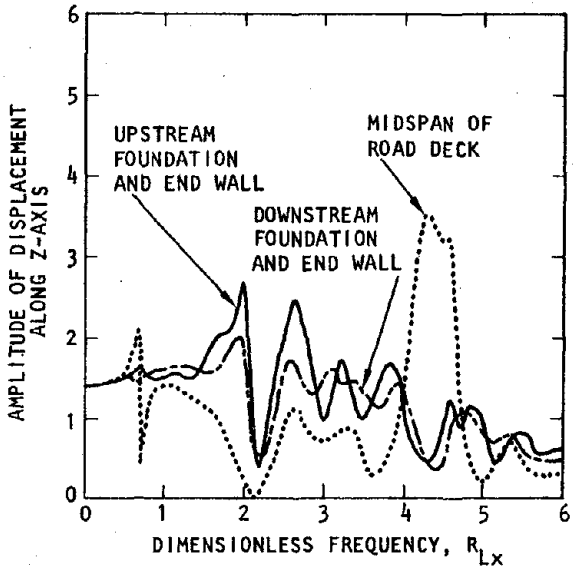

(b) Displacement along z-axis

FIGURE 4-16. FREQUENCY-DEPENDENT RESPONSE AMPLITUDES OF BRIDGE SUBJECTED TO INCIDENT SV-WAVES WITH θ_H = 0 DEG, θ_V = 45 DEG

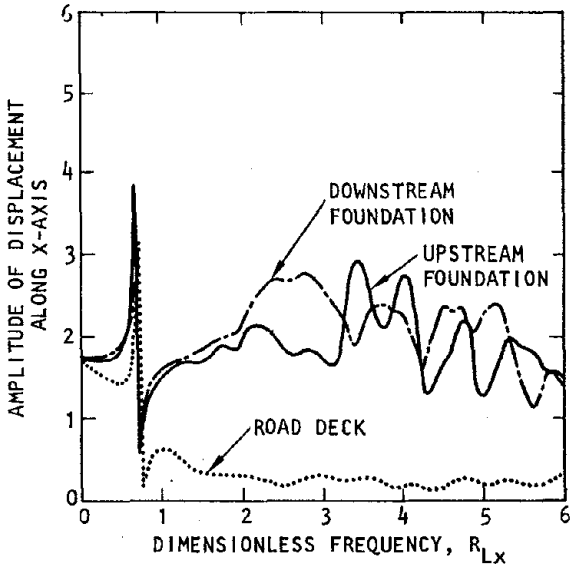

(a) Displacement along x-axis

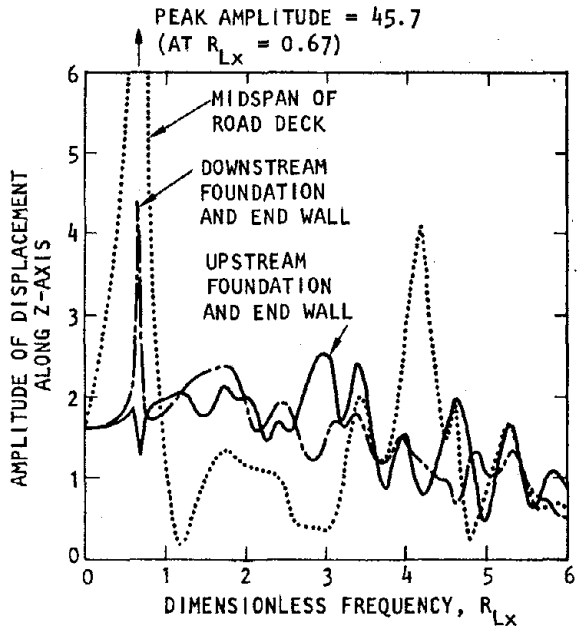

(b) Displacement along z-axis

FIGURE 4-17. FREQUENCY-DEPENDENT RESPONSE AMPLITUDES OF BRIDGE SUBJECTED TO INCIDENT SV-WAVES WITH θ_H = 0 DEG, θ_V = 55 DEG

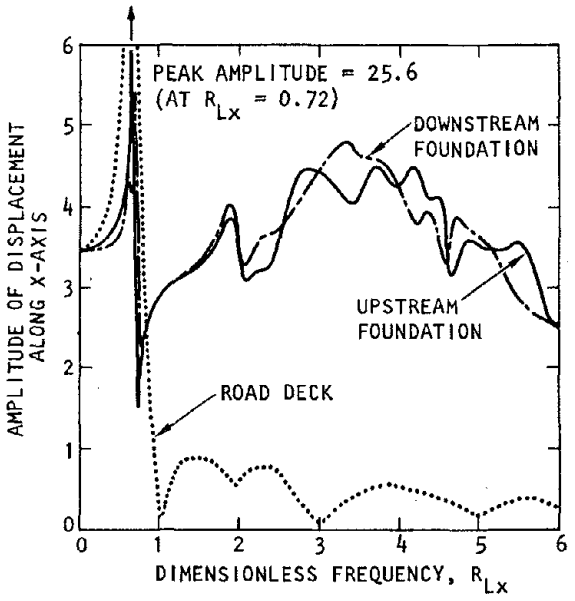

(a) Displacement along x-axis

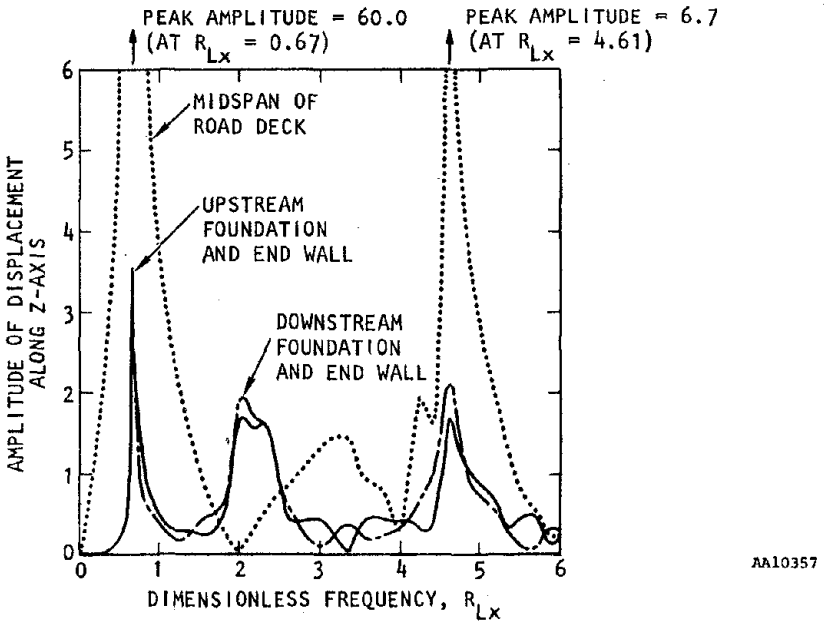

(b) Displacement along z-axis

FIGURE 4-18. FREQUENCY-DEPENDENT RESPONSE AMPLITUDES OF BRIDGE SUBJECTED TO INCIDENT SV-WAVES WITH θ_H = 0 DEG, θ_V = 60 DEG

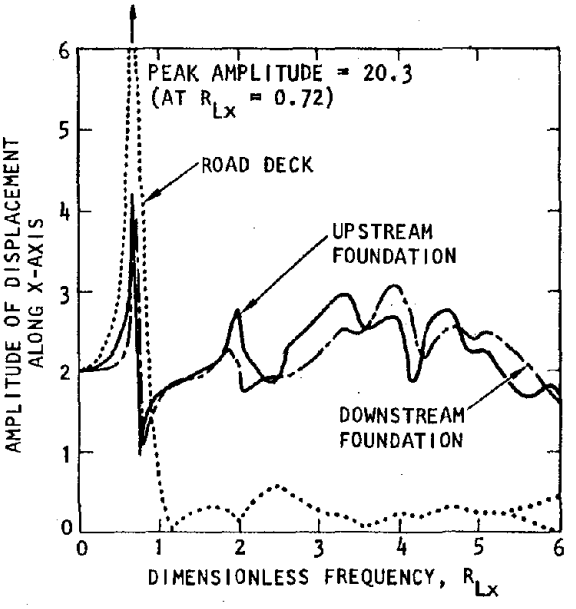

(a) Displacement along x-axis

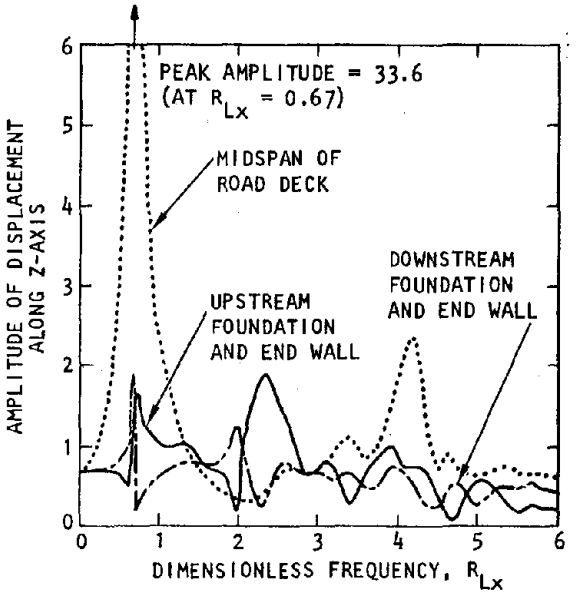

(b) Displacement along z-axis

FIGURE 4-19. FREQUENCY-DEPENDENT RESPONSE AMPLITUDES OF BRIDGE SUBJECTED TO INCIDENT SV-WAVES WITH θ_H = 0 DEG, θ_V = 65 DEG

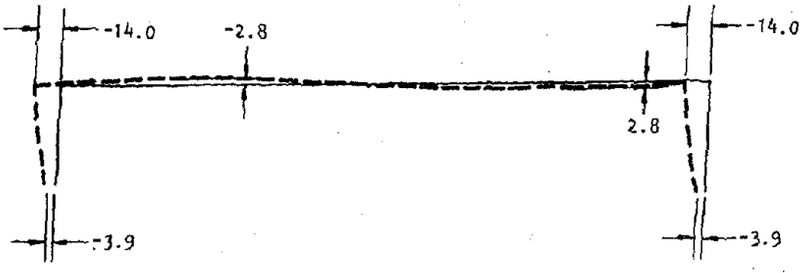

(a) θ_V = 90 deg

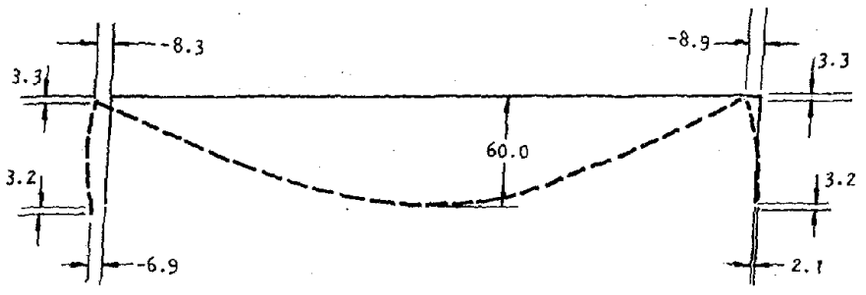

(b) θ_V = 60 deg

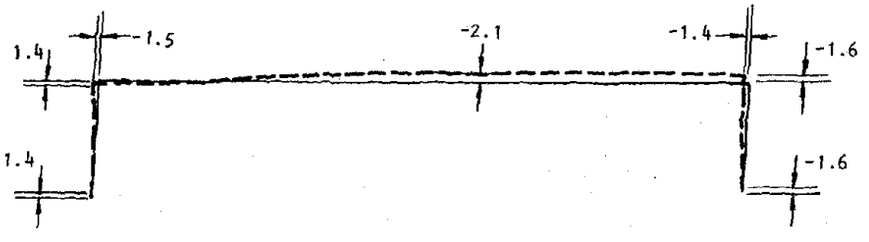

(c) θ_V = 45 deg

AA10263

FIGURE 4-20. CASE 2 (θ_H = 0 DEG): DEFORMED SHAPES OF BRIDGE AT TIMES OF PEAK RESONANT RESPONSE TO SV-WAVE EXCITATIONS (R_{Lx} = 0.67, f = 2.8 Hz)

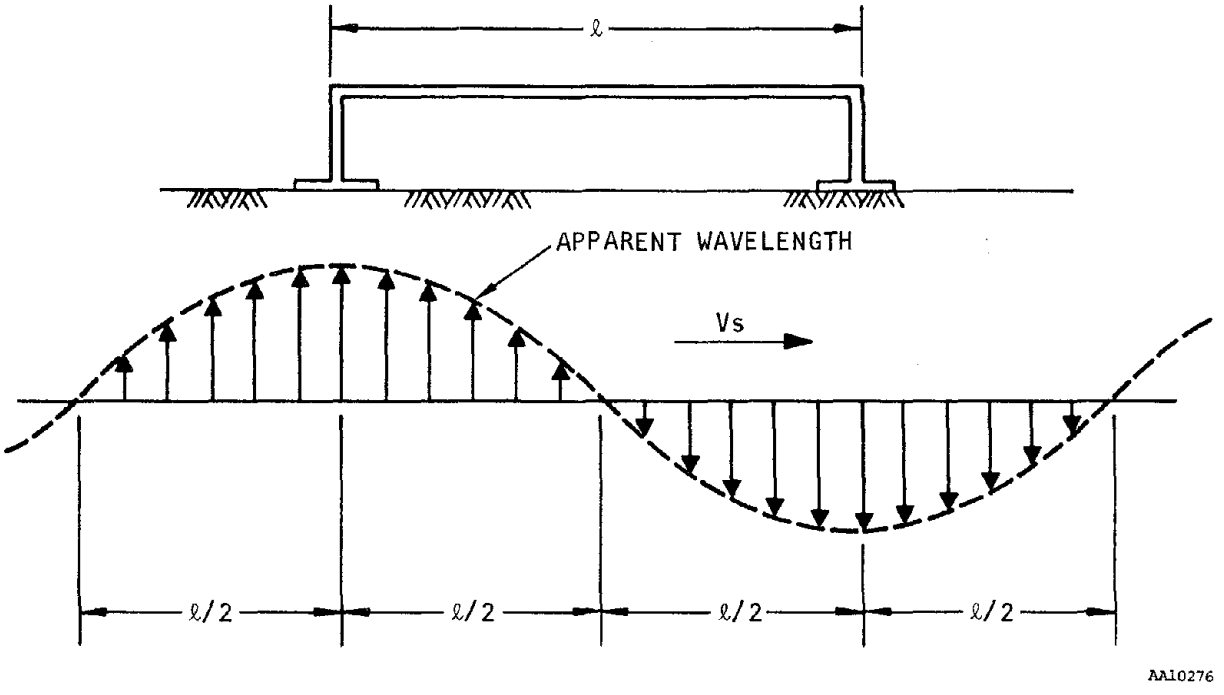

FIGURE 4-21. VERTICAL EXCITATIONS APPLIED TO BRIDGE FOUNDATIONS BY SV-WAVE WHOSE APPARENT WAVELENGTH = 2 x SPAN LENGTH

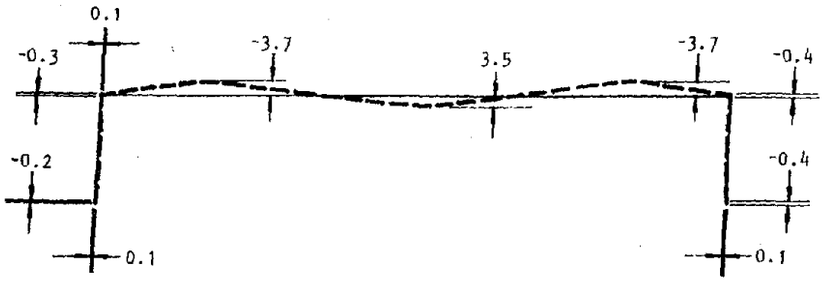

(a) θ_V = 45 deg, R_{Lx} = 4.26 (f = 17.75 Hz)

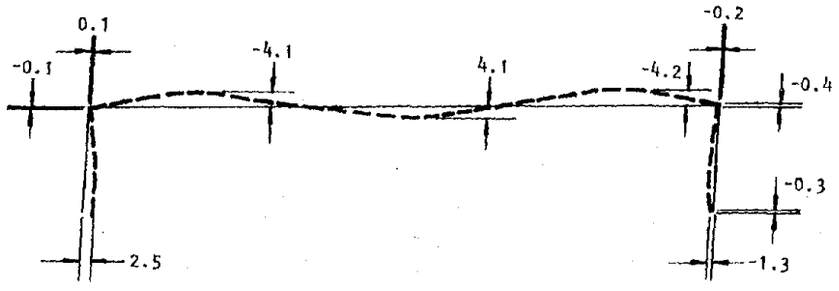

(b) θ_V = 55 deg, R_{Lx} = 4.14 (f = 17.25 Hz)

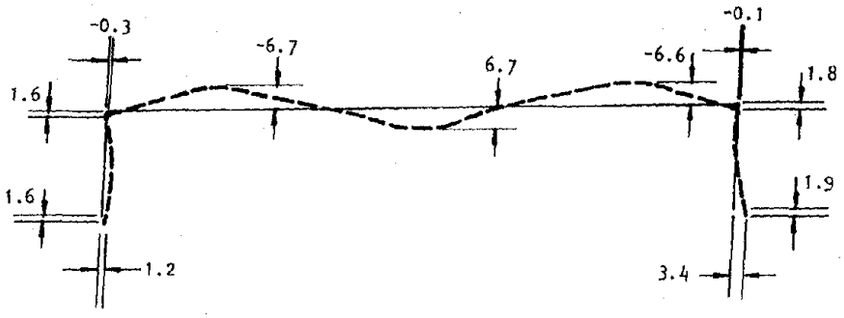

AA10333

(c) θ_V = 60 deg, R_{Lx} = 4.61 (f = 19.21 Hz)

FIGURE 4-22. CASE 2 (θ_H = 0 DEG): DEFORMED SHAPES OF BRIDGE AT TIMES OF PEAK RESONANT RESPONSE TO HIGHER FREQUENCY SV-WAVE EXCITATIONS

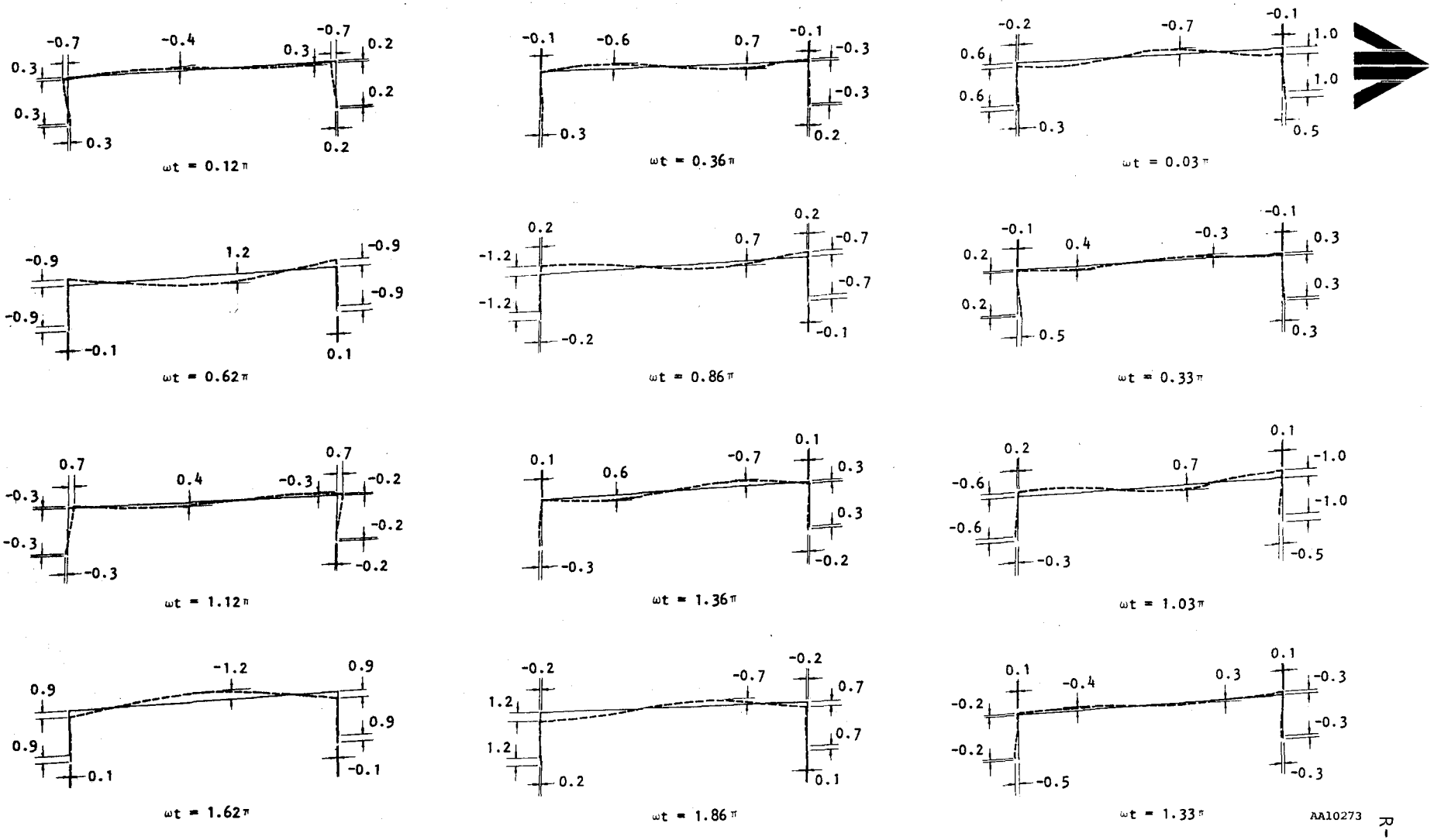

(a) $R_{Lx} = 1.06 \left(\frac{1.0}{\cos 20 \text{ deg}} \right)$ (b) $R_{Lx} = 2.13 \left(\frac{2.0}{\cos 20 \text{ deg}} \right)$ (c) $R_{Lx} = 3.19 \left(\frac{3.0}{\cos 20 \text{ deg}} \right)$

FIGURE 4-23. CASE 2 (θ_H = 0 deg): BRIDGE RESPONSE TO FREE-FIELD SV-WAVE EXCITATIONS OF EQUAL AMPLITUDE AND EQUAL PHASE AT THE TWO FOUNDATIONS WHEN θ_V = 20 deg

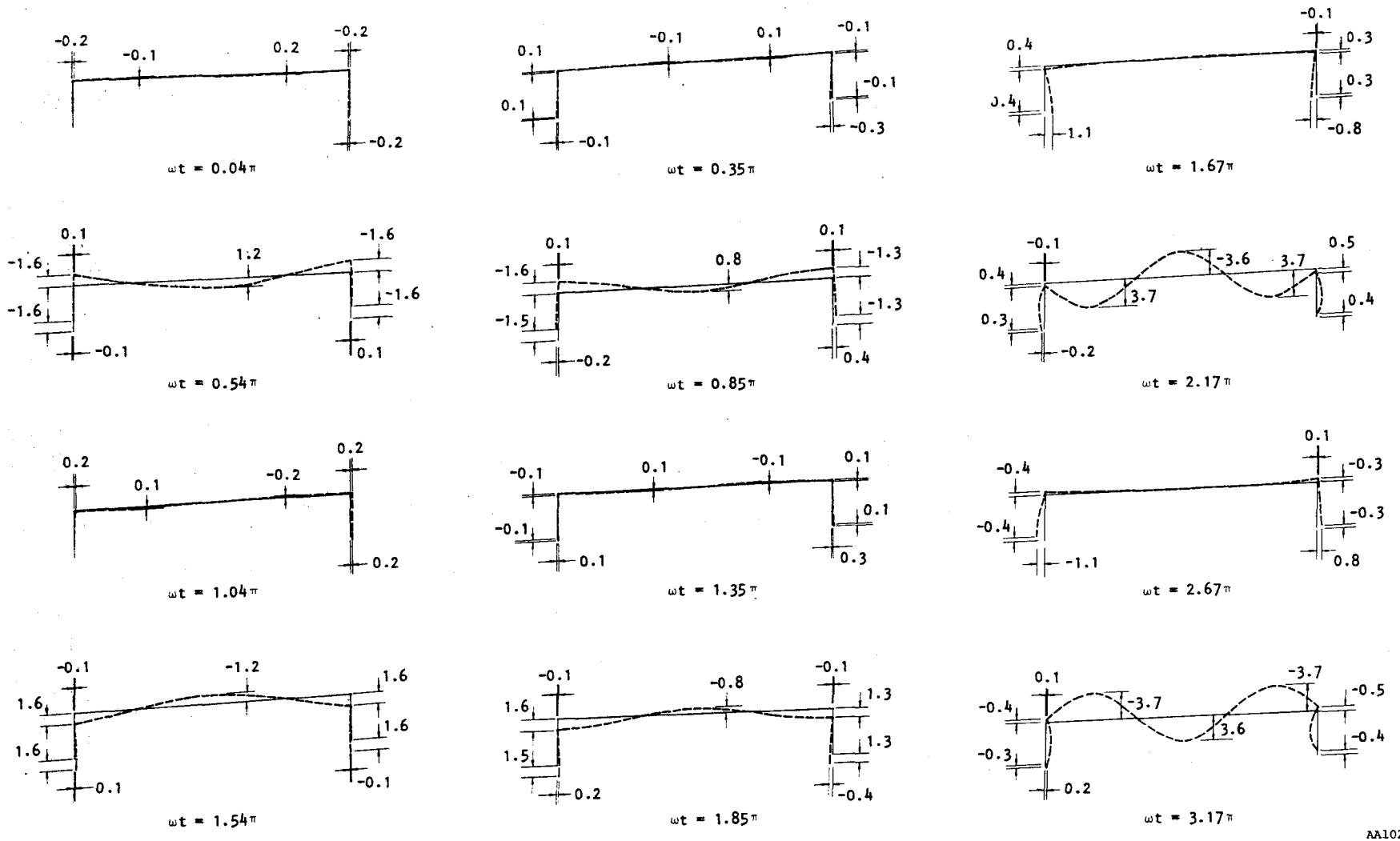

(a) $R_{Lx} = 1.41 \left(\frac{1.0}{\cos 45 \text{ deg}} \right)$ (b) $R_{Lx} = 2.83 \left(\frac{2.0}{\cos 45 \text{ deg}} \right)$ (c) $R_{Lx} = 4.24 \left(\frac{3.0}{\cos 45 \text{ deg}} \right)$

FIGURE 4-24. CASE 2 (θ_H = 0 deg): BRIDGE RESPONSE TO FREE-FIELD SV-WAVE EXCITATIONS OF EQUAL AMPLITUDE AND EQUAL PHASE AT THE TWO FOUNDATIONS WHEN θ_V = 45 deg

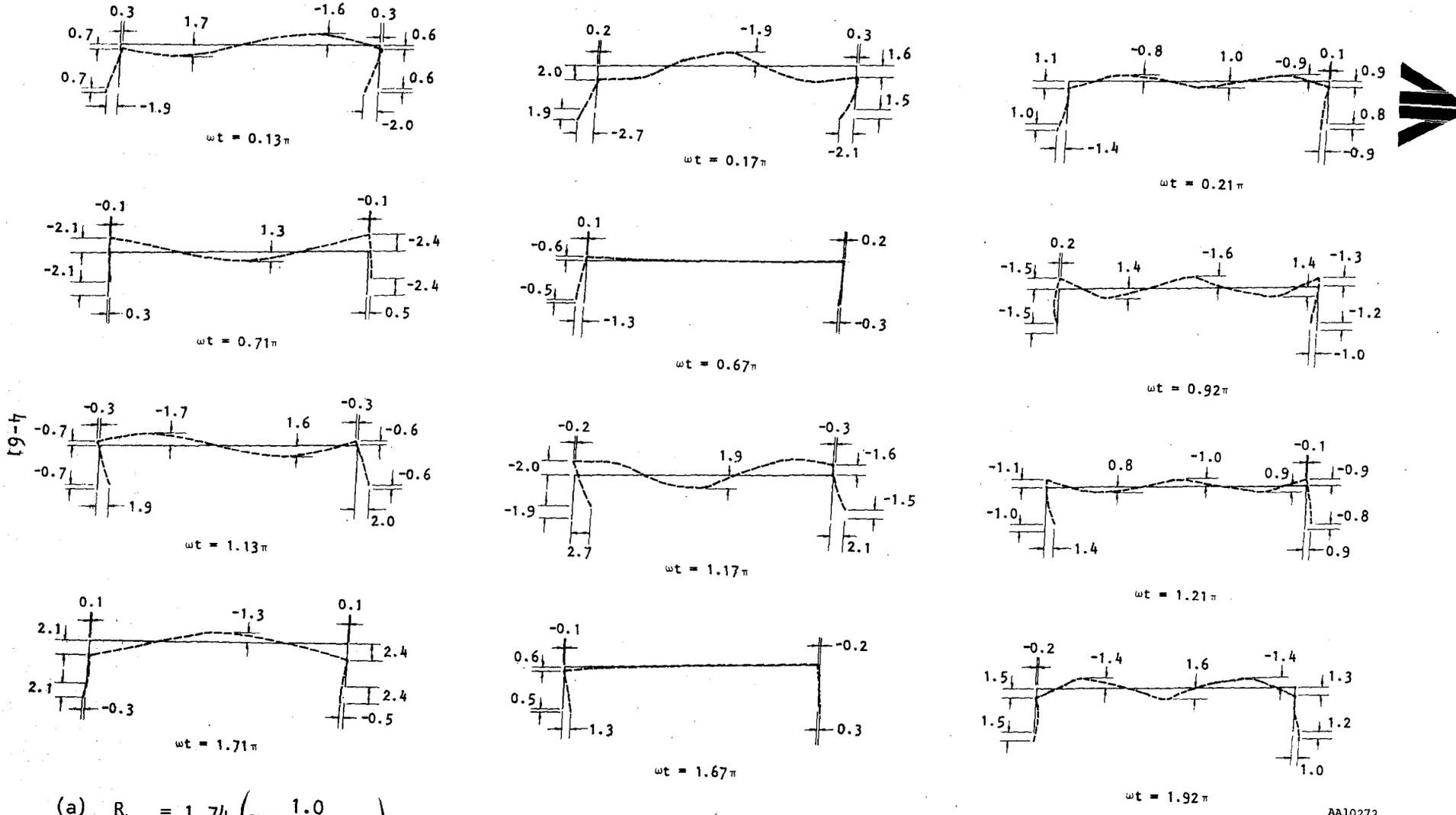

(a) $R_{Lx} = 1.74 \left(\frac{1.0}{\cos 55 \text{ deg}} \right)$

(b) $R_{Lx} = 3.49 \left(\frac{2.0}{\cos 55 \text{ deg}} \right)$

(c) $R_{Lx} = 5.23 \left(\frac{3.0}{\cos 55 \text{ deg}} \right)$

FIGURE 4-25. CASE 2 (θ_H = 0 deg): BRIDGE RESPONSE TO FREE-FIELD SV-WAVE EXCITATIONS OF EQUAL AMPLITUDE AND EQUAL PHASE AT THE TWO FOUNDATIONS WHEN θ_V = 55 deg

R-7911-5008

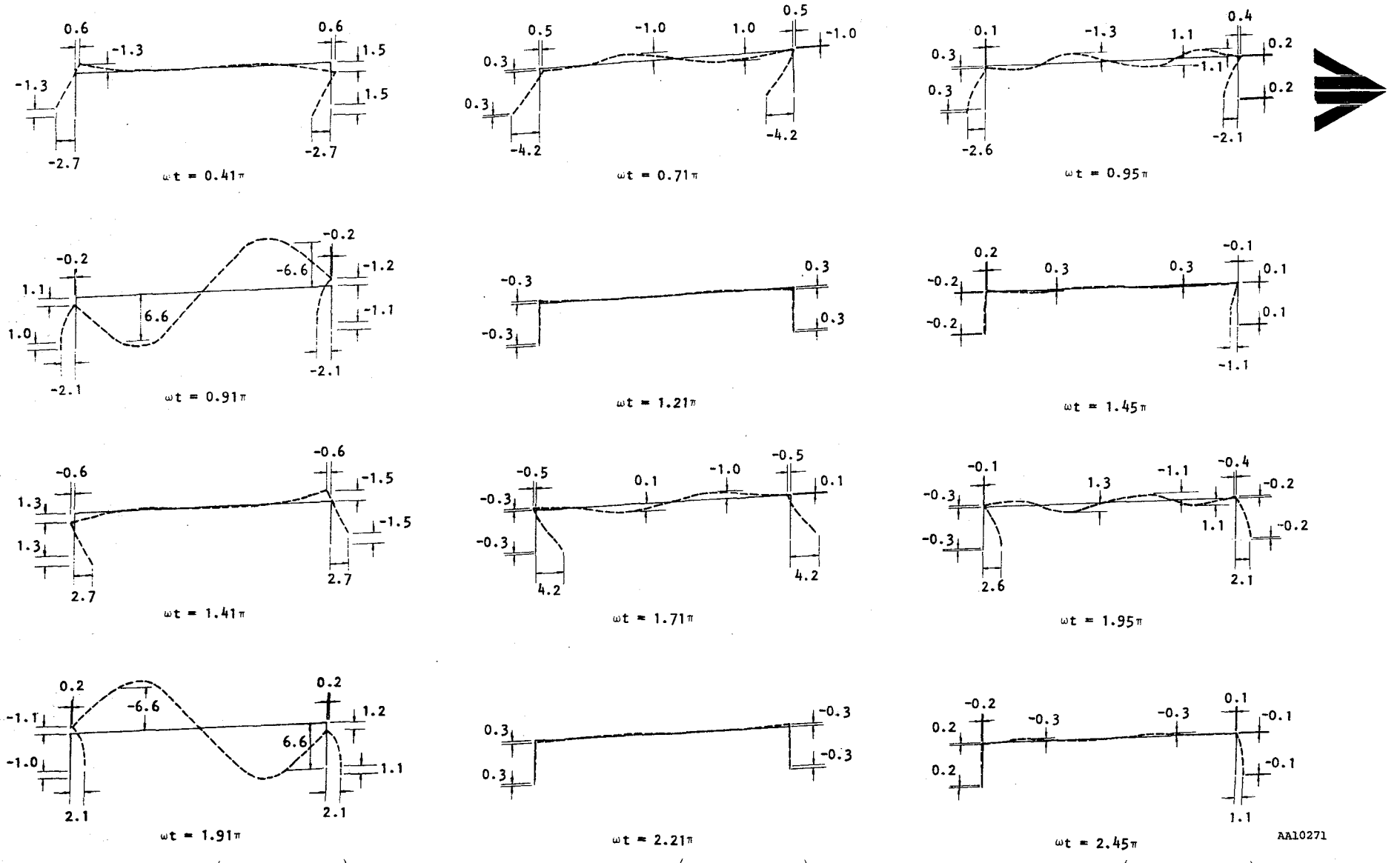

(a) $R_{Lx} = 2.0\left(\frac{1.0}{\cos 60 \text{ deg}}\right)$ (b) $R_{Lx} = 4.0\left(\frac{2.0}{\cos 60 \text{ deg}}\right)$ (c) $R_{Lx} = 6.0\left(\frac{3.0}{\cos 60 \text{ deg}}\right)$

FIGURE 4-26. CASE 2 (θ_H = 0 deg): BRIDGE RESPONSE TO FREE-FIELD SV-WAVE EXCITATIONS OF EQUAL AMPLITUDE AND EQUAL PHASE AT THE TWO FOUNDATIONS WHEN θ_V = 60 deg

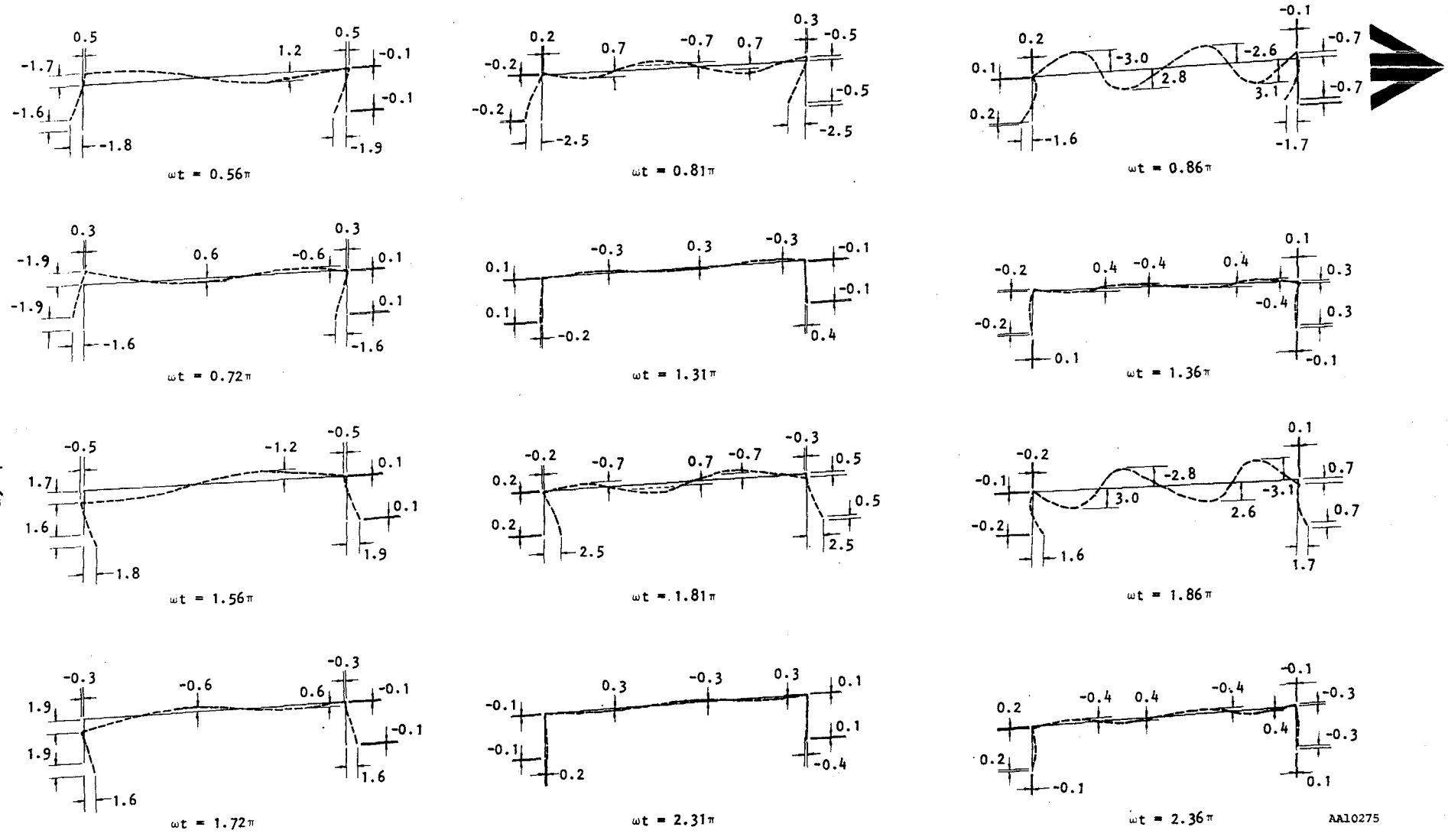

(a) $R_{Lx} = 2.37 \left(\frac{1.0}{\cos 65 \text{ deg}} \right)$ (b) $R_{Lx} = 4.73 \left(\frac{2.0}{\cos 65 \text{ deg}} \right)$ (c) $R_{Lx} = 7.10 \left(\frac{3.0}{\cos 65 \text{ deg}} \right)$

FIGURE 4-27. CASE 2 (θ_H = 0 deg): BRIDGE RESPONSE TO FREE-FIELD SV-WAVE EXCITATIONS OF EQUAL AMPLITUDE AND EQUAL PHASE AT THE TWO FOUNDATIONS WHEN θ_V = 65 deg

R-7911-5008

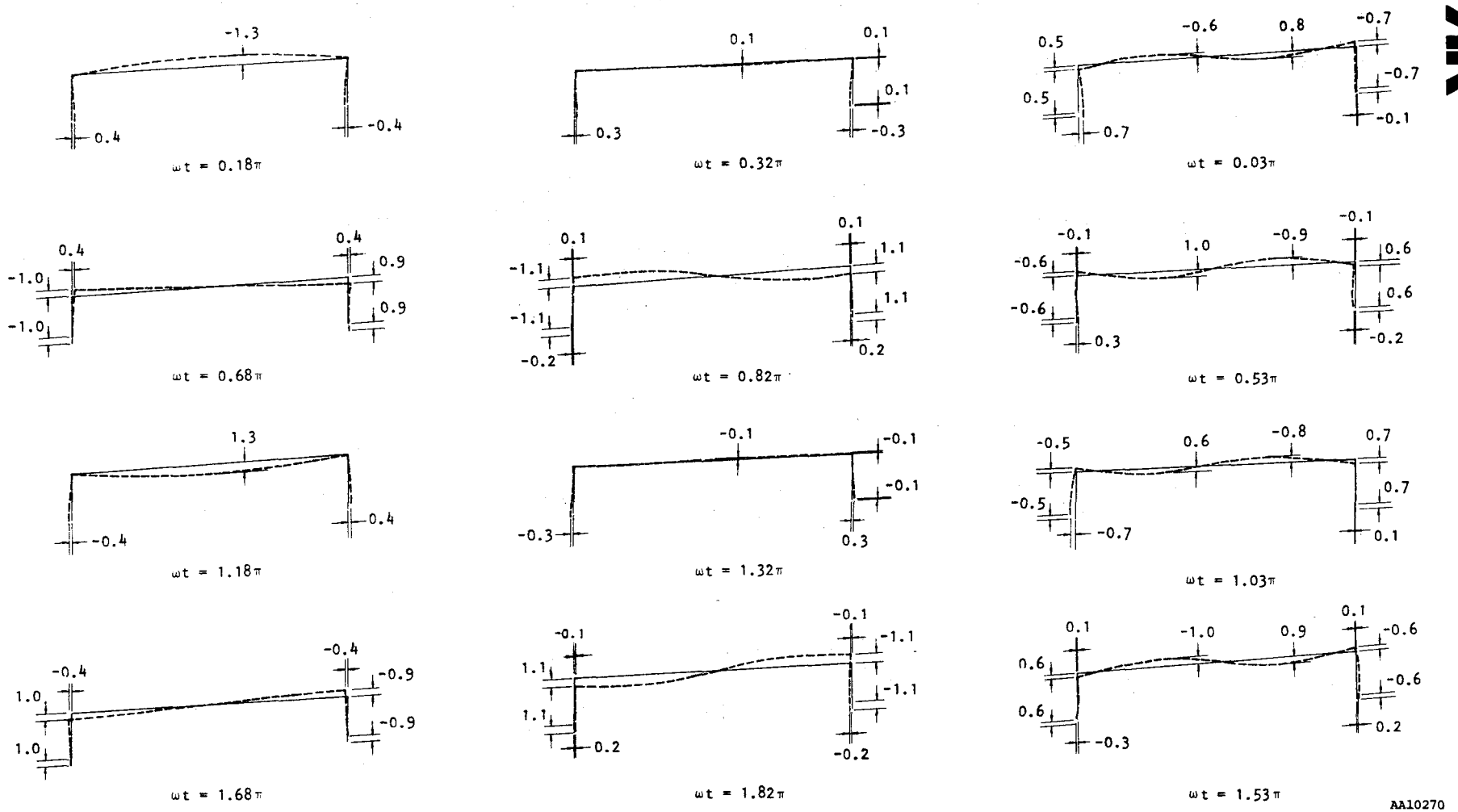

(a) $R_{Lx} = 0.53\left(\frac{0.5}{\cos 20 \text{ deg}}\right)$ (b) $R_{Lx} = 1.59\left(\frac{1.5}{\cos 20 \text{ deg}}\right)$ (c) $R_{Lx} = 2.66\left(\frac{2.5}{\cos 20 \text{ deg}}\right)$

FIGURE 4-28. CASE 2 (θ_H = 0 deg): BRIDGE RESPONSE TO FREE-FIELD SV-WAVE EXCITATIONS OF EQUAL AMPLITUDE AND OPPOSITE PHASE AT THE TWO FOUNDATIONS WHEN θ_V = 20 deg

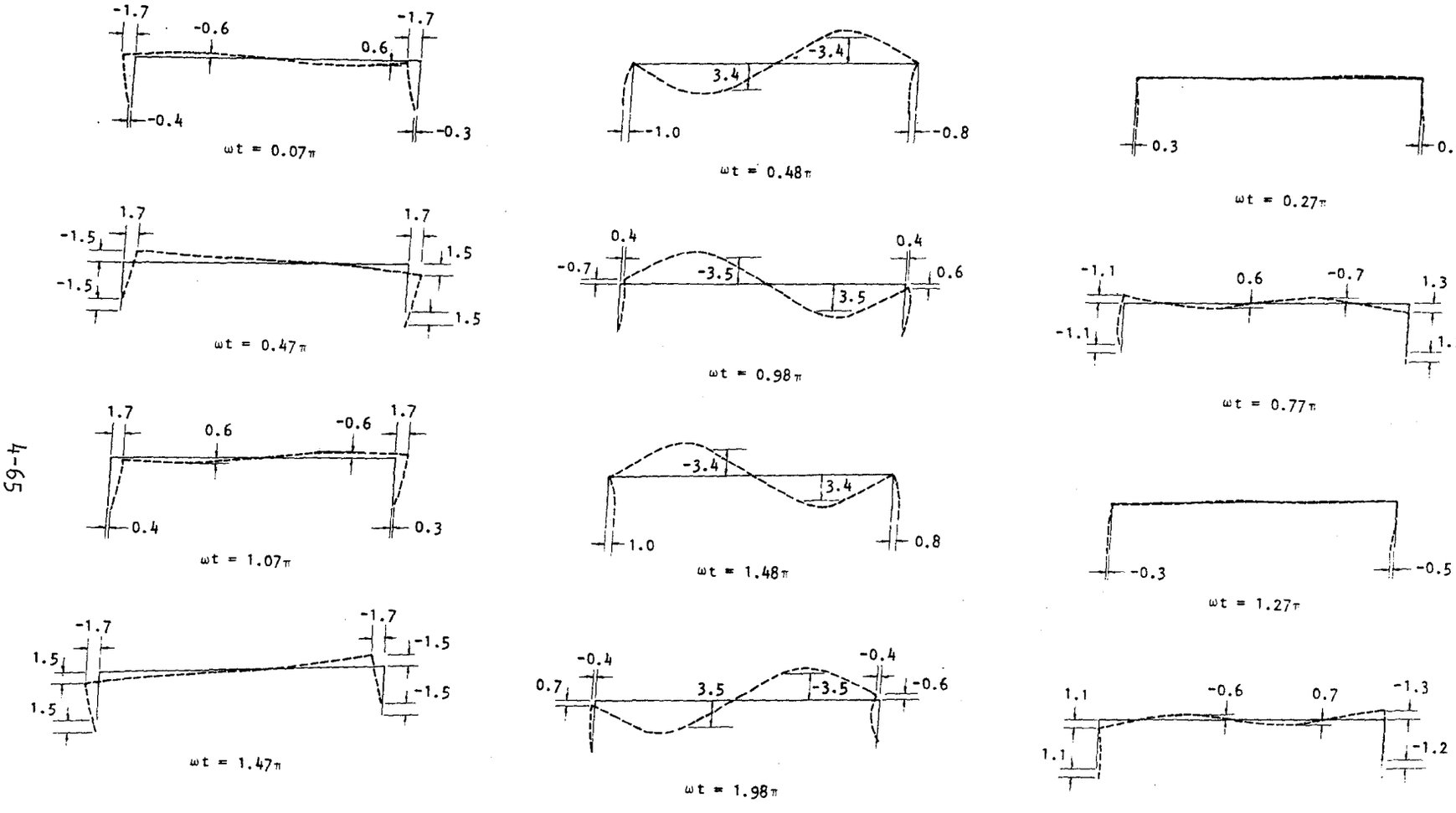

(a) $R_{Lx} = 0.71 \left(\frac{0.5}{\cos 45 \text{ deg}} \right)$ (b) $R_{Lx} = 2.12 \left(\frac{1.5}{\cos 45 \text{ deg}} \right)$ (c) $R_{Lx} = 3.53 \left(\frac{2.5}{\cos 45 \text{ deg}} \right)$

FIGURE 4-29. CASE 2 (θ_H = 0 deg): BRIDGE RESPONSE TO FREE-FIELD SV-WAVE EXCITATIONS OF EQUAL AMPLITUDE AND OPPOSITE PHASE AT THE TWO FOUNDATIONS WHEN θ_V = 45 deg

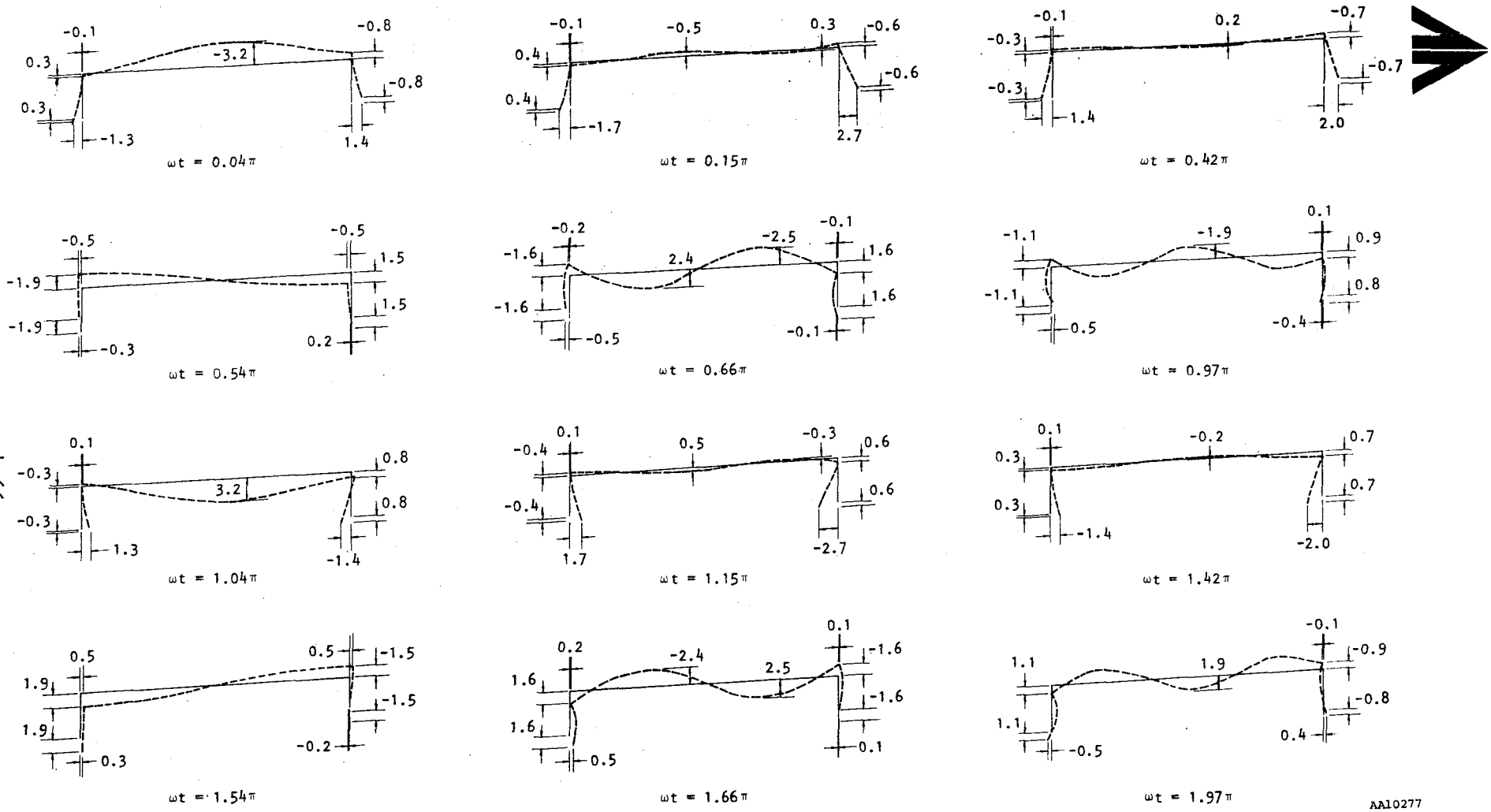

(a) $R_{Lx} = 0.87\left(\frac{0.5}{\cos 55 \text{ deg}}\right)$ (b) $R_{Lx} = 2.62\left(\frac{1.5}{\cos 55 \text{ deg}}\right)$ (c) $R_{Lx} = 4.36\left(\frac{2.5}{\cos 55 \text{ deg}}\right)$

FIGURE 4-30. CASE 2 (θ_H = 0 deg): BRIDGE RESPONSE TO FREE-FIELD SV-WAVE EXCITATIONS OF EQUAL AMPLITUDE AND OPPOSITE PHASE AT THE TWO FOUNDATIONS WHEN θ_V = 55 deg

R-7911-5008

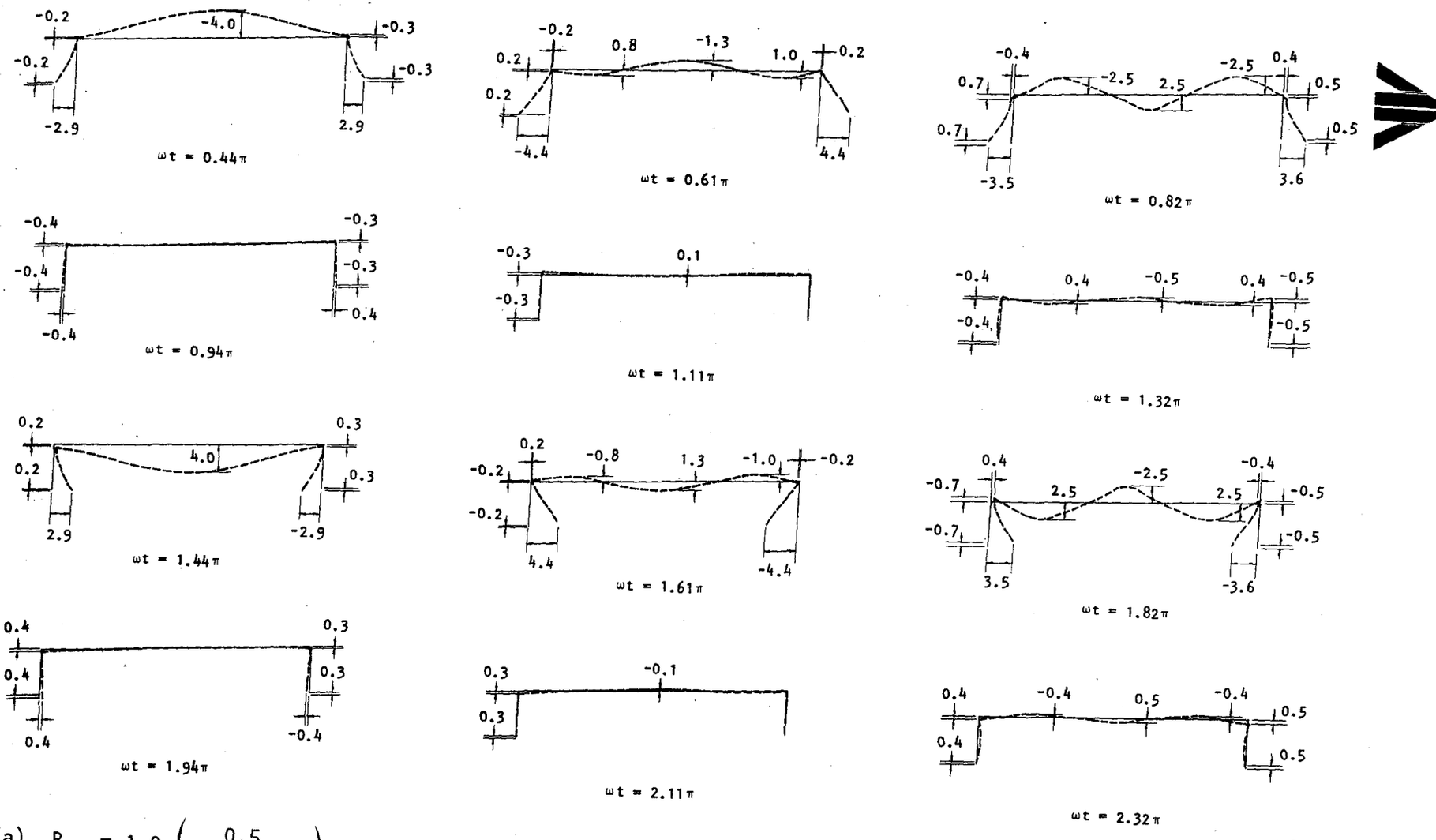

(a) $R_{Lx} = 1.0 \left(\frac{0.5}{\cos 60 \text{ deg}} \right)$

(b) $R_{Lx} = 3.0 \left(\frac{1.5}{\cos 60 \text{ deg}} \right)$

(c) $R_{Lx} = 5.0 \left(\frac{2.5}{\cos 60 \text{ deg}} \right)$

FIGURE 4-31. CASE 2 (θ_H = 0 deg): BRIDGE RESPONSE TO FREE-FIELD SV-WAVE EXCITATIONS OF EQUAL AMPLITUDE AND OPPOSITE PHASE AT THE TWO FOUNDATIONS WHEN θ_V = 60 deg

R-7911-5008

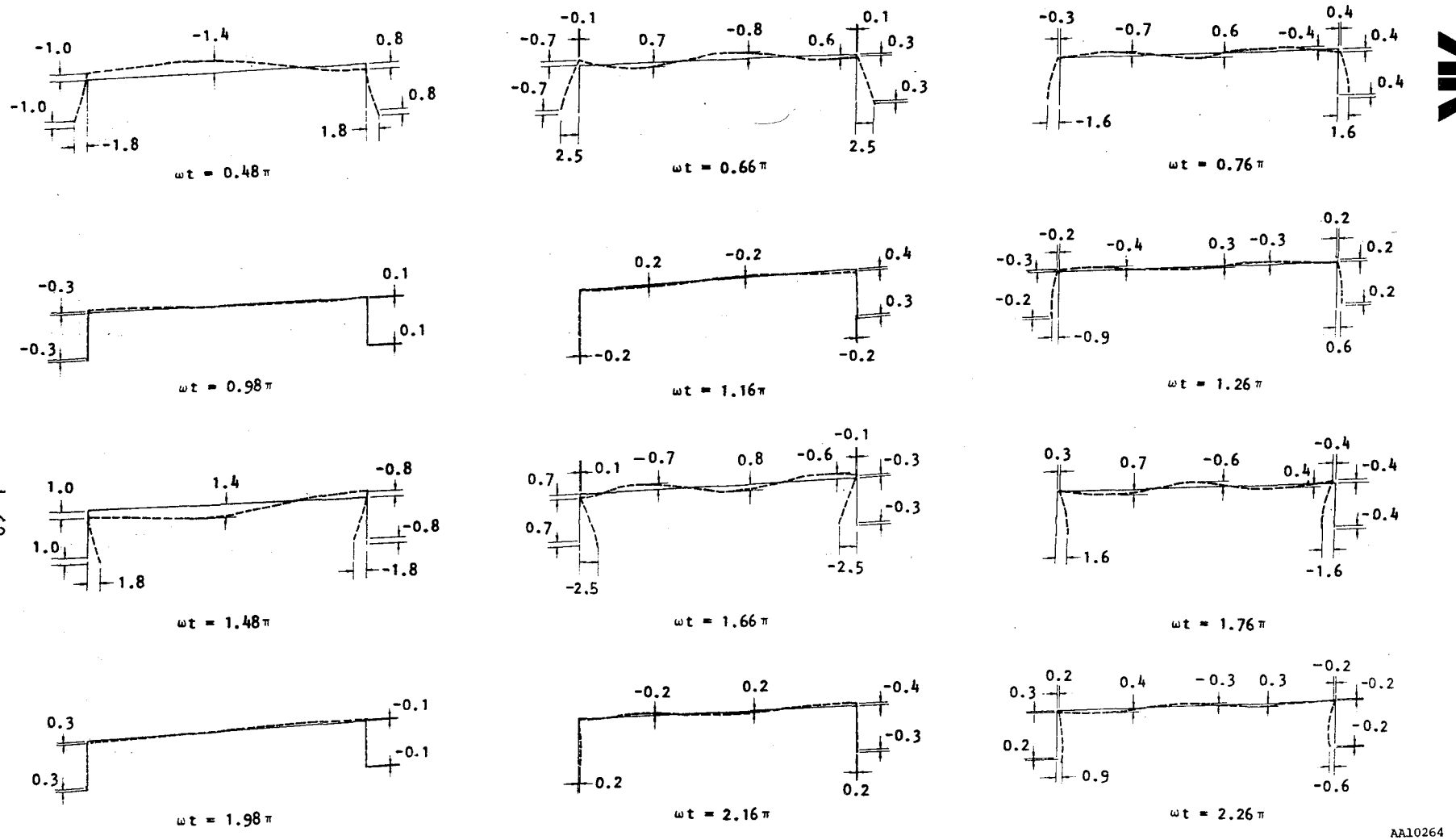

(a) $R_{Lx} = 1.16\left(\frac{0.5}{\cos 65 \text{ deg}}\right)$ (b) $R_{Ly} = 3.55\left(\frac{1.5}{\cos 65 \text{ deg}}\right)$ (c) $R_{Lx} = 5.86\left(\frac{2.5}{\cos 65 \text{ deg}}\right)$

FIGURE 4-32. CASE 2 (θ_H = 0 deg): BRIDGE RESPONSE TO FREE-FIELD SV-WAVE EXCITATIONS OF EQUAL AMPLITUDE AND OPPOSITE PHASE AT THE TWO FOUNDATIONS WHEN θ_V = 65 deg

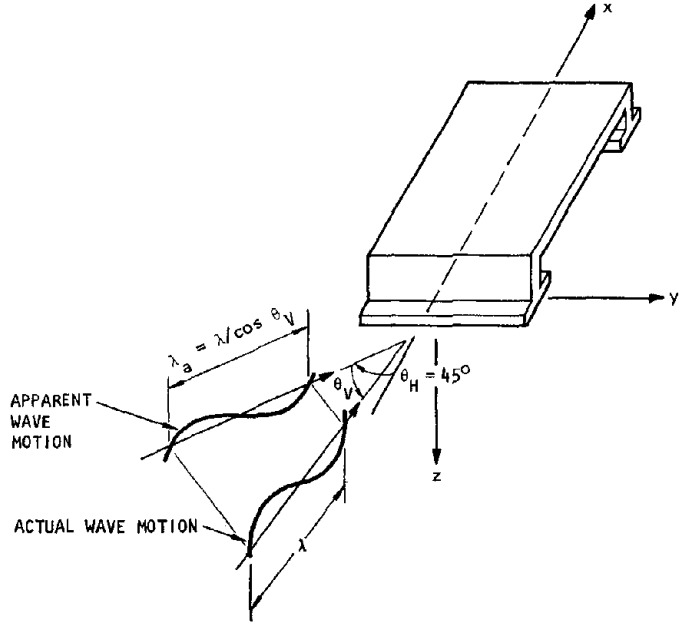

(a) Actual and apparent wave motion

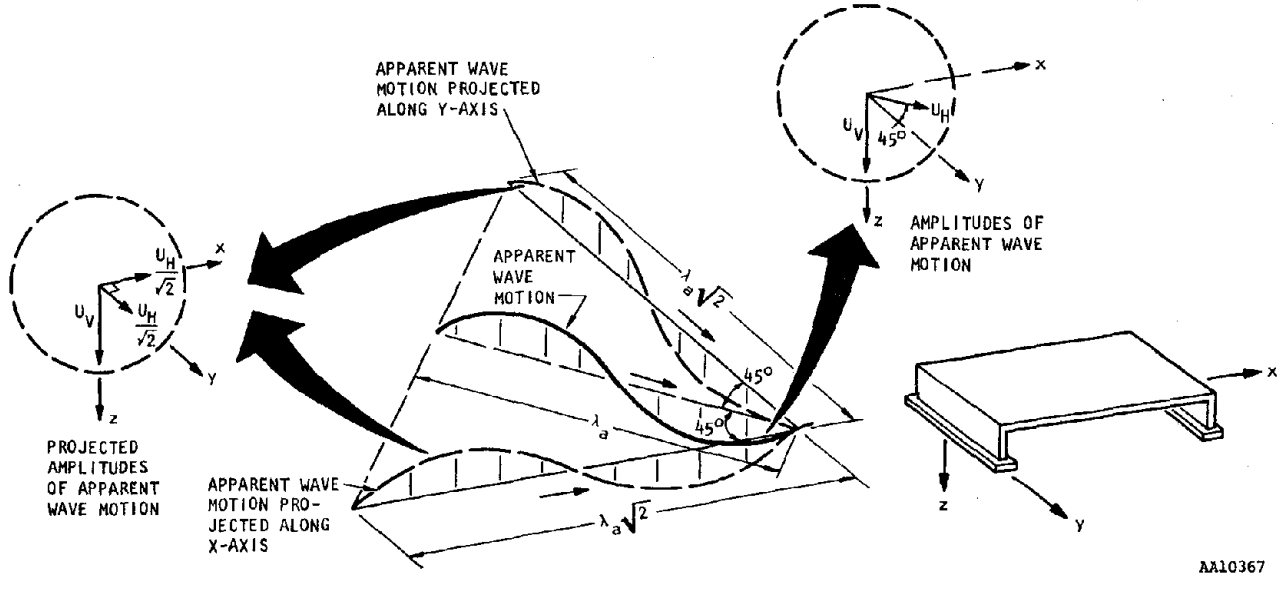

(b) Apparent wave motion projected along x- and y- axes of bridge

FIGURE 4-33. FREE-FIELD EXCITATIONS FROM INCIDENT SV-WAVES FOR CASE 3 (θ_H = 45 deg)

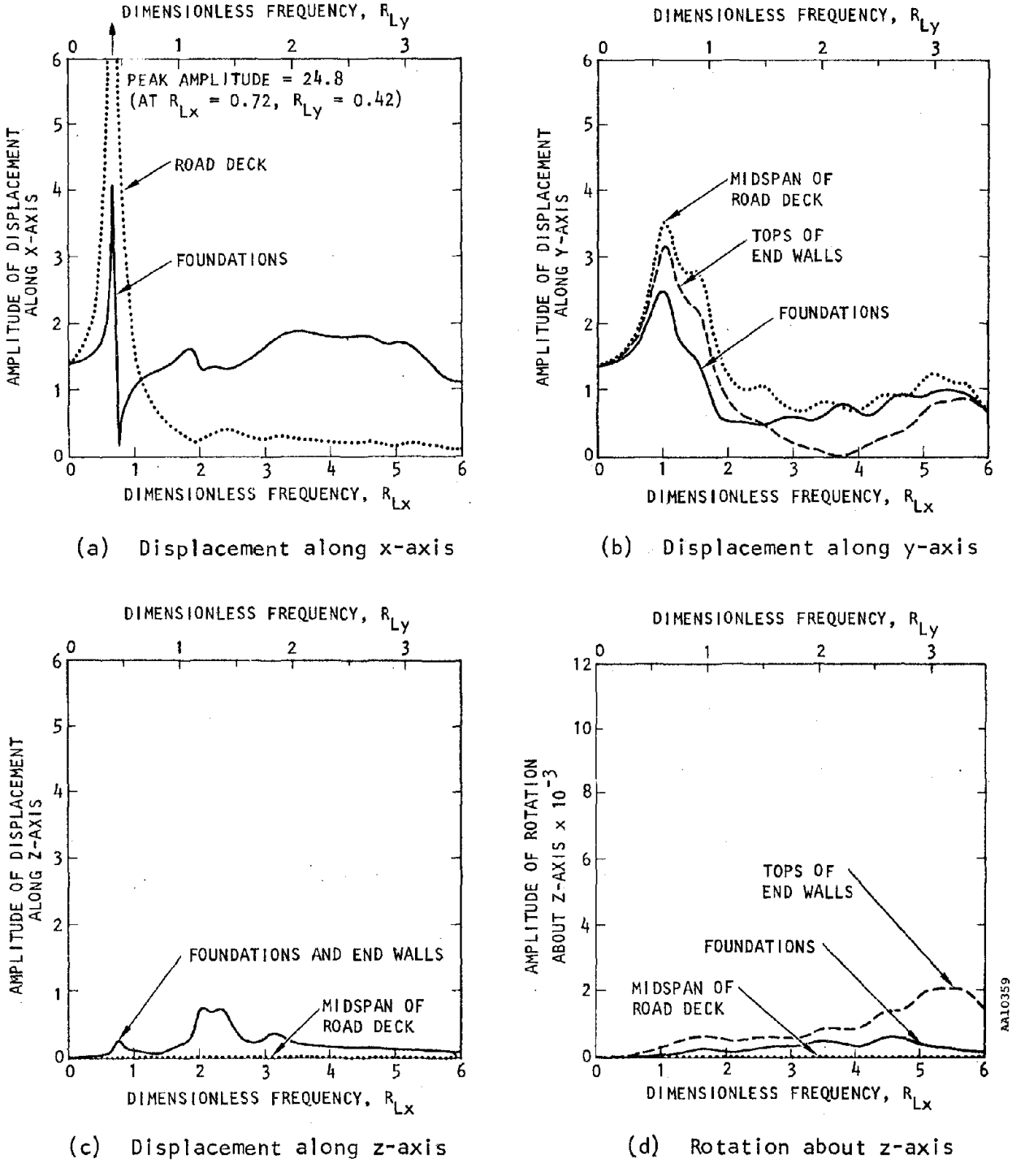

FIGURE 4-34. FREQUENCY-DEPENDENT RESPONSE AMPLITUDES OF BRIDGE SUBJECTED TO INCIDENT SV-WAVES WITH θ_H = 45 DEG, θ_V = 90 DEG

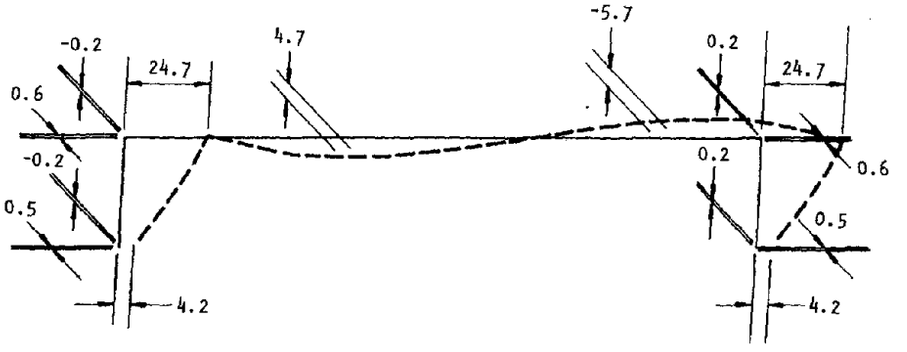

(a) $R_{Lx} = 0.72$, $R_{Ly} = 0.42$ (f = 3.0 Hz)

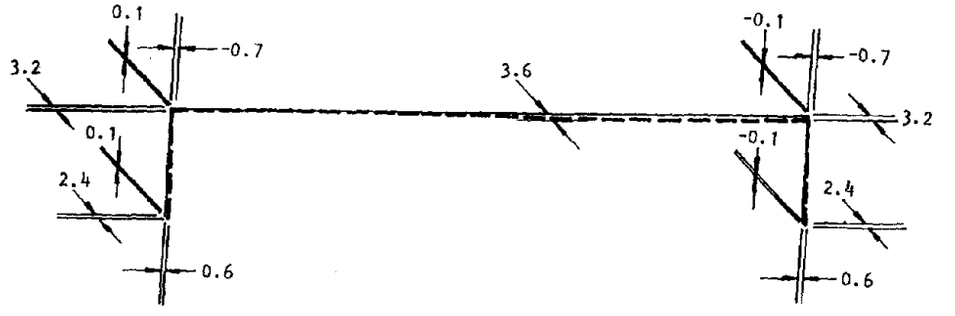

(b) $R_{Lx} = 1.00$, $R_{Ly} = 0.58$ (f = 4.2 Hz)

FIGURE 4-35. CASE 3 (θ_H = 45 DEG): DEFORMED SHAPES OF BRIDGE AT TIMES OF PEAK RESONANT RESPONSE TO SV-WAVE EXCITATIONS WITH θ_V = 90 DEG

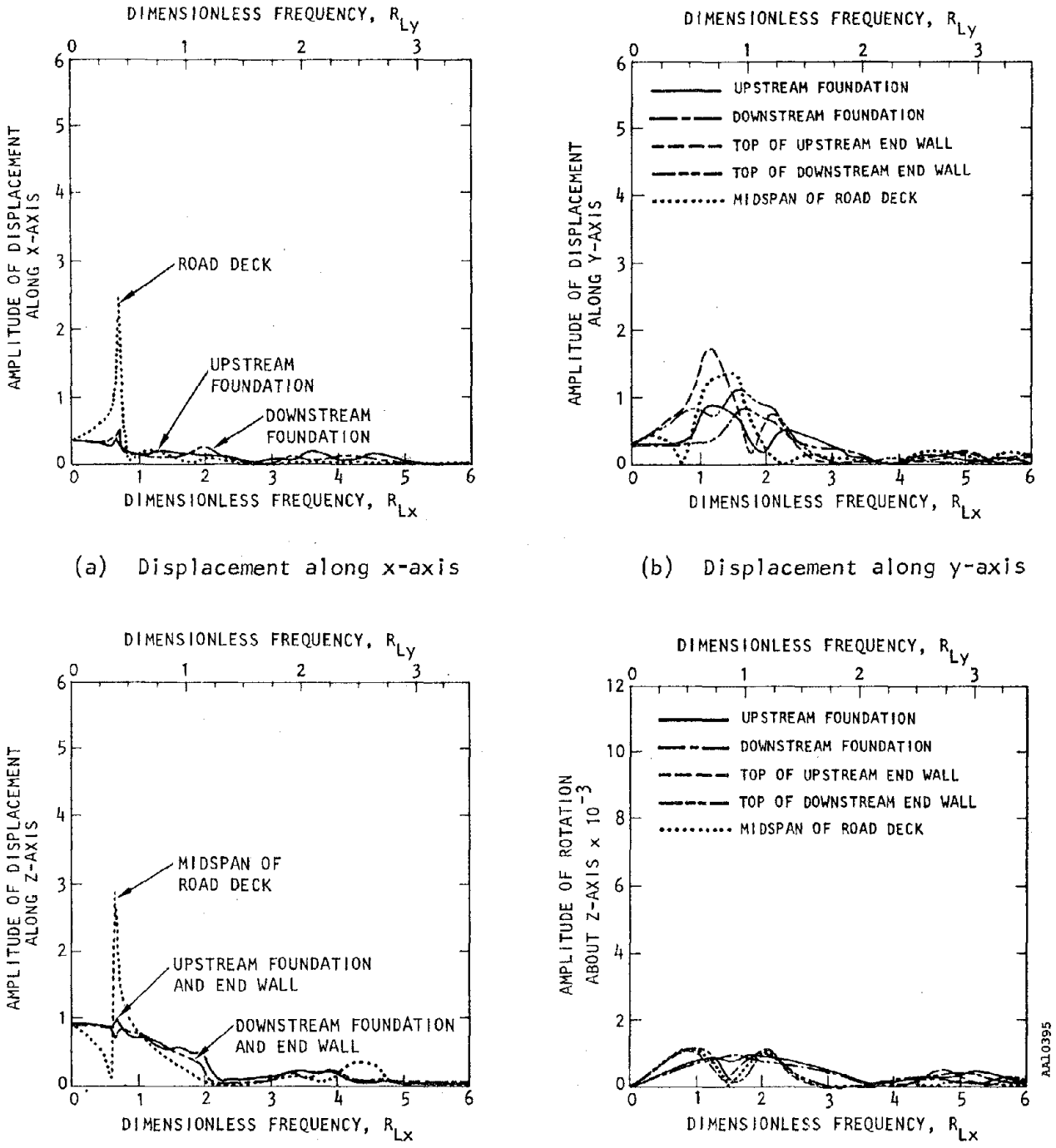

FIGURE 4-36. FREQUENCY-DEPENDENT RESPONSE AMPLITUDES OF BRIDGE SUBJECTED TO INCIDENT SV-WAVES WITH θ_H = 45 DEG, θ_V = 20 DEG

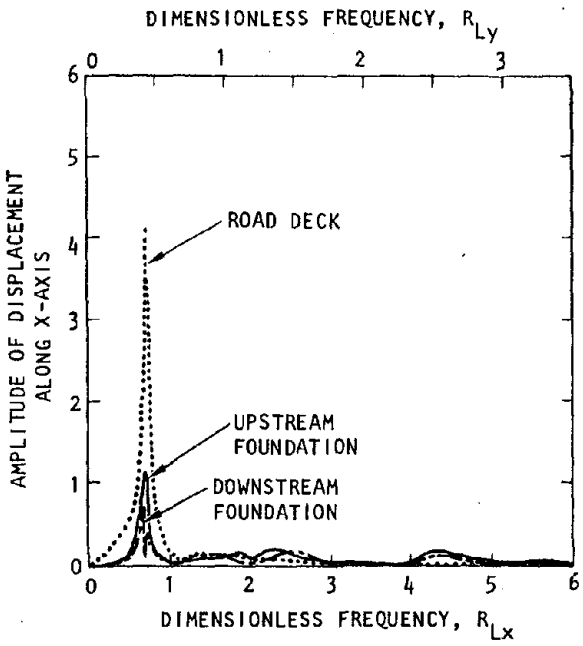

(a) Displacement along x-axis

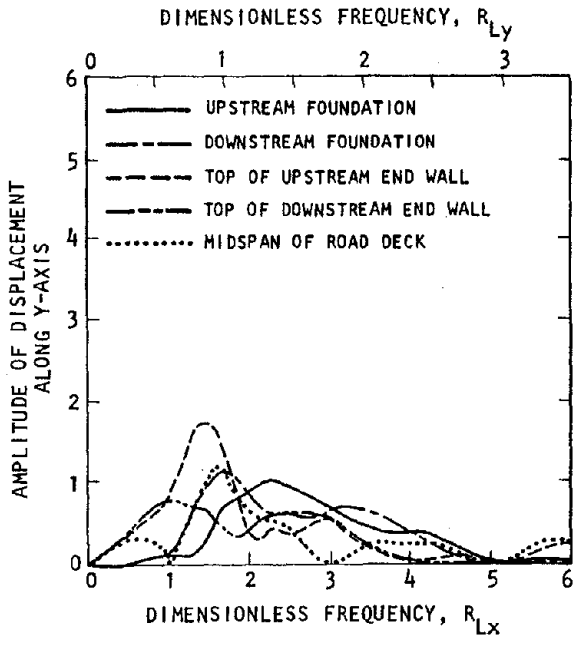

(b) Displacement along y-axis

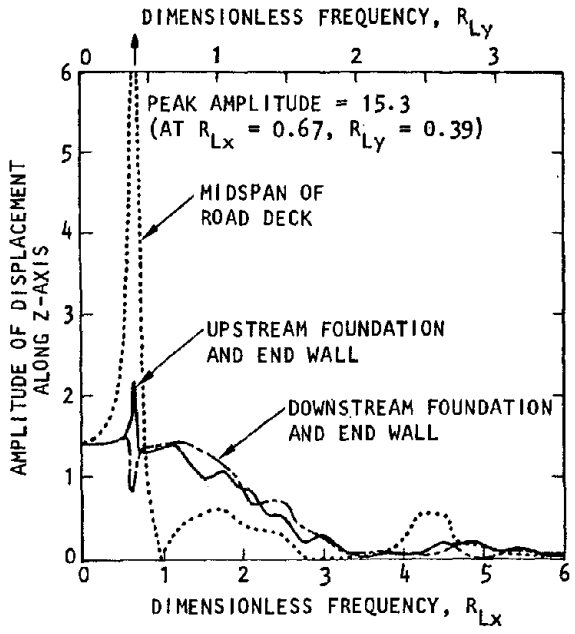

(c) Displacement along z-axis

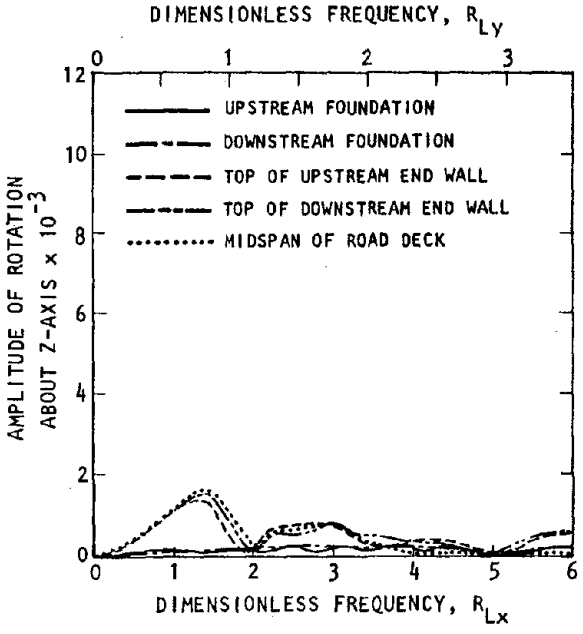

(d) Rotation about z-axis

FIGURE 4-37. FREQUENCY-DEPENDENT RESPONSE AMPLITUDES OF BRIDGE SUBJECTED TO INCIDENT SV-WAVES WITH $\theta_H = \theta_V = 45$ DEG

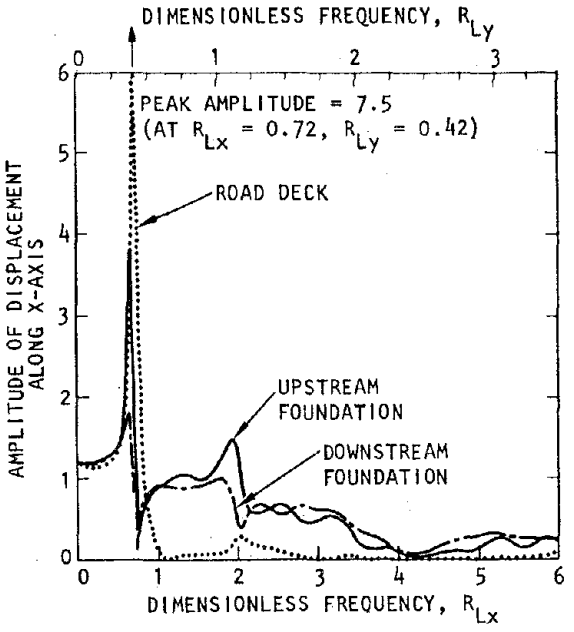

(a) Displacement along x-axis

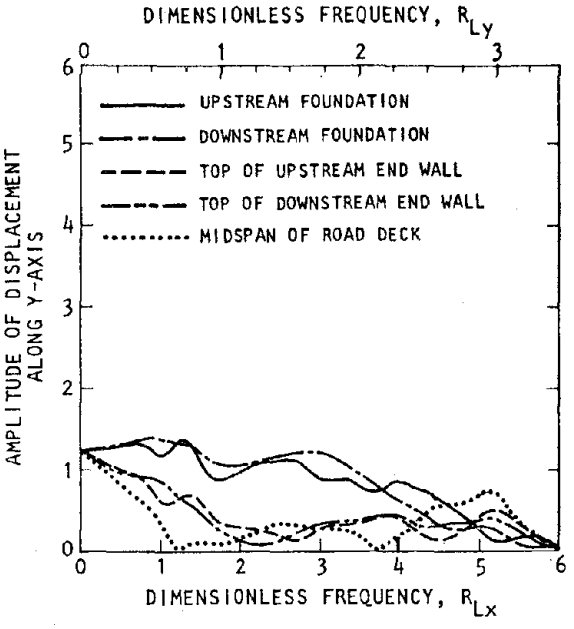

(b) Displacement along y-axis

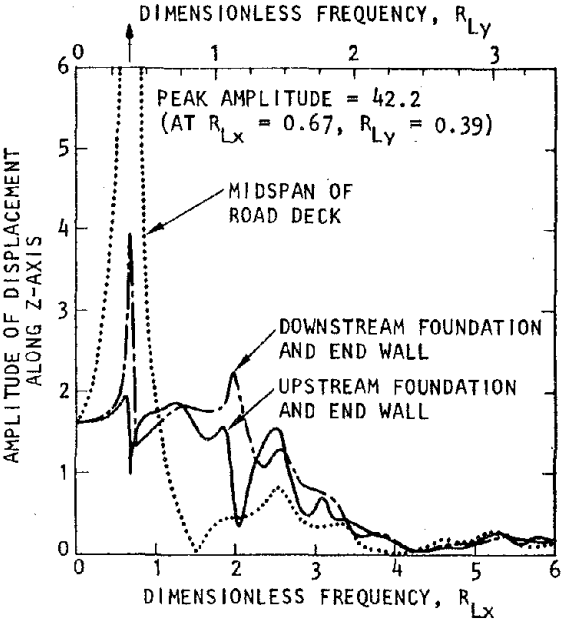

(c) Displacement along z-axis

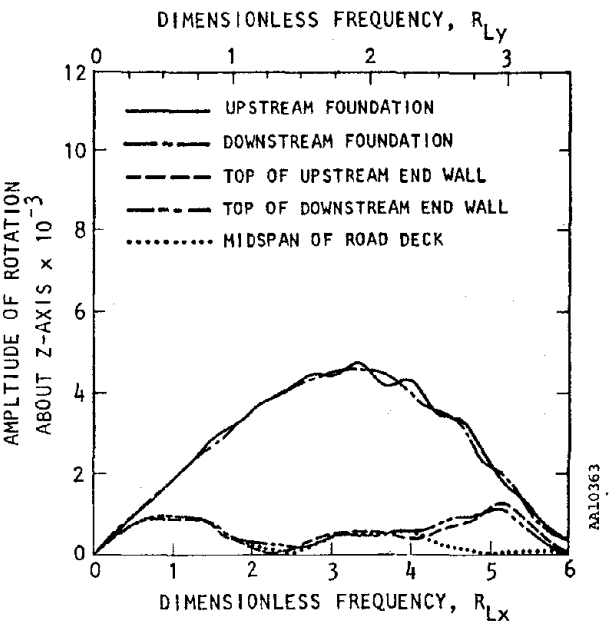

(d) Rotation about z-axis

FIGURE 4-38. FREQUENCY-DEPENDENT RESPONSE AMPLITUDES OF BRIDGE SUBJECTED TO INCIDENT SV-WAVES WITH θ_H = 45 DEG, θ_V = 55 DEG

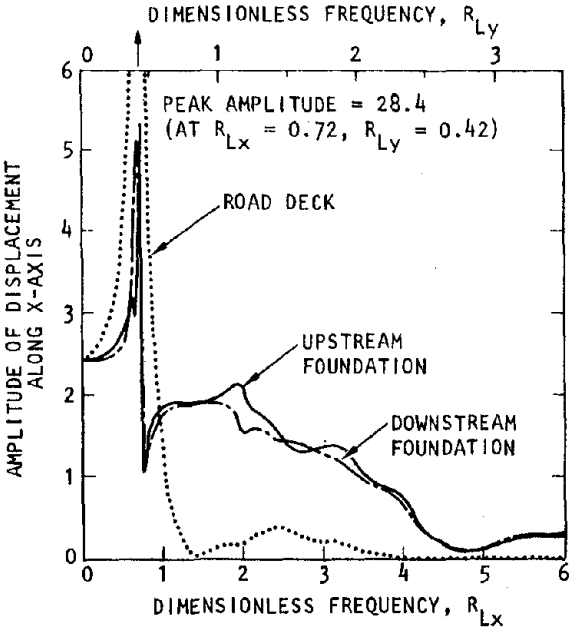

(a) Displacement along x-axis

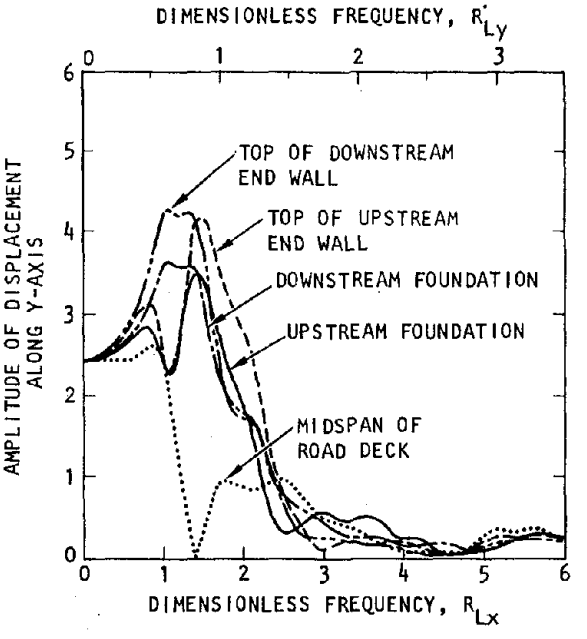

(b) Displacement along y-axis

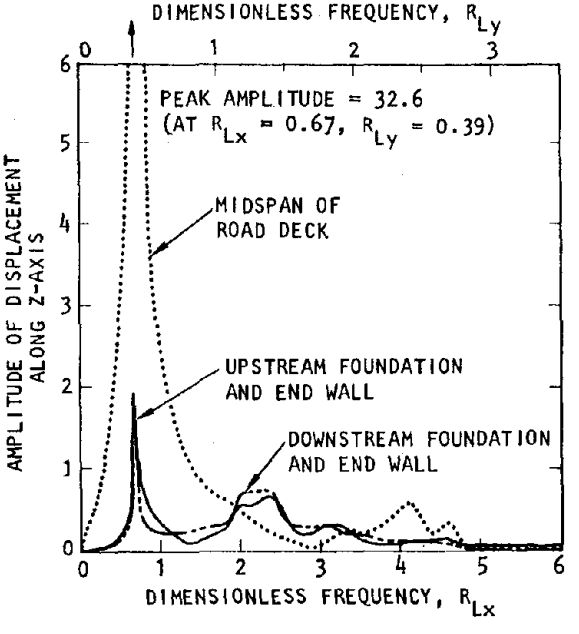

(c) Displacement along z-axis

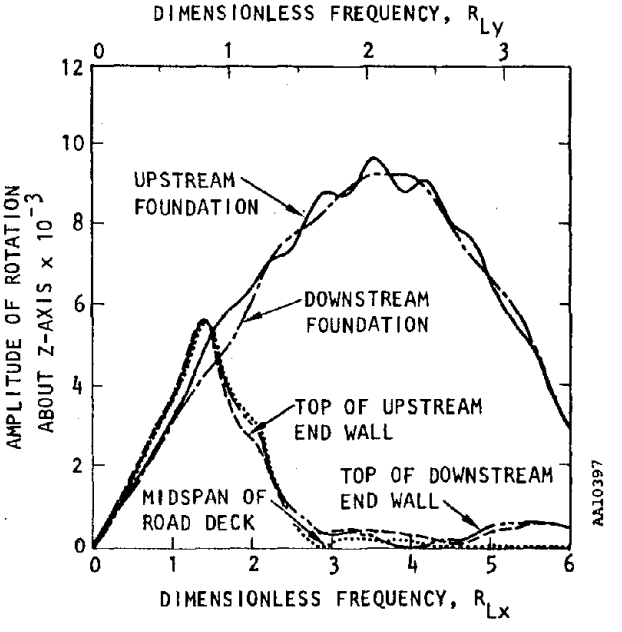

(d) Rotation about z-axis

FIGURE 4-39. FREQUENCY-DEPENDENT RESPONSE AMPLITUDES OF BRIDGE SUBJECTED TO INCIDENT SV-WAVES WITH θ_H = 45 DEG, θ_V = 60 DEG

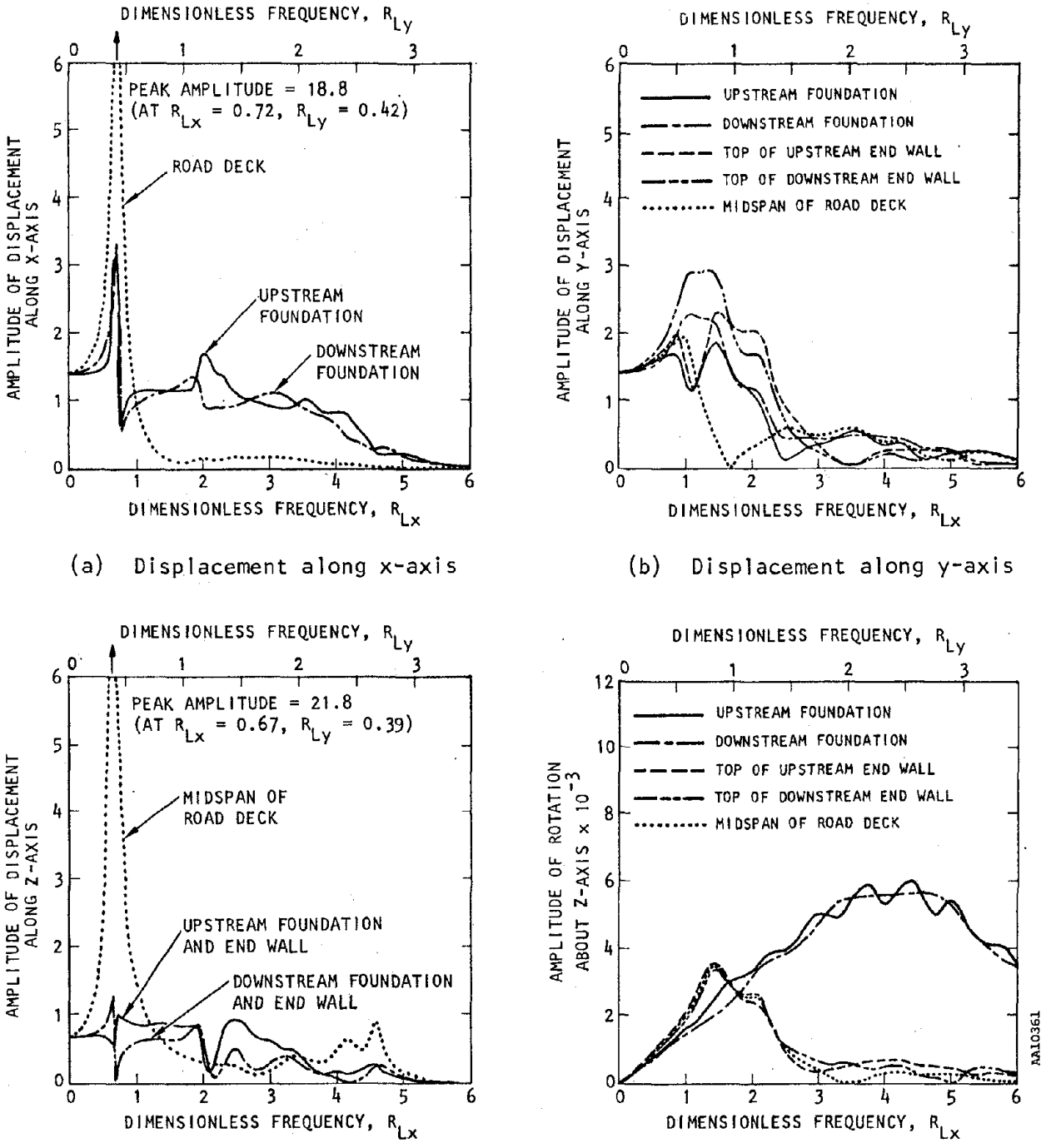

FIGURE 4-40. FREQUENCY-DEPENDENT RESPONSE AMPLITUDES OF BRIDGE SUBJECTED TO INCIDENT SV-WAVES WITH θ_H = 45 DEG, θ_V = 65 DEG

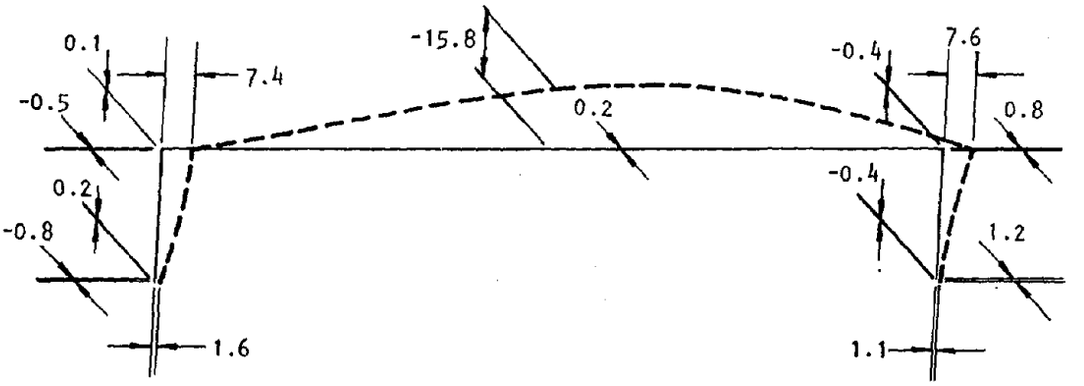

(a) θ_V = 55 deg

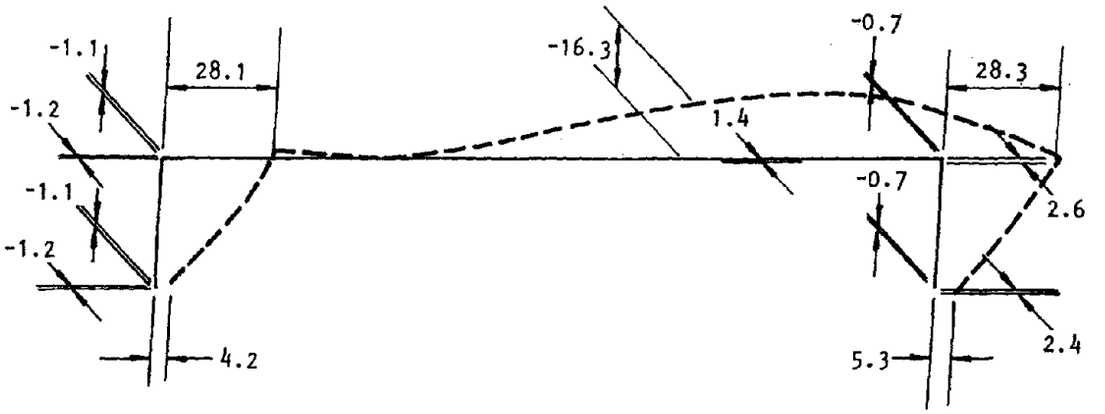

(b) θ_V = 60 deg

AA10424

FIGURE 4-41. CASE 3 (θ_H = 45 DEG): DEFORMED SHAPES OF BRIDGE AT TIMES OF PEAK RESONANT RESPONSE TO SV-WAVE EXCITATIONS (R_{Lx} = 0.72, R_{Ly} = 0.42, f = 3.0 Hz)

THIS PAGE INTENTIONALLY BLANK

CHAPTER 5

P-WAVE ANALYSIS

5.1 GENERAL DISCUSSION

Of the various wave types addressed in this report, P-waves are the simplest. Unlike the Rayleigh waves and SV-waves considered in prior chapters of the report, the horizontal and vertical components of the free field P-wave excitation are always real and in-phase with one another, regardless of θ_V. However, the amplitudes of the horizontal and vertical excitations do vary with θ_V.

There have been only a few studies of the response of structures to traveling P-waves and, as with SV-waves and Rayleigh waves, these studies have been limited to consideration of very simple structural elements. For example, Scanlan (1976) considered the response of a rigid rectangular foundation on distributed soil springs that was subjected to horizontally incident P-waves with variable wavelength. These calculations showed that when excitations were applied to P-waves whose wavelength was short relative to the foundation length, the resulting foundation displacements became small when compared to those of the free field; this reduction in foundation displacements, which was also observed for short-wavelength SH-wave excitation by Scanlan and by other investigators, did not occur when the wavelength of the excitation was long relative to the foundation length. Wong and Luco (1978) analyzed a rigid rectangular foundation bonded to the surface of an elastic half-space and subjected to arbitrarily incident P-wave excitation. They showed that nonvertically incident P-waves generated significant rocking of the foundation; such rocking responses were not excited by vertically incident P-waves. Wolf and Obernhuber (1979) analyzed a rigid circular foundation and elastic half-space that supported a simple single-mass structure. Their results showed that at higher excitation frequencies where translational motions of the foundation centroid are reduced, rocking of the foundation causes significant vertical translations of the edge of the foundation and prominent horizontal displacements of the single-mass structure.

This chapter presents results from the analysis of the single-span bridge subjected to arbitrarily incident P-waves. The remainder of the chapter first describes the nature of the free field P-wave excitations to which the bridge is subjected. Then, analysis results are presented for seven different cases in which each case corresponds to a particular set of angles of incidence, θ_H and θ_V. These cases are listed in Table 5-1.

5.2 EXCITATION

The free field motion generated along the ground surface by a P-wave with angles of incidence θ_H and θ_V (Fig. 5-1), amplitude p, and circular frequency ω is

$$\left\{ U_{ff} \right\} = \left\{ \begin{matrix} U_x \\ U_y \\ U_z \end{matrix} \right\} \exp \left[i\omega \left(t - \frac{x}{c} \cos \theta_H - \frac{y}{c} \sin \theta_H \right) \right] \qquad (5\text{-}1)$$

where U_x, U_y, and U_z are the amplitudes of motion along the x, y, and z axes (Fig. 5-1) and c is the phase velocity. It is noted that Equation 5-1 is identical to Equation 4-1 for SV-wave motions, except that now c is expressed in terms of the P-wave velocity V_p as $V_p/\cos \theta_V$. Also, as for SV-waves, U_x, U_y, and U_z can be expressed in terms of the amplitudes of the horizontal and vertical P-wave motion in the plane of the wave (U_H and U_V, respectively) as

$$\left\{ \begin{matrix} U_x \\ U_y \\ U_z \end{matrix} \right\} = \left[\begin{matrix} \cos \theta_H & 0 \\ \sin \theta_H & 0 \\ 0 & 1 \end{matrix} \right] \left\{ \begin{matrix} U_H \\ U_V \end{matrix} \right\} \qquad (5\text{-}2)$$

In Equation 5-2, U_H and U_V are computed considering that an incident P-wave gives rise to a reflected P-wave and a reflected SV-wave (Fig. 5-1). Expressions for these displacement components are (Ewing et al., 1957)

$$U_H = p\left[\frac{4 \sin \theta_V \tan f (\tan^2 f + 1)}{4 \tan \theta_V \tan f + (\tan^2 f - 1)^2}\right]$$

$$U_V = p\left[\frac{-2 \sin \theta_V (\tan^2 f - 1)(\tan^2 f + 1)}{4 \tan \theta_V \tan f + (\tan^2 f - 1)^2}\right] \qquad (5\text{-}3)$$

where p is the amplitude of the incident P-wave and θ_V and f are, respectively, the angles that the incident and reflected P-waves and the reflected SV-wave make with the ground surface (Fig. 5-1). These angles are related through the expression

$$\cos f = \frac{V_s}{V_P} \cos \theta_V \qquad (5\text{-}4)$$

where V_P and V_s are the P-wave and S-wave velocities of the elastic half-space. In terms of the Poisson's ratio of the elastic half-space, ν, it can be shown that the angle f is expressed as

$$\tan f = \sqrt{\frac{2(1 - \nu)}{(1 - 2\nu)} (1 + \tan^2 \theta_V) - 1} \qquad (5\text{-}5)$$

The substitution of Equation 5-5 into 5-3 shows that U_H and U_V are functions solely of the incident P-wave amplitude p, the angle of incidence θ_V, and the Poisson's ratio ν. Also, it is noted from Equation 5-4 that f attains a maximum value, f_{max}, of

$$f_{max} = \cos^{-1} \frac{V_s}{V_P}$$

Since $V_S < V_P$, then Equation 5-4 shows that f is always real; i.e., there is always a reflected SV-wave regardless of the value of θ_V. From this, Equation 5-3 indicates that U_H and U_V are also always real and are in phase with one another. Only the amplitudes of U_H and U_V vary with θ_V, as shown in Figure 5-2 for the case where $p = 1$ and $\nu = 1/3$.

5.3 RESULTS FOR CASE 1: VERTICALLY INCIDENT P-WAVES

The first case to be considered corresponds to vertically incident P-waves (Fig. 5-3). Amplitudes and phase angles for this case are tabulated at selected frequencies in Table 5-2, and frequency-dependent displacement amplitudes are shown in Figure 5-4. These results are shown only for displacements in the x- and z-directions; all other response components are negligible for this case. The following trends are observed from these results:

- Two resonant responses are seen to occur. The primary resonant response takes place at a frequency of 2.8 Hz ($R_{Lx} = 0.34$ and $R_{Ly} = 0.20$) and corresponds to bending of the road deck in its x-z plane; it features symmetric vertical displacements that are large at the midspan of the road deck, together with smaller equal-and-opposite horizontal displacements (along the x-axis) of the two foundations and end walls. A secondary resonant response at 19.9 Hz ($R_{Lx} = 2.39$ and $R_{Ly} = 1.39$) corresponds to more complex bending of the road deck and end walls (see the deformed shapes in Figure 5-5 and the tabulated results in Table 5-2).*

- Because of the symmetry of the bridge and the vertically incident P-wave excitation for this case, the above results can be generalized to all other excitation frequencies; i.e., at all frequencies, the bridge response is characterized solely by symmetric vertical displacements of the bridge and by

*The frequency of this resonant response is slightly higher than the frequency of the corresponding fixed base mode (Mode 4 of Fig. 2-6a, which is 18.4 Hz). This phenomenon, also noted for some higher frequency resonant responses to incident Rayleigh waves and SV-waves, may be attributable to effects of three-dimensional soil/structure interaction and the phased input motions (see footnote on p 3-6).

equal-and-opposite horizontal displacements (along the x-axis) of the two foundations and end walls. No rocking response of this bridge is induced by the vertically incident P-waves.

5.4 RESULTS FROM CASES 2 THROUGH 7: NONVERTICALLY INCIDENT P-WAVES

5.4.1 FREE-FIELD MOTIONS

This section presents results that illustrate the extent to which nonvertically incident P-waves cause bridge responses that differ from bridge responses induced by vertically incident P-waves. These results are from calculations based on P-waves that propagate in planes normal to the span of the bridge (θ_H = 90 deg), parallel to the span of the bridge (θ_H = 0 deg), and oblique to the span of the bridge (θ_H = 45 deg). For each value of θ_H, two different angles of vertical incidence are considered: θ_V = 10 deg and θ_V = 45 deg. The amplitudes of the horizontal and vertical components of the P-wave motion are given in Figure 5-2 for these two values of θ_V. This figure indicates that:

- The amplitudes of the horizontal component of the P-wave motion (U_H) and the vertical component (U_V) are both greater when θ_V = 45 deg than when θ_V = 10 deg.
- When θ_V = 45 deg, U_H and U_V have similar amplitudes, with U_V being only slightly greater. In contrast, when θ_V = 10 deg, U_H exceeds U_V by a factor of nearly 2.0.

Therefore, both the absolute values and the relative values of the amplitudes of U_H and U_V differ markedly for these two θ_V angles.

5.4.2 CASES 2 AND 3: NONVERTICALLY INCIDENT P-WAVES WITH θ_H = 90 DEG

Cases 2 and 3 both correspond to nonvertically incident P-waves that are propagating in a plane normal to the span of the bridge, or parallel to its y-z plane (θ_H = 90 deg, as shown in Fig. 5-6). Case 2 represents the results for θ_H = 90 deg and θ_V = 10 deg, while Case 3 represents the results for θ_H = 90 deg and θ_V = 45 deg. Results for these two cases are presented as tabulated amplitudes and phase angles at specific frequencies

(Table 5-3), as amplitude vs. dimensionless frequency plots (Figs. 5-7 and 5-8) and as deformed shapes at times of peak resonant response (Fig. 5-9). These results show that:

- Overall, the principal response components generated by these P-wave excitations are the displacements along the y- and z-axes. However, displacements along the x-axis and rotations about the z-axis are also generated over certain isolated frequency ranges. At 2.8 Hz (R_{Ly} = 0.20), opposite-phased x-displacements of the two foundations occur in conjunction with the very large symmetrical vertical displacements of the road deck that are occurring as a resonant response at that frequency (Figs. 5-7a,c and 5-8a,c). At a frequency band around 5.1 Hz (R_{Ly} = 0.36), small z-rotations at the tops of the two end walls are generated as a consequence of the road-deck bending in the x-y plane that occurs within this band. Because these z-rotations are slightly larger than those of the foundations, the end walls undergo small torsional deformations.

- Two types of resonant response are excited by the nonvertically incident P-waves with θ_H = 90 deg. The first occurs at 2.8 Hz (R_{Ly} = 0.20) and is essentially identical to the resonant response induced at this same frequency by the vertically incident P-waves. The second resonant response occurs at 5.1 Hz (R_{Ly} = 0.36) and features horizontal rocking displacements of the bridge in the y-direction that are coupled with vertical displacements of the road deck, end walls, and foundations.* This second resonant response is not induced by vertically incident P-waves. Deformed shapes at times of peak response for each of these resonant frequencies are shown in Figure 5-9.

*The frequency at which this maximum y-displacement occurs is slightly larger (20%) for P-waves than for SH-, SV-, and Rayleigh waves. This may be related to the fact that: (a) at this frequency, the wavelength is longer for P-waves than for shear waves and Rayleigh waves, thereby resulting in a different net loading applied along the foundations; and (b) the phasing of the horizontal and vertical free-field excitations is different for P-waves than for the other wave types; this could result in coupling effects that alter the net driving forces and drive the bridge at a slightly different frequency.

- The bridge displacements along the y-axis and the x-axis both exhibit common characteristics with regard to the dimensionless frequency R_{Ly}. The largest displacements of the bridge occur when R_{Ly} is small, which corresponds to apparent wavelengths of the P-waves that are long relative to the 70-ft length of the bridge foundations in the y-direction. As R_{Ly} becomes large, which corresponds to apparent wavelengths of the P-waves that are short relative to the foundation length, the bridge displacements become small relative to the free-field displacements (given as the zero-frequency displacement amplitudes in Figs. 5-7 and 5-8). Two aspects of this response are as follows: (a) it can be attributed to a self-canceling effect whereby the net loading applied by the incident waves to a rigid foundation becomes small when the wavelength becomes short relative to the foundation length (Werner et al., 1977); and (b) this phenomenon is expected to be somewhat less pronounced when flexible rather than rigid foundations are considered.

- There are two main differences between the response characteristics of Case 2 (θ_V = 10 deg) and Case 3 (θ_V = 45 deg). First, the bridge displacements are all larger for Case 3, a direct consequence of the larger free-field displacements that occur for that case. Second, the previously noted self-canceling effect, which leads to bridge displacements that are small relative to the free field, first occurs at higher dimensionless frequencies for Case 3 than for Case 2. This spreading of the frequency scale is caused by apparent wavelength effects (Sec. 2.3). Also, the reduction in bridge displacements due to self-canceling effects is less pronounced for Case 3.

5.4.3 CASES 4 AND 5: NONVERTICALLY INCIDENT P-WAVES WITH θ_H = 0 DEG

Cases 4 and 5 both correspond to nonvertically incident P-waves that are propagating in a plane parallel to the x-z plane of the bridge, or along its span (θ_H = 0 deg, as shown in Fig. 5-10). Case 4 represents the results for θ_H = 0 deg and θ_V = 10 deg, while Case 5 represents the results for θ_H = 0 deg and θ_V = 45 deg. Results for these cases are shown in Table 5-4

as tabulated amplitudes and phase angles at specific frequencies and in Figures 5-11 and 5-12 as amplitude vs. dimensionless frequency plots. These results are discussed first for resonant responses and then for phased-input-induced responses.

5.4.3.1 Resonant Response Characteristics

Figures 5-11 and 5-12 indicate that the excitations for these cases induce two resonant responses at closely spaced frequencies. The first is at f = 2.8 Hz (R_{Lx} = 0.34) and corresponds to essentially the same resonant response and deformed shape as was induced at that frequency by the vertically incident P-wave excitations of Case 1 and by the nonvertically incident P-wave excitations of Cases 2 and 3 (Fig. 5-13a). The second occurs at f = 3.0 Hz (R_{Lx} = 0.36) and consists of horizontal sidesway response in the x-direction coupled with significant vertical displacements of the road deck (Fig. 5-13b). These resonant responses are induced by the excitations from Case 4 (θ_H = 0 deg, θ_V = 10 deg) as well as Case 5 (θ_H = 0 deg, θ_V = 45 deg), the only difference being that the displacement amplitudes are greater for Case 5. The sidesway resonant response was not excited by the vertically incident P-waves of Case 1.

5.4.3.2 Phased-Input-Induced Response Characteristics

To illustrate additional effects of the phasing of the P-wave excitations on the nonresonant bridge response, two sets of results are presented. The first set corresponds to free-field P-wave excitations that are of equal amplitude and opposite phase at the two foundations; this occurs when the ratio of the bridge span length to the apparent wavelength of the incident wave is 0.5, 1.5, 2.5, etc. The second set of results corresponds to free-field excitations that are identical in both amplitude and phase at the two foundations; this occurs when the ratio of the bridge span length to the apparent wavelength of the incident waves is 1.0, 2.0, 3.0, etc.

These results are presented as tabulated amplitudes and phase angles in Table 5-5 and as time-dependent deformed shapes of the bridge in

Figures 5-14 to 5-17. They show that the bridge response depends on the phasing of the excitations applied at the two foundations and, in addition, on the frequency of the excitations for a given phasing. Furthermore, these response characteristics are seen to be markedly different from those induced by the vertically incident P-waves of Case 1. In particular, it is observed that

- The equal-amplitude and opposite-phase P-wave excitations induce bridge deformations that are neither symmetric nor antisymmetric about the midspan of the road deck. No horizontal sidesway is induced by these excitations (Figs. 5-14, 5-16).

- The equal-amplitude and equal-phase P-wave excitations induce horizontal sidesway displacements of the bridge (in the x-direction) that are coupled with the vertical displacements of the foundations, end walls, and road deck (Figs. 5-15, 5-17). These response characteristics are clearly different from those induced by the equal-amplitude and opposite-phase excitations, illustrating the importance of the phasing of the P-wave excitations applied at the two foundations.

- For a given phasing of the applied excitations, the deformed shape of the bridge becomes more complex as R_{Lx} is increased. As noted in the Rayleigh wave and SV-wave results, this is a consequence of the increased influence of wave diffraction and scattering and the higher modes of vibration.

- The bridge displacements of Case 5 are larger than those of Case 4, particularly in the vertical direction. This is because of the larger free-field P-wave displacements, particularly in the vertical direction, that result as θ_V is increased from 10 deg to 45 deg. Also, for a given frequency, the phasing of

the free-field excitations applied to the two foundations differs in Cases 4 and 5 because of apparent wavelength effects; this contributes to some of the differences between the bridge responses that result for these two cases.

5.4.4 CASES 6 AND 7: NONVERTICALLY INCIDENT P-WAVES WITH θ_H = 45 DEG

Cases 6 and 7 both correspond to nonvertically incident P-waves that are propagating in a plane that makes an angle of 45 deg with the x-z plane of the bridge (θ_H = 45 deg as shown in Fig. 5-18). Case 6 represents the results for θ_H = 45 deg and θ_V = 10 deg, while Case 7 represents the results for $\theta_H = \theta_V$ = 45 deg. Results for these cases are shown in Tables 5-6 and 5-7 as tabulated displacement amplitudes and phase angles at specific frequencies, and in Figures 5-19 and 5-20 as amplitude vs. dimensionless frequency plots. In addition, deformed shapes at times of peak resonant response and time-dependent deformed shapes that depict phased-input-induced response characteristics are presented in Figures 5-21 to 5-24.

These results show that, in contrast to the results for θ_H = 90 deg and θ_H = 0 deg, the bridge response from Cases 6 and 7 is now fully three dimensional over the entire frequency range. The particular response characteristics for these cases are summarized as follows:

- Resonant responses are excited at frequencies of 2.8 Hz and 3.0 Hz (Table 5-6). These resonances have both been excited in one or more of the prior P-wave cases and, as before, involve primary responses in the x-z plane. For example, the resonance at 2.8 Hz, which was excited in all prior cases, features symmetric bending of the road deck in the z-direction with a very large vertical displacement at the midspan of the road deck (Fig. 5-21a). The resonance that occurs at 3.0 Hz involves sidesway in the x-direction coupled with vertical displacements of the road deck (Fig. 5-21b).

- It was previously shown that the Case 2 and Case 3 excitations (θ_H = 90 deg) led to a resonant response at 5.1 Hz (R_{Ly} = 0.36) involving bending of the road deck in the y-direction and large y-displacements of the midspan of the road deck (Table 5-3, Fig. 5-9b). This resonant response, which is symmetric about the midspan of the road deck, is not excited when θ_H = 45 deg because this oblique angle of horizontal incidence introduces phase differences between the y-components of free-field excitation applied to the two foundations; these phase differences destroy the symmetry of the y-components of excitation applied to the two foundations. As shown in Figures 5-22 and 5-23, the deformed shapes of the bridge that result at 5.1 Hz when θ_H = 45 deg are markedly different from the resonance conditions occurring when θ_H = 90 deg; nevertheless, they still feature relatively large displacements in the y-direction (also see Table 5-7).

- Because of the phase differences that are introduced between the free-field excitations at the two foundations when θ_H = 45 deg, the bridge response over the entire frequency range differs from that induced by the excitations of Cases 2 to 5. (This is clearly shown by comparing Figures 5-19 and 5-20 with the figures for the corresponding components of response from Cases 2 to 5.) One important consequence of these phase differences is the out-of-phase rocking displacements (in the y-direction) that occur at the two end walls; these, in turn, lead to torsional deformations in the road deck.

- Significant rotations about the z-axis for various elements of the bridge are excited by the free field P-wave excitations for Case 6 and Case 7 (Fig. 5-19d, 5-20d). The most significant rotations occur in the foundation elements at $R_{Lx} > 1.0$.

At these higher frequencies, the foundation rotation amplitudes substantially exceed the road deck rotation amplitudes, indicating that the end walls (which interconnect the foundations and road deck) are undergoing prominent torsional deformations. At lower values of R_{Lx}, the differences between the road deck and foundation rotation amplitudes are smaller; however, because the road deck and foundation rotations are not in phase (Table 5-5), the end walls undergo torsional deformations at these lower frequencies as well. These torsional deformations were not induced by the P-wave excitations from Cases 1, 4, and 5 and were induced on a smaller scale by the excitations from Cases 2 and 3.

- The bridge response of Case 7 differs from that of Case 6 because of the larger amplitudes of free-field excitation that result when θ_V is increased and, in addition, because of apparent wavelength effects that alter the phasing of the excitations applied to the two foundations at a given frequency (Table 5-7).

TABLE 5-1. LIST OF CASES FOR ANALYSIS OF BRIDGE SUBJECTED TO ARBITRARILY INCIDENT P-WAVES

Case No.	Description	Horizontal Angle of Incidence, θ_H, deg	Vertical Angle of Incidence, θ_V, deg
1	Vertically incident P-waves	Arbitrary	90
2	Nonvertically incident P-waves propagating in plane normal to span of bridge	90	10
3			45
4	Nonvertically incident P-waves propagating in plane parallel to span of bridge	0	10
5			45
6	Nonvertically incident P-waves propagating in plane oblique to span of bridge	45	10
7			45

Note: See Figure 2-1 for definition of θ_H and θ_V.

TABLE 5-2. BRIDGE RESPONSE TO VERTICALLY INCIDENT P-WAVES (CASE 1)(1)

Description of Response	Excitation Frequency(2)			Component of Response	Upstream Foundation		Downstream Foundation		Top of Upstream End Wall		Top of Downstream End Wall		Midspan of Road Deck	
	R_{Lx}	R_{Ly}	f, Hz		Amplitude	Phase Angle, rad	Amplitude	Phase Angle, rad	Amplitude	Phase Angle, rad	Amplitude	Phase Angle, rad	Amplitude	Phase Angle, rad
Resonance with fundamental bending mode of road deck in x-z plane	0.34	0.20	2.83	Displacement along x-axis	7.389	-0.586π	7.389	0.414π	0.635	-1.573π	0.635	-0.573π	Small	--
				Displacement along z-axis	6.116	0.438π	6.116	0.438π	6.295	0.438π	6.295	0.438π	121.340	0.425π
Resonance with higher bending mode of road deck in x-z plane	2.39	1.39	19.89	Displacement along x-axis	1.888	-3.960π	1.888	-2.960π	0.209	-3.961π	0.209	-2.961π	Small	--
				Displacement along z-axis	2.246	0.713π	2.246	0.713π	2.243	0.708π	2.242	0.708π	5.289	-1.210π

Note: (1) Free-field displacement at the ground surface (vertical only) has amplitude of 2.0 and zero phase angle when $\theta_V = 90$ deg.

(2) R_{Lx} = ratio of bridge span length (120 ft) to wavelength of incident P-wave

R_{Ly} = ratio of foundation length (70 ft) to wavelength of incident P-wave

f = excitation frequency (Hz)

AA10241

TABLE 5-3. BRIDGE RESPONSE TO NONVERTICALLY INCIDENT P-WAVES WITH θ_H = 90 DEG (CASES 2 AND 3)(1)

Description of Response	Angle of Incidence, θ_V, deg	Excitation Frequency(2)		Component of Response	Upstream Foundation		Downstream Foundation		Top of Upstream End Wall		Top of Downstream End Wall		Midspan of Road Deck	
		R_{Ly}	f, Hz		Amplitude	Phase Angle, rad	Amplitude	Phase Angle, rad	Amplitude	Phase Angle, rad	Amplitude	Phase Angle, rad	Amplitude	Phase Angle, rad
Resonance with fundamental bending mode of road deck in x-z plane	10	0.20	2.83	Displacement along x-axis	1.836	-0.571π	1.836	-1.571π	0.158	0.422π	0.158	-0.558π	Small	--
				Displacement along y-axis	1.073	-0.011π	1.073	-0.011π	1.191	0.040π	1.191	0.040π	1.242	0.040π
				Displacement along z-axis	1.520	-1.547π	1.520	-1.547π	1.564	-1.547π	1.564	-1.547π	30.151	-1.559π
	45	0.20	2.83	Displacement along x-axis	5.207	-0.580π	5.207	0.420π	0.448	0.433π	0.447	-0.567π	Small	--
				Displacement along y-axis	1.636	-0.007π	1.636	-0.007π	1.839	0.060π	1.839	0.060π	1.919	0.060π
				Displacement along z-axis	4.310	-1.556π	4.310	-1.556π	4.436	-1.557π	4.436	-1.557π	85.503	-1.569π
Resonance with fundamental sidesway mode of bridge in y-direction	10	0.36	5.10	Displacement along y-axis	2.716	-0.326π	2.716	-0.326π	3.657	-0.330π	3.657	-0.330π	4.215	-0.330π
				Displacement along z-axis	0.500	-0.988π	0.500	-0.988π	0.500	-0.988π	0.500	-0.988π	0.462	-1.981π
	45	0.36	5.10	Displacement along y-axis	4.779	-0.309π	4.779	-0.309π	6.350	-0.305π	6.350	-0.305π	7.319	-0.305π
				Displacement along z-axis	1.508	-1.004π	1.508	-1.004π	1.510	-1.004π	1.510	-1.004π	1.395	-1.997π

Note: (1) Free-field displacement components at the ground surface (U_x, U_y, and U_z in Eq. 5-1) have amplitudes of 0.0, 0.879, and 0.528 when θ_V = 10 deg, and 0.0, 1.285 and 1.457 when θ_V = 45 deg. Also, these components have a zero phase angle at the upstream foundation, which is the origin of the coordinate system for this analysis.

(2) R_{Ly} = Ratio of foundation length (70 ft) to wavelength of incident P-wave

f = Excitation frequency (Hz)

AA10242

TABLE 5-4. RESONANT RESPONSE OF BRIDGE TO NONVERTICALLY INCIDENT P-WAVES WITH θ_H = 0 DEG (CASES 4 AND 5)(1)

Description of Response	Angle of Incidence, θ_V, deg	Excitation Frequency(2)		Component of Response	Upstream Foundation		Downstream Foundation		Top of Upstream End Wall		Top of Downstream End Wall		Midspan of Road Deck	
		R_{Lx}	f, Hz		Amplitude	Phase Angle, rad	Amplitude	Phase Angle, rad	Amplitude	Phase Angle, rad	Amplitude	Phase Angle, rad	Amplitude	Phase Angle, rad
Resonance with fundamental bending mode of road deck in x-z plane	10	0.34	2.83	Displacement along x-axis	3.279	-0.447π	1.044	-1.474π	3.959	-0.401π	4.364	-0.414π	4.182	-0.408π
				Displacement along z-axis	2.257	-1.536π	2.780	0.373π	2.320	-1.536π	2.837	0.375π	40.803	-1.525π
	45	0.34	2.83	Displacement along x-axis	5.821	-0.506π	2.976	-1.819π	8.779	-0.293π	9.231	-0.318π	9.046	-0.306π
				Displacement along z-axis	3.781	-1.588π	5.461	0.344π	3.896	-1.588π	5.574	0.344π	76.586	0.380π
Resonance with fundamental sidesway mode of bridge in z-direction	10	0.36	3.0	Displacement along x-axis	1.184	-0.804π	1.675	-0.786π	7.508	-0.794π	7.605	-0.795π	7.601	-0.795π
				Displacement along z-axis	0.041	-1.925π	0.801	0.210π	0.056	-1.912π	0.810	0.208π	7.163	-1.900π
	45	0.36	3.0	Displacement along x-axis	3.055	-0.750π	3.703	-2.641π	17.485	-0.689π	17.596	-0.691π	17.645	-0.690π
				Displacement along z-axis	0.418	-0.943π	1.385	0.386π	0.392	-0.945π	1.387	0.382π	13.228	0.007π

NOTE: (1) Free-field displacement components at the ground surface (U_x and U_z in Eq. 5-1) have amplitudes of 0.879 and 0.528 when θ_V = 10 deg, and 1.285 and 1.457 when θ_V = 45 deg. Also, these components have a zero phase angle at the upstream foundation, which is the origin of the coordinate system for this analysis.

(2) R_{Lx} = Ratio of bridge span length (120 ft) to wavelength of incident P-wave

f = Excitation frequency (Hz)

AA10283

TABLE 5-5. PHASED-INPUT-INDUCED RESPONSE OF BRIDGE SUBJECTED TO NONVERTICALLY INCIDENT P-WAVES WITH θ_H = 0 DEG (CASES 4 AND 5)(1)

Description of Response	Angle of Incidence, θ_V, deg	Excitation Frequency(2) R_{Lx}	Excitation Frequency(2) f, Hz	Component of Response	Upstream Foundation Amplitude	Upstream Foundation Phase Angle, rad	Downstream Foundation Amplitude	Downstream Foundation Phase Angle, rad	Top of Upstream End Wall Amplitude	Top of Upstream End Wall Phase Angle, rad	Top of Downstream End Wall Amplitude	Top of Downstream End Wall Phase Angle, rad	Midspan of Road Deck Amplitude	Midspan of Road Deck Phase Angle, rad
Response to free-field excitations of equal amplitude and opposite phase applied at the two foundations	10	$\frac{0.5}{\cos 10\ deg}$ (0.508)	4.23	Displacement along x-axis	0.691	-1.999π	0.734	-1.002π	0.009	-1.179π	0.049	-0.999π	0.029	-1.027π
				Displacement along z-axis	0.567	-1.023π	0.787	-0.033π	0.566	-1.023π	0.792	-0.033π	0.852	-1.971π
		$\frac{1.5}{\cos 10\ deg}$ (1.523)	12.69	Displacement along x-axis	1.093	-2.085π	1.387	-3.222π	0.054	-2.315π	0.057	-0.963π	0.032	-0.654π
				Displacement along z-axis	0.702	-1.382π	0.590	-2.331π	0.712	-1.383π	0.598	-2.331π	0.359	-2.194π
	45	$\frac{0.5}{\cos 45\ deg}$ (0.707)	5.89	Displacement along x-axis	1.239	-2.001π	1.128	-3.016π	0.168	-2.134π	0.122	-2.226π	0.147	-2.172π
				Displacement along z-axis	1.984	0.897π	2.312	-0.105π	1.998	0.897π	2.332	-0.105π	0.552	0.046π
		$\frac{1.5}{\cos 45\ deg}$ (2.121)	17.68	Displacement along x-axis	1.752	-2.528π	1.869	-5.559π	0.118	-4.537π	0.118	-3.601π	0.016	-4.077π
				Displacement along z-axis	0.783	0.241π	1.431	-0.626π	0.845	0.244π	1.450	-0.625π	2.310	-0.662π
Response to free-field excitations of equal amplitude and opposite phase applied at the two foundations	10	$\frac{1.0}{\cos 10\ deg}$ (1.015)	8.46	Displacement along x-axis	0.664	-2.105π	0.922	-2.153π	0.227	-0.855π	0.229	-0.857π	0.239	-0.856π
				Displacement along z-axis	0.775	-1.413π	1.220	-1.070π	0.791	-1.416π	1.233	-1.067π	0.438	-2.193π
		$\frac{2.0}{\cos 10\ deg}$ (2.031)	16.92	Displacement along x-axis	1.224	-2.358π	1.320	-4.331π	0.130	-3.343π	0.117	-1.337π	0.151	-1.340π
				Displacement along z-axis	0.238	-1.434π	0.198	-3.671π	0.249	-1.441π	0.218	-3.658π	0.560	-2.576π
	45	$\frac{1.0}{\cos 45\ deg}$ (1.414)	11.79	Displacement along x-axis	2.034	-2.104π	1.008	-4.132π	0.265	-2.966π	0.321	-3.001π	0.322	-2.985π
				Displacement along z-axis	2.048	0.721π	3.140	0.615π	2.088	0.719π	3.203	0.616π	1.728	-0.321π
		$\frac{2.0}{\cos 45\ deg}$ (2.828)	23.57	Displacement along x-axis	1.115	-2.503π	0.834	-6.722π	0.121	-5.850π	0.041	-3.513π	0.111	-5.771π
				Displacement along z-axis	0.487	0.347π	0.495	0.554π	0.514	0.342π	0.523	0.553π	0.344	0.533π

NOTE: (1) Free-field displacement components at the ground surface (U_x and U_z in Eq. 5-1) have amplitudes of 0.879 and 0.528 when θ_V = 10 deg, and 1.285 and 1.457 when θ_V = 45 deg. Also, these components have a zero phase angle at the upstream foundation that is the origin of the coordinate system for this analysis.

(2) R_{Lx} = Ratio of bridge span length (120 ft) to wavelength of incident P-wave
f = Excitation frequency (Hz)

AA10284

TABLE 5-6. RESONANT RESPONSE OF BRIDGE SUBJECTED TO NONVERTICALLY INCIDENT P-WAVES WITH θ_H = 45 DEG (CASES 6 AND 7)

Description of Response	Angle of Incidence, θ_V, deg	Excitation Frequency(2) R_{Lx}	R_{Ly}	f, Hz	Component of Response	Upstream Foundation Amplitude	Upstream Foundation Phase Angle, rad	Downstream Foundation Amplitude	Downstream Foundation Phase Angle, rad	Top of Upstream End Wall Amplitude	Top of Upstream End Wall Phase Angle, rad	Top of Downstream End Wall Amplitude	Top of Downstream End Wall Phase Angle, rad	Midspan of Road Deck Amplitude	Midspan of Road Deck Phase Angle, rad
Resonance with fundamental bending mode of road deck in x-z plane	10	0.34	0.20	2.83	Displacement along x-axis	2.533	-0.461π	0.924	-1.301π	4.045	-0.313π	4.276	-0.331π	4.181	-0.322π
					Displacement along y-axis	0.732	-0.029π	0.757	-0.459π	0.788	0.014π	0.828	-0.399π	0.671	-0.198π
					Displacement along z-axis	1.611	-1.553π	2.115	0.381π	1.657	-1.553π	2.159	0.382π	30.418	-1.571π
					Rotation about z-axis x 10^{-3}	0.524	-1.486π	0.536	0.007π	0.669	-0.669π	0.667	-0.695π	0.676	-0.682π
	45	0.34	0.20	2.83	Displacement along x-axis	5.333	-0.543π	4.081	-1.807π	7.227	-0.223π	7.470	-0.257π	7.377	-0.241π
					Displacement along y-axis	1.130	-0.025π	1.154	-0.327π	1.244	0.036π	1.293	-0.251π	1.190	-0.111π
					Displacement along z-axis	3.649	-1.620π	4.986	0.351π	3.764	-1.621π	5.101	0.351π	77.549	0.353π
					Rotation about z-axis x 10^{-3}	0.544	-1.495π	0.559	0.144π	0.761	-0.573π	0.757	-0.617π	0.767	-0.595π
Resonance with fundamental sidesway mode of bridge in x-direction	10	0.36	0.21	3.00	Displacement along x-axis	1.390	-0.749π	1.644	-2.666π	8.040	-0.706π	8.096	-0.708π	8.116	-0.707π
					Displacement along y-axis	0.747	-0.033π	0.775	-0.486π	0.807	0.010π	0.857	-0.423π	0.677	-0.214π
					Displacement along z-axis	0.047	-1.013π	0.513	0.412π	0.037	-1.056π	0.514	0.408π	5.287	-1.944π
					Rotation about z-axis x 10^{-3}	0.555	-1.484π	0.567	-0.021π	0.719	-0.681π	0.716	-0.708π	0.726	-0.695π
	45	0.36	0.21	3.00	Displacement along x-axis	2.688	-0.716π	3.051	-2.537π	14.575	-0.620π	14.635	-0.623π	14.692	-0.622π
					Displacement along y-axis	1.163	-0.029π	1.191	-0.345π	1.291	0.032π	1.352	-0.267π	1.234	-0.121π
					Displacement along z-axis	0.491	-0.928π	1.012	0.552π	0.468	-0.928π	1.002	0.547π	13.475	-0.022π
					Rotation about z-axis x 10^{-3}	0.573	-1.494π	0.592	0.124π	0.826	-0.579π	0.820	-0.626π	0.832	-0.603π

NOTE: (1) Free-field displacement components at the ground surface (U_x, U_y, and U_z in Eq. 5-1) have amplitudes of 0.622, 0.622, and 0.528 when θ_V = 10 deg, and 0.909, 0.909, and 1.457 when θ_V = 45 deg. Also, these components have a zero phase angle at the upstream foundation, which is the origin of the coordinate system for this analysis.

(2) R_{Lx} = Ratio of bridge span length (120 ft) to wavelength of incident P-wave

R_{Ly} = Ratio of foundation length (70 ft) to wavelength of incident P-wave

f = Excitation frequency (Hz)

AA10281

TABLE 5-7. COUPLED THREE-DIMENSIONAL RESPONSE OF BRIDGE SUBJECTED TO NONVERTICALLY INCIDENT P-WAVES WITH θ_H = 45 DEG (CASES 6 AND 7)

Angle of Incidence, θ_V, deg	Excitation Frequency(2)			Component of Response	Upstream Foundation		Downstream Foundation		Top of Upstream End Wall		Top of Downstream End Wall		Midspan of Road Deck	
	R_{Lx}	R_{Ly}	f, Hz		Amplitude	Phase Angle, rad	Amplitude	Phase Angle, rad	Amplitude	Phase Angle, rad	Amplitude	Phase Angle, rad	Amplitude	Phase Angle, rad
10	0.61	0.36	5.1	Displacement along x-axis	0.471	-1.983π	0.490	-2.851π	0.074	-1.520π	0.070	-1.413π	0.073	-1.468π
				Displacement along y-axis	0.721	-0.157π	1.403	-0.920π	0.660	-1.279π	1.733	-0.876π	0.778	-0.765π
				Displacement along z-axis	0.612	-1.044π	0.696	0.074π	0.620	-1.044π	0.701	0.074π	0.325	-2.008π
				Rotation about z-axis x 10^{-3}	1.040	-1.461π	0.973	-0.379π	1.634	-0.933π	1.439	-0.954π	1.565	-0.943π
	1.44	0.84	11.97	Displacement along x-axis	0.464	-2.084π	0.265	-4.057π	0.064	-2.951π	0.074	-2.987π	0.076	-2.971π
				Displacement along y-axis	0.402	-0.449π	0.429	-2.446π	0.018	-0.468π	0.049	-2.439π	0.100	-2.447π
				Displacement along z-axis	0.397	-1.250π	0.625	-1.378π	0.404	-1.253π	0.638	-1.376π	0.348	-2.311π
				Rotation about z-axis x 10^{-3}	2.220	-1.540π	2.347	-1.535π	0.076	-2.419π	0.071	-1.478π	0.017	-2.384π
45	0.61	0.36	5.1	Displacement along x-axis	0.680	-1.949π	0.815	-2.604π	0.275	-1.317π	0.287	-1.281π	0.285	-1.299π
				Displacement along y-axis	1.465	-0.396π	3.132	-0.715π	1.663	-0.455π	4.094	-0.678π	3.151	-0.615π
				Displacement along z-axis	1.880	-1.031π	1.728	0.300π	1.887	-1.031π	1.737	0.299π	0.894	-0.157π
				Rotation about z-axis x 10^{-3}	1.068	-1.433π	1.075	-0.134π	2.465	-0.763π	1.684	-0.838π	2.102	-0.793π
	2.00	1.17	16.67	Displacement along x-axis	0.636	-4.324π	0.758	-4.302π	0.074	-3.318π	0.058	-3.267π	0.080	-3.296π
				Displacement along y-axis	1.188	-0.760π	1.190	-2.767π	0.071	-1.068π	0.081	-0.945π	0.522	-2.000π
				Displacement along z-axis	0.325	-1.494π	0.303	-1.580π	0.345	-1.498π	0.327	-1.576π	0.680	-0.553π
				Rotation about z-axis x 10^{-3}	4.156	-1.646π	4.483	-1.640π	0.652	-1.994π	0.635	-1.008π	0.013	-0.581π

NOTE: (1) Free-field displacement components at the ground surface (U_x, U_y, and U_z in Eq. 5-1) have amplitudes of 0.622, 0.622, and 0.528 when θ_V = 10 deg, and 0.909, 0.909, and 1.457 when θ_V = 45 deg. Also, these components have a zero phase angle at the upstream foundation, which is the origin of the coordinate system for this analysis.

(2) R_{Lx} = Ratio of bridge span length (120 ft) to wavelength of incident P-wave

R_{Ly} = Ratio of foundation length (70 ft) to wavelength of incident P-wave

f = Excitation frequency (Hz)

AA10282

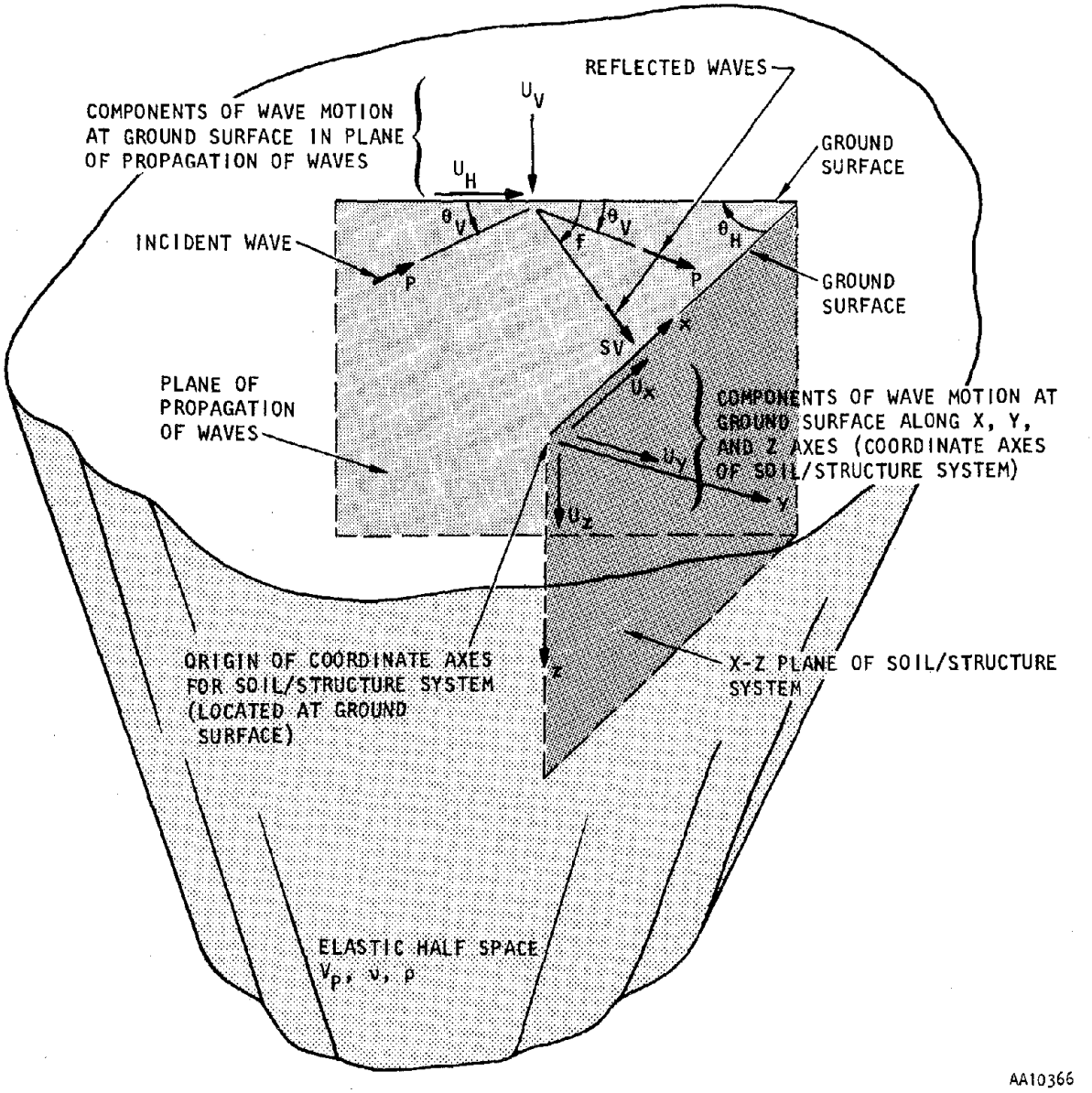

FIGURE 5-1. FREE-FIELD P-WAVE GROUND MOTION

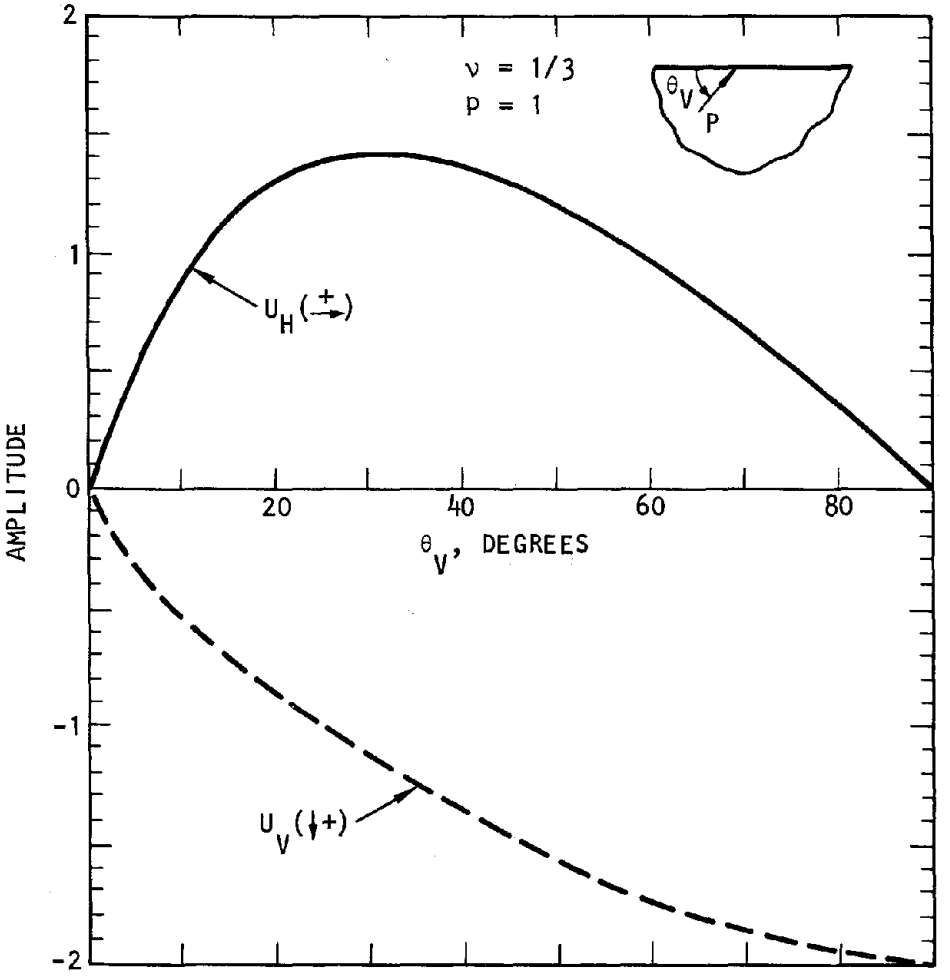

FIGURE 5-2. HORIZONTAL AND VERTICAL P-WAVE GROUND SURFACE DISPLACEMENT AMPLITUDES FOR POISSON'S RATIO = 1/3

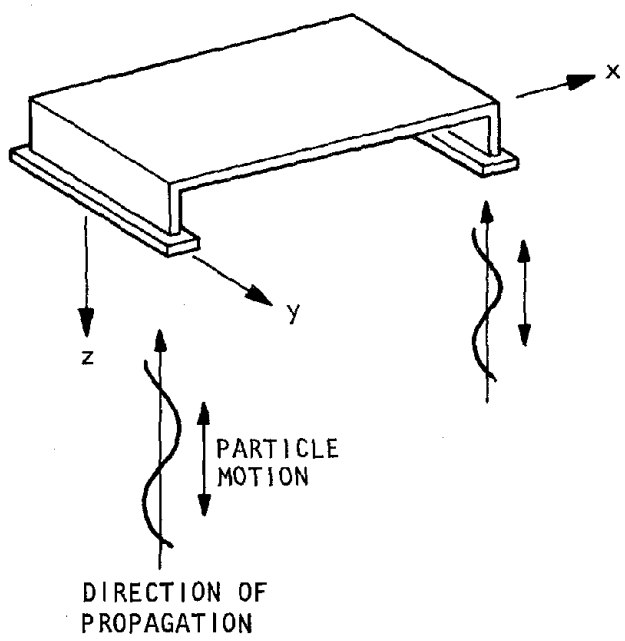

FIGURE 5-3. FREE-FIELD EXCITATIONS FROM INCIDENT P-WAVES FOR CASE 1 (θ_H = ARBITRARY, θ_V = 90 deg)

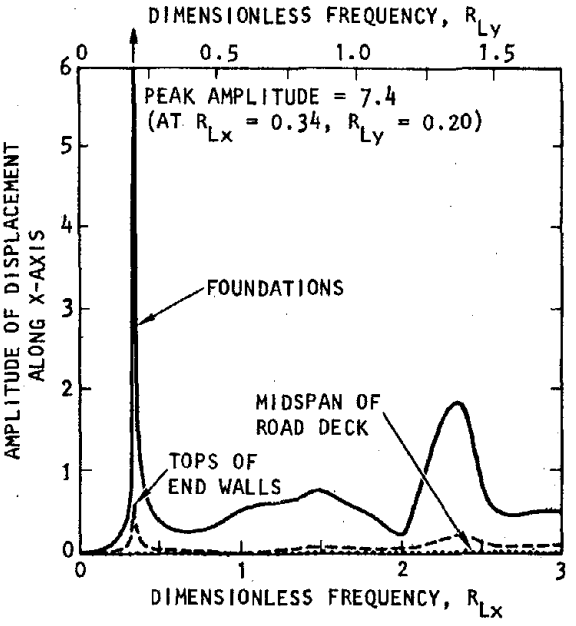

(a) Displacement along x-axis

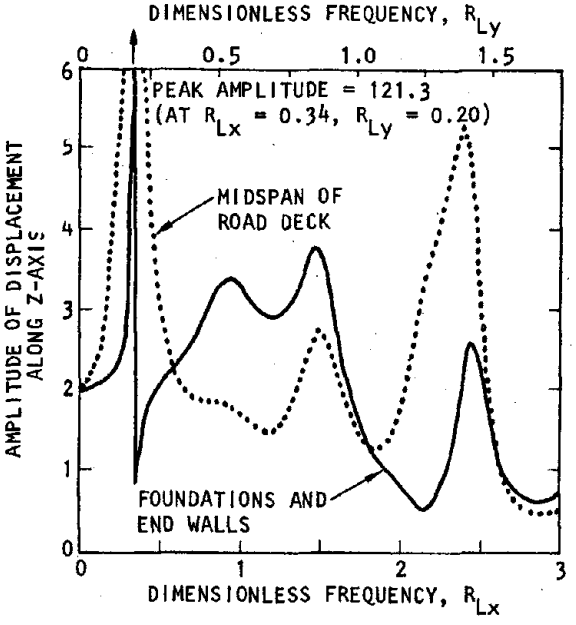

(b) Displacement along z-axis

FIGURE 5-4. FREQUENCY-DEPENDENT RESPONSE AMPLITUDES OF BRIDGE SUBJECTED TO VERTICALLY INCIDENT P-WAVES (θ_V = 90 DEG, θ_H ARBITRARY)

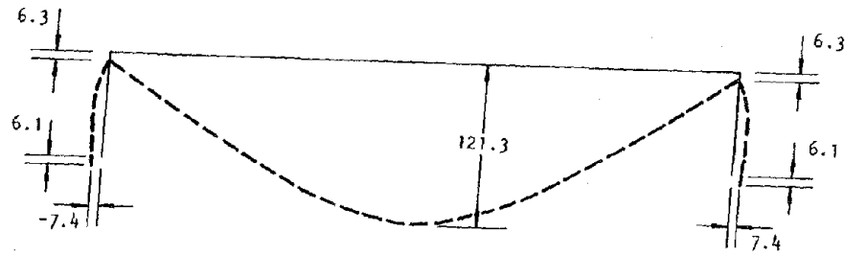

(a) R_{Lx} = 0.34 (f = 2.8 Hz)

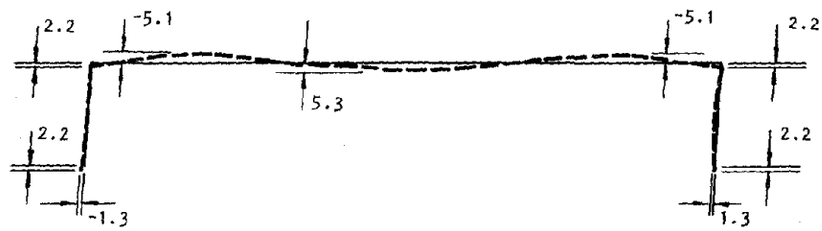

(b) R_{Lx} = 2.39 (f = 19.9 Hz)

AA10259

FIGURE 5-5. CASE 1 (θ_V = 90 deg): DEFORMED SHAPES OF BRIDGE AT TIMES OF PEAK RESONANT RESPONSE TO P-WAVE EXCITATIONS

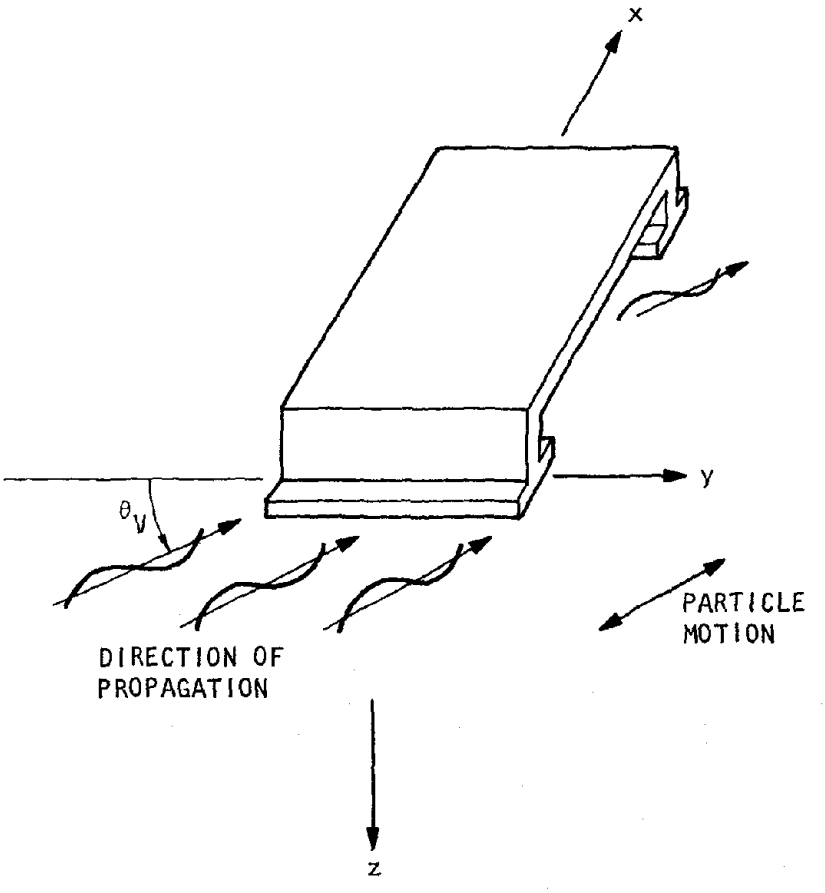

FIGURE 5-6. FREE-FIELD EXCITATIONS FROM INCIDENT P-WAVES FOR CASES 2 AND 3 (θ_H = 90 deg)

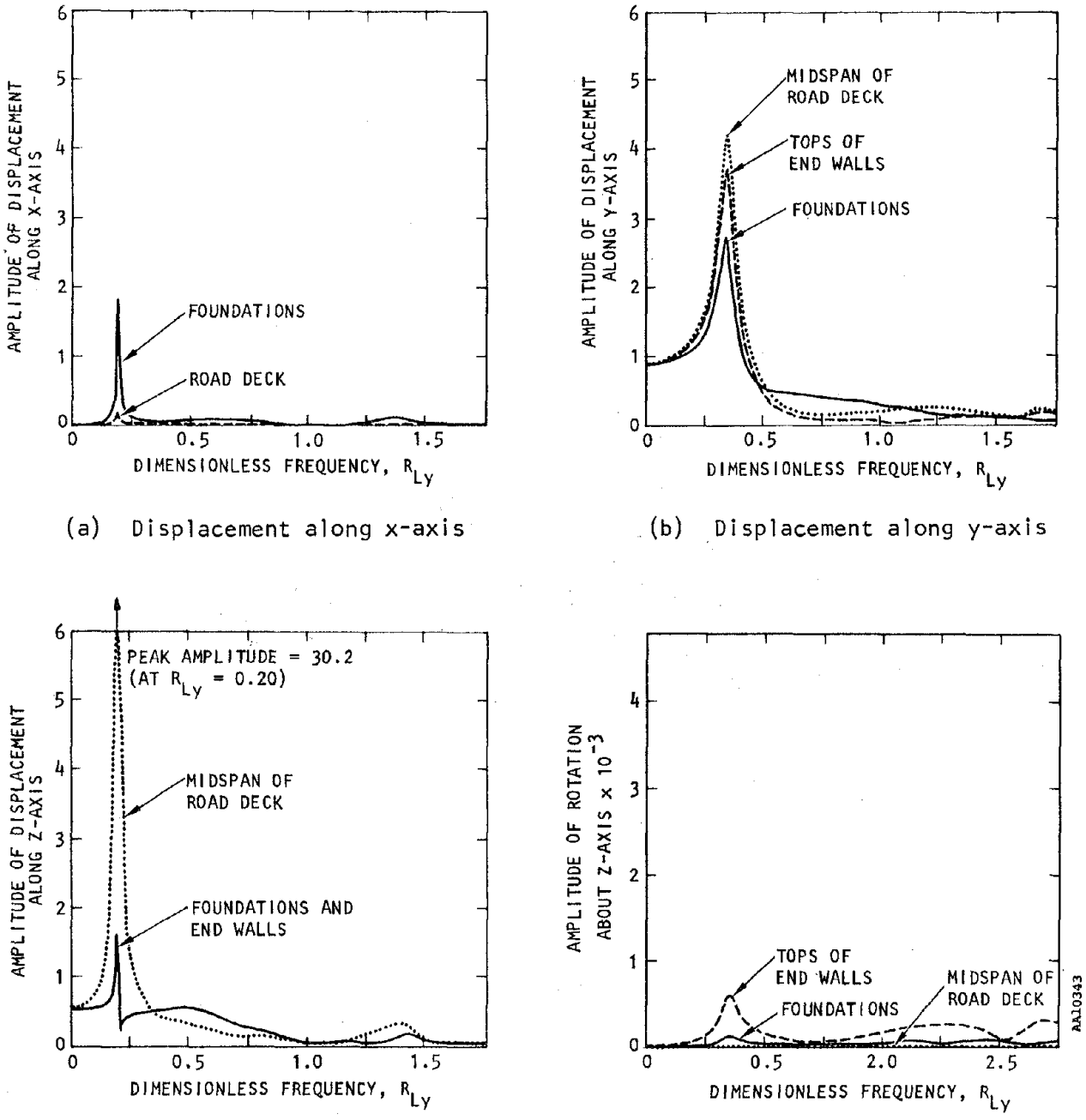

(a) Displacement along x-axis

(b) Displacement along y-axis

(c) Displacement along z-axis

(d) Rotation about z-axis

FIGURE 5-7. FREQUENCY-DEPENDENT RESPONSE AMPLITUDES OF BRIDGE SUBJECTED TO INCIDENT P-WAVES WITH θ_H = 90 DEG AND θ_V = 10 DEG

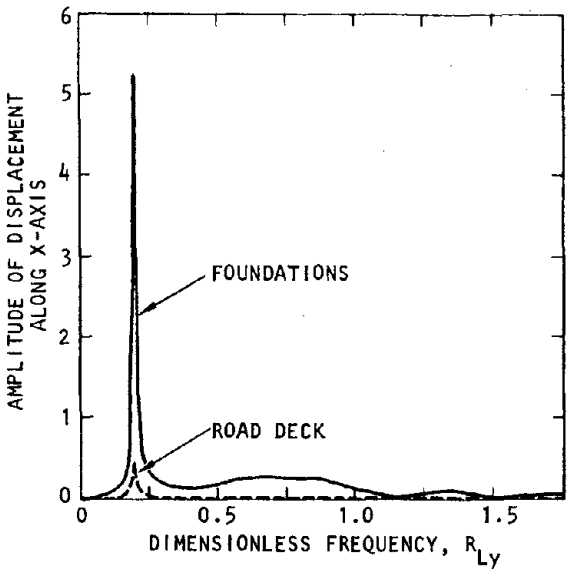

(a) Displacement along x-axis

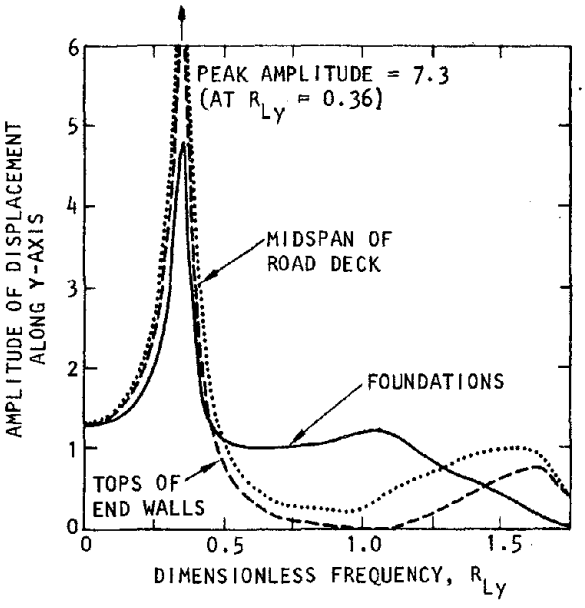

(b) Displacement along y-axis

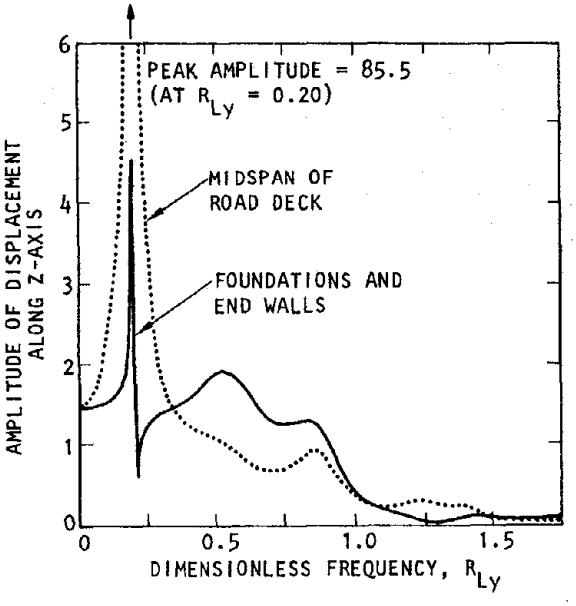

(c) Displacement along z-axis

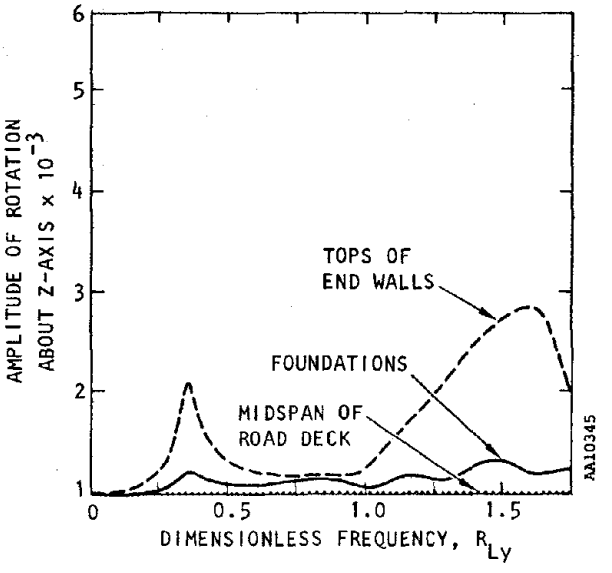

(d) Rotation about z-axis

FIGURE 5-8. FREQUENCY-DEPENDENT RESPONSE AMPLITUDES OF BRIDGE SUBJECTED TO INCIDENT P-WAVES WITH θ_H = 90 DEG AND θ_V = 45 DEG

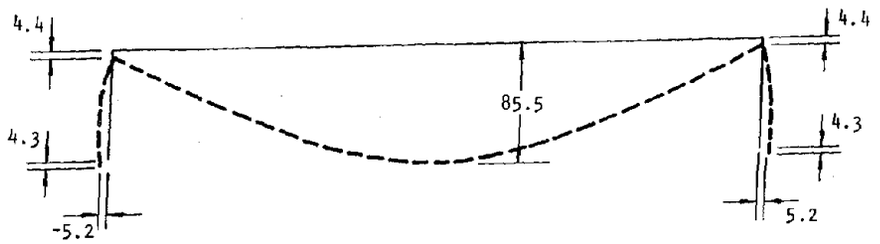

(a) R_{Ly} = 0.20 (f = 2.8 Hz)

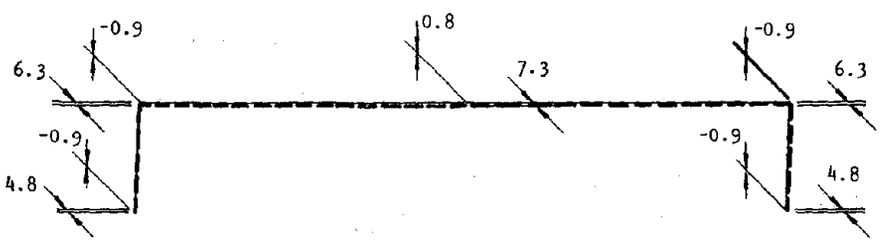

(b) R_{Ly} = 0.36 (f = 5.1 Hz)

NOTE: RESONANT FREQUENCIES AND DEFORMED SHAPES SHOWN ABOVE ARE ESSENTIALLY THE SAME AS THESE FOR CASE 2 (θ_H = 90 deg, θ_V = 10 deg), EXCEPT THAT, FOR THAT CASE, THE BRIDGE DISPLACEMENT AMPLITUDE ARE SMALLER (See Figures 5-7 to 5-8 and Table 5-3)

AA10258

FIGURE 5-9. CASE 3 (θ_H = 90 deg, θ_V = 45 deg): DEFORMED SHAPES OF BRIDGE AT TIMES OF PEAK RESONANT RESPONSE TO P-WAVE EXCITATIONS

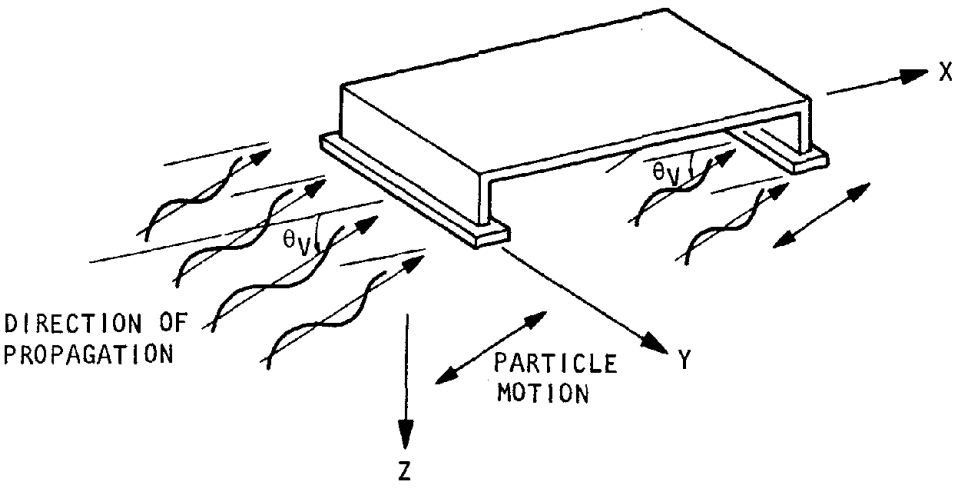

FIGURE 5-10. FREE-FIELD EXCITATIONS FROM INCIDENT P-WAVES FOR CASES 4 AND 5 (θ_H = 0 deg)

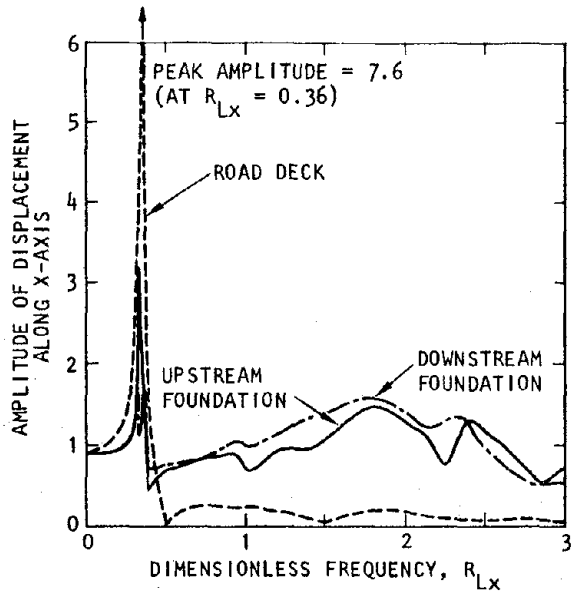

(a) Displacement along x-axis

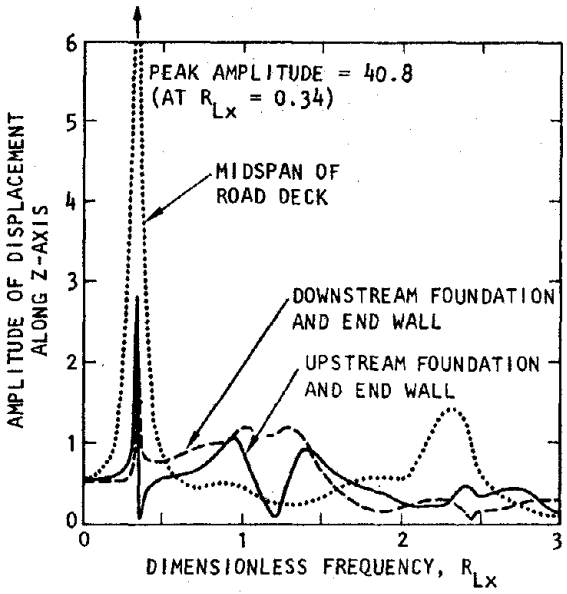

(b) Displacement along z-axis

FIGURE 5-11. FREQUENCY-DEPENDENT RESPONSE AMPLITUDES OF BRIDGE SUBJECTED TO INCIDENT P-WAVES WITH θ_H = 0 DEG AND θ_V = 10 DEG

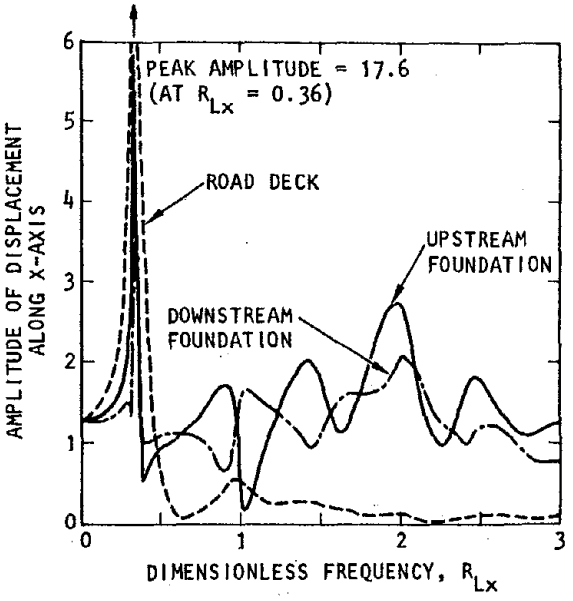

(a) Displacement along x-axis

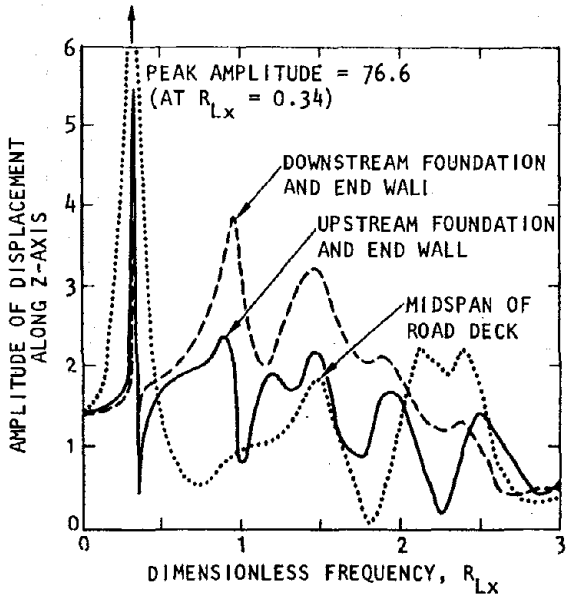

(b) Displacement along z-axis

FIGURE 5-12. FREQUENCY-DEPENDENT RESPONSE AMPLITUDES OF BRIDGE SUBJECTED TO INCIDENT P-WAVES WITH θ_H = 0 DEG AND θ_V = 45 DEG

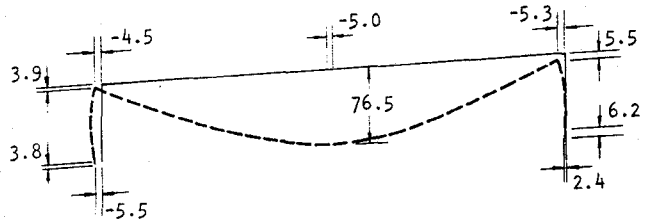

(a) R_{Lx} = 0.34 (f = 2.8 Hz)

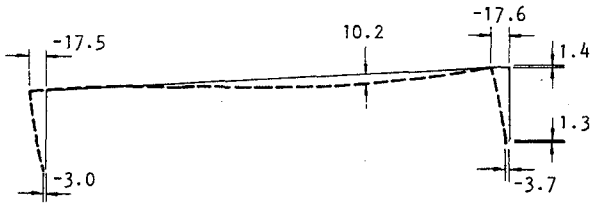

MAXIMUM SIDESWAY RESPONSE

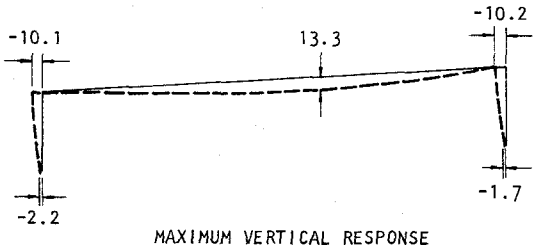

MAXIMUM VERTICAL RESPONSE

(b) R_{Lx} = 0.36 (f = 3.0 Hz)

AA10249

NOTE: RESONANT FREQUENCIES AND DEFORMED SHAPES SHOWN ABOVE ARE ESSENTIALLY THE SAME AS FOR CASE 4 (θ_H = 0 deg, θ_V = 10 deg) EXCEPT THAT, FOR THAT CASE, THE BRIDGE DISPLACEMENT AMPLITUDES ARE SMALLER (See Figures 5-11 to 5-12 and Table 5-4)

FIGURE 5-13. CASE 5 (θ_H = 0 deg, θ_V = 45 deg): DEFORMED SHAPES OF BRIDGE AT TIMES OF PEAK RESONANT RESPONSE TO P-WAVE EXCITATIONS

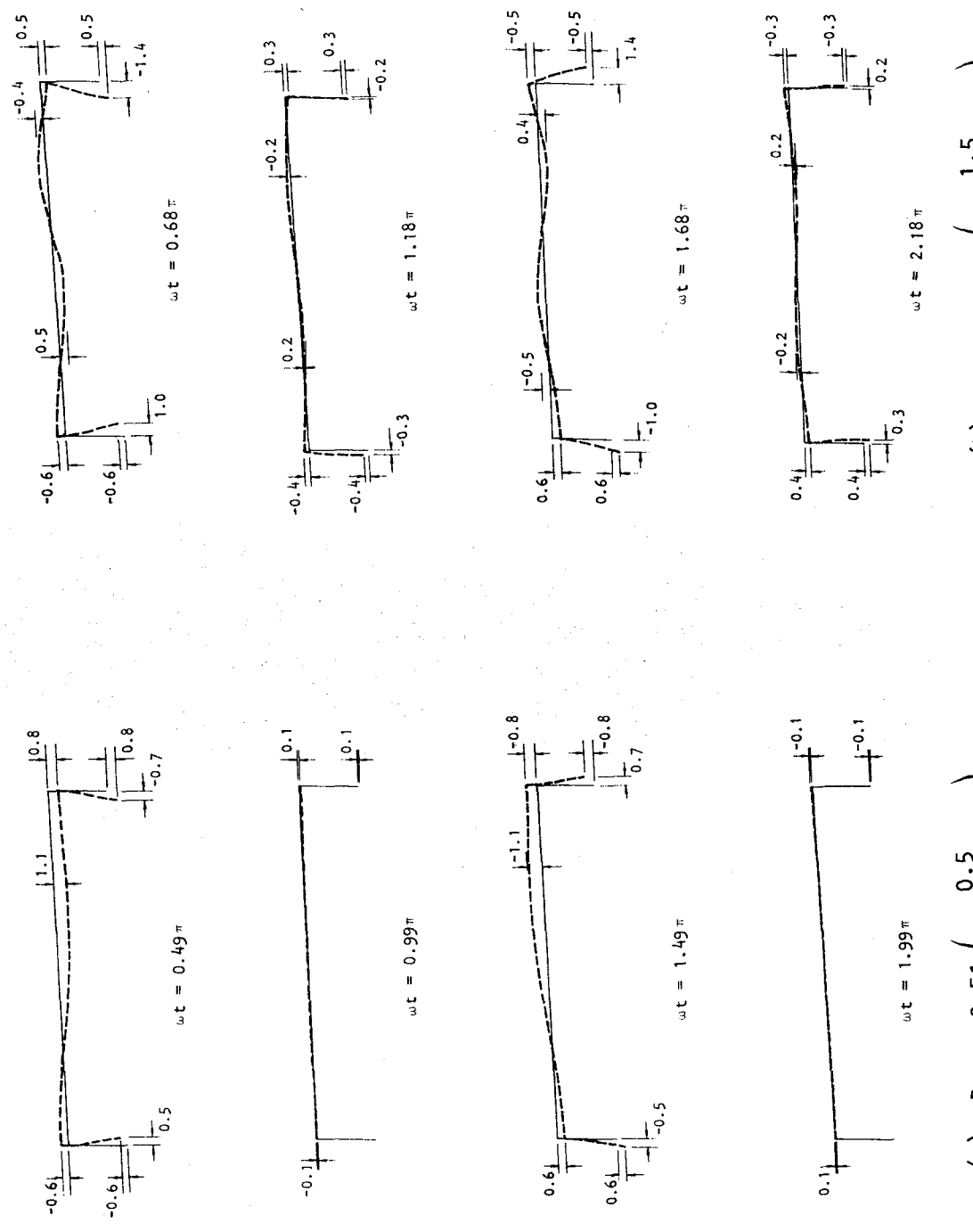

(a) $R_{Lx} = 0.51 \left(\frac{0.5}{\cos 10 \text{ deg}} \right)$ (b) $R_{Lx} = 1.52 \left(\frac{1.5}{\cos 10 \text{ deg}} \right)$

FIGURE 5-14. CASE 4 (θ_H = 0 deg, θ_V = 10 deg): BRIDGE RESPONSE TO APPLIED P-WAVE EXCITATIONS OF EQUAL AMPLITUDE AND OPPOSITE PHASE AT THE TWO FOUNDATIONS

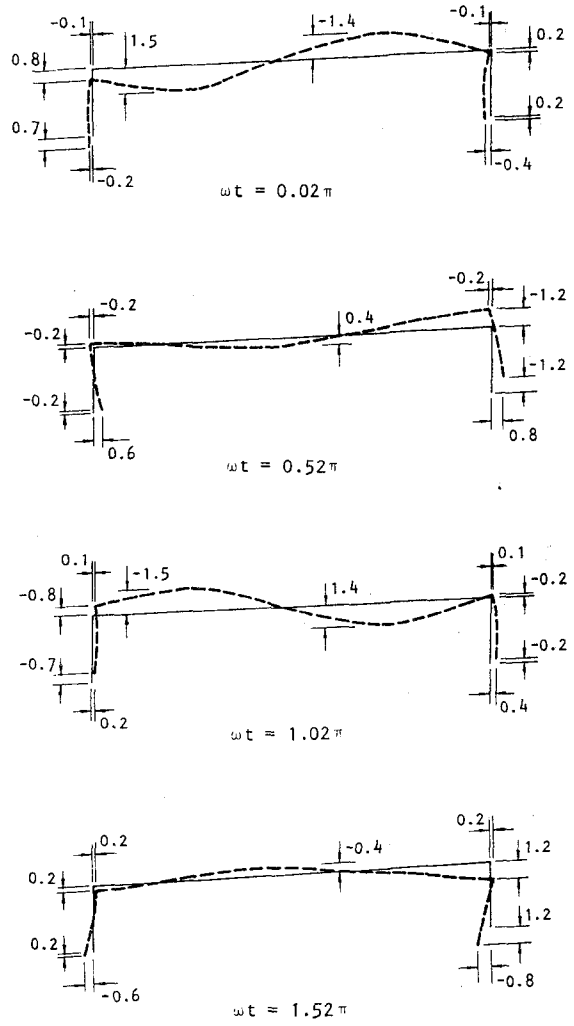

(a) $R_{Lx} = 1.02 \left(\frac{1.0}{\cos 10 \text{ deg}} \right)$

(b) $R_{Lx} = 2.03 \left(\frac{2.0}{\cos 10 \text{ deg}} \right)$

AA10251

FIGURE 5-15. CASE 4 (θ_H = 0 deg, θ_V = 10 deg): BRIDGE RESPONSE TO APPLIED P-WAVE EXCITATIONS OF EQUAL AMPLITUDE AND EQUAL PHASE AT THE TWO FOUNDATIONS

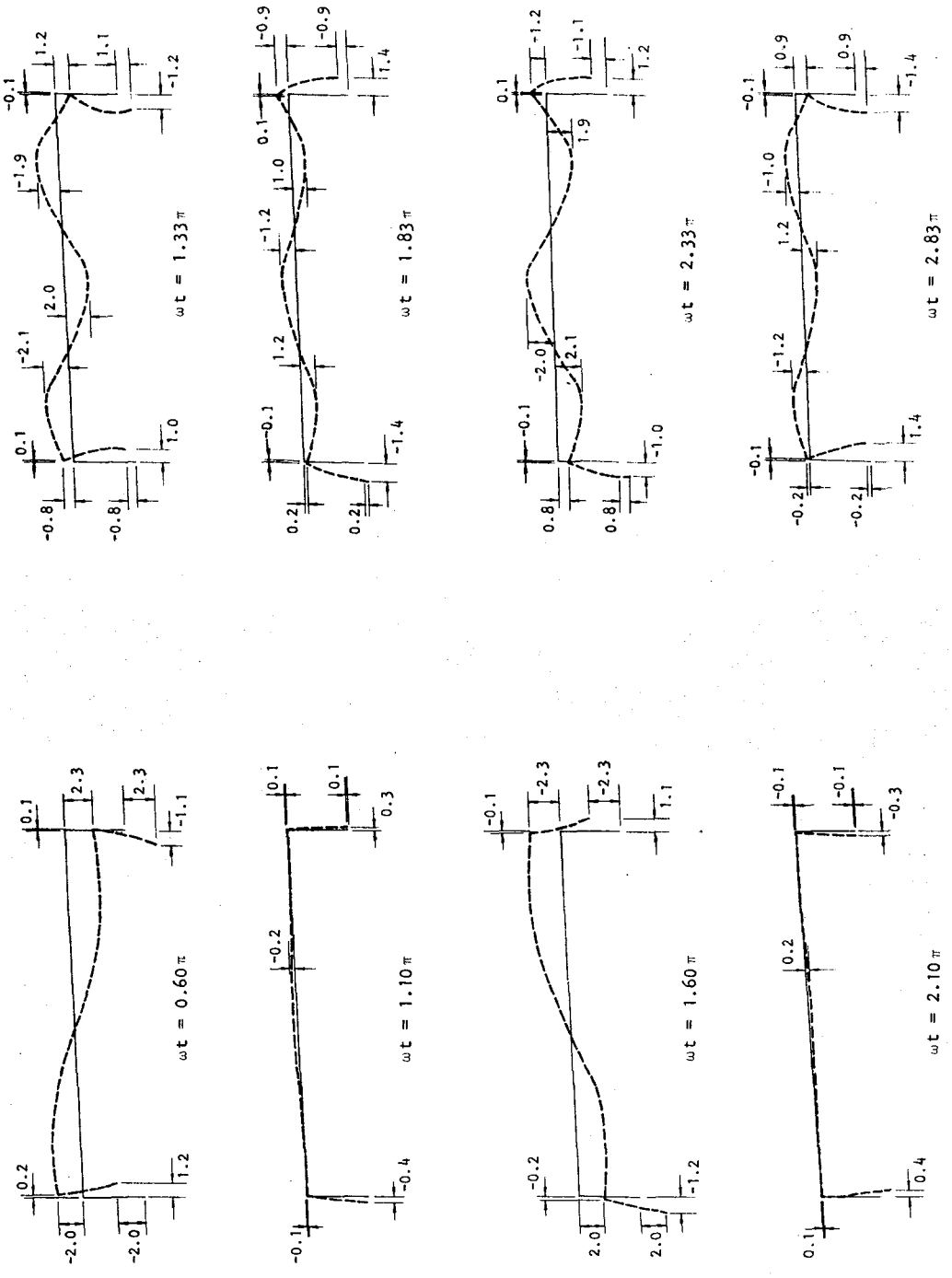

(a) $R_{Lx} = 0.71 \left(\frac{0.5}{\cos 45 \text{ deg}} \right)$ (b) $R_{Lx} = 2.12 \left(\frac{1.5}{\cos 45 \text{ deg}} \right)$

FIGURE 5-16. CASE 5 (θ_H = 0 deg, θ_V = 45 deg): BRIDGE RESPONSE TO APPLIED P-WAVE EXCITATIONS OF EQUAL AMPLITUDE AND OPPOSITE PHASE AT THE TWO FOUNDATIONS

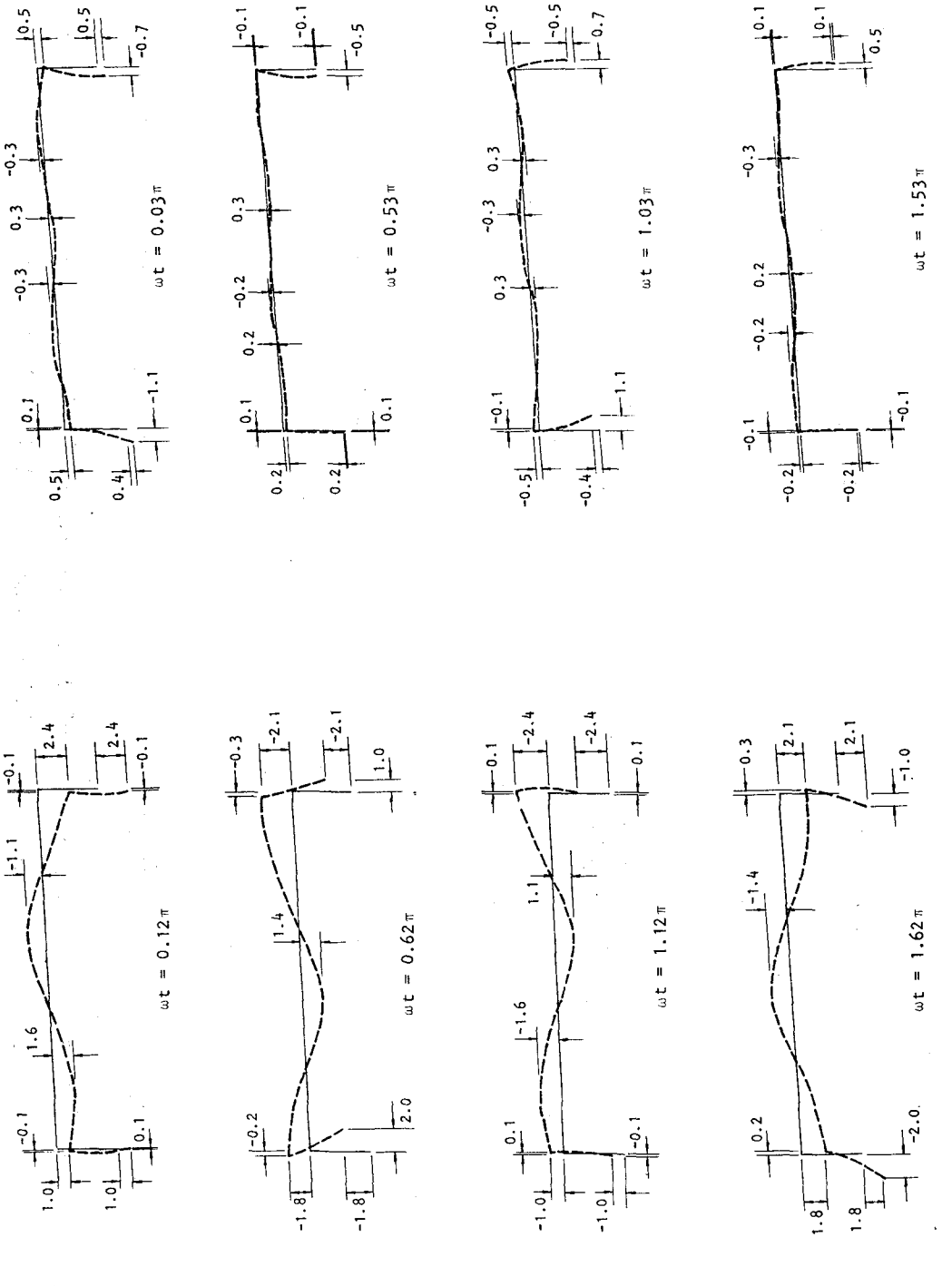

(a) $R_{Lx} = 1.41 \left(\frac{1.0}{\cos 45 \text{ deg}}\right)$ (b) $R_{Lx} = 2.82 \left(\frac{2.0}{\cos 45 \text{ deg}}\right)$

FIGURE 5-17. CASE 5 (θ_H = 0 deg, θ_V = 45 deg): BRIDGE RESPONSE TO APPLIED P-WAVE EXCITATIONS OF EQUAL AMPLITUDE AND EQUAL PHASE AT THE TWO FOUNDATIONS

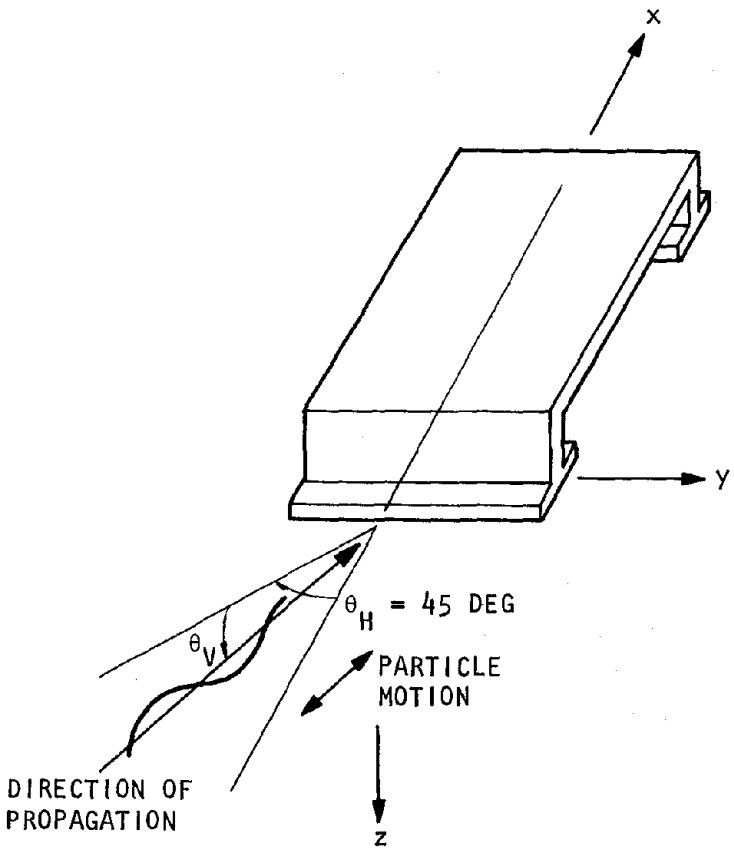

FIGURE 5-18. FREE-FIELD EXCITATIONS FROM INCIDENT P-WAVES FOR CASES 6 AND 7 (θ_H = 45 deg)

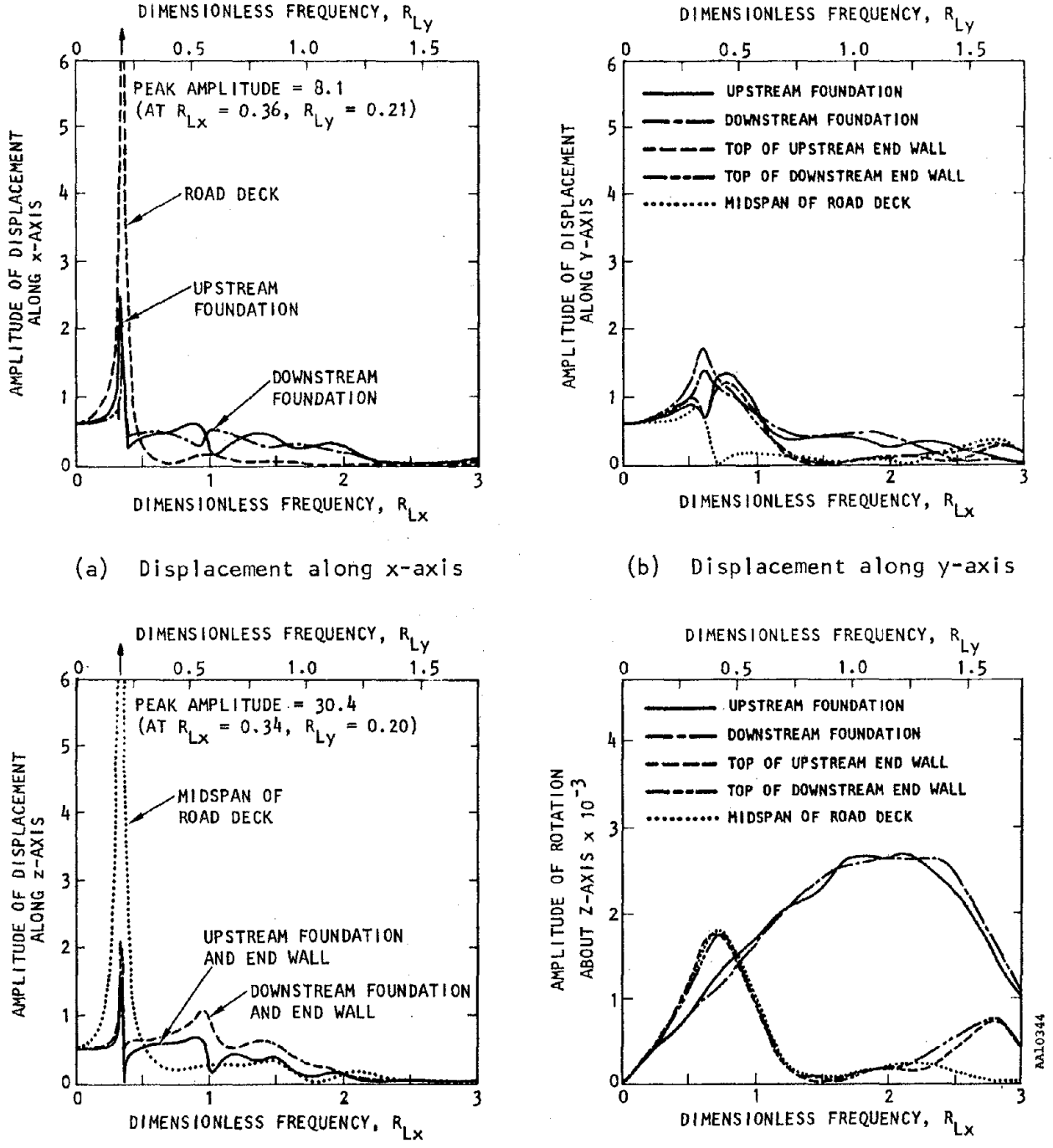

FIGURE 5-19. FREQUENCY-DEPENDENT RESPONSE AMPLITUDES OF BRIDGE SUBJECTED TO INCIDENT P-WAVES WITH θ_H = 45 DEG AND θ_V = 10 DEG

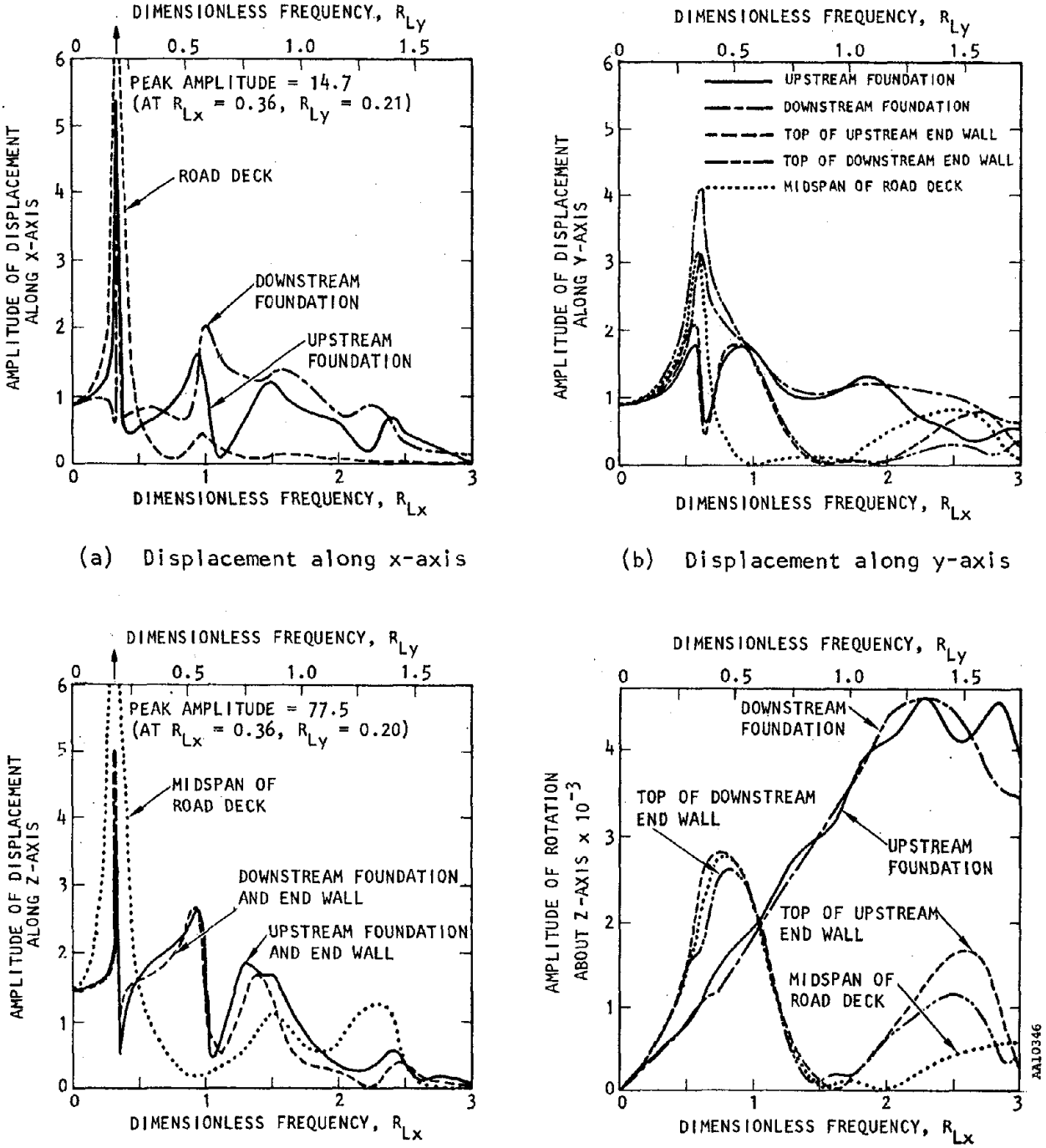

(a) Displacement along x-axis

(b) Displacement along y-axis

(c) Displacement along z-axis

(d) Rotation about z-axis

FIGURE 5-20. FREQUENCY-DEPENDENT RESPONSE AMPLITUDES OF BRIDGE SUBJECTED TO INCIDENT P-WAVES WITH $\theta_H = \theta_V = 45$ DEG

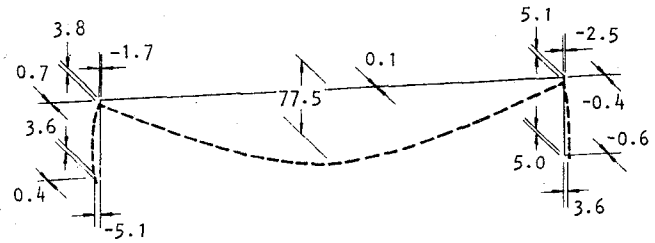

(a) $R_{Lx} = 0.34$, $R_{Ly} = 0.20$ (f = 2.8 Hz)

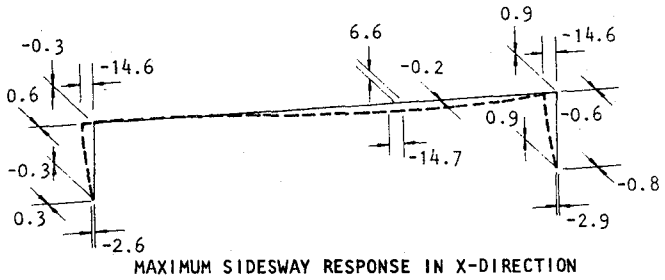

MAXIMUM SIDESWAY RESPONSE IN X-DIRECTION

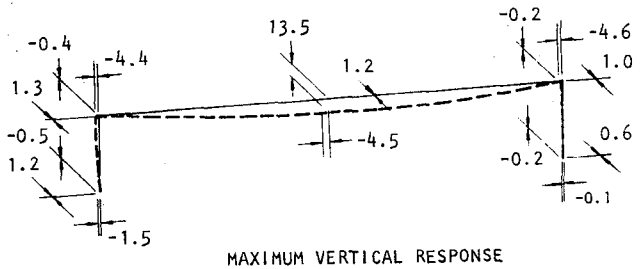

MAXIMUM VERTICAL RESPONSE

(b) $R_{Lx} = 0.36$, $R_{Ly} = 0.21$ (f = 3.0 Hz)

NOTE: RESONANT FREQUENCIES AND DEFORMED SHAPES SHOWN ABOVE ARE ESSENTIALLY THE SAME AS THOSE FOR CASE 6 (θ_H = 45 deg, θ_V = 10 deg) EXCEPT THAT, FOR THAT CASE, THE BRIDGE DISPLACEMENT AMPLITUDE ARE SMALLER (See Figures 5-19 to 5-20 and Table 5-6)

AA10254

FIGURE 5-21. CASE 7 ($\theta_H = \theta_V$ = 45 deg): DEFORMED SHAPES OF BRIDGE AT TIMES OF PEAK RESONANT RESPONSE TO P-WAVE EXCITATIONS

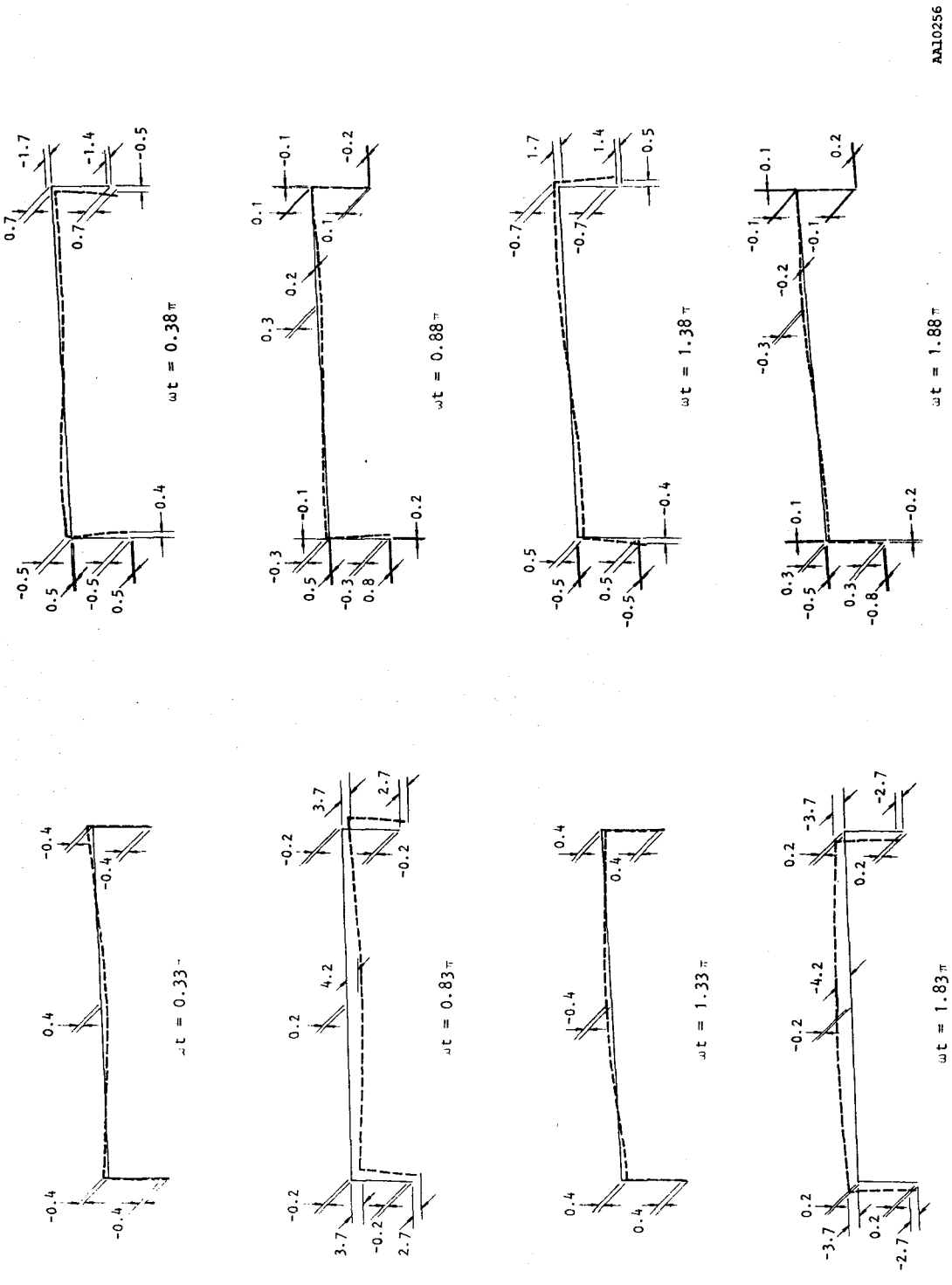

(a) Case 2 (θ_H = 90 deg, θ_V = 10 deg) (b) Case 6 (θ_H = 45 deg, θ_V = 10 deg)

FIGURE 5-22. COMPARISON OF TIME-DEPENDENT DEFORMED SHAPES OF BRIDGE INDUCED BY INCIDENT P-WAVES AT R_{Ly} = 0.36 (f = 5.1 Hz)

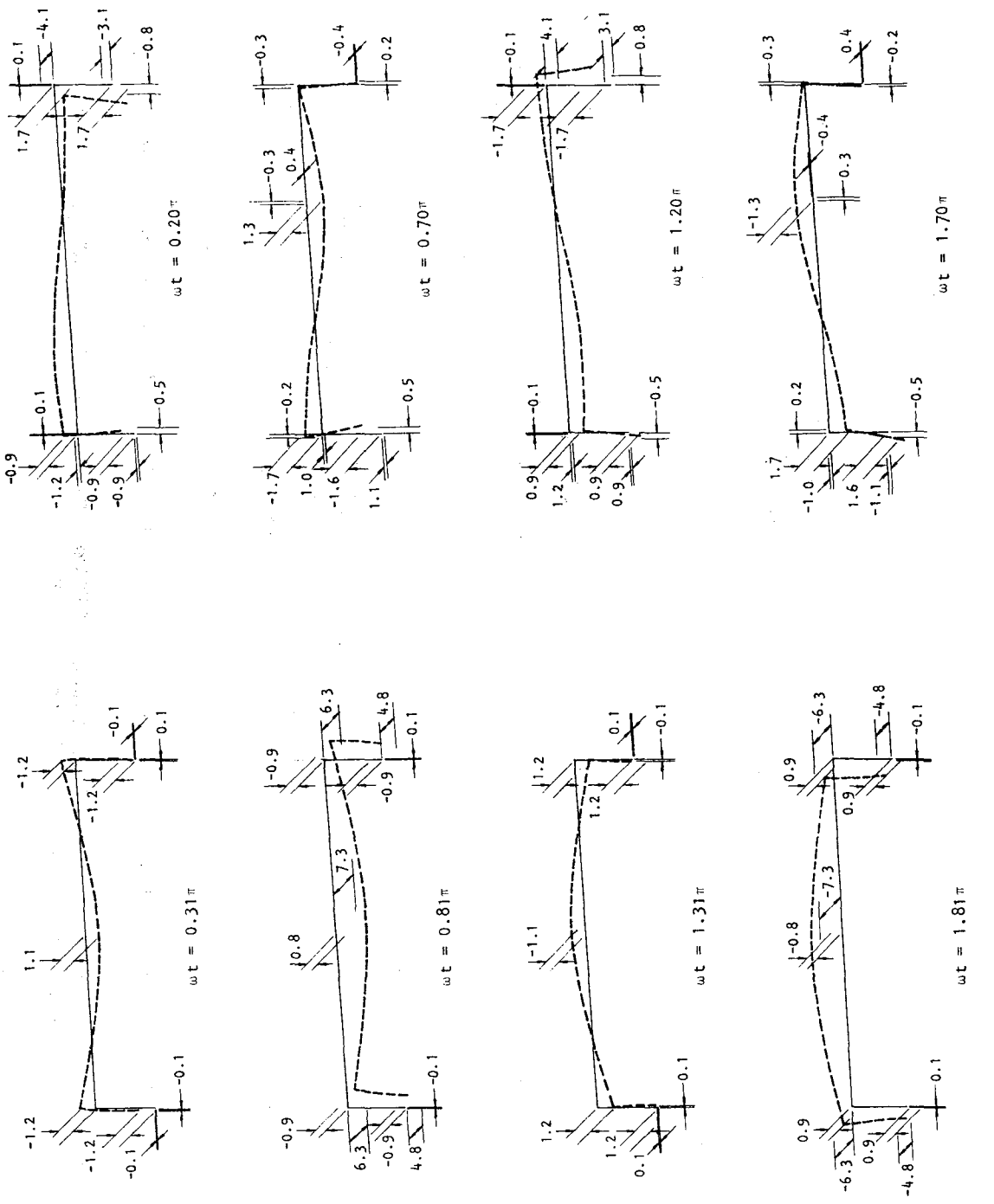

(a) Case 3 (θ_H = 90 deg, θ_V = 45 deg)

(b) Case 7 ($\theta_H = \theta_V$ = 45 deg)

FIGURE 5-23. COMPARISON OF TIME-DEPENDENT DEFORMED SHAPES OF BRIDGE INDUCED BY INCIDENT P-WAVES AT R_{Ly} = 0.36 (f = 5.1 Hz)

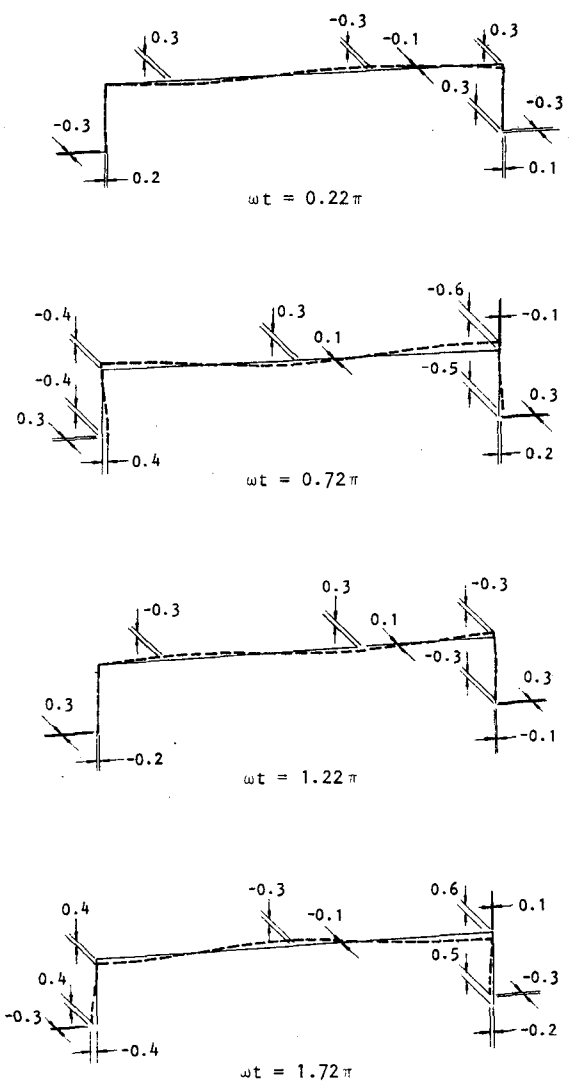

(a) θ_V = 10 deg (R_{Lx} = 1.44, R_{Ly} = 0.84)

(b) θ_V = 45 deg (R_{Lx} = 2.00, R_{Ly} = 1.17)

FIGURE 5-24. CASES 6 AND 7 (θ_H = 45 deg): TIME-DEPENDENT DEFORMED SHAPES OF BRIDGE INDUCED BY INCIDENT P-WAVES AT HIGHER EXCITATION FREQUENCIES

THIS PAGE INTENTIONALLY BLANK

CHAPTER 6

REFERENCES

Anderson J. (1974) "A Dislocation Model for the Parkfield Earthquake," *Bull. Seismol. Soc. of Amer.*, 64:3, pt 1, Jun, pp 671-686.

Bathé, K.J. and Wilson, E.L. (1972) "Large Eigenvalue Problems in Dynamic Analyses," *J. of the Eng. Mech. Div., ASCE*, 98:6, Dec, pp 1471-1486.

----. (1973) "Eigensolution of Large Structural Systems with Small Bandwidth," *J. of the Eng. Mech. Div., ASCE*, 99:3, Jun, pp 467-480.

Bathé, K-J.; Wilson, R.L.; Peterson, V.E. (1974) *SAP IV, A Structural Analysis Program for Static and Dynamic Response of Linear Systems*, EERC-73-11, rev. 1. Berkeley, CA: Univ. of Calif. Earthquake Eng. Res. Center, Apr. (PB 221 967)

Clough, R.W. and Penzien, J. (1975) *Dynamics of Structures*. New York: McGraw-Hill.

Ewing, W.M.; Jardetsky, W.S.; and Press, F. (1957) *Elastic Waves in Layered Media*. New York: McGraw-Hill.

Gutierrez, J.A. and Chopra, A.K. (1978) "A Substructure Method for Earthquake Analysis of Structures, including Structure-Soil Interaction," *Earthq. Eng. & Struct. Dyn.*, 6:1, Jan-Feb, pp 51-70.

Hartzel, S.H.; Brune, J.N.; and Prince, J. (1978) "The October 6, 1974 Acapulco Earthquake: An Example of Short Period Surface Waves in Strong Ground Motion," *Bull. Seismol. Soc. of Amer.*, 68:6 Dec, pp 1663-1678.

Hanks, T.C. (1975) "Strong Ground Motion of the San Fernando California Earthquake," *Bull. Seismol. Soc. of Amer.*, 65:1, Feb, pp 193-225.

Knopoff, L. (1952) "On Rayleigh Wave Velocities," *Bull. Seismol. Soc. of Amer.*, 42:4, Oct, pp 307-308.

Luco, J.E. and Wong, H.L. (1977) "Dynamic Response of Rectangular Foundations for Rayleigh Wave Excitation," *Proc. 6th World Conf. on Earthq. Eng., New Delhi, India, Jan 1977*, Vol. 4, pp 4-85 to 4-90.

Newmark, N.M.; Hall, W.J.; and Morgan, J.R. (1977) "Comparison of Building Response and Free-Field Motion in Earthquakes," *Proc. 6th World Conf. on Earthq. Eng., New Delhi, India, Jan 1977*, Vol. 3, pp 3-01 to 3-06.

REFERENCES (CONCLUDED)

Scanlan, R.H. (1976) "Seismic Wave Effects on Soil-Structure Interaction," *Earthq. Eng. & Struct. Dyn.*, 4:4, Apr-Jun, pp 379-388.

Simpson, I.C. (1978) "On the Interaction of Rayleigh Surface Waves with Structures," *Earthq. Eng. & Struct. Dyn.*, 6:3, May-Jun, pp 247-263.

Trifunac, M.D. (1971) "A Method for Synthesizing Realistic Strong Ground Motion," *Bull. Seismol. Soc. of Amer.*, 61:6, Dec, pp 1739-1753.

Trifunac, M.D. (1979) Personal communication to S.D. Werner, December.

Werner, S.D.; Lee, L.C.; Wong, H.L.; and Trifunac, M.D. (1977) *An Evaluation of the Effects of Traveling Seismic Waves on the Three-Dimensional Response of Structures*, R-7720-4514. El Segundo, CA: Agbabian Associates, Oct.

Wolf, J. and Obernhuber, P. (1979) "Traveling Wave Effects in Soil-Structure Interaction," *Trans. of 5th Int. Conf. on Struct. Mech. in React. Technology*, Vol. K(a), paper K5/1, Berlin, Germany, Aug 13-17.

Wong, H.L. (1975) *Dynamic Soil/Structure Interaction*, EERL-75-01. Ph.D. dissertation. Pasadena, CA: Calif. Inst. of Tech. May.

Wong, H.L. and Luco, J. (1978) "Dynamic Response of Rectangular Foundations to Obliquely Incident Seismic Waves," *Earthq. Eng. & Struct. Dyn.*, 6:1, Jan-Feb, pp 3-16.

APPENDIX A

USE OF CAST-1 TO ANALYZE EFFECTS OF TRAVELING LOVE WAVES IN A LAYERED HALF-SPACE

The results contained in this report and in our prior work (Werner et al,, 1977) describe the bridge response to a complete set of arbitrarily incident wave types that can be encountered in an elastic half-space (i.e., P-, SV-, SH-, and Rayleigh waves). However, an additional surface wave type that occurs only in layered media--Love waves--is also important and can be considered using the CAST-1 elastic half-space results, as described below (Trifunac, 1979).

Consider a soil profile with a uniform, continuous, elastic layer of thickness H that has a shear modulus G_1 and shear wave velocity V_{S_1}; this layer overlies an elastic half-space with shear modulus G_2 and shear wave velocity V_{S_2}. Applying equations of motion to this profile together with appropriate boundary conditions* leads to the following classical Love wave period equation (Ewing et al., 1957):

$$\tan \frac{\omega H}{V_{S_1}} \sqrt{1 - \frac{V_{S_1}^2}{C^2}} = \frac{G_2}{G_1} \frac{V_{S_1}}{V_{S_2}} \sqrt{\frac{\frac{V_{S_2}^2}{C^2} - 1}{1 - \frac{V_{S_1}^2}{C^2}}} \qquad \text{(A-1)}$$

where ω is the excitation frequency and C is phase velocity. Equation A-1 represents relationships between ω and C that are of the form shown in Figure A-1.

Now consider a structure whose foundations rest on the surface of the soil medium. The response of this structure to nonvertically incident SH-waves propagating through an elastic half-space will be the same as the response to a Love wave in a layered medium, provided the phase velocity of

*These boundary conditions correspond to a zero shear stress at the ground surface and compatibility of displacements and stress of the layer and the half-space at their interface.

the SH-wave and Love wave are identical. Equation A-1 shows that the phase velocity for the Love wave is dependent only on the mode number and excitation frequency, whereas for the elastic half-space it is computed as

$$C = \frac{V_S}{\cos \theta_V} \qquad \text{(A-2)}$$

where V_S is the shear wave velocity of the elastic half-space and θ_V is the angle of vertical incidence of the incident SH-wave, measured from the horizontal. Therefore, it is simply necessary to properly select θ_V (assuming V_S is fixed) in order to establish equivalence between the SH-wave results and the Love wave results for a given frequency and mode.

To illustrate this concept, consider the layered half-space to which Equation A-1 is applied in order to obtain the curves shown in Figure A-1. Also, suppose that we are only interested in the first mode shown in Figure A-1. Therefore, for a given frequency, we proceed as follows:

- Enter Figure A-1 at this frequency and obtain the phase velocity of the Love wave, C.
- Compute the required angle of vertical incidence of the SH-wave results as

$$\theta_V = \cos^{-1} \frac{V_S}{C}$$

- Carry out SH-wave calculations at this frequency for an elastic half-space with shear wave velocity V_S and an angle of incidence of the SH-wave of θ_V. The resulting structural response will be identical as that caused by the first mode of Love waves in the medium shown in Figure A-1.
- Repeat the above steps for each frequency and mode of interest.

Figure A-1 shows one important trend that has some practical significance--namely, the existence of a significant frequency range over which the phase velocity of the Love wave is constant. Over this range, it is not necessary to vary θ_V for the SH-waves; instead, the results from a single set of SH-wave results are identical to those from the Love waves. The extent of this range is dependent on the layer thickness and properties of the layer and the underlying half-space. For a given set of material properties and a given excitation frequency, the phase velocity approaches V_{S_1} (the shear wave velocity of the layer) as the layer thickness increases.

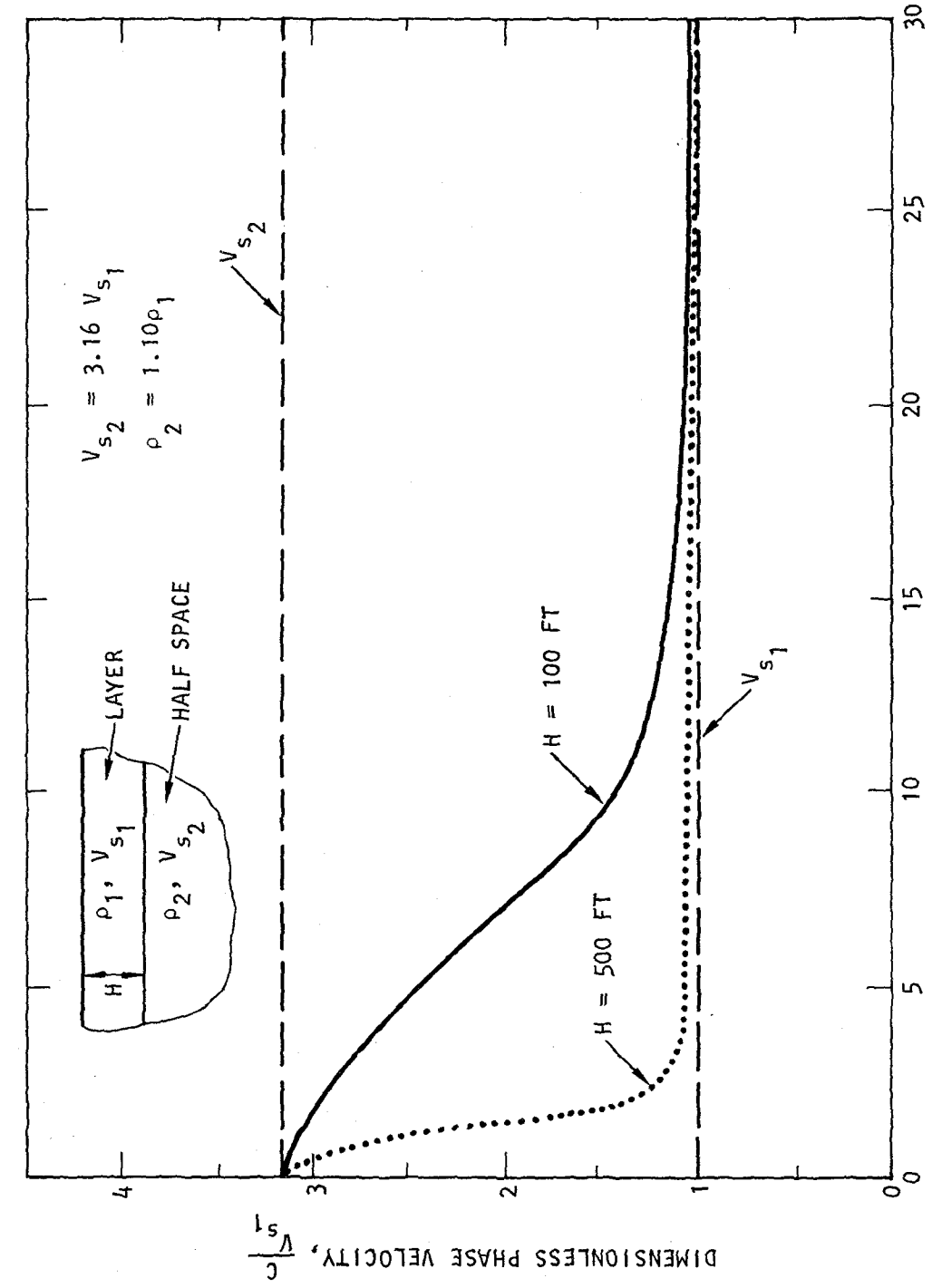

FIGURE A-1. LOVE WAVE PHASE VELOCITY (FIRST MODE) VS. EXCITATION FREQUENCY